SCUOLA NORMALE SUPERIORE

Classe di Scienze

Corso di perfezionamento in

Neuroscienza

XXXII ciclo

“Comprehensive Techniques to Study Activity-dependent and Neurogenic Mechanisms in Stem Cell-derived Neuron Models”

Settore Scientifico Disciplinare **Biologiá/Neurobiologiá**

Candidato
Dr. Keagan Dunville

Relatore:

Prof. Federico Cremisi

Anno accademico 2021

Table of Contents

Abstract: Accurately modeling human-related neuronal phenomena remains at the forefront of neuroscience. This thesis utilizes already-established *in vitro* models of mouse embryonic stem cells, designing an efficient method to optogenetically stimulate neurons derived from mouse stem cells and expounds upon their scope with novel protocols to generate hippocampal neurons from human induced pluripotent stem cells. First, a novel platform for optogenetic stimulation was built and tested on mouse embryonic stem cells to demonstrate functionality of optogenetic channels in mouse embryonic stem cell-derived neurons. The device was built from 3D printed materials and validated with oscilloscopy and spectrophotometry while neurons were cultured for over 30 days *in vitro* and assayed first for electrical activity by electrophysiology, calcium signaling, and small molecule activation of glutamatergic receptors. When verified that both device and neurons were functional, cells were transduced with a ChannelRhodopsin variant, ChR2-eYFP-NpHR, and were stimulated over several light cycle parameters and assayed for CFOS expression. Having shown that neurons responded in an activity-dependent manner to the device, I established preliminary studies into human hippocampal embryonic neurogenesis. I derived a novel protocol to differentiate hiPSCs to hippocampal neural progenitors using small molecules and specific laminar substrates unique to the subgranular zone. Hippocampal progenitors were assayed for literature-established genetic markers including WNT7b, WNT8a, PROX1, FOXG1, and ZBTB20, and then allowed to spontaneously differentiate into neurons expressing canonical neural, synaptic, glutamatergic, and constitutive hippocampal markers. These cells were expanded over 200 days *in vitro*. When allowed to spontaneously differentiate or forced to differentiate under NOTCH inhibition, neuronal cultures sustained ZBTB20 and FOXG1 coexpression over the terminal differentiation path though cultures at ~200 days old did not differentiate at the same rate as cultures from ~30 days. When transplanted *in vivo*, human hippocampal progenitors differentiated fully after 4 months, projected toward the CA3 from the dentate gyrus, and established synaptic connections with host neurons identified by staining synaptic markers. In conclusion, several novel findings are demonstrated throughout this thesis, though the most pertinent include:

1.) mESC-derived neurons may be optogenetically stimulated by ergonomic device fabrication.

2.) Sustained or adult neurogenesis is dependent on the laminin isoform expressed in the subgranular zone.

3.) Hippocampal progenitors from human induced pluripotent stem cells behave like neurons and can be optogenetically targeted and are transplantable *in vivo* hippocampus in which they integrate into pre-existing hippocampal networks.

Future investigations include merging activity-dependent Tau phosphorylation in mESC- and hiPSC-derived human hippocampal neurons and transplantation of human hippocampal progenitors into an *in vivo* model to study aging or dementia-related effects on memory and behavior.

Chapter I: Stem cell-derived neurons as a comprehensive model for neuromolecular studies

The over-arching theme of this thesis stems from contemporary questions regarding human hippocampal development and approaches them with genetic engineering approaches to establish novel *in vitro* models and methods reliant on stem cell-derived neuronal cultures. Several emergent fields and techniques are approached during these studies with the long-term goal to concatenate several directions to succinctly understand human embryonic hippocampal neurogenesis. Cellular studies have been conducted to establish reliable *in vitro* investigations into neurodevelopmental or neurodegenerative disorders, The past two decades in stem cell research have nurtured a wealth of protocols and studies for neuronal differentiation into basal ganglia striatal projections (Arber et al., 2015; Fjodorova et al., 2015; Kirkeby et al., 2012), isocortex (Bertacchi, Pandolfini, et al., 2015; Espuny-Camacho et al., 2013, 2017; Gaspard et al., 2008, 2009; Y. Shi, Kirwan, & Livesey, 2012), spinal cord (Wichterle et al., 2002), cerebellar purkinje neurons (Muguruma et al., 2010; Shuyan Wang et al., 2015; Watson et al., 2018), general LGE- and MGE-origin mixed cell type culture (Sandra Ahn et al., 2016; Hsieh & Baraban, 2017), hypothalamus (Bertacchi et al., 2013; Wataya et al., 2008), and hippocampus (Sakaguchi et al., 2015; Sarkar et al., 2018; Terrigno et al., 2018; Diana Xuan Yu et al., 2014). Stem cell-derived neurons have been observed as capable of functional maturity, mimicking voltage gated cation channel expression similar to their respective *in vivo* wild-type (Barth et al., 2014), with exceptional nuances in expression level and current amplitude (Tong et al., 2010). Furthermore, stem cell-derived neuronal cultures and organoids have provided unprecedented insight into questions regarding development (Alenina et al., 2006; Bertacchi et al., 2013; A. M. Paşca et al., 2015), molecular interactions (Bertacchi, Lupo, et al., 2015; He et al., 2016; S. Li et al., 2015; Pandolfini et al., 2016; Rodriguez, 2004; Yalin Zhang et al., 2017), and pathological modeling (S. H. Choi et al., 2016; Iovino et al., 2015; Medda et al., 2016; Ohta et al., 2015; Reilly et al., 2017; Wray, 2017). Considering the studies included in this thesis aim to establish foundations for investigating the archicortical development, reliable and appropriate models of distinct archicortical circuitry need further establishment. While these studies are not necessarily seminal, they aim to provide reliable, accessible,

compatible, and molecularly fidelitous expansions for studying human neuronal development to expand contemporary *in vitro* study limitations in optogenetics and human development.

Embryonic or induced pluripotent stem cells? "2D" adherent cultures or 3D organoids?

Stem cells represent a robust *in vitro* platform to reliably study developmental mechanisms and phenomena as they undergo self-renewal and exhibit totipotency, or the ability to differentiate along all embryonic-derived, somatic and germ-line lineages (Figure 1) (Romito & Cobellis, 2016). Stem cells were first characterized *in vitro* after the discovery of hematopoietic stem cells in the bone marrow of mice and described as highly proliferative in adult (Till & McCulloch, 1961). Embryonic stem cells (ESCs) were instead derived 20 years later by direct isolation from the embryonic germline or mouse blastula (Martin, 1981). Originally sustained on mouse embryonic fibroblast feeder layers, the pluripotency of these stem cells is maintained by serological activation of cytosolic SMAD signaling and additional activation of Leukemia Inhibitory Factor (LIF) signaling pathway. Briefly, excess Bone Morphogenic Protein (BMP) activates BMP receptors to recruit SMAD proteins, activating transcription factor Id4 to inhibit lineage specific differentiation (Ying et al., 2003). Simultaneously, LIF activates the JAK/STAT pathway through gp130 receptor thereby activating Stat3 (Chambers, 2005; Niwa et al., 1998) to recruit Oct4 (Nichols et al., 1998; G. Shi & Jin, 2010), Sox2 (Avilion et al., 2003; Fong et al., 2008), and Nanog (Mitsui et al., 2003; Jianlong Wang et al., 2008), transcription factors crucial in regulating stem cell self-renewal. Alternatively this may be substituted with small molecule inhibition of the MEK-MAPK-ERK pathway, however, to induce Nanog expression by inhibiting ERK1 phosphorylation (Kim et al., 2014). While debated whether b-catenin upregulation contributes to self-renewal in cultured ESCs (Bone et al., 2009; Davidson et al., 2012), Gsk-3b is simultaneously inhibited in parallel to MEK inhibition and LIF signaling activation to promote yet fully elucidated mechanisms of self-renewal, though most likely involves recruitment of pro-proliferation transcription factor complex, TCF1/LEF1 (Aulicino et al., 2020).

Induced pluripotent stem cells (iPSCs), while regulated by the same self-renewal transcription factors as ESCs (Xiaosong Liu et al., 2008), are instead a more recent discovery in which fibroblasts are transiently induced to express Oct3/4, Sox2, and instead of Nanog, c-Myc and Klf4 (Takahashi & Yamanaka, 2006). Overexpression of these 4 factors induces chromatin reopening in differentiated cells and allows accessibility

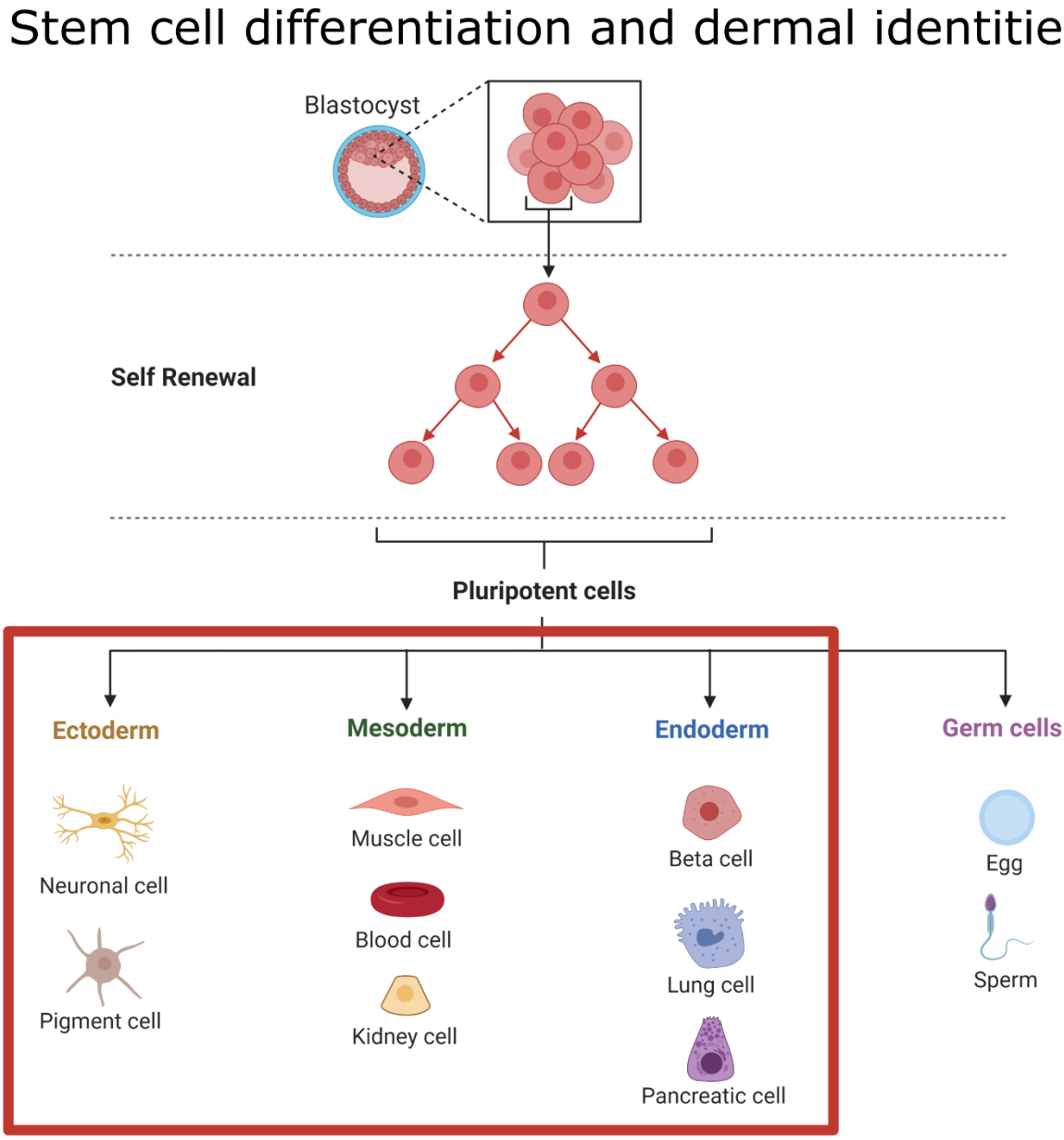

Figure 1. Stem cell differentiation for terminal tissue differentiation. Stem cells intended for cell culture differention are derived from the inner cell mass of the blastocyst. *In vivo*, they undergo self renewal to enrich the available pluripotent niche before proceeding to generate primordial progenitors of 1 of the 4 lines listed. The red box indicates somatic lines that have been most accessible to for functional studies using induced PSCs, however, a recent study has demonstrated that it possible to model the original blastocyst (X. Liu et al., 2021). Figure adapted from Moodley et al., 2013.

to previously inactivated transcription factors, most notably c-Myc's unilateral reactivation of Notch signaling pathway (Xiaosong Liu et al., 2008). Intriguingly, while Nanog dimerization has been demonstrated as a key regulator of pluripotent stem cell renewal (Jianlong Wang et al., 2008), it is otherwise redundant in the conversion of fibroblasts as a Nanog-knockout model of iPSC was demonstrated as more similar to wild type ESC (B. A. Schwarz et al., 2014). Reprogramming differentiated murine cells to a ground state of pluripotency is an unparalleled discovery in that previous terminal differentiation was thought to be irreversible (W. A. Müller, 1997). Furthermore, it lead to the further discovery of conserved mechanisms in other species and thus the establishment of human iPSCs (hiPSCs) (I. H. Park et al., 2008), and most recently has been even further extended to model human blastocysts *in vitro* (Xiaodong Liu et al., 2021). Despite reconversion, ESCs and iPSCs express near-identical molecular profiles in both murine (Takahashi & Yamanaka, 2006) and human lines (Chin et al., 2009) though may be distinguished from each other at the miRNA level (Chin et al., 2010; Marchetto et al., 2009). Regardless of this nuance, induced pluripotent and embryonic stem cells share identical major gene regulatory networks (J. Choi et al., 2015) and provide a robust platform to study developmental mechanisms (Ardhanareeswaran et al., 2017) and model biological processes *in vitro*.

The spatial conformation of the cells during *in vitro* differentiation studies from iPS and ES cells are dependent on the intended study. These culture conformations fall under two categories: two dimensional or "cellular carpets" and three dimensional, free floating organoids. Two dimensional, or adherent, cultures are the standard wherein cultured cells adhere to the bottom of the culture dish and grow outward across its surface. Some cell lines or types require substrates for adhesion, for example primary neurons require poly-d-lysine (Brewer, 1997) or stem cell-derived neural cells require a two-part substrate system of poly-l-ornithine and laminin (Cai & Grabel, 2007), whereas other cell lines like human embryonic kidney cells sufficiently adhere to plastic without additional substrate (Graham et al., 1977). Conversely, 3D organoids are a novel alternative to 2D cultures and support the differentiating stem cell culture is free floating within culture media. The substrate-free system does however is optimized for constant motion of the media (Qian et al., 2016) however and in terms of neuronal differentiation protocols, still requires diluted laminin substrate in the media. The

major difference between 2D and 3D cultures is the intended application or research question: 2D cultures are suitable for shorter maintenance protocols in which limited cell types are probed for molecular changes whereas 3D cultures are optimal for understanding developmental mechanisms over a longer period of time in a more physiological context i.e. cell type emergence during system/organ formation. Because differentiation protocols however typically induce identity along one germ line, 3D cultures are still preliminary in their capacity to understand systems development given that a single organ system may be comprised of differentiating cells from all three lineages (Baker & Chen, 2012). Furthermore, spatially constrained embryogenic phenomena like folding in the cortex are not readily recapitulated in 3D models and thus they are still limited to molecular and cellular study, which often require extracellular stimuli. Three-dimensional matrix cultures are emergent as an alternative which combines 2D and 3D culture systems by providing a porous matrix *in vitro* coated with a substrate to promote 3D growth while conserving 2D surface area availability (Lancaster et al., 2017; Ouyang et al., 2007). *In vitro* matrices are still novel, however, and require further development to refine cellular extraction and analysis. Both major culture systems, 2D and 3D, demonstrate advantages and disadvantages and require consideration before undertaking *in vitro* experiments.

Modeling neurodevelopment and neurodegeneration with stem cells

Stem cells have presented a novel and ethical tool in developmental biology and have provided enormous insight regarding developmental mechanisms *in vitro*. These studies have spanned across nearly all fields of systems biology including skeletomuscular (Brack et al., 2007), cardiovascular (de Carvalho et al., 2019; Millard et al., 2017), neurological (Gaspard et al., 2009; Y. Shi, Kirwan, Smith, et al., 2012), adipogenesis (Schie et al., 2008), cancer (Z. Yu et al., 2012), renal (Kramer et al., 2006), immune response (Hasselmann et al., 2019), and epidermis (J. Lee et al., 2020) to name a few. The capacity for multilineage differentiation makes stem cell biology an attractive complement to *in vivo* study for understanding body compartments that are difficult to

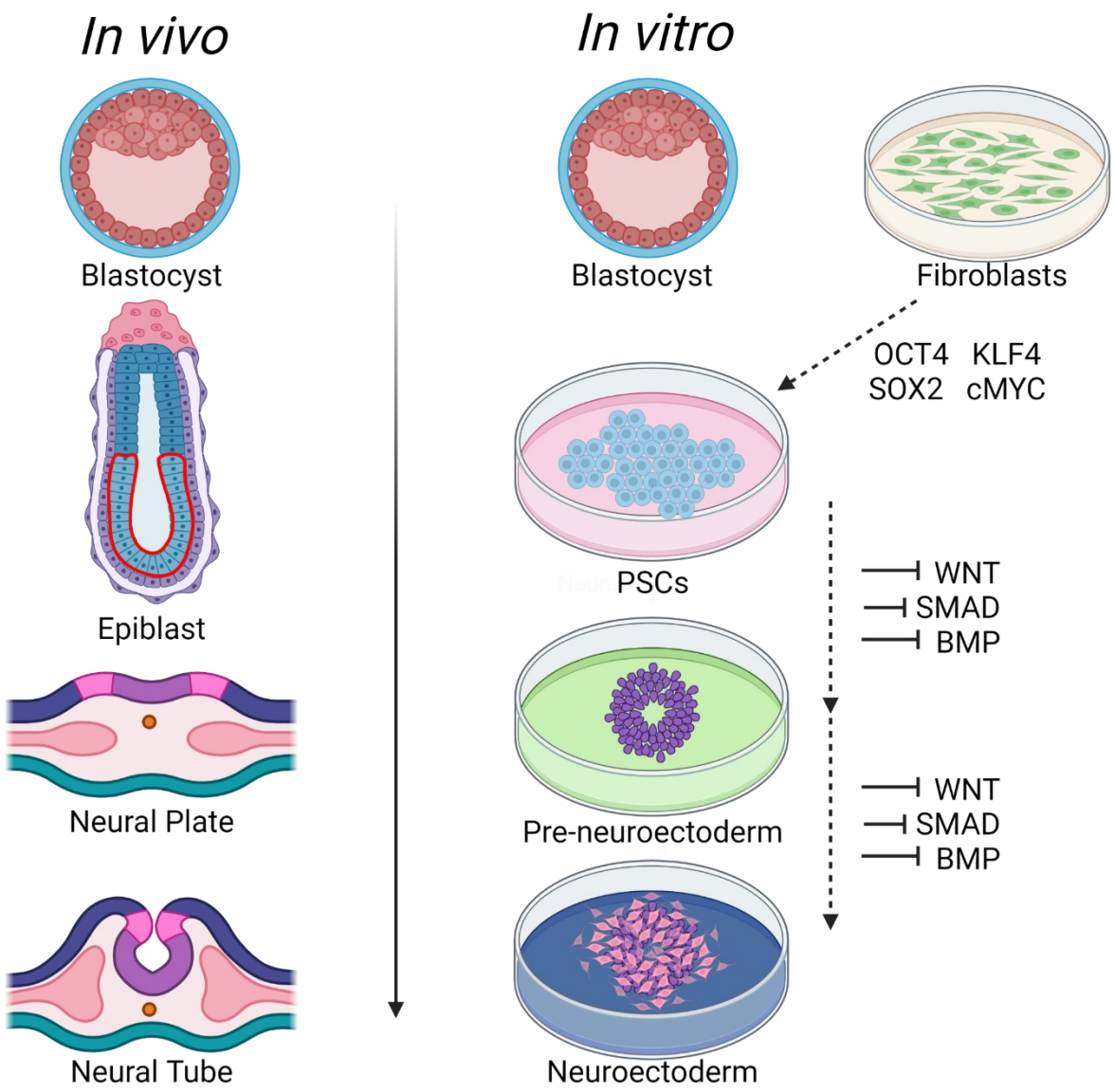

Figure 2. In vitro recapitulation of neural folding events in vivo. ESCs are derived from the blastocyst by inner cell mass extraction OR iPSCs are derived from young fibroblasts by transient overexpression of Yamanaka factors (Park et al, 2008; Takahasi & Yamanaka, 2006). Transition from an epiblastic state using pluripotent stem cells (either ESCs or iPSCs) to invaginated neural tube in human models is recapitulated by simultaneous inhibition of WNT, SMAD, and BMP signals (Shi et al., 2012). Compared to mouse ESC telencephalic induction (Bertacchi et al, 2015), induction of human PSCs requires additional SMAD inhibition to reproduce early embryonic neuralization events. Figure adapted from Lupo et al, 2014.

access. The potential for stem cells in biological study application is exhaustive and thus for the sake of this section, highlighted studies will demonstrate major findings in neurodevelopmental and neurodegeneration *in vitro* models.

One of the more important findings in modeling brain development through hiPSCs differentiation and organoid culture establishment is the conservation of embryogenic mechanics between *in vitro* "pseudo-development" compared to *in vivo* (Amiri et al., 2018; Gordon et al., 2021; Raja et al., 2016). These studies demonstrate that there is a cellular conservation in maturation signals that take place during embryogenesis (detailed in Figure 2) which are inherently encoded and executed to essentially recapitulate the *in vivo* molecular environment (Camp et al., 2015), a retention in self-organization of the cortical plate (Lancaster et al., 2017), and finally the reconstitution of cell-type diversity within cerebral organoids (Quadrato et al., 2017; Velasco et al., 2019) in the same birth-order as observed *in vivo* corticogenesis (Eiraku et al., 2008). Secondly, retention of neuron-specific characteristics such as functional channel expression and synaptic network establishment have also been demonstrated in stem cell-derived *in vitro* models (Miura et al., 2020; Perny et al., 2017; Quadrato et al., 2017; Y. Shi, Kirwan, & Livesey, 2012; Y. Shi, Kirwan, Smith, et al., 2012), elaborating that not only are *in vivo* molecular mechanisms conserved but also the physiology of the terminally differentiated cell is conserved. This is key in demonstrating the validity and weight of stem cell differentiation protocols in that signaling events prior to differentiation generate a physiologically relevant context (S. J. Yoon et al., 2019). Extensive *in vitro* stem cell modeling has demonstrated that neurodevelopmental and neurodegenerative pathway signaling are also highly conserved and functionally alter differentiation outcome (Ying Zhang et al., 2013) thereby increasing the utility of stem cell-derived cultures in understanding human disorders.

Stem cell models of human disorders explore mechanistic dysregulations in both neurodevelopmental and neurodegenerative contexts, particularly with the publication of patient-derived induced pluripotent stem cells (Brennand et al., 2011; Israel et al., 2012; Soldner et al., 2009). Key findings have been demonstrated using the conserved neurological mechanisms with the intent for therapy or management, uncovering pathways that are otherwise ethically difficult to study *in vivo*. These models and their findings are extensive (Ardhanareeswaran et al., 2017) and select examples will be introduced. The Autism Spectrum is extensively studied using human stem cell models (Cheffer et al., 2020). Fragile X Syndrome, a disorder on the Autism

Spectrum characterized by intellectual impairment, is a prime example of novel mechanistic discovery. Stem cell-derived Fragile X Syndrome models have uncovered that Fragile X Mental Retardation Protein (FMRP), responsible for disorder manifestation, regulates synaptogenesis despite neurogenic retention in neural stem cell populations (Telias et al., 2013) and is most likely becomes dysfunctional through inhibited retinoic acid signaling (Z. Zhang et al., 2018). Impaired cortical network establishment was further expanded in that FMRP ultimately regulates axonal pathfinding networks, including *DCC*, a netrin receptor expressed at the growth cone, and that Fragile X Syndrome mutation in FMRP impairs cortical pathfinding signals through *DCC* downregulation (Halevy et al., 2015). Fragile X is not the only ASD studied using stem cell models. Management and potential therapies for Rett Syndrome, an orphan disease which selectively affects female infants and terminates fatally in childhood, have advanced significantly. KCC2, a potassium channel sensitive to GABAergic activation of NSCs during embryogenesis, has been shown to not only be deficient in Rett Syndrome but that compensatory expression in its stem cell model rescues cellular impairment (Tang et al., 2016) and alternatively rescued through iHDAC6 compensatory expression (Landucci et al., 2018) offering preliminary studies to future therapeutic investigations. As a final example, developmental mechanisms of Schizophrenia have been studied using iPSCs, first demonstrating that iPSC-derived neuron models also exhibit decreased neuronal network connectivity (Brennand et al., 2011). Furthermore, this effect was further compounded in an iPSC-derived model of genetic risk factor CYFIP1 and that its mutation disrupts adherens junction at the neural stem cell stage (K. J. Yoon et al., 2014). In a patient-derived iPSC-derived model of CA3 neurons, it was elaborated that schizophrenia-afflicted neurons exhibited decreased intrinsic neuronal activity (Sarkar et al., 2018) giving an overall perspective that the Schizophrenia genotype impairs critical development processes in cytoarchitectural establishment and cellular functionality. iPSC-derived neurodevelopmental disorder models are not limited to these fields, however, and include other disorders categorized within the Autism Spectrum, including Angelman Syndrome (Fink et al., 2017), Timothy Syndrome (S. P. Paşca et al., 2011), Phelan-McDermid Syndrome (Huang et al., 2019), and Kleefstra Syndrome (Frega et al., 2019) as well as disorders outside of ASD like lysosomal storage disorders (Luciani et al., 2020) and pediatric epilepsy (Tukker et al., 2018).

Stem cell cultures, gene-editing, and patient-derived iPSCs have not only supported neurodevelopmental disorders however and have been exploratorily used in neurodegeneration research. *In* vitro models for Huntington's (Arber et al., 2015; Fjodorova et al., 2019), Alzheimer's disease (Bergström et al., 2016; Israel et al., 2012), Parkinson's disease (Beevers et al., 2017; Soldner et al., 2009), and amyotrophic lateral sclerosis or motor neuron disease as well as Frontotemporal dementia (S. Lee & Huang, 2017). These models have succeeded in recapitulating the pathological molecular environment, often in the upregulation of increased markers of pathological neurodegeneration like neurofibrillary tangles (S. H. Choi et al., 2016; Medda et al., 2016; Ohta et al., 2015). Studies using these models have demonstrated that disordered and pathologically aggregating protein, microtubule associated protein Tau (MAPT) induces early maturation of neurons in these models (Beevers et al., 2017; Iovino et al., 2015). However, while these studies have effectively demonstrated that the pathomolecular environment can be reconstructed *in vitro*, no study has successfully demonstrated disrupted synchronization of networks otherwise present in *in vivo* models (Etter et al., 2019; Gillespie et al., 2016). Furthermore, these studies, while novel and intuitive to understanding microtubule binding protein mechanisms in an developmental axonal context, may not accurately reflect the pathological state as some pathological markers, like hyperphosphorylated MAPT, are comparatively expressed during development (Brion et al., 1993; Goedert et al., 1993; Riederer, 1992). Thus not only are these studies limited in their capacity to study physiological effects like behavior and demonstrated network signaling, but without accounting for the approximate culture age these model may be studied in an inadequate context as observed death may be a function of cell-autonomous programming (S. H. Choi et al., 2016; Raja et al., 2016). This is further compounded by the assumption that any neuronal type from any cerebral compartment will suffer equivocally in pathological conditions. From recent literature, it is apparent that cell type dictates neurodegenerative effects, for example TAU-mediated neurodegeneration (Andrews-Zwilling et al., 2010) is commonly accepted to start in the medial entorhinal cortex and propagate in a transsynaptic manner to the dentate gyrus and cornu ammonis (L. Liu et al., 2012; Vermersch et al., 1992). This is likely mediated by glutamatergic projection neurons as they exhibit heightened susceptibility to TAU

phosphorylation and aggregation (Ghosal & Pimplikar, 2011; Siano et al., 2019; Sun et al., 2016) and selectively die during early Alzheimer's pathogenesis (Kobro-Flatmoen et al., 2016). Modelling neurodegeneration *in vitro* then demands that the respective affected compartment be modeled as well, though currently only one *in vitro* model for the CA3 exists (Sarkar et al., 2018). This point transitions to the remaining obstacle in stem cell models that not all compartments have been adequately modeled *in vitro* nor has a succinct process for aging stem cell-derived models been published. This is due to unique regional differences transcriptional activation and timing of signal transduction. The most widely studied of such developmental molecular organizers, and thus the most prevalent to this thesis, is the evolutionarily conserved Wnt protein.

Wnt signaling in neurodevelopment and recapitulation in vitro

Wnt protein is a long-studied molecule whose developmental function was first introduced in *Drosophila melanogaster* in ortholog Wingless gain and loss of function models. Wingless was demonstrated as responsible for organizing body segments in a gradient expressive manner along the anterior-posterior axis (Cadigan & Nusse, 1996; Kadowaki et al., 1996; Van den Heuvel et al., 1993). In mammals, this gradient-wise organizational control during development is highly conserved and Wnt is expressed through 19 isoforms in the murine and human and denominated as: Wnt1 (Nusse et al., 1984)/WNT1 (Arheden et al., 1988), Wnt2 (McMahon & McMahon, 1989)/WNT2 (Wainwright et al., 1988), Wnt2b (Wnt13) (Zakin et al., 1998)/WNT2b (WNT13) (M Katoh et al., 1996), Wnt3 (H. Roelink et al., 1990)/WNT3 (Henk Roelink et al., 1993), Wnt3a (Greco et al., 1996)/WNT3a (Saitoh et al., 2001), Wnt4 (Gavin et al., 1990)/WNT4 (Huguet et al., 1994), Wnt5a (Gavin et al., 1990)/WNT5a (Clark et al., 1993), Wnt5b (Gavin et al., 1990)/WNT5b (Saitoh & Katoh, 2001b), Wnt6 (Gavin et al., 1990)/WNT6 (Rankin et al., 1999), Wnt7a (Gavin et al., 1990)/WNT7a (Ikegawa et al., 1996), Wnt7b (Gavin et al., 1990)/WNT7b (Kirikoshi et al., 2001b), Wnt8a (Bouillet et al., 1996)/WNT8a (Saitoh & Katoh, 2001a), Wnt8b (Richardson et al., 1999)/WNT8b (Majlinda Lako et al., 1996), Wnt10a (J Wang & Shackleford, 1996)/WNT10a (Kirikoshi et al., 2001a), Wnt10b (J Wang & Shackleford, 1996)/WNT10b (Bui et

al., 1997), Wnt11 (Adamson et al., 1994)/WNT11 (M. Lako et al., 1998), WNT14 (Saitoh et al., 2001), Wnt15/WNT15 (Bergstein et al., 1997), and Wnt16/WNT16 (Fear et al., 2000). Wnt is responsible for not only organizing compartments in development but has also been associated in post-mitotic neurons as crucial to maintaining electrical functionality (Rosso & Inestrosa, 2013). Wnt signaling is divided into 2 pathways: canonical modulates b-catenin activity (Figure 3) and non-canonical induces intracellular Ca^{2+} influx (Masaru Katoh, 2017). While Wnt signaling is crucial to all body compartments, this thesis will focus primarily

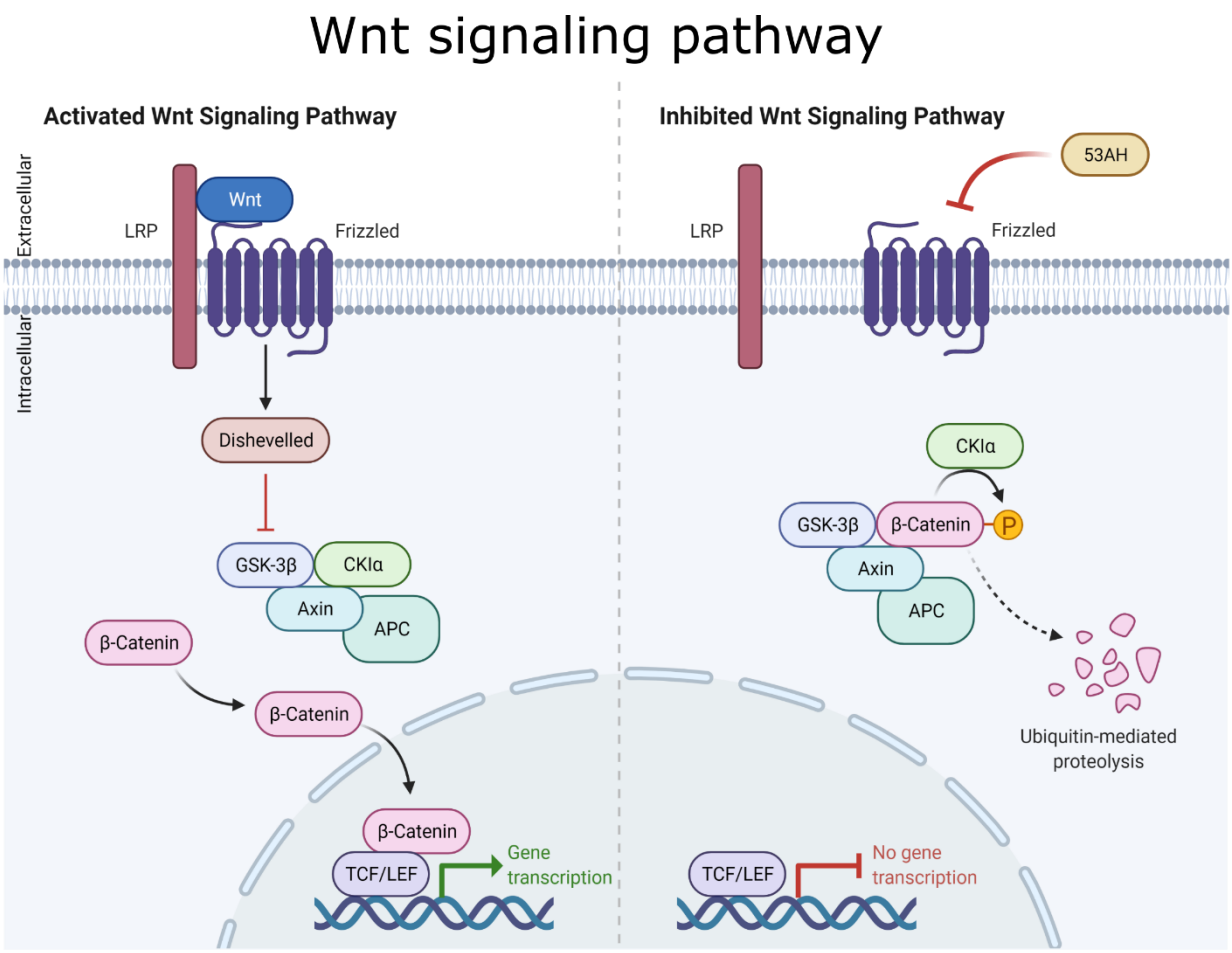

Figure 3. Molecular signaling in canonical Wnt pathway. Wnt binds first to TMP receptor, Frizzled and recruits lipoprotein receptor-related protein (LRP) thereby activating dishevelled. Dishevelled inhibits a proteolytic induction complex, organized by GSK-3β and comprised of Casein Kinase 1 alpha (CKIα), Axin, and adenomatous polyposis coli (APC). β-Catenin accumulates and enters the nucleus and binds to T-cell factor/lymphoid enhancer factor (TCF/LEF) to induce downstream genes including those regulating cell cycle, cell identity, and terminal differentiation. WNT pathway inhibition is commonly used to induce a neuroepithelial identity from ESC or iPSC to induce proteolysis of GSK-3β-phosphorylated β-catenin. In this thesis, small molecule Frizzled inhibitor, 53AH, is employed to induce a telencephalic identity from both ESC and iPSC by blockade of Frizzled transmembrane receptor. Figure adapted from Mulligan et al, 2013 and Miller et al, 2002.

on canonical Wnt signaling pathway in relation to cell culture and its involvement in inducing neural plate-like stages.

Several Wnt genes are involved in regulating the neural plate and neural tube formation (Bouillet et al., 1996; Grove et al., 1998; Mulligan & Cheyette, 2012; Ni et al., 2021; H. Roelink & Nusse, 1990) and are expressed in discreet patterns as the neural tube progresses to form more definitive regions in the central nervous system (Parr et al., 1993) thus the timing and the isoform expressed are crucial to positional identity within the mammalian brain (Figure 4). Wnt is more strongly expressed posteriorly whereas its functional antagonist, Secreted frizzled-related protein 1 (Sfrp1) is more strongly expressed anteriorly but both are expressed in an opposing gradient along the anterior-posterior axis (Figure 4A)(H. Roelink & Nusse, 1990).

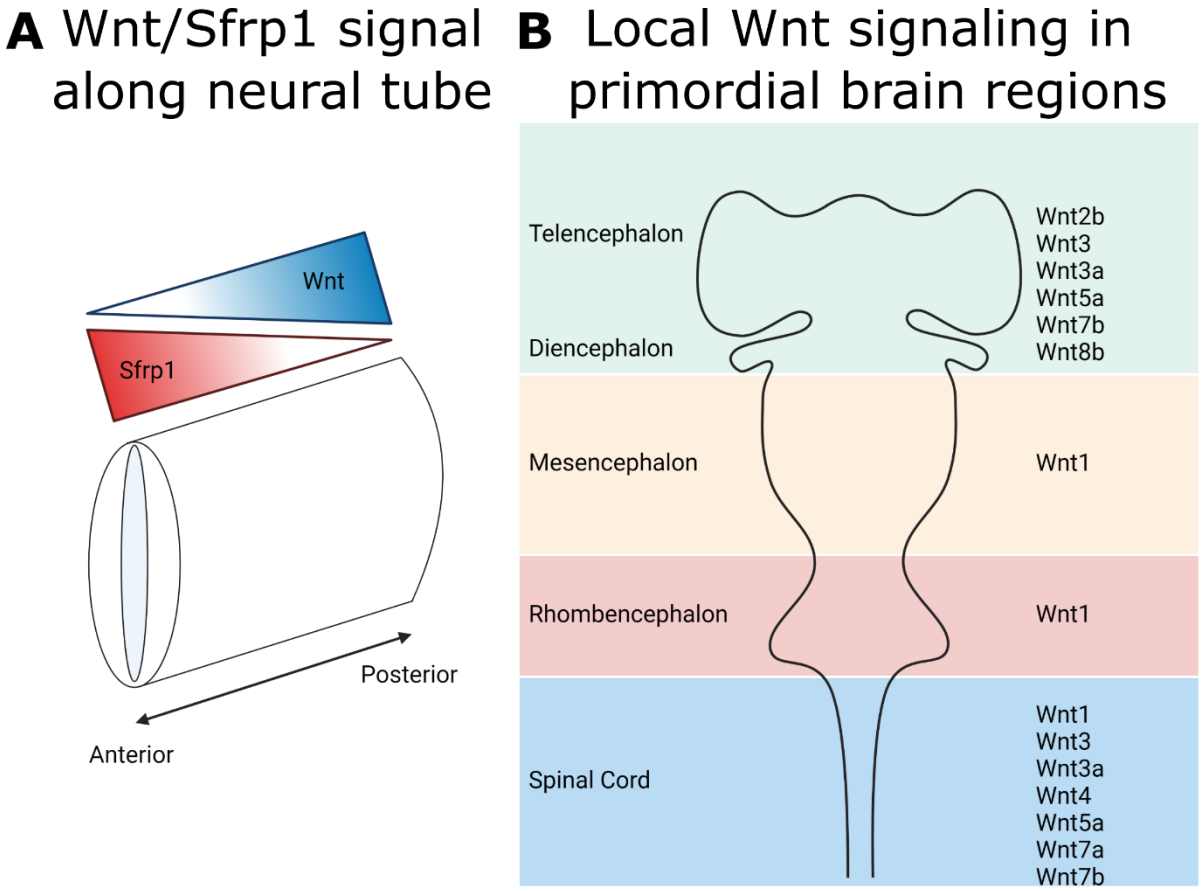

Figure 4. Physiological Wnt signaling during early polarization and regional fating events during embryonic neuralization. (A) During the formation of the nural tube, Sfrp1 and Wnt generate the anterior and posterior poles of the neural tube, respectively. Their expression is graded along the anterior-posterior axis wherein Wnt preliminarily organizes posterior structures and Sfrp1 organizes anterior structures. (B) After the neural tube has been established, primitive structures arise from which more specified cortices and brain compartments will be derived. These embryonic structures include the telencephalon, diencephalon, mesencephalon, rhombencephalon, and spinal cord. Corresponding local Wnt signals are to the right of the depicted structure. Figure adapted from Mulligan et al, 2013.

These conflicting signals give rise to the polarization events that dictate the formation of the telencephalon, diencephalon, mesencephalon, metencephalon, and spinal cord. Once these structures have been formed in the embryo, local Wnt expressions arise in the resulting structures (Figure 4B) (Mulligan & Cheyette, 2012). To derive a telencephalic identity, these signaling patterns are recapitulated starting from stem cells wherein Wnt and BMP are inhibited by small molecules to drive dorsal-anteriorization patterns observed *in vivo* (Y. Shi, Kirwan, & Livesey, 2012; Y. Shi, Kirwan, Smith, et al., 2012; Theil et al., 2002). These molecular signals, while seemingly few, are sufficient in driving neuronal fate specific to telencephalic identities representing their *in vivo* counterpart .

Aims and hypotheses

Utilizing the extensive studies established previously, this thesis sets out a novel protocol for deriving dentate gyrus neurons from hiPSCs and to incorporate an emergent and under-utilized field in *in vitro* neuroscience. Human iPSC-derived dentate gyrus neurons will be accompanied by the introduction of a new platform by which optogenetic experiments may be conducted *in vitro.* The aims and hypotheses are as follows:

Aim 1: Establish an optogenetic platform suited for stem cell-derived neurons to preliminarily assay function by electrophysiological protein markers.

> Hypothesis 1-1: If mouse ESC-derived neurons are functional, then they should demonstrate electrophysiologically active ion channels and should upregulate molecular activation pathways, like cFOS, in response to historically utilized neuronal activators. This thesis hypothesizes that ESC-derived neurons will express voltage-gated ion channels and will respond in a cFOS-dependent manner to neuronal actuators and silencers.
>
> Hypothesis 1-2: If a suitable platform for optogenetics can be constructed, then functional ESC-derived neurons should upregulate cFOS in a similar manner to those chemical actuators assessed in the

preceding hypothesis. This thesis hypothesizes that ESC-derived neurons optogenetically targeted with light-gated sodium channels will upregulate cFOS when stimulated with blue-light.

Aim 2: Establish a robust neurogenic model of the human dentate gyrus using small molecules and hiPSCs.

Hypothesis 2-1: If hiPSCs-derived cells are neuronal in nature, then they should express neuronal and telencephalic identity markers demonstrated using the same protocols published previously. This thesis hypothesizes that hiPSC-derived telencephalic-identity neurons will be able to be generated using previously established protocols and will upregulate mature neuronal markers as well as cortical identity markers at the protein and mRNA level, in particular FOXG1 and PAX6.

Hypothesis 2-2: If hiPSC-derived neurons are hippocampal in nature, then they should express markers that are associated with the hippocampus. This thesis hypothesizes that by adapting previous protocols, telencephalic identity NSCs will be fated toward a hippocampal identity and will upregulate markers associated with the hippocampus at the protein and mRNA level, in particular ZBTB20.

Aim 3: Longitudinally maintain hippocampal neural stem cell proliferation in a 2D culture to understand if and how the subgranular niche of the dentate gyrus can be recapitulated *in vitro*.

Hypothesis 3-1: If laminin substrate exerts a role in neural stem maintenance, then NSCs markers should be supported and neuronal differentiation markers suppressed in short term experiments (duration of 1 week). This thesis hypothesizes that laminin isoform 511 and simultaneous activation of Wnt will maintain NSC markers and prevent differentiation by proxy of maturing neurocytoskeleton detection over short term culture.

Hypothesis 3-2: If laminin substrate exerts a longitudinal role in neural stem maintenance within the context of the subgranular zone, then NSC markers should be maintained and neuronal differentiation markers suppressed in long term experiments (duration of several months up to 1 year). This thesis hypothesizes that laminin isoform 511 and simultaneous activation of Wnt will maintain NSC markers and prevent differentiation by proxy of maturing neurocytoskeleton detection over long term culture.

Aim 4: Demonstrate that ZBTB20 plays a sustained role in human hippocampal neurogenesis.

Hypothesis 4: If neuronal cells in the hippocampus constitutively express ZBTB20 over mammalian lifespan, then ZBTB20 must play a crucial role to hippocampal cytoarchitecture maintenance, most likely through newborn neurons in the dentate gyrus. This thesis hypothesizes that ZBTB20 will have a conserved role in cell culture and that it directly regulates the neural stem cell cycle, regardless of timepoint *in vitro*.

Aim 5: Demonstrate that neurons derived from hiPSCs fated with a dentate gyrus identity are physiologically relevant.

Hypothesis 5-1: If dentate gyrus neurons are functional, then they should exhibit physiological characteristics of neurons, like cFOS upregulation after stimulation. This thesis hypothesizes that by using the OPAL and optogenetically targeted hiPSC-derived dentate gyrus neurons, neuronal cells will upregulate cFOS in response to blue light.

Hypothesis 5-2: If dentate gyrus neurons are molecularly similar to *in vivo* dentate gyrus, then they will integrate into dentate gyrus tissue post-transplantation. This thesis hypothesize that hiPSC-derived NSCs will extend axonal processes from the dentate gyrus to synaptic targets, like the CA3, and will establish synapses with the host model.

In combining emergent techniques, this thesis overall aspires to contribute meaningful and accessible methods to advance the field of *in vitro* neuroscience.

Section I: Optogenetics and assembly of a device for optogenetic stimulation *in vitro*

CHAPTER II: Introduction to Optogenetics

Optogenetics and Electrical Signaling

Optogenetics emerged at the onset of the millennia as a novel, minimally intrusive method for functionally stimulating neurons but, thanks to fast-paced development in genetic engineering, rapidly evolved several unique avenues including neuronal inhibition, excitation of cardiomyocytes, and even serve as a novel delivery for cancer therapy. Most utilized in neuroscience is a second-generation channelrhodopsin, ChannelRhodopsin-2 (ChR2), a "blue-light" activated sodium channel. ChR2 is an inward cation channel, expressed transmembranally, and often conjugated to an optimized fluorescent reporter (Nagel et al., 2003). When exposed to a strong light source with wavelengths associated to visible blue light, ChR2 "gates" open (akin to voltage gated cation channels), allow inward cationic currents to enter the cytoplasm, and close when the blue light stimulus is absent. These characteristics are variable across channelrhodopsin species, and each has unique kinetics including onset of opening, sustainment of open conformation, and latency of closing. Minimally, optogenetics requires three essential components: a strong light source, a target cell to be modulated, and a light-activated channelrhodopsin. The target cell is genetically engineered to express the channelrhodopsin virally or by transfection, called optogenetic targeted, and becomes photocurrent activatable when the channelrhodopsin is sufficiently expressed along the cell surface. The nature of investigation dictates the model organism or system to be studied; investigations involving movement, afferent/efferent pathways, and broader cell type characterization are typically performed in *C. elegans* as the set-up requires minimal isolation and the target neurons can be stimulated; social behavior, pathologies, degeneration and more complicated cell typing rely minimally on mouse models expressing the channels in target areas though studies have been hierarchically adapted to nonhuman primate models; finally, to assess cellular behavior, molecular dynamics, or neuronal ensemble signaling in response to stimulation, an *in vitro* model is more suitable.

Emergence of Optogenetics

Typically credited to Karl Deisseroth and Edward Boyden, the birth of optogenetics, or inducing light-mediate ionic flux across cellular membrane barriers, takes place across several laboratories simultaneously including those of Stefan Herlitze, Lynn Landmesser, Hiromu Yawo, Zhuo-Hua Pan, Alexander Dizhoor, Richard Kramer, Gero Miesenbock, and Georg Nagel (Vlasits, 2016). This is not to undermine or diminish Deisseroth's and Boyden's contributions, in fact their 2005 study demonstrated that ChR2 was sufficient by itself to stimulate neurons *in vitro* and did not require supplementing retinoids or ATP to an optogenetically targeted neuron despite thorough thought experiments from other optogenetic contemporaries at the time (Sjulson, 2020). Furthermore, their publication led to the development and discovery of other light-gated channels and light-activated pumps (Wietek & Prigge, 2016). While light-activated ion channels were known to be expressed by halobacteria (Oesterhelt and Stoeckenius, 1971), algae (Hegemann et al., 1991; Kianianmomeni et al., 2009), and specific fungi (Bieszke et al., 1999) their functional expression was not introduced into animal models until 2001, wherein *Xenopus laevis* oocytes were lentivirally transduced with Chop1, the algal gene encoding for ChannelRhodopsin-1 (ChR1). When electrophysiologically recorded, optogenetically active oocytes were stimulated with blue light and an inward proton current was detected (Nagel et al., 2002). Shortly thereafter, the same group isolated Chop2, the unconjugated predecessor of ChR2 and demonstrated that while Chop1 and Chop2 were both expressed endogenously by *Chlamydomonas reinhardtii*, their photoconductivity dynamics differed significantly. Nagel et al predicted from quaternary structure analysis that ChR2 was a cation-selective channel and quantitatively demonstrated that while stimulation of ChR1 elicited proton-selective photocurrents, ChR2 instead increased membrane permissivity to larger cationic species, namely Li^+, Na^+, and to a lesser extent, larger Group I cations including K^+, Cs^+, and Rb^+. They also observed that the membrane activity was an innate channel property of ChR2, that the pore was slightly larger than voltage gated sodium channel pores, and that ChR2 behavior was cell-line and species independent as they expressed and induced nearly identical photocurrents in BHK and HEK cell lines as well as Xenopus oocytes (Nagel et al., 2003). Concurrently, Miesenbock's group developed "chARGe," a technique to selectively photostimulate vertebrate

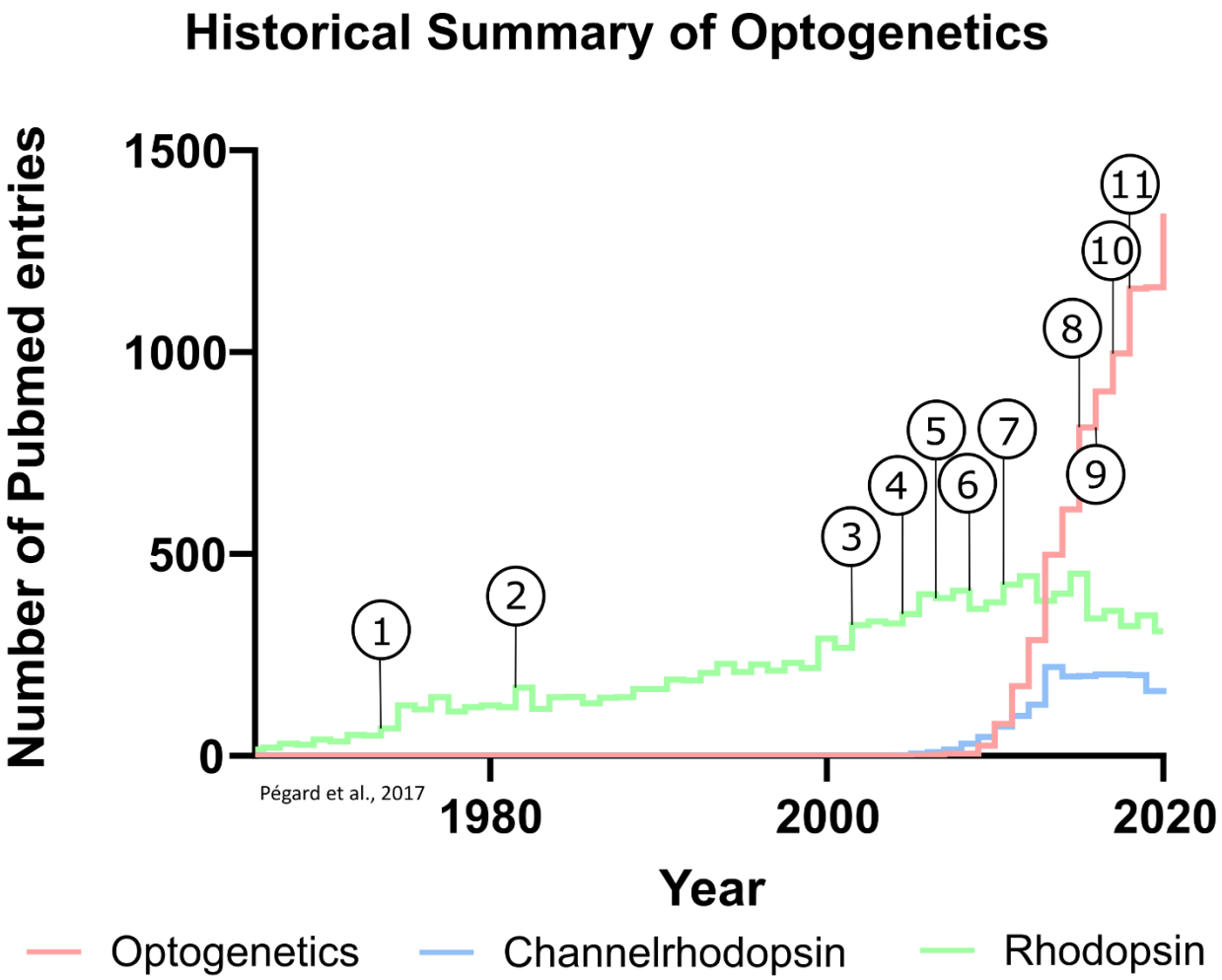

Figure 5. Graphical representation of optogenetic research growth over the past half-century. Colored steps represent a search term in the pubmed database, major events are numbered and labeled in chronological order:

1. 1971: Bacteriorhodopsin described in Oesterhelt and Stoeckenius, 1971
2. 1982: Halorhodopsin described in Schobert and Lanyi, 1982
3. 2002: Channelrhodopsin described in Nagel et al, 2002
4. 2005: Channelrhodopsin first expressed in mammalian cells in Boyden et al, 2005
5. 2007: Fiberoptic interface in freely moving mammals described
6. 2009: Optogenetic experiments in nonhuman primates
7. 2011: Chimeric construct (CheYNa in thesis) derived in Kleinogel et al, 2011
8. 2015: gTaCr1 and gTaCr2 introduced in characterized in Govorunova et al, 2015
9. 2016: Axion Lumos systems becomes commercially available as first *in vitro* platform
10. 2017: ST-ChRoME and 3D SHOT Holography are introduced in Pegard et al, 2017
11. 2018: ChrimsonR is introduced to a mouse model of retinopathy to rescue signal degeneration in Cheong et al, 2018

Run-off: ChrimsonR is introduced to human retinopathy patients for functional treatment in Sahel et al, 2021

Figure adapted from Deisseroth, 2010

neurons *ex vivo*. Transgenic expression of *Drosophila* arrestin-2, NinaE bound to retinal (blue-sensitive opsin of R1-R6 photoreceptors), and a G-protein α subunit was demonstrated to transduce a stimulatory photocurrent in primary rat hippocampal neurons when exposed to broad-spectrum light

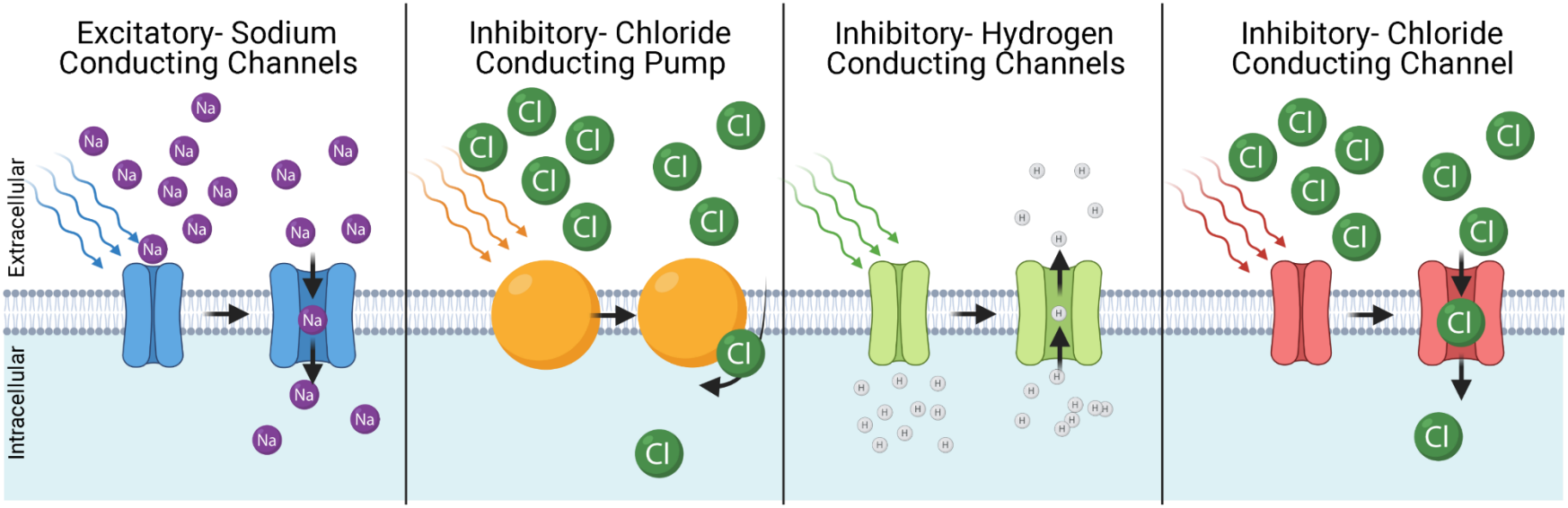

Derived from:	Variant	Description	Publication
Channelrhodopsins: cation channels from Chlamydomonas reinhardtii	ChR2	Blue light activatable gated cation channel from Chlamydomonas reinhardtii (CrChR2)	Boyden et al, 2005
	ChR2/H134	Blue light activatable, most commonly used variant with larger photocurrent compared to CrChR2	Nagel et al, 2005
	ChETA	Blue light activatable, ChR2 harboring E123T mutation, exhibits faster kinetics but reduced photocurrent amplitude	Berndt et al, 2011
	XXL	Blue light activatable, sensitive to low intensity light, prolonged tau off and delayed gate closure	Dawydow et al, 2013
	ReaChR	Red-light activatable variant of ChR2	Lin, J. et al 2013
Channelrhodopsins: cation channels from other species	VChR1	Green-light activatable channelrhodopsin from Volvox carteri	Zhang, F. et al 2008
	VChR2	Blue-light shifted Channelrhodopsin from Volvox carteri, slower kinetics than ChR2	Kianianmomeni et al, 2009
	Chronos	Green-light activatable high-speed, light-sensitive channel from Stigeoclonium helveticum	Klapoetke et al, 2014
	ST-ChRoME	Green-light activatable , high-speed, rapid reovery, light-sensitive channel from Chronos	Pégard et al, 2017
	Chrimson	Red-light activatable channel from Chlamydomonas noctigama. ChrimsonR carries K176R mutation.	Klapoetke et al, 2014
	ChrimsonR	Red-light activatable channel from Chlamydomonas noctigama carrying K176R mutation.	Klapoetke et al, 2014
	CoChR	Blue-light activatable Channelrhodopsin from Chloromonas oogama	Klapoetke et al, 2014
	MChR1	Red-light shifted channelrhodopsin from Mesostigma viride, slow kinetics	Govorunova et al, 2011
	SdChR	Blue-light activatable, derived from Scherffelia dubia	Klapoetke et al, 2014
	TsChR	Blue- and UV-light activatable channelrhodopsin, derived from Tetraselmis striata	Klapoetke et al, 2014
	CheRiff	Blue-light activatable, derived from SdChR	Hochbaum et al, 2014
Channelrhodopsins: cation channels- chimeras	ChEF	Blue-light activatable; Engineered by chimeragenesis of Chop1 transmembrane domains 1-5 and Chop2 transmembrane domains 6-7	Lin et al, 2009
	ChiEF	Blue-light activatableDerived from ChEF by I90V mutation	Lin et al, 2009
Halorhodopsins	Halo/NpHR	Orange light-activatable inward chloride pump from Natronomonas pharaonis as neuronal inhibitor, fast tau off but slow kinetics	Schobert et al, 1982
	eNpHR 3.0	Orange light-activatable NpHR with additional trafficking signal for improved membrane targeting via Kir2.1, fast tau off but slow kinetics	Gardinaru et al, 2008
Archaerhodopsins	Arch	Green light-activatable outward proton pump derived from Halorubrum sodomense	Chow et al, 2010
	ArchT	Green light-activatable outward proton pump with improved light sensitivity compared to Arch.	Han et al., 2011
	C1V1	Blue-light activatable, chimera of VChR1 transmembrane domains 1-2 and ChR1 transmembrane domains 3-7 expressing E122T and E162T mutati	(Yizhar, Fenno, Prigge, et al., 2011
Channelrhodopsins: chloride channels	ChloC	Blue-light activatable chloride-conducting channel, permissible to cations	Wietek et al 2014
	GtACR1	Green-light activatable chloride-conducting channel from Guillardia theta	Govorunova et al, 2015
	GtACR2	Blue-light activatable chloride-conducting channel from Guillardia theta	Govorunova et al, 2015

Figure 6. Classes of ChannelRhodopsins common to optogenetics. Table colors correspond to channel class and describe activating light and the source of discovery. From left to right: blue-labeled channels correspond to inward soidium channels, orange-labeled channels correspond to chloinward chloride pumps, green-labeled channels correspond to outward hydrogen channels and red-labeled channels correspond to inward chloride channels. Figure adapted from Addgene (https://www.addgene.org/guides/optogenetics/).

(Zemelman et al., 2002). This method, while seemingly preliminary to demonstrate light-mediated neuronal activity, requires exogenous retinal bathing to reconstitute metarhodopsin after photoconversion. Attempting *in vivo* experiments would imply introducing exogenous trans-retinal and sure induction of confounding side-reactions. Ultimately, Nagel et al 2002 and 2003 inspired Deisseroth's flagship paper in 2005 as Nagel gifted the ChR2 construct to Deisseroth. Deisseroth's student, Boyden, characterized the construct in rat primary hippocampal neurons thereby providing evidence that ChR2 could be expressed in mammalian systems to drive neurons at biologically relevant frequencies (Boyden et al., 2005). Simultaneously, Zhuo-Hua Pan's group expressed ChR2 longitudinally in rodentia inner retinal neurons, demonstrating several key findings including ChR2 independence from retinal, the innate ability of ChR2 to stabilize its own chromophore after multiple stimulation cycles, immutable long-term expression, and that inner retinal neurons could remain vital and functional despite photoreceptor death if stimulated via ChR2 (Bi et al., 2006). Figure 5 depicts the major events regarding optogenetic history while Figure 6 provides schematic overviews accompanied by classification of channelrhodopsins introduced in this section. Overall, these seminal studies constitute a gateway into almost limitless neuroscientific endeavors and since these highlighted publications, the field of optogenetics has expanded well beyond *Chlamydomonas reinhardtii*.

Evolution and discovery in optogenetics: stimulatory Channelrhodopsins

Channelrhodopsin-2, ChR2, refers to the Chop-2 cation protein channel, without C-terminal intracellular domain, conjugated to a reporter fluorophore, typically enhanced Green Fluorescent Protein (eGFP), or enhanced Yellow Fluorescent Protein (eYFP). Chop-2, as detailed above, consists of 7 transmembrane domains selectively permeable to cationic species attributed to AAR Glu90 (Eisenhauer et al., 2012), namely sodium (Nagel et al., 2003), and is variably sensitive to light at wavelength with ranges between 400-520 nm but peak activity between 470-490 nm. Channelrhodopsin-2's kinetics permit temporally resolute neuronal activation, faithfully reproducing photocurrent at 5 Hz (Boyden et al., 2005). Characterized in the

same investigation, ChR2's recovery time between spikes lasted ~ 5 s, averaged 10 ms pulse exposure independent of light stimulus frequency, and expressed a negatively correlated relationship between light frequency and probability of spike generation (Boyden et al., 2005). While, at the time, these recordings were unprecedented, progress central to the merging of optogenetics and neuroscience demanded improved ChR2 function.

A contemporary critique of ChR2, persists that inward sodium currents are low-fidelity as they fail to maintain consistent dynamics during reproducibility trials or frequent spike experiments; these shortcomings include extended gate-opening latency, weak photocurrent magnitude, inadvertent doublet induction, increased recovery time between open states, and inability to surpass spike trains of frequencies greater than 40Hz (Boyden et al., 2005; Ishizuka et al., 2006; Wietek & Prigge, 2016). ChR2 was additionally found to behave as a leaky inward proton pump even in the absence of light stimuli (Feldbauer et al., 2009). Arguably, these inadequacies potentially confound or influence cumulative molecular or behavioral output. In response, optogenetic discovery bifurcates: an several research groups undertook re-engineering of Chop-2's genetic motif to optimize or compensate for higher temporal resolution, lowered light intensity activation threshold, or facilitation of increased magnitude photocurrent whereas another set of research groups mined evolutionary niches yet probed for alternative, sequence-homologous light-activated cation channels.

The first optimal point mutation to ChR2's motif exchanges histidine-134 for arginine and is known as ChR2 H134R. The mutations mimics a structural motif found in bacteriorhodopsin compulsory for proton-pump activity and when present in Chop-2's code, facilitates larger photocurrent amplitude and decreases permeability to divalent cation species like Ca^{2+} in *C. elegans* neurons and HEK cells (Nagel et al., 2005). Kinetically, however, ChR2 lacks temporal sensitivity at which higher frequency action potentials can be driven. Two ChR2 variants emerged to address gating kinetics: ChEF, and ChIEF. ChEF, a chimera of the first 5 Chop-1 transmembrane domains and the sixth and seventh Chop-2 transmembrane domains, demonstrated no differences in channel kinetics compared to ChR2. Instead, mutating isoleucine-190 in ChEF's motif to valine drastically improved kinetics and resulted in a channelrhodopsin capable of mediating reliable spike trains

upward of 50 Hz (Lin et al., 2009). Though surpassing the gamma frequency threshold delimited ChR2 constraints, a host of disadvantages persisted as did the exigency for driving neurons at potentiation frequencies.

Another AAR, E123, in ChR2's motif provided the solution for unwanted doublets and generating faster spike trains by mutation to tyrosine. ChETA, the mutated ChR2 E123T variant, would enhance channel opening and closing kinetics in response to nanosecond light pulses. Both frequency threshold and probability of spiking increased up to 100Hz in response to light pulses greater than 2 ms in width (Gunaydin et al., 2010). However, ChETA's mutation blunted photocurrent magnitude by desensitization to light source intensity thereby decreasing the probability of successful spikes, indicated by Gunaydin et al, 2010's results when ChETA is exposed to narrower light pulse widths (1 ms). Where frequency of photocurrent induction was improved, risk of long-term cell exposure to powerful blue-green light sources and photon scattering increased due to ChETA's light exposure requirements. Subsequently, a modification study rectified ChETA's light sensitivity with a second AAR mutation and comparatively analyzed single-component and double mutants. Tyrosine-159 was mutated to cysteine in ChR2 and ChETA motif to understand the individual residue's role in ChR2's dynamics; where the single mutant ChR2 T159C increased latency of response and decreased sensitivity in comparison to wild type ChR2, the double mutant, E123T/T159C demonstrated accelerated kinetics compared to ChETA and, to an extent, rectified the compromise between photocurrent amplitude and velocity of activation (Berndt et al., 2011). The authors note, however, that light sensitivity is only increased in the T159C single mutation variant and that the double mutant is not activatable in response to low-light intensity.

One ChR2, Channelrhodopsin-2 extra high expression and long open state (ChR2-XXL), exhibits increased sensitivity to low-intensity stimulus by mutation of aspartic acid-159 to cysteine by prolonging ChR2's open conformation; however, due to its elongated open state, ChR2-XXL's utility ends with low frequency stimulation (Dawydow et al., 2014). Two robust, blue-light neuronal actuators were published alongside ChR2-XXL in 2014, CoChR (Klapoetke et al., 2014) and CheRiff (Hochbaum et al., 2014). CoChR, a channelrhodopsin isolated from *Chloromonas oogama*, was observed to generate photocurrents six times greater in magnitude

than ChR2, independent of fluorescent reporter expression. CoChR further exhibits rapid activation onset kinetics, reliable probability of peak current generation during train stimuli, but slow τ_{off} kinetics; because its closing is markedly delayed from ChR2, it is most likely overshadowed in the publication by its sister discovery, Chronos (Klapoetke et al., 2014). By co-expression with red-light activated channelrhodopsin, ChRimson, CoChR proves instrumental in generating signal gradients to elucidate discreet neuronal signaling patterns in motor sensory neurons in *C. elegans* (Schild & Glauser, 2015). In hiPSC-derived neurons, CheRiff and an archaerhodopsin-based voltage sensor were co-expressed in a single plasmid to establish an electrophysiological imaging tool. Stimulation of *Scherffelia dubia* channelrhodopsin (SdChR) by blue laser generated previously unobserved photocurrents (>2 nA at 500 mW/mm^2) though exhibited robust activation to far-red light sources as well. Inclusion of Kir2.1 membrane signal and point mutation of glutamate-154 to alanine absolved red-light activation and decreased gate-closing latency (Hochbaum et al., 2014). The same group continued to pursue "Optopatch" *in vivo* and generated a Cre-dependent mouse model to characterize variegated cell types (Lou et al., 2016) and utilized it to identify a previously unknown mutation to SOD1 in ALS patient-derived hiPSC-derived neurons (Kiskinis et al., 2018).

Despite ChR2's pitfalls, it persists in neuroscience studies as an immeasurably useful tool and ultimately, if utilizing ChR2, variant-dependent idiosyncrasies can be paradigmatically compensated or emphasized; not every ChR2 variant is right for every experiment, but the nature of the experiment can guide the appropriateness in selecting and applying ChR2.

Advances in SNP engineering of ChR2 dynamics were accompanied by investigations into red-shifted cationic channels to accommodate a broader range of light sources, increase compatibility between co-expressed chromophores or conjugated fluorophores in concurrent systems, and to minimize both potential biological damage and photon scattering induced by blue light lasers. Red-shifted channel development less convoluted than its blue-shifted counterpart and the race for neuronal applicability though pioneers in the field remain at the emergent-publication forefront. Deisseroth's group discovered and characterized a spectrally shifted, light-gated cationic-permissible protein channel similar in activity to ChR2 but with slower dynamics.

Derived from *Volvox carteri*, this channelrhodopsin was named "VChR1" and was published under a pseudonymous title claiming that its nature was stimulable by wavelengths in the red spectrum (F. Zhang et al., 2008). However, the abstract elucidates that VChR1 is in fact "yellow-shifted" while the data suggest instead that VChR1 is green-shifted in that it is optimally activated by 525 nm wavelength light and only exhibits ~20% of peak cationic influx activity when stimulated by 580 nm wavelength light. Despite misleading publication headlines, several groups expounded on this work and either optimized VChR1 for truer red-shift activation or sought new opsin channels altogether. Though a second *Volvox*-derived channelrhodopsin, VChR2, was discovered and analogized to *Chlamydonas*-derived ChR2 (Kianianmomeni et al., 2009), its chromophore was characterized as sensitive to blue-shifted wavelengths. Another group demonstrated attempted to demonstrate that *Mesostigma viride*, a flagellated species of algae, exploited a "red-shifted" cation channel, MChR1 to undergo flagella-mediated motility. Like Zhang et al 2008, however, MChR1 was more optimally activated at 525 nm and exhibited reduced activation probability when exposed to longer wavelengths (Govorunova et al., 2011). Progress toward red-light activated cation channels would not converge upon red-light activation until the genetic manipulation of VChR1 to give two distinct channelrhodopsins: C1V1 and red-activatable channelrhodopsin (ReaChR).

To access the medial prefrontal cortex and modulate excitatory-inhibitory balance during social behavior tasks, a red-shifted channelrhodopsin was necessary to decrease blue photon scattering, leading to C1V1. Generation of C1V1 hearkens to ChEF/ChIEF's generation, in that C1V1 is chimeric and consists of the first two transmembrane helices of VChR1 and the last five of ChR1, fused at tryptophan-163 of ChR1. Electrophysiological characterization of C1V1 indicated that while ion selectivity was similar to ChR2 and its photocurrents exceeded 1000 pA, on average, its onset and offset were delayed by greater than 100 ms (Yizhar, Fenno, Prigge, et al., 2011). Conclusive results regarding excitatory/inhibitory imbalance were obtained, however, C1V1's *in* vivo activity was dependent on coexpression of a step-function opsin. Its nucleotide structure would serve as the template for ReaChR. Though several mutative steps were required to reach ReaChR, Lin et al demonstrated ReaChR as an inward cation channel optimally activated at ~590 nm with

increased membrane expression and increased photocurrent SNR 4-fold and 16-fold when stimulated with a 590 nm laser and compared to VChR1 and C1V1, respectively (Lin et al., 2013). ReaChR's activation, though still not entirely responsive to monochromatic red-light, was later demonstrated as restorative to retinal cell function *in vivo* in mouse and *ex vivo* in macaque and human while decreasing cell damage otherwise facilitated by blue-wavelength laser (Sengupta et al., 2016).

Transcriptomic mining of various algae species revealed a host of light-activated cation channels including previously undiscovered red-shifted channelrhodopsin from *Chlamydomonas noctigama*, CnChR1 or ChRimson. Electrophysiological characterization established its spectral peak at ~590 nm but still robustly activatable at ~660 nm in mouse primary hippocampal neuron cultures. ChRimson's structure was further optimized by the SNP K176R to enhance channel kinetics, increasing stimulation rates to a 20 Hz threshold or decreasing tau-off time by ~5 ms, and most notably, retained activity at ~725 nm wavelength (Klapoetke et al., 2014). ReaChR's inferior dynamics and spectral sensitivity compared to ChRimsonR, however, ceded modeling and application to ChRimsonR; the optimized channelrhodopsin was functionally demonstrated and integrated throughout models of human retinal organoids (Garita-hernandez et al., 2018), zebrafish (Antinucci et al., 2020; Förster et al., 2017), and a parallel study to Sengupta et al, 2016 demonstrating photocurrent-mediated rescue of retinal cells in a degenerative photoreceptor model (Cheong et al., 2018). Despite emergent holographic stimulation techniques suggesting attenuation of kinetic independence between ReaChR and ChRimsonR (I. W. Chen et al., 2019), ChRimsonR's co-applicability with other popular fluorophores, like GcAMP-6 (Cheong et al., 2018) and its further optimization in conjunction with holographic stimulation techniques (Pégard et al., 2017) may provide a robust and reliable tool in multi-fluorophore/chromophore expressing models.

One of the latest modified channelrhodopsin structure accompanied a technological advancement in high-fidelity stimulation of multi neuron ensembles. ChRoME is a somatically expressed variant of Chronos, a green-shifted variant of channelrhodopsin which already boasts high response fidelity and the most rapid recorded gating dynamics (Klapoetke et al., 2014). The modification to Chronos adds a somatic messenger signal to augment and concentrate somatic inward sodium currents thereby increasing the probability of action

potential induction via proximity to axon hillock, called ST-Chronos. A mutation to ST-Chronos, methionine-140 to glutamate, increases cationic transmembrane flux due to the negative charge glutamate exerts in a water-shielded pore (Mardinly et al., 2018). ST-ChRoME was adapted for novel stimulation by 3D-SHOT holography, a light scattering technique which permits precise volumetric light columns to stimulate optogenetically enabled neurons (Pégard et al., 2017). Dual application of ChRoME and 3D-SHOT remain at the forefront of optogenetic stimulation as their concatenated use has been demonstrated to be capable of activating up to 50 neurons in a single ensemble with one pulse of stimulus. Though yet novel, dual application of ST-ChRoME and 3D-SHOT holography has the potential to become the standard for studying photoinduced network activity, especially within the context of behavior, memory, and learning, as single units are not singularly responsible for these large-scale, ultra-processing phenomena.

Neuronally inhibitive Channelrhodopsins

Neurons endogenously conduct electrical currents by inward voltage gated sodium channel and outward voltage gated potassium channels. Though early optogenetic constructs were able to artificially induce sodium channel activation via photocurrent stimulation, light-mediated hyperpolarization became an obvious ad subsequent demand for neuroscientists. Hyperpolarization is endogenously mediated by an array inward potassium channels whose expression is cell-type- and compartmentally dependent. Potassium, a cationic species, is similar in size and quantum charge to sodium and, consequentially, already known to be permissible through Chop species (Nagel et al., 2003). This characteristic of channelrhodopsins implies that if an inward channel is permeable to cations of potassium's size or smaller, then cationic sodium would enter if the hypothetical gate were open, potentially negating any hyperpolarizing effect inward potassium could have (Eventually, a light-activatable potassium channel, HyLighter, would emerge, however, akin to the chimeric nature of chARGE but was introduced after several inhibitory pump publications (Janovjak et al., 2010). The incorporation of optogenetic tools tends to avoid these fabricated chimeras and preferentially utilizes evolutionarily derived channelrhodopsins.). Consequently, deriving a light-gated inward potassium channel or

discovering an evolved potassium-exclusive channel would prove problematic. Instead, interrogation of aquatic, photosynthetic prokaryotic and simple eukaryotic candidates would shine a light on *Natronomonas pharaonis*, a haloalkyphilic archaeon expressing a unique chloride pump. Characterized two decades prior to its first expression in mammalian neurons, *Natronomonas pharaonis*'s chloride pump, halorhodpsin, was observed to actively increase halorhodopsin-expressing vesicle volume in response to broad-spectrum light (Schobert & Lanyi, 1982). To recapitulate action potential cycles reliably and precisely, *Natronomonas pharaonic* halorhodopsin (NpHR) was more critically assayed and characterized in *Xenopus laevis* oocytes against *Halobacterium salinarum* halorhodopsin (HsHR). Despite their equivocal dynamics, HsHR was omitted as its peak activation spectrum overlapped with that of ChR2 as opposed to NpHR, whose peak activation occurs at ~590 nm. NpHR, once suitable for mammalian expression, was shown to suppress closely timed spikes in primary rat hippocampal neurons at 200 pA step injections, though its temporal dynamics were shown as much more delayed than ChR2 (t_{on} ~= 26 ms, t_{off} ~= 26 ms). Despite its latency in activation cycle, NpHR was elaborately utilized *in vitro* to demonstrate its coexpression with ChR2, its facilitation of action potentials generated by ChR2 activation, and the possibility to control firing of dual-expressing neurons *in vivo* (F. Zhang et al., 2007). NpHR was prone to aggregation and thus its activation and cellular expression was unreliable. Re-engineering the NpHR, enhanced NpHR (eNpHR), with the N-terminus of Chop-2 would inhibit aggregation and subsequently augment the cellular depolarization magnitude two-fold (Gradinaru et al., 2008). Suppressing neuronal action potentials by chloride photocurrents, however, would not serve as the singular avenue for inhibitory optogenetics.

As several ionic species are conducive to eliciting stimulatory photocurrents in neurons, so too are they inhibited by several ionic species. Bacteriorhodopsins (Oesterhelt & Stoeckenius, 1971), a family of light-activatable proton pumps, were discovered across several species of *Halorubrum*, including archaerhodopsins-1 (Mukohata et al., 1988), -2 (Uegaki et al., 1991), and -3 (Ihara et al., 1999) as well as opsins from *Haloarcula*, called cruxrhodopsins (Chan et al., 2014; Sugiyama et al., 1994). Archaerhodpsin-3 (Arch) however served as the template bacteriorhodopsin for optogenetically silencing neurons as it was demonstrated functional in

subduing endogenous sodium currents compared to other microbial opsins (Chow et al., 2010). When exposed to monochromatic yellow light, Arch has the capability to suppress currents approaching 900 pA with a spike-silencing probability 2-fold greater than NpHR at various illumination strengths; moreover, Arch autonomously recovers post activation as opposed to NpHR. In the same paper, Chow et al, 2010, the researchers characterize a second, blue-green light activatable proton pump derived from the fungus *Leptosphaeria maculans*, called Mac. While Mac has been demonstrated as inhibitive with comparable dynamics to NpHR, its utility is limited within the literature as its dynamics seems overshadowed by Arch (Chow et al., 2010). Indeed, though Mac has been utilized in *C. elegans* models for circuit mapping investigation (Husson et al., 2012), Mac's involvement in any neuroscientific study abruptly ends with Husson et al. 2012. Arch's application, on the other hand, is latently sustained, first by SNP optimization of Arch to ArchT for improved dynamics (Han et al., 2011) and second by Boyden's persistent integration of optimized ArchT in mammalian circuitry modeling studies (Rueckeman et al., 2016). Ultimately, however, Archaerhodopsin-3 has yielded its potential in neurobiological research instead to voltage-gated sensing and finds greater utility in detecting voltage-dependent neurocytosolic pH changes (Flytzanis et al., 2014) possibly as a result of a review detailing rhodopsins' preferential efficiency in voltage sensing (Looger, 2012). Furthermore, inhibitory photocurrents mediated by anion and proton pumps are proportionally stoichiometric in activation wherein one photon absorbed permits one ionic species to transgress the membrane. While the utility and dynamics of inhibitory channelrhodopsins seem underwhelming in comparison to their stimulatory counterparts, an emergent inhibitory channel protein offers a drastically improved alternative to inhibitory neurobiological study.

Per the theme of optogenetic tool development, anionic channelrhodopsins were discovered in species evolutionarily primed toward phototaxis. Anionic channelrhodopsins 1 and 2 (ACR1, ACR2, respectively) were screened from the nuclear genome of a flagellate cryptophmonadic algae, *Guillardia theta*. Where all cationic channelrhodopsins are derived from chlorophytic species, ACR1 and ACR2 seem to be the earliest demonstrated cryptophytic-derived channelrhodopsins. GtACR1 and GtACR2 are comprised of 7 transmembrane domains, express peak activation wavelengths at 515 nm and 470 nm, respectively, and are

exclusively permissible to anionic species smaller than SO_4^{-2} and therefore mimic neuronal chloride channels (Govorunova et al., 2015). When comparatively assessed against and a modified channelrhodopsin permissible to chloride anions, ChloC (Wietek et al., 2014), GtACR's activation sensitivity was reported as ~10 times greater than that of either Arch or ChloC (3.7 nA [GtACR2] vs ~0.4 nA [ChloC/Arch] photocurrent at 10 mW/mm^2), fully suppressed neuronal spiking in rat primary hippocampal neurons at 0.005 mW/mm^2, and whose temporal dynamics are exponentially faster (tau onset = 0.04 s, tau off = 2.4 s). Though Govorunova et al 2015 experimentally emphasizes GtACR2, both GtACR isoforms hold enormous potential for inhibitory photocurrents as their functionality improves photocurrent activation sensitivity providing a robust and fidelitous avenue for optogenetically silencing neurons.

The realm of optogenetics is seemingly limitless in application and activatable spectra. However, channelrhodopsin activation interestingly occurs within the confines of the visible spectrum. Presently, no utile channelrhodopsins exclusively activated by ultraviolet or infrared wavelengths exist. Arguably, a channelrhodopsin derived from *Tetraselmis striata*, TsChR, has a peak activation is ~430 nm and an activation tail sensitive to UV light (Klapoetke et al., 2014). Likewise, while ChRimson and ChRimsonR have been demonstrated as sensitive to IR frequencies (Klapoetke et al., 2014), no investigation has uncovered an IR-specific channelrhodopsin. One group claims to perform Near IR stimulation in deep tissues, however, this protocol relies lanthanide nanoparticles to "up-convert" NIR frequencies to higher frequency photons after whose ejection stimulates ChR2 (Hososhima et al., 2015).

Chimeric multiplexed channelrhodopsins

The discoveries and engineering of novel channelrhodopsins have not been limited to altering kinetics, current dynamics, ionic transport, and activation wavelength shift. Several groups have attempted dimerizing and even trimerizing individual channelrhodopsins. While the pan-spectra activatable "white-opsin," a trimeric construct comprised of red-, green-, and blue-light activatable ChR2 variants in series, frivolously fails to

address research needs (Batabyal et al., 2015), other chimeras offer practicality by recapitulating a naturally occurring action potential. A longstanding criticism of ChR2 is that its overexpression contributes to an imbalance between sodium-channels and endogenous potassium channels thereby compromising the innate activity of the genetically altered neuron. Furthermore, it well understood that because of this imbalance, ChR2 activation does not consistently induce action potentials in the presence of blue light stimuli as endogenous inward rectifying currents may not compensate quickly enough to repolarize the neuron. Aside from optimized ChR2 variants, some listed prior, two sects of chimerization have been introduced to address the inequity of stimulations of single neurons by ChR2. The first approach conjugates ChR2 to an unaltered potassium channel cassette, though its use is sparse and the expression of distinct potassium channels potentially confounding depending on cell type. A more controllable option for stoichiometric expression instead was designed earlier than the ChR2-Venus-VGKC2.1 and conjugates ChR2 H134R to eNpHR or bR (Kleinlogel et al., 2011). When illuminated by alternating laser pulses in wavelengths of 470 nm and 580 nm more reliable depolarization and repolarization phases could be induced within a patched CA3 pyramidal neuron. Despite scrutiny against inward proton pumps and its induction of cytoplasmic acidification, it stands to reason that utilizing chimeric constructs which dually express stimulatory and inhibitive channels may improve the fidelity of neuronal firing. This would further facilitate the integrity of endogenous firing pattern behavior in a neuron and offer optimized avenues by which sophisticated input signals could be studied within single cells and neuronal ensembles.

Optogenetic approaches for in vivo and in vitro neuronal stimulation

Techniques and methods to stimulate optogenetically targeted neurons *in vivo* has experienced a paramount of growth and development from targeting since sole use of external laser. These techniques have evolved through fiber optic implant for free movement, past dual optic modules in single, and into manipulating holography and virtual energy states to stimulate nonrandom ensembles of neuronal colonies reliably, precisely, and volumetrically. Named three-dimensional scanless holographic optogenetics with

temporal focusing (3D-SHOT), holographically stimulating neurons was shown to scatter light in a controlled, precision, and replicable manner that simultaneously homogenizes power distribution curve and maintains photocurrent amplitude. By reducing tissue induced axial aberrations and optimizing volumetric scattering, neurons of sequential layers may be more reliably stimulated without affecting neighboring layers or orthogonal ensembles within its offered micrometric confines (Pégard et al., 2017). As rapidly as channelrhodopsins evolved, so did methods for *in vivo* stimulation.

Despite accelerated revolutions in animal model optogenetic techniques, cell culture optogenetic simulation falls short and consequentially underutilized. Axion biosystems made commercially available the first patented device intended for *in vitro* optogenetic stimulation. The device, "Lumos," allegedly provides LED-mediated stimulation in up to 96 individual wells, allows 4 different spectra to support activation of virtually any channelrhodopsin, hosts its own temperature-controlled incubation chamber, and is programmable to allow varied stimulation paradigms in independent wells. Furthermore, Axion markets the Lumos as compatible with their multi-electrode array (MEA) technology "Maestro" and that large, multiplexed matrices of electrophysiological, extracellular media, immunocytodetection, and nucleotide/protein extraction data are possible to simultaneously acquire in one experiment. Despite its wide applicability and efficiency in data-generation, since its commercial release it has only been cited in three peer-reviewed articles, one of which include its own validation studies alongside a chapter citation (Elena et al., 2016; Millard et al., 2017), one pharmaceutical study investigating polyarrhythmic side-effects of a subset of small molecules , and one neuronal study providing inconclusive results when attempting to improve peripheral nerve regrowth with electrical activity (McGregor et al., 2019). While this study expected inconclusive results based on the BDNF V66M mutation as a dependent variable of impeding activity-mediated nerve regrowth, the lack of positive demonstrable utility of Axion's Lumos system in *in vitro* neuronal cultures is discouraging. Notwithstanding the inconsistent citation in literature, Axion's system does not seem to be well suited for central nervous system *in vitro* applications as several key features either seem misleading or are completely absent from its design as well. First, the isolated chamber lacks a CO_2 inlet which discourages the user from performing longitudinal or

continuous experiments. Second, the LEDs are mounted above sample wells and with dead space between the LEDs and the culture plate cover. This implies several malfeasances in light delivery including radial decay of light intensity during the distance of light trajectory, several refraction indices changes (see Figure) which risks random scattering and augmented intensity decay, and non-isolated LEDs to individual wells further risking random scattering and incidental crosstalk between target wells. Furthermore, the 192 LEDs are 48 of each blue, red, orange, and green and indicate that 96 wells could in fact not be targeted individually and uniquely as at least 2 wells would share one LED. When inquired about the software, Axion could not demonstrate that customizable frequencies were possible nor that the software was accessible to the user to hard code new stimulation frequency paradigms. Finally, the Lumos system alone comes at an estimated 22.500,00 EUR not including the set-up and demonstration fee (~5.000,00 EUR) and one-time use culture plates (~350,00 EUR/10 plates). For a typical laboratory, this price is discouraging considering the lack of experimental freedoms and absence of prior studies citing the technique.

Alternatively, an open-source platform intended for photobiological applications was introduced the same year and addressed several of Lumos' critical drawbacks. The platform was designed where the LEDs illuminate cell cultures from the underside of the well, decreasing both the distance traveled by light and minimizing the total changes between refractive indices. LEDs could also be changed manually to allow dual-chromatic cisphasic or contraphasic stimulation and the researchers assessed more than one hundred uniquely manufactured LEDs including UV and IR specialized modules. Furthermore, the LED chambers were optimized to increase light exposure surface area and were optically separate from neighboring chambers, eliminating the possibility of cross-well interference. The platform was adapted to cell culture incubators and the total volume occupies ~15 cm x 10 cm x 20 cm, can be securely and semi-permanently attached to the incubator shelf-grid for security, and tens of units can be powered in series to perform multiple experiments/replicates in parallel. All components and hardware could be easily and ergonomically obtained, assembled, and used, estimated at a cost of ~200,00 USD for three platforms in total. Finally, the accompanying software is claimed to be editable and enables true well-paradigm independence in a P24 well plate (Gerhardt et al., 2016).

Likewise, and more recently, an updated iteration of under-well optogenetic stimulation has been developed in the literature, boasting higher frequency of stimulation between independent wells and a larger capability for its stimulation matrix. This increase in power is in part delivered by a significantly more powerful microprocessor, like that used in Axion Biosystem's. Subsequently, the increase in computing power demands an increase in input voltage and contrives a problem previously unseen in prior art, the need to autonomously cool the stimulation system. Ultimately this renders an otherwise compact device bulky with heat sink material and with the need for increase wattage, introduces cables to the incubator system.

While this and a handful of other microprocessor-based platforms for photobiology exist, none have become utilized to a broad extent in terms of reliability, access, and neurobiological application. Withal, the application of the open-source platform is significantly more constrained than its authors deemed: the software is not truly editable and only allows light intensity fluctuation in terms of waveform (i.e., square vs triangle vs sinusoidal), all 24 wells are all concatenated, and the "independence" arises from a temporal offset. Finally, most of the components listed are outdated or retired including the internal memory card upon which experimental light patterns are installed. Overall, in comparison to *in vivo* apparatuses, the availability and performance scope for *in vitro* optogenetic stimulation platforms are underwhelmingly limited, posing an inconvenient obstacle for studying electrical activity-mediated phenomena in cell cultures. An *in vitro* device intended for optogenetic experiments must mirror the extensiveness of optogenetic capabilities, biological relevance, and paradigmatic needs of the researcher.

I thus undertook first establishing a device which can be ergonomically built and is suited for already established cell culture laboratories to optogenetically stimulate neurons *in vitro*. This was accomplished by 3D printing a housing unit upon which a microprocessor, 24 RGB LEDs, and an internally battery were housed and assayed for spectral qualities. Optogenetically expressing mouse ESC-derived neurons were further demonstrated to serve as a robust model to assay physiological activation via cFOS expression after light exposure and offered further insight into the potential of stoichiometrically co-expressing excitatory and inhibitory channelrhodopsins.

CHAPTER III: Construction and validation of OPAL: an *in vitro* Optogenetics Platform for Adaptable Light-paradigms (Methods)

OPAL design

Utilizing a 3D vector graphic software (Google SketchUp), a housing unit was designed in two pieces to minimize complicated printing and lengthy assembly time but still maintain accessibility to the circuitry post-assembly. The first piece, the LED platform grid (Figure 7A-B) is a simple, rectangular plate which houses 24 LED units (WS2812B). Conversely, the housing unit (Figure 7C-F) is more complicated as it securely contains the circuitry. The housing itself is 138mmx96mmx40mm (lwh), is thus compact, and has been inscribed with OPAL on the side (Figure 7C). From the top (Figure 7D-F) it is possible to view the breadboard partition (L-shape), a design to securely fasten a half-breadboard, and the LED platform support rail, the rectangular outline circumventing the interior of the upper rim. The design includes an access port face (Figure 7E-F) that includes three access ports: (left to right, Figure 7G) the micro-USB port (elliptical rectangle), the 5V-phono jack port (circle), and the USB-B male port (rectangle). These are oriented proximally to the intended breadboard location (Figure 7E-F) to optimize wire length. The OPAL inscription further serves to orientate the access ports with respect to the breadboard (Figure 7H).

Though the dimensions are recorded automatically within the software and object files, they have been measured and provisionally recorded in Table 1 or alternatively with more complicated dimensions to describe orientations on the port access face, in Figure 7G. The circuitry itself was designed and theoretically confirmed using practical circuitry drawing software (Fritzing, Figure 8A). Each hardware component is labeled using red Arabic numerals and indicated by black lines. The red numerals correspond to their make and vendor (Table 2), of which most are generic and can be acquired from any microelectronics supplier or starter kit, apart from the microprocessor, voltage regulator, and piezo speaker. Hardware can also be allocated to their pin position on the breadboard (Table 3) except for the LEDs, which are instead connected to the wire terminals (ground, +5V) or by extension wire to pins J8-J11 (data), and the 9V adaptor which is directly connected to the

voltage regulator (explicit connections listed in Table 3). The circuitry diagrams have been provided for the wiring of the LEDs (Figure 8B), the capacitor (Figure 8C) and the voltage regulator in series with a 9V batter (Figure 8D) to provide further schematic detail of the most complicated components of the circuitry.

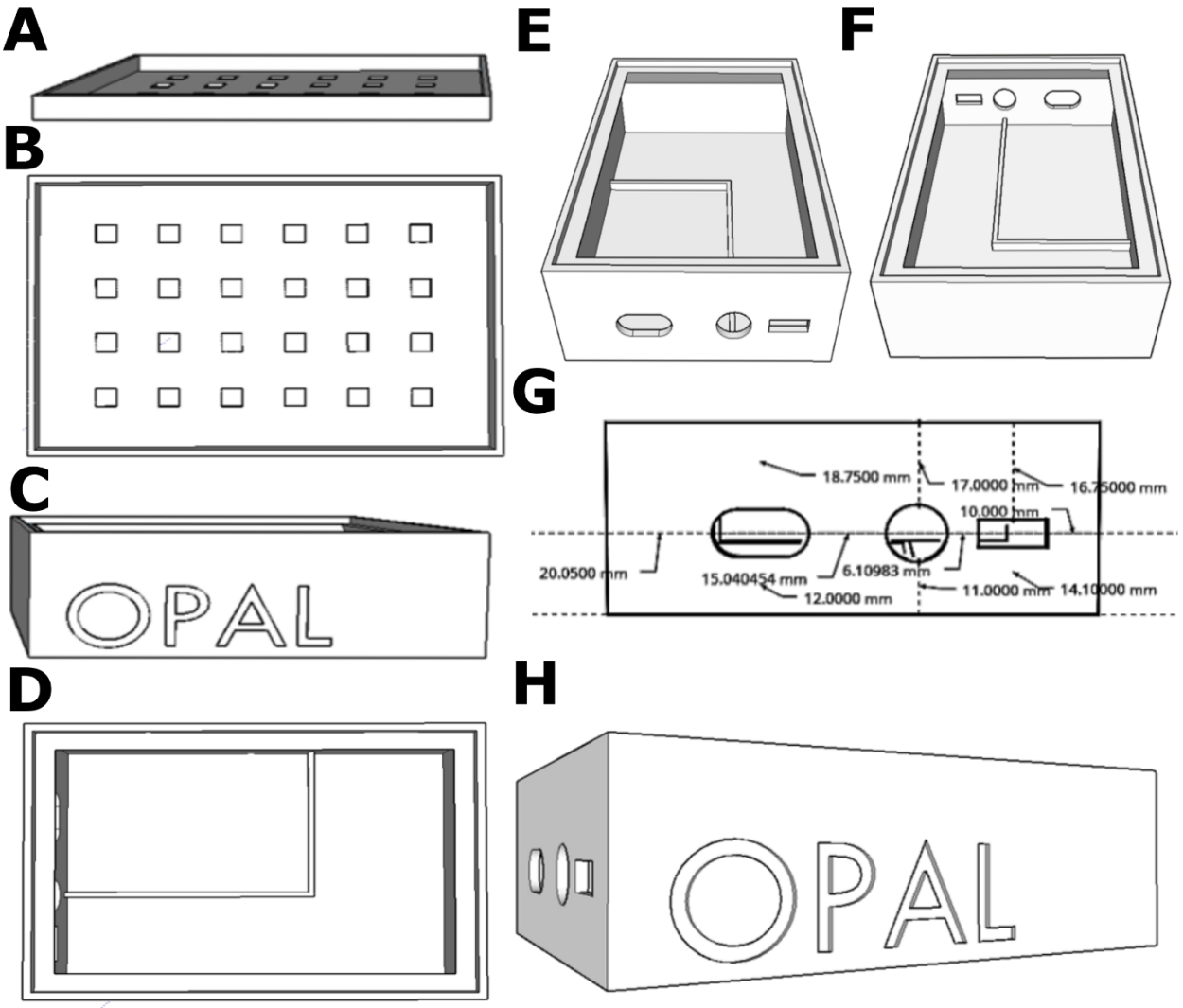

Figure 7. Three-dimensional rendering of the OPAL housing and the LED grid platform. (A) side view of platform; (B) top view of platform exposing LED ports; (C) side view of the lower housing chamber; (D) top view of the lower housing chamber, breadboard partition, and platform support rail; (E) orientation of the access port with respect to breadboard partition (F) reverse-orientation of the access port with respect to breadboard partition; (G) Positions and dimensions of the access ports, from left to right: microcontroller access port, 5V input jack port, USB-B port; dimensions are included in the .obj files; (H) orientation of the access port with respect to the OPAL inscription. All dimensions are included Table 1 as well as the .obj file. Renderings made in Google SketchUp.

OPAL Housing Dimensions

Platform Grid	mm	Housing	mm	USB-A port	mm
Outer perimeter length	132	Length	138	Length	13.5
Inner perimeter length	128	Width	96	Width	5.8
Outer perimeter width	90	Height	40	Thickness	2.5
Inner perimeter width	86	Platform partition		5V plug port (diameter)	12
Outer height	7.5	Length	133	USB-B port (microcontroller access)	
Inner height	6	Width	91	Rectangular length	9
Platform thickness	1.5	Height	3	Rectangular width	10
lip width	4	Platform support rail		Arc radius	5
LED port		Outer Length	133	Breadboard Partition	
Length	6	Inner Length	121	Outer Length	87
Width	6	Outer Width	91	Inner Length	85
Height	1.5	Inner Width	79	Outer width	59
Distance between ports (length-wise)	12	Slope of support wall	11.66194	Inner Width	57
Distance between ports (width-wise)	12	Inner wall height (pre slope)	27	Height	4
Distance from wall (length-wise)	13		Radial degrees		
Distance from wall (width-wise)	16	Slope of support wall	~31		

Table 1. Dimensions of OPAL housing. Each housing piece has been measured such that the dimensions are accurately recorded and are capable of being corroborated with the object files included or scaled up/down as necessary. The platform grid itself refers to the diagrams in Fig 1 and includes inner and outer perimeters separated by the "lip" or small 3D wall which circumvents the perimeter. Furthermore, all 24 LED ports are identical in dimensions and their orientation on the grid is symmetrical. Likewise, the housing dimensions are representative of the diagrams in Fig. 1 and include the exterior measurements and breadboard partition measurements as well as the measurements for the "support rail," the support on which the platform grid rests. It should be noted that the support rail circumvents the interior and is sunk with respect to the housing wall thus creating a loose bevel with the platform grid when assembled. The support rail is also printed triangularly with its hypotenuse facing inwardly and at a slope 31^{O}. Finally, the dimensions of access ports on the port face found in Fig. 1E and viii can be found here. Their orientations with respect to the face are instead listed in Fig1a.viii. All dimensions recorded using Google SketchUp.

OPAL assembly

In line with ease of accessibility, I have provided a schematic by which assembly does not require niche hardware and that the housing itself can be printed as two pieces. Once completed printing, allow to cure at room temperature overnight or if using a different composite, as suggested by the manufacturers' advice. To assemble, it is first necessary to attach the LEDs to the upper stage grid (Figure 9A-B). Alignment arrows are manufacturer-provided and should be aligned in the same orientation to support correct current flow. Each

OPAL Circuitry Components

Diagram Number	Part	Quantity	Product Number	Manufacturer
1	LED	24	WS2812B	Adafruit
2	Piezo speaker	1	PKM22EPP-40S1-B0	Murata
3	Half-breadboard	1	Generic	Supplied by Adafruit (Product id:64)
4	Battery power switch	1	Generic	
5	LED grid switch	1	Generic	
6	Voltage regulator	1	LM2596	Texas Instrument
7	1000 mF capacitor	1	Generic	
8	Screw terminals	2	Generic	
9	USB-B Female Port	1	Generic	
10	5V input port	1	Generic	
11	USB to serial chip CH340	1	CH340	WCH
12	Wire pin adapters	4	Generic	
13	9V input	1	Generic	

Table 2. List of circuitry hardware and their manufacturer. If listed as generic, these pieces are available in Arduino/Generic microelectronic starter kits.

LED should fit snugly and should be attached within the openings, fixed semi-permanently with an adhesive. While waiting for adhesive to cure part of the circuitry can be loaded and fixed. The +5V phono jack (part #10) and USB-B male ports (part #9) need to be included and sealed around the gaps with a permanent, waterproof adhesive (Figure 9C). After the LED adhesive has cured, each LED needs to be wired in series, connecting each of the three pins to the corresponding pins (Figure 9D) on the subsequent LED within their respective rows (60 intermittent wires, four rows total, a completed circuit will result in 4 separate circuits of 6 LEDs, Figure 3D, red bracket). It is important to note that within the rows, the shorter connecting wires never cross over each other. Twelve (12) wires should overhang from the LED grid (three wires per LED, 1 +5V, 1 ground, 1 data) and will connect to the input pins of the four remaining (Figure 9D); these will serve to connect the LEDs to the breadboard. Each LED is positioned in the approximate center of each well and position the LEDs 50-60 µm from the bottom of the well plates. Following soldering the LED circuits, the backs of the LEDs, wires, and solder should be sealed with a waterproof covering to prevent use-based oxidation (Figure 9D). I used a two-part epoxy and gently brush applied so as not to disturb or break the connections. Once the completed LED grid has been sealed, it can be connected to the microcontroller by fusing the four corresponding overhang wires together and leading them to their respective breadboard positions. The exception is with the data pin wires, wherein each overhang wire terminates in its own breadboard pin (Figure 9D, number 12, Table 3). Once the connections are established it is necessary to test the connections and ensure that they are functional (Figure 9B). With the fully assembled circuit and breadboard, load “test.” onto the Arduino and allow the microcontroller to proceed with its function. A series of tones will be emitted from

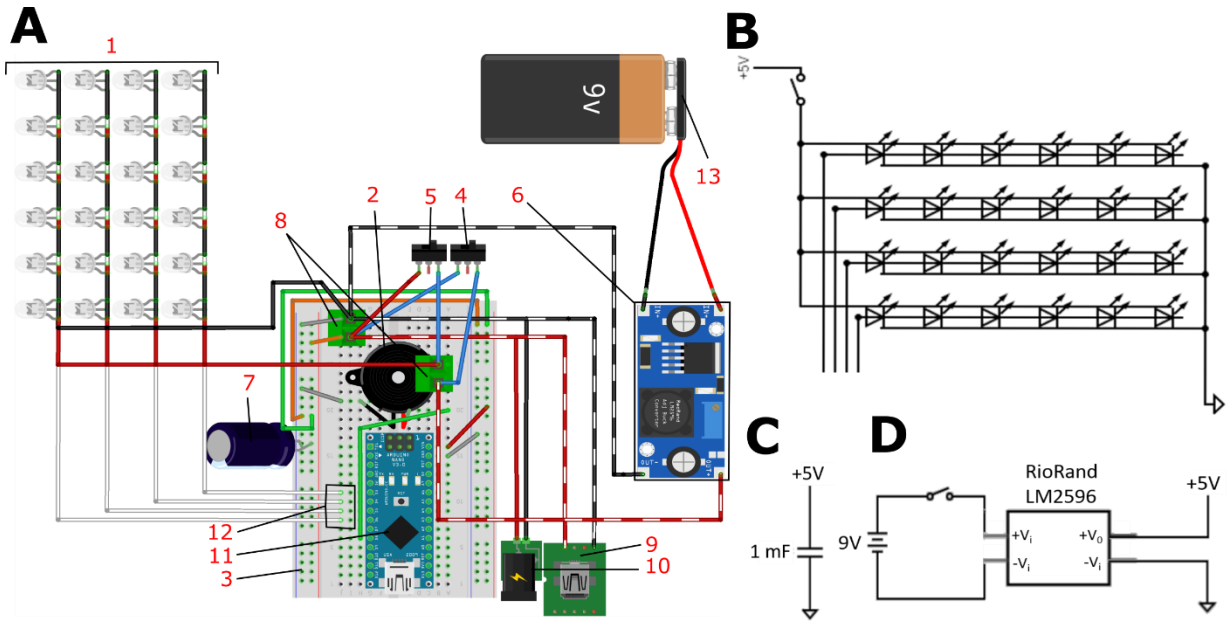

Figure 8. Schematics for the assembly of OPAL electrical circuitry. (A) Wired connections conceptualized in Fritzing, each numbered part is identified in Tables 2 and 3, for part identification (Table 2) and its corresponding pin location on the breadboard (Table 3). (B) Electrical schematic of the LEDs; (C) Electrical schematic of 1000 mF capacitor connected to rail and ground; (D) Electricacl schematic of the voltage regulator.

the small speaker followed by an activation of the LEDs in synchrony, row 1 in blue, 2 in green, 3 in red, and 4 in yellow. After testing the LED connections and priming the access ports, reconstruct the bread board. Breadboard pin locations for individual components are listed in Table 3 and should be followed while using the guidance of the Fritzing schematic (Figure 8A). Intra-breadboard connections are completed with generic copper wires. LED ground and rail connectors are comprised of 4 individual wires connecting from their respective LED pins and fused to one copper wire of slightly larger diameter connected to the screw terminal (ST, position of each listed). Two simple toggle switches control the LED array and battery power. Switches may be adhered as seen fit. Carefully load the completed breadboard (Figure 9D) into the partition (Figure 9E). The only piece of hardware not securely fastened is the voltage regulator (Figure 9F-G) and it can be temporarily placed next to the breadboard to easily change the battery if needed. lower chassis is a simple box with an inner-basement partition that allows for stabilizing the breadboard as well as three input ports: the microcontroller port, a 5V input jack, and USB-B male. The microcontroller port permits changing frequential programs without disturbing The LED grid may be switched off while keeping the processor active: this is to prevent shorting the LED array while uploading new sketches. The battery power switch allows for remote

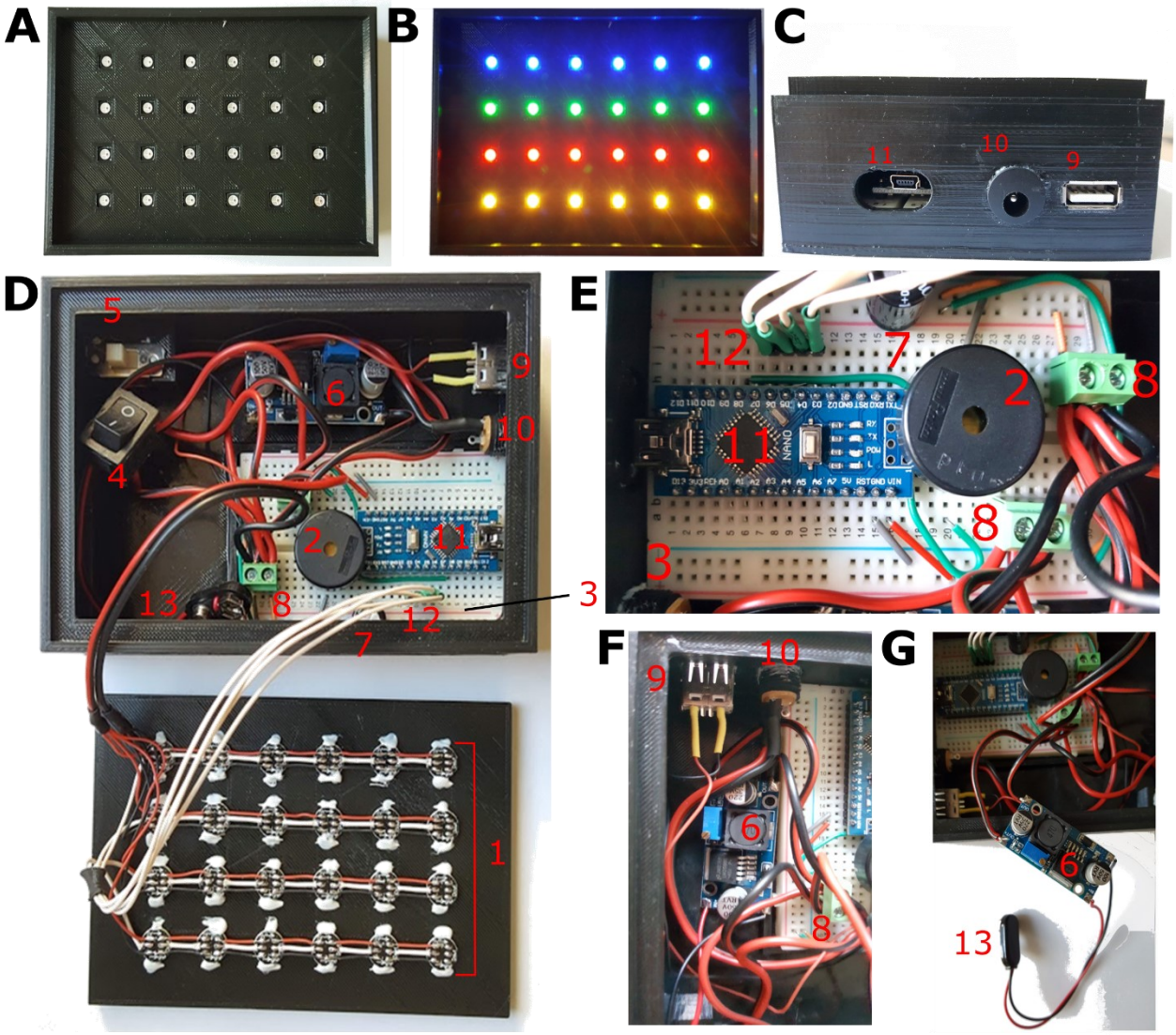

Figure 9. Post assembly of OPAL housing and circuits. Red numbers correspond to part number from Table 2. (A) Post-assembly of LED conformation in a 4x6 grid from above. (B) LEDs in "test" phase: blue, green, red, and "yellow" have been called within the program. (C) Face view of access ports including the USB-B Female Port (9), SV input port (10), and USB to serial chip CH340 (11). (D) Circuitry and its orientation after integration with the housing. Parts 1-13 are all listed within Tables 2 and 3. The breadboard (3) is securely nestled within its partition while the other parts (2, 4-13) remain undisturbed in their positions with enough room to accommodate the wiring. There are duplicates of the screw terminals (8) purposefully. (E) Higher resolution layout of the breadboard (3) arrangement of the piezo speaker (2), capacitor (7), screw terminals (8), the microprocessor (11), and the LED pin array (12). (F) the voltage regulator is situated next to the breadboard between the 5V phono jack port (5), the USB-B port (9) and one of the screw terminals. (G)) Higher resolution of niched pieces including the voltage regulator (6) connected to the screw terminals (left side) and terminating with the 9V connector.

powering of the device and is especially useful in cases when a 5V connection is unavailable or distal to the incubator. The upper stage grid complete with LEDs can now be positioned on top of the chassis and should rest securely. An adhesive is not recommended to attach the upper stage to the lower chassis as access to the

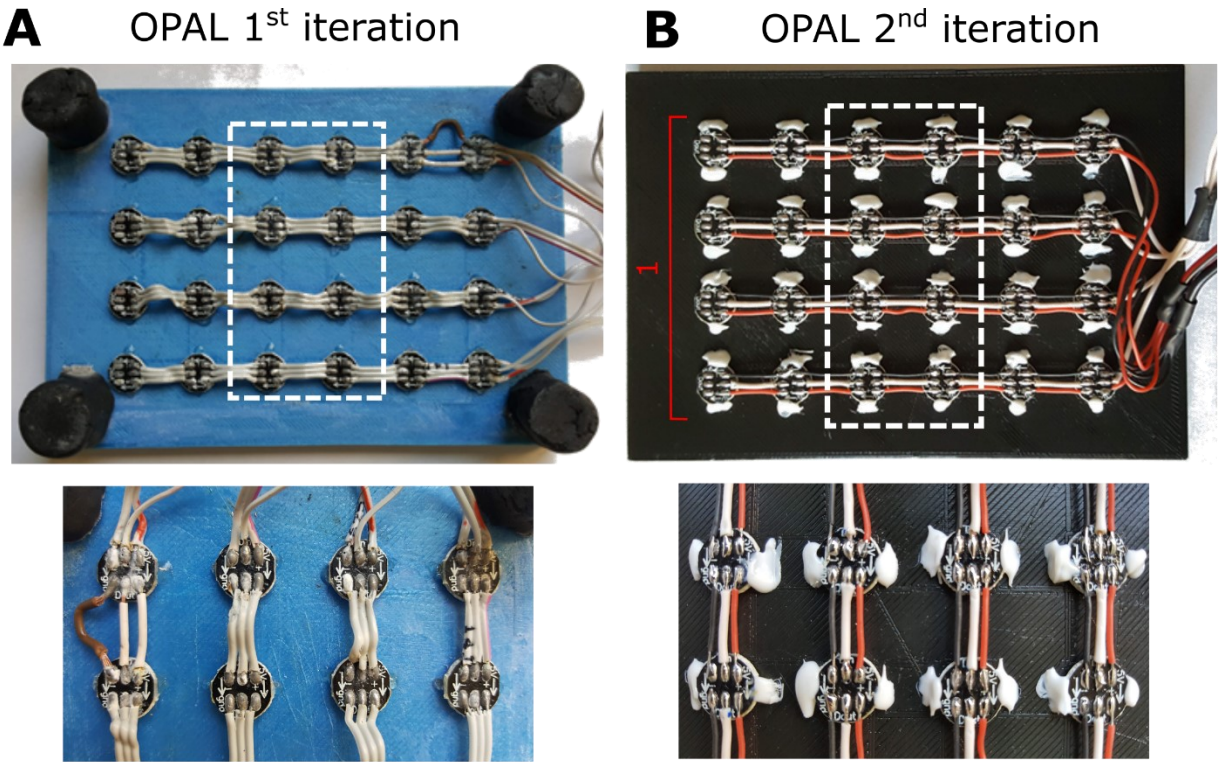

Figure 10. Oxidization of exposed, unhoused LED junctions. (A) First iteration of OPAL and its oxidation, blow-out picture below is indicated by white dashed box surounding middle circuitry showing tarnish on soldered junctions. (B) Second iteration of OPAL and its oxidation after the same number of uses; blow-out picture below is indicated by white dashed box surounding middle circuitry showing lack of tarnish post-epoxy waterproofing and enclosure of circuitry.

internal components may be needed. Re-execute test.file to ensure the connections were not loosened or destroyed during attachment. At this point, the device is ready to be applied for experimental procedures. Custom experimental light parameters can be designed by using the macros provided in this paper or from scratch. Epoxy is highly recommended for waterproofing as the first iteration of the OPAL included neither lower housing unit nor epoxy and suffered oxidation at the LED solder junctions (Figure 10A). The epoxy serves strongly as a preventive measure for intra-incubator corrosion (Figure 10B).

Software for light patterns

All patterns for light stimulation were constructed within Arduino software and can be downloaded from the following link: https://github.com/kleagsand/Neuroware/branches. Arduino IDE open-source

software, v 1.8.9. Briefly, these programs allowed for square wave LED oscillations of activation-deactivation, producing a "flickering" effect. This was achieved by alternating cycles: first cycle lasting 5 ms and second cycle on delay of 5 ms but also lasting 5 ms. LEDs were activated by calling each row with the desired wavelength ranges (i.e., led[0]= Blue to induce 450-490 nm, "Red," and "Green.").

LED Validation

To validate the wavelength ranges emitted by the Adafruit LEDs, an AvaSpec-ULS3648 High-resolution Spectrometer (Avantes) was used. The detector of the fiber optic cable was positioned at a fixed 10 cm while the Arduino executed programs to give constitutive "red," "green," "blue," and "yellow" perceived light. The spectrum from 300 nm-1000 nm was measured. Resultant wavelength spectra are averaged from N=2 measurements. An oscilloscope was used to assay the temporal fidelity of the microprocessor. The one used to perform these measurements is a Tektronix TBS 1072B (Tektronix). Generic red and blue LEDs were used to receive input from the device LEDs. The receiver LEDs were positioned fixedly and proximal to the device LEDs while the test program was performed. The test program induced on-off oscillations at 100 Hz of the blue LED, the red LED, and dual contraphasic blue and red (such that when the blue LED is activated, the red LED is deactivated and vice-versa). The resultant measurements are taken from after five minutes real time monitoring and displayed as 10 milliseconds and 1 second.

Lentiviral constructs

Three lentiviral constructs were implemented to manipulate the electrical responses of mESC-derived neurons: two constructs previously demonstrated to function *in vivo* eYFP-ChR2 and eYFP-NpHR, and ChR2-eYFP-β-NpHR. ChR2-eYFP-βHK-NpHR was subcloned from its parent plasmid15 and inserted into pLV-EF1a-IRES-Puro, a plasmid containing EF-1α and α-intron promoter upstream of the MCS followed by IRES promoter

with a puromycin resistance cassette (Addgene Plasmid #85132, RRID:Addgene_85132) (Hayer et al., 2016). Primers were designed using SnapGene Reader.

Primer sequences:

Forward Primer: 5'-CGAAGGATCCACCATGGATTATGGAGGCGCCCTG-3'

Reverse Primer: 5'- CGTAACGCGTTCAGTCGTCAGCGGGAGTGC-3'.

The forward primer contains a BamHI (R0136, New England Biolabs) restriction site at its 5' end and the reverse primer contains a MluI (R0198, New England Biolabs) restriction site at its 5' end. Subcloning was performed using the Q5 DNA polymerase protocol (M0491, New England Biolabs). Lentivirus were prepared using an adapted version of the protocol from Addgene's lentivirus protocol page (https://www.addgene.org/protocols/lentivirus-production/#). Channelrhodopsin-containing plasmids were packaged by incubating 15 µg of psPAX2 (Addgene plasmid # 12260 ; http://n2t.net/addgene:12260 ; RRID:Addgene_12260), 5 µg pMD2.G (Addgene plasmid # 12259 ; http://n2t.net/addgene:12259 ; RRID:Addgene_12259), and 20 µg of plasmid construct in RT reduced-serum OptiMEM GLUTAMAXTM media and 0.12 µg/ml linear polyethyleneimine (PEI, MW: 25,000, CAS Number 9002-98-6)(Wiseman et al., 2003). HEK 293T cells were transfected for 6 hours at 37°C in OptiMEM GLUTAMAX whereupon the transfection media was removed from the culture and replaced with fresh OptiMEM (Lattanzi et al., 2010; Naldini et al., 1996). Virally active media was collected at 48 hours after transfection and immediately added to cell culture plates. Transgenic expressions were assayed via live cell monitoring throughout time course leading up to experiments on an inverted Leica epifluorescent microscope, Western Blots, and immunocytochemical detection.

ICC detection of transgene expression in HEK cells

At ~DIV-35, transduced neuronal cells were fixed in 2% PFA and washed 3 times in 1X PBS following fixation. Cultures were then blocked in 3% FCS/3% BSA/0.5% Triton-X and incubated at RT for 1 hour. Blocking buffer was aspirated and replaced with primary antibody solution containing 3% FCS/3% BSA/0.1% Triton-X,

1:1000 anti-GFP (rabbit, A-11122, Invitrogen, RRID:AB_221569) and 1:500 anti-NeuN (chicken, ABN91, EMD, RRID:AB_11205760), allowed to incubate overnight at 4°C. Primary antibody solution was aspirated, samples were washed 3 times in 1X PBS, 10 minutes per wash, and then allowed to incubate 2 hr at RT in secondary antibody solution containing 3% FCS/3% BSA, 1:500 Goat anti-rabbit AlexaFluor 488 (A-11008, Invitrogen, RRID:AB_143165) and 1:500 Goat anti-chicken AlexaFluor 546 (A-11040, Invitrogen, RRID:AB_2534097). Secondary antibody solution was aspirated, samples were washed 3 times in 1X PBS, 10 minutes per wash, and during the last wash included 1:1000 DAPI. Samples were mounted with a few drops of AquaPolymount (18606, Polysciences Inc.) and allowed to cure 72 hours before confocal acquisition.

Neuronal Cell Culture

In brief, neurons were differentiated from mouse E14 embryonic stem cells outlined previously (Bertacchi, Pandolfini, et al., 2015; Y. Shi, Kirwan, & Livesey, 2012; Terrigno et al., 2018). Starting from days *in vitro* (DIV) -1plated at a density of 30,000 cells/cm2 on 1% porcine gelatin (G1890, Sigma Aldrich), maintained overnight in 2i + LIF medium based in GMEM BHK-21 (11710035, ThermoFisher Scientific) and containing 2mM Glutamine (25030, ThermoFisher Scientific), 1 mM Sodium Pyruvate (11360070, ThermoFisher Scientific), 100 U/ml Penicillin-streptomycin (15140, ThermoFisher Scientific), 1mM Non-essential amino acids (11140, Sigma Aldrich), 0.05mM β-mercaptoethanol (M3148, Sigma Aldrich), CHIR 99201, 5 µM (SML1046, Sigma Aldrich), PD 0325901, 5 µM (sc-205427, Santa Cruz Biotechnologies), Mouse Leukemia Inhibitory Factor (LIF), 10 ng/ml (GFM200-100, Cell Guidance Systems), N-2 Supplement 100X (175020, ThermoFisher Scientific), and B-27 Supplement minus Vitamin A 50X (125870, ThermoFisher Scientific). Cells were then introduced to isocortical neuronal differentiation medium containing Wnt/BMP inhibitors and based in DMEM/F12 1:1 (21331-046, ThermoFisher Scientific) containing 2mM Glutamine (25030, ThermoFisher Scientific), 1 mM Sodium Pyruvate (11360070, ThermoFisher Scientific), 100 U/ml Penicillin-streptomycin (15140, ThermoFisher Scientific), 1mM Non-essential amino acids (11140, Sigma Aldrich), 0.05mM β-mercaptoethanol (M3148, Sigma Aldrich), 10 µM

53AH (C5324-10, Cellagen Technology), 10 μM LDN193189 hydrochloride (SML0559, Sigma Aldrich), N-2 Supplement 100X (175020, ThermoFisher Scientific), and B-27 Supplement minus Vitamin A 50X (125870, ThermoFisher Scientific). Differentiating cells were maintained in WiBi until DIV11 where the media was changed to Neurobasal (gNb) based in Neurobasal (21103049, ThermoFisher Scientific) and containing 2mM Glutamine (25030, ThermoFisher Scientific), 1 mM Sodium Pyruvate (11360070, ThermoFisher Scientific), 100 U/ml Penicillin-streptomycin (15140, ThermoFisher Scientific), 0.05mM β-mercaptoethanol (M3148, Sigma Aldrich), Ascorbate, 0.5 mM (A92902, Sigma Aldrich), Recombinant human BDNF, 20 ng/ml (NBP2-52006, Novus Biologicals), and B-27 Supplement minus Vitamin A 50X (125870, ThermoFisher Scientific); gNb was maintained until DIV 25.

After DIV 25 the media was changed to Neurobasal-A, vNb, based in Neurobasal-A (10888022, ThermoFisher Scientific) and containing 2mM Glutamine (25030, ThermoFisher Scientific), 1 mM Sodium Pyruvate (11360070, ThermoFisher Scientific), 100 U/ml Penicillin-streptomycin (15140, ThermoFisher Scientific), 0.05mM β-mercaptoethanol (M3148, Sigma Aldrich), Ascorbate, 0.5 mM (A92902, Sigma Aldrich), Recombinant human BDNF, 20 ng/ml (NBP2-52006, Novus Biologicals), and B-27 Supplement 50X (17504044, ThermoFisher Scientific); vNb was maintained until DIV 37. Eppendorf's glass bottom P24 imaging plates (H 0030 741 021, Eppendorf) were chosen for these experiments as the culture chamber walls are light impermissible, diminishing cross-talk between wells while the LED programs are active. After differentiation, cells were plated on poly-l-ornithine, (P3655, Sigma Aldrich) and purified mouse Laminin (CC095-M, Merck Millipore).

Tripartite chambers were cultured according to methods previously published (J. W. Park et al., 2006; Taylor et al., 2005) using silicone tripartite chambers (Xona Microfluidics, TCND1000). It is important to note that the silicone chambers should be attached to the glass microscope slide before starting the coating. If XonaChips are used instead of silicone devices, do not use Zeiss immersion oil during microscopy acquisition and instead use Leica Type F. Neuronal cell medium was changed exactly as aforementioned except that less than 200 μl of media was added to each compartment and sequentially decreased from the first to the third

chamber to promote 1-directional axonal growth (e.g., 1st chamber receives 200 µl, 2nd chamber receives 180 µl 3rd chamber receives 160 µl). At DIV 35, only the first culture was treated with 100 µM glutamate in vNb. Media was allowed to equilibrate for 2 hours before fixation with 2% PFA.

Lentiviral transduction

At DIV 10, lentiviral transduction was performed as described above. Prior to the cell culture exchange with virally active OptiMEM, 8ug/ml polybrene (TR-1003-G, Sigma-Aldrich) was added to 300 µl/well of viral OptiMEM and mixed thoroughly. Cultures were incubated for 4 hours at 37oC with viral transduction media after which, the media was disposed in biohazard containers and replaced with WiBi.

Stimulation Parameters

DIV 35-37 cells were given fresh vNb BDNF and glutamine and were either exposed to LEDs at different corresponding patterns of stimulation and wavelengths or given chemical synaptic activators and inhibitors. Light patterns were built in Arduino software. As controls, chemical inhibitors/activators were given in parallel to the light courses and were similarly terminated by removal of media after 60 minutes and 360 minutes. Chemicals include: VGNaC blocking (1 µM tetrodotoxin), GABAA receptor inhibition (20 µM bicuculine), and NMDA/AMPA receptor agonist (100 µM glutamate). To test blue light activation, ChR2 and CheYNa cultures were given 100 Hz for 10 minutes followed by 5 minutes of rest, repeated 4 times for a total experimental duration of 60 minutes. Repeated in combination with 1 µM tetrodotoxin. Similarly, to test red light activation: ChR2 and CheYNa Cultures were given 100 Hz for 10 minutes followed by 5 minutes of rest, repeated 4 times for a total experimental duration of 60 minutes. eNpHR cultures were given 3 hours of continuous red light, +/- 100 µM glutamate. Finally, contraphasic activation with alternating blue and red light was performed by

exposing CheYNa cultures to 100 Hz blue light with 100 Hz red light in alternating phases for 10 minutes followed by 5 minutes of rest, repeated 4 times for a total experimental duration of 60 minutes.

Immunocytochemical Acquisition

Cells were fixed with 2% PFA/1X PBS for 15 min at RT after which the PFA was aspirated and replaced with fresh 1X PBS. For immunocytochemical detection, a previous immunohistochemical protocol was adapted for ICC (Mainardi et al., 2009). In short, cells were washed 3 times in 1X PBS after fixation and permeabilized and blocked in 3% FCS/3% BSA/0.5% Triton-X and incubated at RT for 1 hour. Blocking buffer was aspirated and replaced with primary antibody solution containing 3% FCS/3% BSA/0.1% Triton-X, 1:1000 cFOS (rabbit, ABE457, EMD, RRID:AB_2631318), and 1:200 MAP2 (mouse, sc-74421, Santa Cruz Biotechnology, RRID:AB_1126215) and allowed to incubate 72 hours at 4oC. Primary antibody solution was aspirated, samples were washed 3 times in 1X PBS, 10 minutes per wash, and then allowed to incubate 2 hr at RT in secondary antibody solution containing 3% FCS/3% BSA, 1:500 Goat anti-rabbit AlexaFluor 546 (A-11010, Invitrogen), and 1:500 Goat anti-mouse AlexaFluor 633 (A-21126, Invitrogen, RRID:AB_2535768). Secondary antibody solution was aspirated, samples were washed 3 times in 1X PBS, 10 minutes per wash, and during the last wash include 1:1000 DAPI (10236276001, Sigma Aldrich) or 1:500 Hoechst 33258 (H3569, ThermoFisher Scientific, RRID:AB_2651133). Samples were mounted with a 3-4 drops of AquaPolymount (18606, Polysciences Inc.) and allowed to cure 72 hours before confocal acquisition. Cultures were assayed on a Leica SP2 confocal microscope with an oil 40x objective and images were taken in z-stack format.

Image analysis

Once z-stacks were acquired, an in-house batch cell counter was applied through Image J (Fiji, RRID:SCR_002285), which parsed cells and counted circular, nuclear bodies expressing above a user-defined

intensity threshold throughout all cFOS+ images. Counts were summed across all slices, every third slice, and the first 15 to account for multiplicate counts of cFOS+ nuclei. The cell batch counter is available at this link: https://github.com/kleagsand/Neuroware/branches/Cell-Counter

Electrophysiology

Patch-clamp recordings were performed by Gianluca Pietra, Institute of Neuroscience of National Research Council of Pisa, in the laboratory of Professor Tommaso Pizzorusso. Plates containing cells at 37 days of differentiation were withdrawn from incubator and directly put under a microscope axioskop (Zeiss, Oberkochen, Germany) equipped with a 60X lens. While recording the petri were continually perfused by 1 ml/min flux at 35° C of artificial cerebrospinal fluid (ASCF; composition in mM: NaCl 119, KCl 2.5, NaHPO4 1.25, NaHCO3 15, HEPES 10, glucose 12.5, CaCl2·4H2O 2, MgSO4·7H2O 2; pH=7.3±0.1; osmolarity: 295mOsm).
The recording was performed with a borosilicate pipette (diameter: inner, 0.86mm; ext, 1.5mm - World Precision Instruments, Sarasota, FL) pulled by P-97 puller (Sutter Instruments, Novato, CA) to exhibit a resistance of 3-5 MΩ. Once the tip was in the bath and capillary was filled with intracellular solution (mM: KCl 120, K-Gluconate 10, HEPES 10, EGTA 1, CaCl2 0.3, MgCl2 1, ATP 4, GTP 0.3, phosphocreatine 5- pH=7.3±0.1; osmolarity 285mOsm). The pipette was electrically linked by Multiclamp 700° amplifier controlled by Clampex 8.2 and sampled by a Digidata 1322A (Molecular Devices, San José, CA) connected to a PC from which the experiments were controlled. During the cell approach, soft pressure was applied. Once within proximity of the cell, the pressure was released to achieve a Giga-seal. The cell membrane was broken within the pipette tip and entered in whole-cell configuration. Recordings were made in voltage-clamp (VC) holding the cell at -70 mV and applying a positive voltage step to -20 mV to check Na+ and K+ voltage-gated currents. Cells with a membrane resistance less than 150 MΩ and input resistance greater than 30 MΩ were discarded.

Experimental Design and Statistical Analyses

All ICC experiments were performed by acquiring at least n=3 biological replicates but no more than n=4. Each biological replicate consists of 5 technical replicates, each of which range from 12-17 µm z-stack images. Summations and averages were calculated of cFOS+ nuclei, cell counts were exported to GraphPad PRISM v 7.0 and one-way or two-way ANOVAs with post-hoc multiple t-test or Tukey comparisons were performed. A CI of 95% and power of 80% were imposed as the standard for significance.

CHAPTER IV: OPAL construction validation in mESC derived neuronal cultures (Results)

OPAL Device Assembly:

An open-source and readily programmable device, the OPAL is adapted for high-throughput optogenetic experiments *in vitro* and securely supports and illuminates a P24 well plate. Its structural composition and water-resistant interior allow the OPAL to withstand incubator conditions. Reported in this thesis are experiments of one-hour duration, however, I found that the OPAL could remain in the incubator for 72 consecutive hours, unaffected. This eliminates the need for ancillary temperature-controlled chambers and promotes longitudinal study in an already established incubator system. Additionally, the compactness allows minimal disruption to ulterior experiments residing simultaneously in the incubator. With the assistance from above, the OPAL can be assembled and utilized to execute experiments in a cost- and time- efficient manner.

Arduino-microcontroller mediated LED activation and validation:

The individuated LEDs were tested to ensure two critical factors: wavelength emission and temporal fidelity by the ATMega328 processor (https://www.microchip.com/wwwproducts/en/atmega328p). To drive LED-activation I employed an Arduino-based system. Arduino is an open-source electronics platform intended for easily making interactive projects (https://www.arduino.cc/). I first analyzed via broadband spectrophotometry the emitted spectra from each individual LED by uploading and executing an Arduino protocol which sustains perceived LED emission as "red," "green," and "blue," to assay the emitted wavelengths listed in Table 4. Contrary to the manufacturer's reported

LED Factory Emission Spectra

Emitting Color	Model	Wavlength range (nm)
Red	13CBAUP	620-625
Green	13CGAUP	522-525
Blue	10R1MUX	465-467

Table 4. RGB LED characteristic parameter. Table from WS2812B data sheet redrawn to display the three different LEDs integrated into each single LED housing and their respective reported wavelength ranges. From now, whenever a single "LED" is mentioned in the paper, it refers to the integrated triad of LEDs; practically, the OPAL houses 72 independent LEDs but only requires 24 spaces.

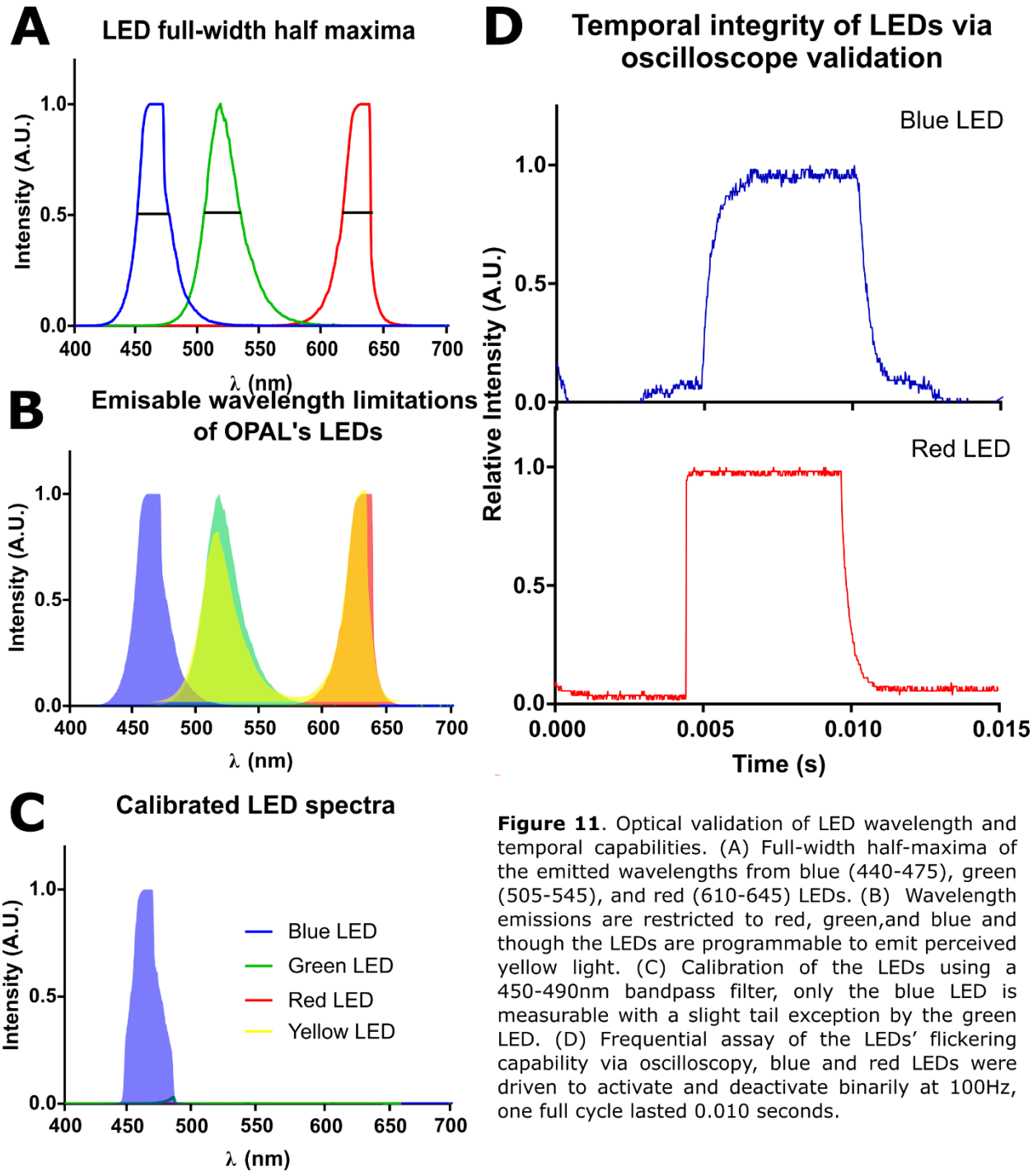

Figure 11. Optical validation of LED wavelength and temporal capabilities. (A) Full-width half-maxima of the emitted wavelengths from blue (440-475), green (505-545), and red (610-645) LEDs. (B) Wavelength emissions are restricted to red, green,and blue and though the LEDs are programmable to emit perceived yellow light. (C) Calibration of the LEDs using a 450-490nm bandpass filter, only the blue LED is measurable with a slight tail exception by the green LED. (D) Frequential assay of the LEDs' flickering capability via oscilloscopy, blue and red LEDs were driven to activate and deactivate binarily at 100Hz, one full cycle lasted 0.010 seconds.

emission ranges (Table 4) which suggest a very narrow spectrum per LED (2-5nm wide), I calculated each full-width half-maximum ranges (Figure 11A) as 450-480nm (blue), 505-535nm (green), and 615-640nm (red). Using the same protocol but including "yellow," I sampled each "color" to confirm that LEDs' perceived colors are correspondent to those reported by the manufacturer and that the LEDs emit light in discreet ranges of

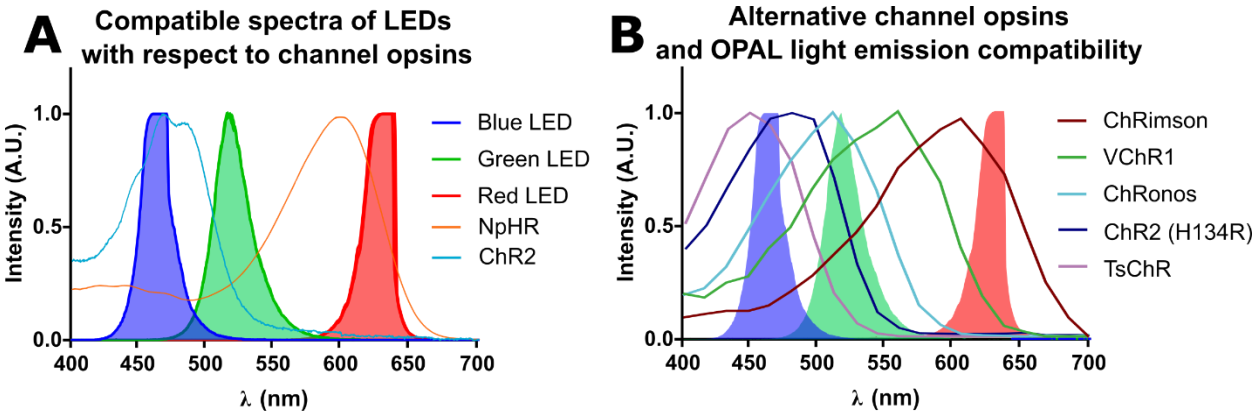

Figure 12. Compatible channelrhodopsin spectra with OPAL emission spectra. (A) Compatibility of channelopsin excitation spectra redrawn from Wood et al and superimposed over LED wavelength spectra. (B) Compatibility of the OPAL LEDs with four alternative channelopsins' excitation spectra redrawn from literature including: ChRimson, VChR1, ChRonos, and TsChR.

~440nm-500nm (perceived blue), ~480nm-550 nm (perceived green), and ~600nm-650nm (perceived red) (Figure 11A).

Furthermore, when prompted for intermediate wavelengths (yellow, Figure 11B), the green and red LEDs produce interfering signals and accordingly give perceived yellow light. However, the LEDs are unable to emit wavelengths between 550nm-600nm and thus are restricted to three wavelength ranges. The LEDs were further calibrated via DAPI filter (Thor Labs, 450-490 nm) and the LED emission spectra of red, green, and blue were remeasured. As expected, only the blue range was detectable alongside a discreet tail from the green range (Figure 11C) indicating high specificity of wavelength ranges and practically negligible cross-signal between LED settings. To give biological relevance to OPAL's performance, I determined the temporal fidelity of the upper-frequency threshold of LED switching. It is well accepted that neurons encode electrical signals intraneuronally via uniquely patterned events, the best characterized are long-term potentiation, thought to basally occur at 100Hz (Andersen & Lømo, 1967; Larson et al., 1986; Rose & Dunwiddie, 1986), and long-term depression exhibiting regionally dependent frequential ranges between 1-10Hz (Staubli & Lynch, 1990; Werk et al., 2006). Thus, LED switching frequencies of the blue and red LEDs were measured at 100 Hz via oscilloscopy (Figure 11D). It was determined that the LEDs are highly fidelitous and complete a symmetrical on-off cycle within 10 ms. It appears that the blue LED is noisier than its red counterpart and exhibits a longer delay when reaching maximum intensity. The red LED appears to exhibit near-perfect square wave nature, with only a slight

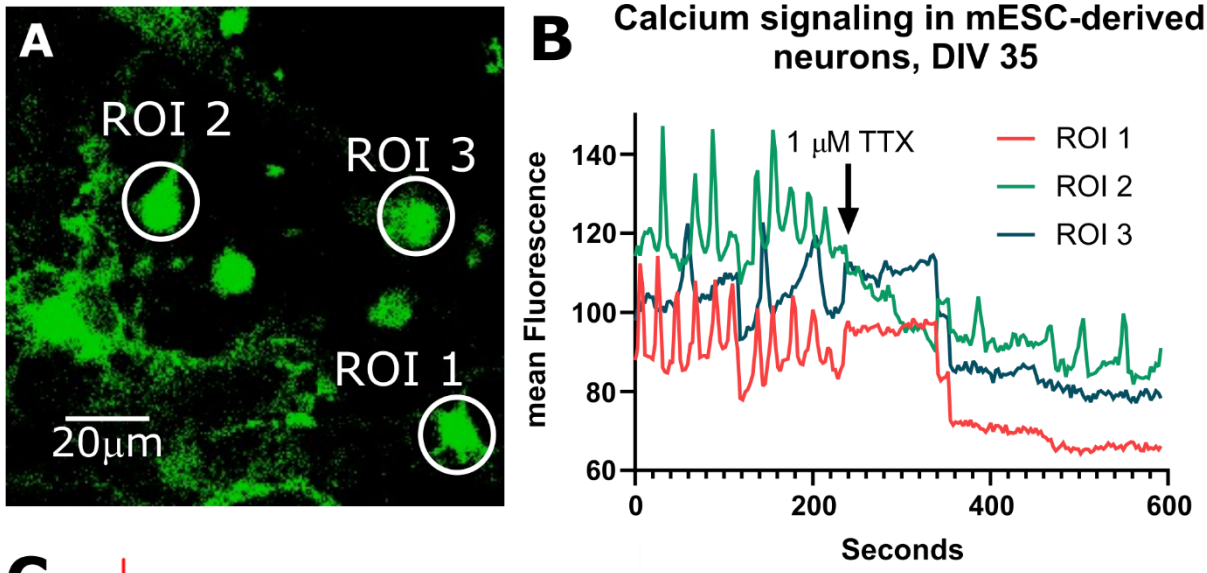

Figure 13. Physiological firing of mESC-derived neurons. Cells were assayed for ionic channel activity by live cell imaging and patch clamp electrophysiology. (A) Thumbnail of video recording in live cell confocal imaging. White circles indicate cells analyzed for calcium wave dynamics using BAPTA Oregon Green. (B) Mean fluorescent changes in respective ROI's sig -nal over time. with the addition of 1 μM TTX at ~220 s, all three cells underwent a decrease in Ca^{2+} fluctuations. N=3 (C) Averaged patch clamp recording from n=6 neurons at DIV 35, cells display a depolarization response during step-wise increase canonical to voltage-gated sodium as well as fast- and slow- voltage-gated potassium channels.

tail while switching off (Figure 11D). In anticipation of compatibility, the excitation spectra of the two channelrhodopsins used in this paper (Figure 12A), ChR2 and NpHR, as well as those from a handful of less common channelrhodopsins (Figure 12B) were redrawn from literature (Klapoetke et al., 2014; Kleinlogel et al., 2011) and overlapped with the LED emission spectra. Of the 6 channelrhodopsins shown, none of the excitation spectra exceed those of the LED limitations. Given that the LED emitted wavelength ranges are theoretically highly compatible with an array of channelrhodopsins and that the LEDs can achieve a switching frequency parallel to neuronal signaling, construction of a device incorporating these LEDs for *in vitro* support was feasible.

Validity of mESC-derived neurons for stimulation experiments:

Before applying the OPAL system, an electrically active culture model first needed to be set up. Previously, mESC-derived neurons have been demonstrated to behave in an electrically canon manner (Barth et al., 2014; Streckfuss-Bömeke et al., 2009), exhibiting mature sodium currents. To assay whether the cells could mature physiologically, cultures at several time points were assayed for calcium wave signals at DIV 35 (Figure 13A). Neuronal cultures were imaged for a total length of 10 minutes in BAPTA Oregon Green calcium detector and were bathed in 1mM TTX at ~minute 3. ROI analysis showed that 3 cells' calcium waves were disrupted for ~100 seconds after the addition of TTX and decreased for the remainder of the experiment (Figure 13B). Cells were further assayed for electrophysiological properties under patch clamp after 25, 35, 37, and 45 days *in vitro*. Only cells at DIV 35 provided a mature voltage-gated sodium current and ten neuronally morphological cells were probed from each time length for mature sodium currents. Despite previous cFOS

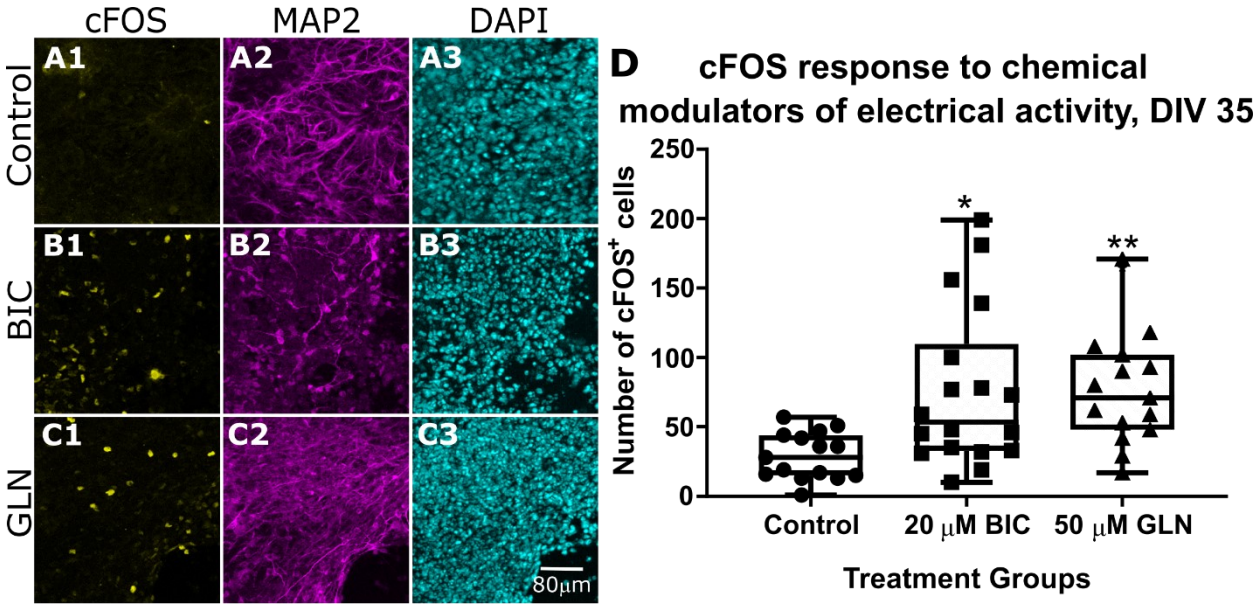

Figure 14. Neuronal activation with bicuculline and glutamine. At DIV 35, cells were treated without small molecule supplements (Control, A), 20 μM bicuculline (BIC, B), or 100μM glutamine (GLN,C) for 1 hour. Thereafter, cells were fixed and immunostained for cFOS (Col. 1), MAP2 (A4) (Col. 2), and DAPI (Col. 3). Z-stack mages were acquired via confocal and cFOS images were processed semi-automatedly in each stack with a batch cell counter macro in ImageJ. (D) Analysis of $cFOS^{+}$ cells from ICD confocal acquisition. Both BIC- and GLN- treated cells upregulated cFOS over 1 hr in comparison to control (+35 cells, +52 cells, respectively). Analysis was performed with a one-way ANOVA followed by a Kruskal-Wallis post-hoc test. Asterisks above box plots indicate comparison to control. *-p-val<0.05, **-p-val<0.01; error bars representative of 99% CI, N=18

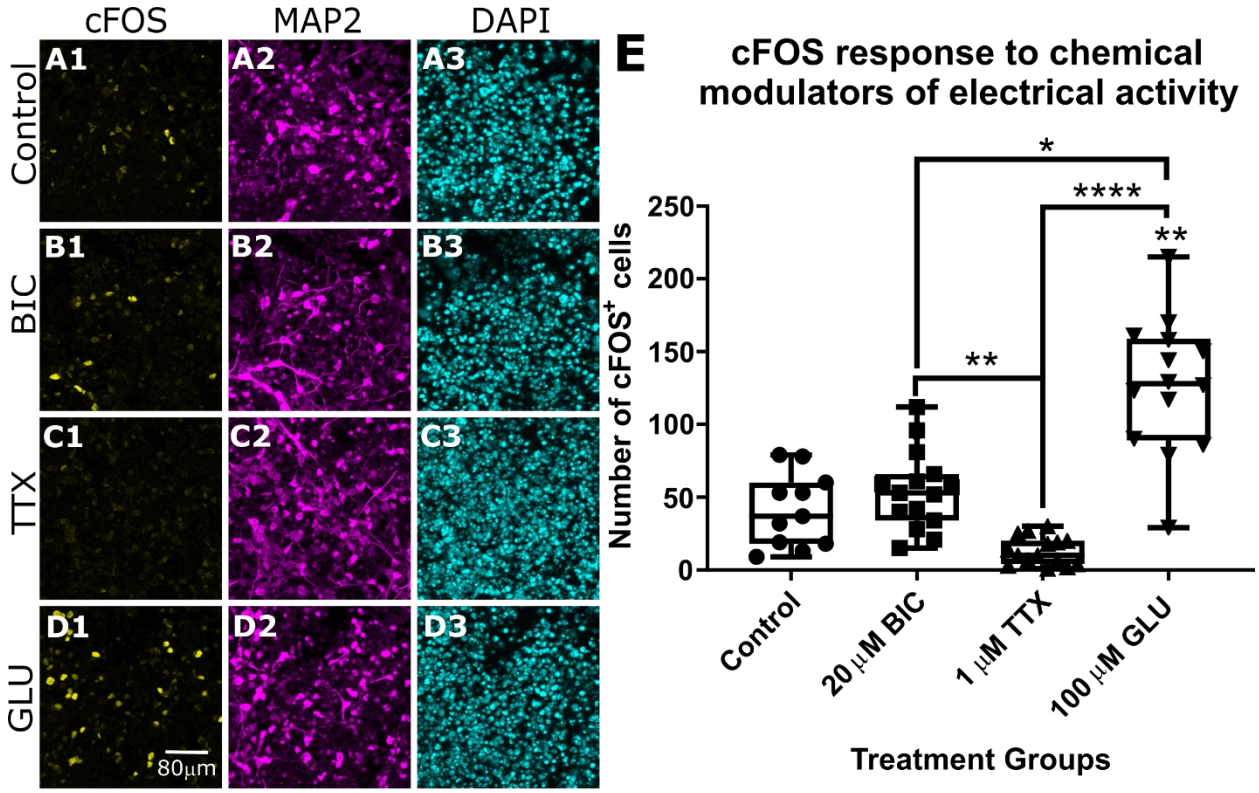

Figure 15. Neuronal activity modulation with canonical ion channel small molecule interactors. At DIV 35, cells were treated without small molecule supplements (Control, A), 20 mM bicuculline (BIC, B), or 1mM tetrodotoxin (TTX,C) or 100mM glutamate (GLU, D) for 3 hours. Thereafter, cells were fixed and immunostained for cFOS (Col. 1), MAP2 (A4) (Col. 2), and DAPI (Col. 3). Z-stack mages were acquired via confocal and cFOS images were processed semi-automatedly in each stack with a batch cell counter macro in ImageJ. (E) Analysis of $cFOS^+$ cells from ICD confocal acquisition. GLU- treated cells significantly upregulated cFOS over hr in comparison to control (+83 cells) as well as BIC (+71 cells). While TTX was not significantly downregulated compared to Control, it did not activate cells and exhibited fewer $cFOS^+$ cells than BIC (-37 cells) and GLU (-108 cells). Analysis was performed with a one-way ANOVA followed by a Kruskal-Wallis post-hoc test. Asterisks above box plots indicate comparison to control whereas asterisks above solid black bars indicate between groups. *-p-val<0.05, **-p-val<0.01, ***-p-val<0.001, ****-p-val<0.0001; error bars representative of 99% CI, N=13

activation analyses (Terrigno et al., 2018), I found that DIV 25 was too early for the appearance of matured sodium channels and found a majority population of mature neurons from DIV 35 (6 of 10 cells, Figure 13C).

To further assay physiological activation, immunofluorescent detection of activity-dependent transcription factor, cFOS, was employed. Wild-type cultures were left in minimal media as control (Figure 14A)

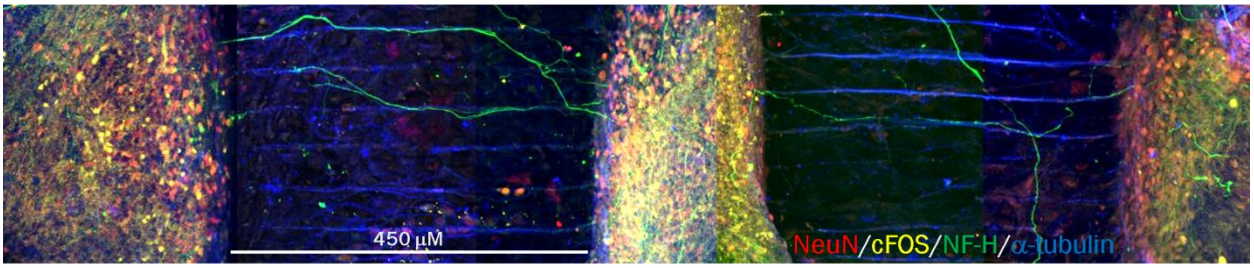

Figure 16. Transynaptic activation of downstream neuronal populations. Cells were plated into tripartite microfluidic chambers. At DIV 35, 100 μM glutamate was added to the first, left-most chamber and incubated for 2 hours. At the end of 2 hours, cells were fixed and immunostained for NeuN, cFOS, Neurofilamentin-Heavy (NF-H), and α-tubulin. cFOS upregulated in the second, middle chamber but not in the third, right-most chamber. N=1

or treated with 20 μM bicuculline (BIC, Figure 14B), 50 μM glutamine (GLN, Figure 8C) for 1 hour. I found that after 1 hr, nuclear cFOS protein is upregulated in neuronal cell cultures at DIV 35 by both BIC and GLN (Figure 14D). While BIC is commonly known to activate neuronal networks by inhibited inhibition, GLN's effect guided the formulation of my experimental media to withdraw GLN from further experiments measuring cFOS. To further assay the nature of cFOS induction I assayed minimal media cultures (Figure 15A) and compared them to 3 hours and compared them to 20 μM bicuculline (Figure 15B), 1mM TTX (Figure 15C), and 100 μM glutamate (GLU, Figure 15D). An observed increase of cFOS expressing cells was sustained over 3 hours by GLU (Figure 15E) although BIC did not increase $cFOS^+$ nuclei (Figure 15E). It was further observed that TTX-mediated inactivation trends as diminishing the number of $cFOS^+$ nuclei below baseline control, though cFOS is significantly decreased between both BIC and GLU treatments (Figure 15E). Finally, I assayed the synaptic nature of DIV 35 neuronal cultures and seeded a tripartite microfluidic chamber to separate three populations of neurons. At DIV 35 only one chamber was given 100 mM of glutamate for 2 hours and the cFOS response in the 1^{st} downstream chamber was upregulated but not in the 2^{nd} subsequent chamber (Figure 16). The combined observations between electrophysiology and chemical modulations to cFOS response sufficed in verifying canonical neuronal activity within these populations.

Neuronal cFOS expression modulation via OPAL

After validating electrical activity in neuronal cultures, I instated the OPAL device to assess practical application and intended use. The EF-1a-ChR2 construct was tested with non-neuronal cells (HEK 293T, RRID:CVCL_0063 (DuBridge et al., 1987; Pear et al., 1993)) and given a short burst of blue light with the same LEDs and microprocessor as the OPAL. When recorded, these cells elicited an inward sodium current (Figure 17A) interpreted as sufficient to drive an action potential in neuronal cells. I next utilized three channelrhodopsin constructs and exposed them to their approximate and respective activation wavelength ranges: blue-light activated ChR2 H134R, red-light activated NpHR, and ChR2-NpHR chimera (CheYNa) (Kleinlogel et al., 2011). I measured cFOS expression to assay the activation of single cells in network clusters. Neuronal cultures transduced with either ChR2 or CheYNa were exposed to a paradigm of 100Hz light trains (Figure 17B), flickering at 100 Hz (Figure 17C), for 10 min followed by 5 minutes of rest/disabled LEDs; this pattern was repeated 4 times over the course of an hour. Unexposed, matched-phenotype cells (Figure 18A) were compared to ChR2-transduced (Figure 18B) and CheYNa-transduced (Figure 18C) cells to assess ChR2-mediated activation of cFOS expression. Wild-type neuronal cultures were found to be insensitive to blue light, as expected (Figure 18D) and instead the light train paradigm from Figure 17B was found to induce cFOS in both ChR2 and CheYNa groups (Figure 18D).

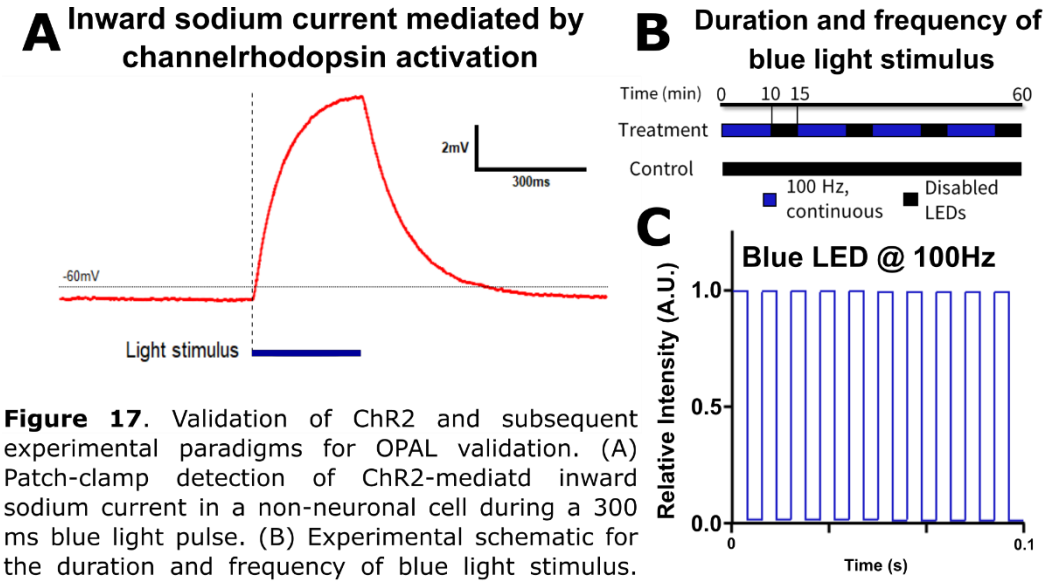

Figure 17. Validation of ChR2 and subsequent experimental paradigms for OPAL validation. (A) Patch-clamp detection of ChR2-mediatd inward sodium current in a non-neuronal cell during a 300 ms blue light pulse. (B) Experimental schematic for the duration and frequency of blue light stimulus. Control remained unexposed to light (solid black bar) whereas ChR2 or CheYNa-transduced neurons were exposed to 10 minutes of blue light pulsing at 100 Hz followed by five minutes of deactivated LEDs; this was repeated 4 times over the course of an hour (blue and black dashed bar). (C) Rendered on/off signal for blue LED switching at 100Hz.

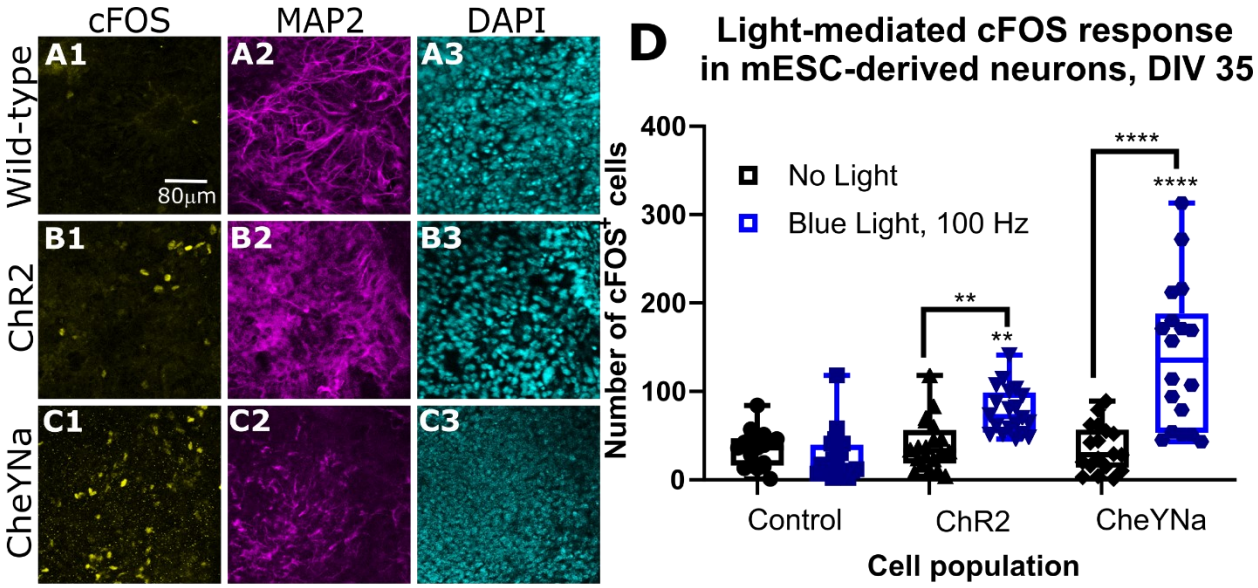

Figure 18. Activation of mESC-derived neurons transduced with ChR2 constructs and blue light. At DIV 35, optogenetically targeted cells were exposed to the 4 light trains pulsed at 100Hz outlined in Fig 11B over the course of 1 hour. Cells were either untransduced (Control, A), expressed ChannelRhodopsin-V134R (ChR2, B), or the CheYNa construct (C). Thereafter, celals were fixed and immunostained for cFOS (Col. 1), MAP2 (A4) (Col. 2), and DAPI (Col. 3). Z-stack mages were acquired via confocal and cFOS images were processed semi-automatedly in each stack with a batch cell counter macro in ImageJ. (D) Analysis of $cFOS^{+}$ cells from ICD confocal acquisition. Blue light did not initiate a cOS response in control wild-type cells. ChR2-transduced cultures exhibited an increase in $cFOS^{+}$ cells compared to control (+28 cells) and its optically inert control (ChR2 No Light, +21 cells). CheYNa-transduced cultures instead exhibited a larger cFOS response with 100Hz blue-light trains compared to both control (+111 cells) and its inert control (CheYNA No Light, +126 cells). Analysis was performed with a one-way ANOVA followed by a Kruskal-Wallis post-hoc test. Asterisks above box plots indicate comparison to control whereas asterisks above solid black bars indicate between groups. **-p-val<0.01, ****-p-val<0.0001; error bars representative of 99% CI, N=20

Furthermore, the results suggest that while ChR2 exposure induces cFOS expression, CheYNa is more sensitive to the experimental paradigm, though this difference is not significant. To assess whether this activation was mediated by sodium currents, I replicated the experimental outline of Figure 17B and Figure 18 but supplemented 1 μM TTX over the course of an hour in parallel to the light treatment. Control cells (Figure 19A) were included in the analysis to demonstrate baseline activation and 3-hour TTX treated cells from Figure 15 were incorporated to demonstrate TTX preventative effect. ChR2 (Figure 19B) and CheYNa (Figure 19C) were instead co-incubated with TTX. Blue-light mediated cFOS upregulation in both optogenetically transduced cell populations is prevented by TTX co-incubation despite repeated blue-light exposure (Figure 19D). As TTX is a well-known inhibitor of voltage gated sodium channel opening (R. Chen & Chung, 2014; Narahashi et al., 1964)

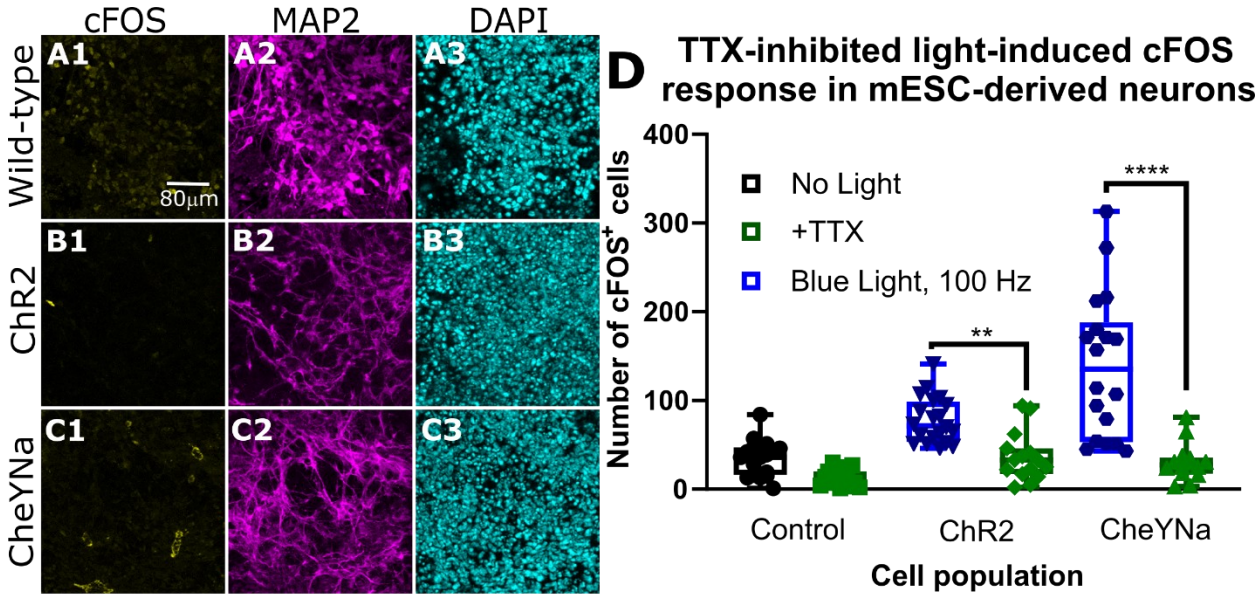

Figure 19. Activation of mESC-derived neurons transduced with ChR2 constructs and blue light. At DIV 35, optogenetically targeted cells were exposed to the 4 light trains pulsed at 100Hz outlined in Fig 11B over the course of 1 hour. Cells were either untransduced (Control, A), expressed ChannelRhodopsin-V134R (ChR2, B), or the CheYNa construct (C) and given the same parameter as in Fig 12 but were cotreated with 1 μM tetrodotxin (TTX) over the hour long treatment, with the exception of wild-type (matched with TTX 3 hours from Fig 9E). Thereafter, cells were fixed and immunostained for cFOS (Col. 1), MAP2 (A4) (Col. 2), and DAPI (Col. 3). Z-stack mages were acquired via confocal and cFOS images were processed semi-automatedly in each stack with a batch cell counter macro in ImageJ. (D) Analysis of $cFOS^+$ cells from ICD confocal acquisition. Addition of TTX to light-train treatment prevented cFOS upregulation in both ChR2-transduced cells (-43 cells) and CheYNa-transduced cells (-115 cells). Analysis was performed with a one-way ANOVA followed by a Kruskal-Wallis post-hoc test. Asterisks above box plots indicate comparison to control whereas asterisks above solid black bars indicate between groups. **-p-val<0.01, ****-p-val<0.0001; error bars representative of 99% CI, N=20

it may be inferred that my neuronal cells transduce calcium-dependent nuclear signals downstream from voltage-gated sodium channel activation in a canonical neuronal pathway.

After validating that the blue LED was sufficient to elicit a response in my transduced neuronal populations, subsequent validation of the red LED followed. Replicating previous finding of selective wavelength activation (Boyden et al., 2005), the specificity of ChR2 and CheYNa to blue-light was first assessed by enabling red LEDs under the same parameters as the blue LED experiments (Figure 17B): 10 minutes of 100Hz, 4 times over the course of 1 hr but with the red LED active instead of the blue LED. cFOS response in control cells (Figure 20A) was compared to the responses in ChR2-transduced (Figure 20B) and CheYNA-transduced (Figure 20C) cell cultures. I anticipated minimal activation, as ChR2 is reported to express a “tail” inclusive of 600 nm-NIR in its activation spectrum. When administered in the same oscillation parameters,

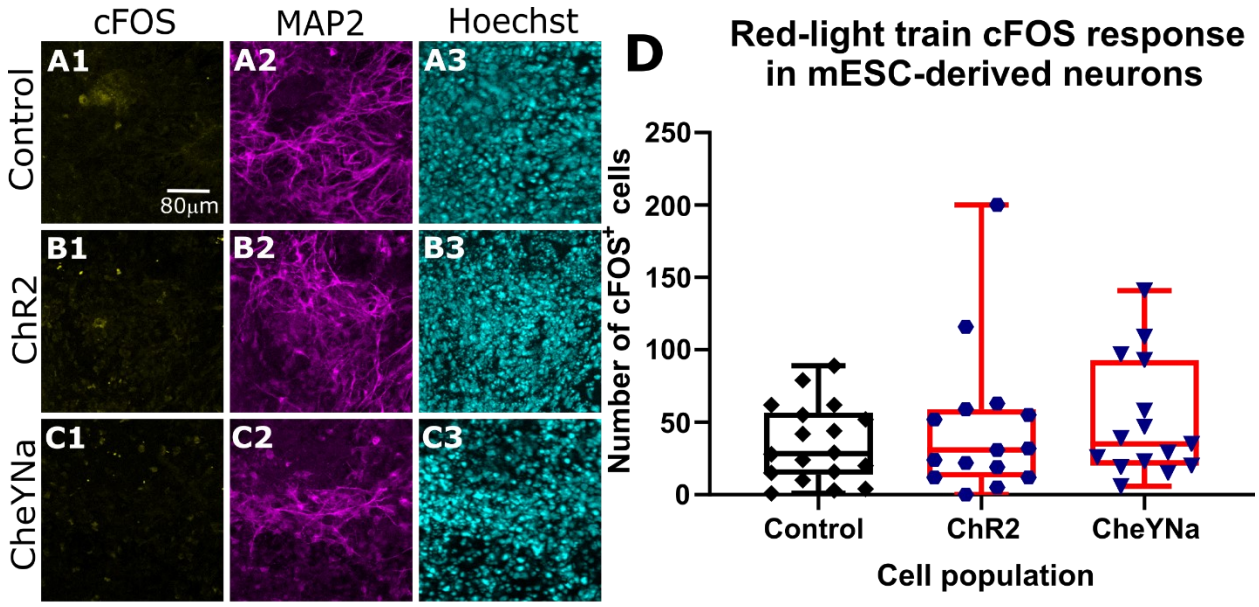

Figure 20. Selective activation of mESC-derived neurons transduced with ChR2 constructs and red light. At DIV 35, optogenetically targeted cells were exposed to the 4 light trains pulsed at 100Hz outlined in Fig 11B over the course of 1 hour except the red LED was initialized instead of the blue LED. Cells were either untransduced (Control, A), expressed ChannelRhodopsin-V134R (ChR2, B), or the CheYNa construct (C) . Thereafter, cells were fixed and immunostained for cFOS (Col. 1), MAP2 (A4) (Col. 2), and DAPI (Col. 3). Z-stack mages were acquired via confocal and cFOS images were processed semi-automatedly in each stack with a batch cell counter macro in ImageJ. (D) Analysis of cFOS+ cells from ICD confocal acquisition. cFOS was unchanged between all groups and was not upregulated in response to 100Hz red light. Analysis was performed with a one-way ANOVA followed by a Kruskal-Wallis post-hoc test. Asterisks above box plots indicate comparison to control whereas asterisks above solid black bars indicate between groups. Error bars representative of 99% CI, N=15

however, the red LED does not elicit a significant cFOS response in either optogenetically targeted culture (Figure 20D). A slight trend appears in cFOS activation with regards to CheYNa-transduced cultures. Following these experiments, monomeric NpHR activation was tested by administering constitutive red light to NpHR-transduced cultures. It was evident from the TTX-treated cells (Figure 15E) that a prolonged treatment time is necessary to diminish the cFOS signal in these cell populations. I recapitulated these parameters by exposing NpHR-transduced cultures to 3 hours of sustained red LED exposure. The continuous red light, in theory, would mimic the continuous presence of TTX and should downregulate cFOS expression. cFOS response in control cells was assessed against NpHR-transduced (Figure 21A) and NpHR-transduced co-incubated in 100 mM glutamate (Figure 21B). When exposed to constitutive red LED exposure for 3 hours, the cFOS signal was not significantly elevated in NpHR-transduced cell population in comparison to the wild-type 3-hour control, suggesting no inhibitive effect on cell cultures (Figure 21C). Furthermore, this effect is exacerbated by the

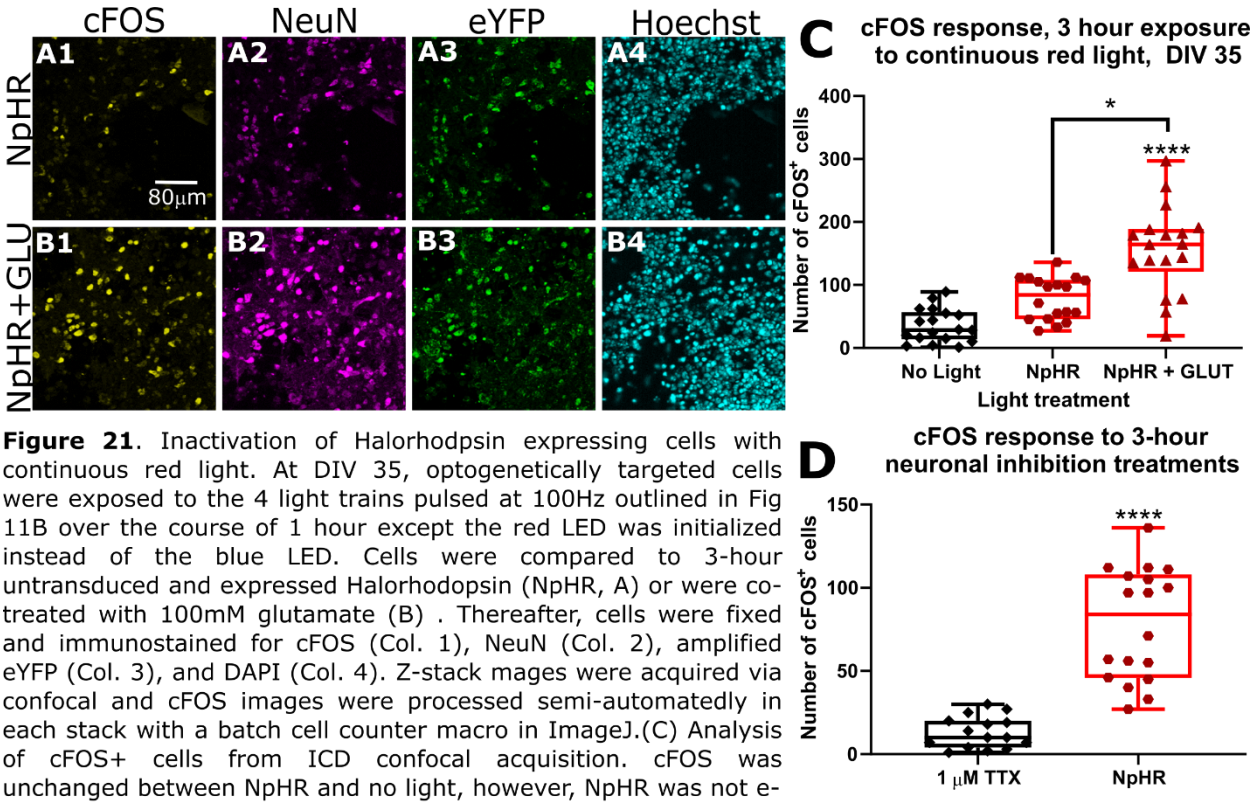

Figure 21. Inactivation of Halorhodpsin expressing cells with continuous red light. At DIV 35, optogenetically targeted cells were exposed to the 4 light trains pulsed at 100Hz outlined in Fig 11B over the course of 1 hour except the red LED was initialized instead of the blue LED. Cells were compared to 3-hour untransduced and expressed Halorhodopsin (NpHR, A) or were co-treated with 100mM glutamate (B) . Thereafter, cells were fixed and immunostained for cFOS (Col. 1), NeuN (Col. 2), amplified eYFP (Col. 3), and DAPI (Col. 4). Z-stack mages were acquired via confocal and cFOS images were processed semi-automatedly in each stack with a batch cell counter macro in ImageJ.(C) Analysis of cFOS+ cells from ICD confocal acquisition. cFOS was unchanged between NpHR and no light, however, NpHR was not e-nough to prevent glutamate-mediated upregulation of cFOS compared to Control (+130 cells) and NpHR alone (+73 cells). Analysis was performed with a one-way ANOVA followed by a Kruskal-Wallis post-hoc test. (D) NpHR-transduced cells were compared by Mann-Whitney ranked parametric t-test against 3-hour TTX treated cells from Fig 9E, demonstrating that NpHR activation does not prevent cFOS expression (+59 cells). Asterisks above box plots indicate comparison to control whereas asterisks above solid black bars indicate between groups. *-p-val<0.05, ****-p-val<0.0001 Error bars representative of 99% CI, N=17

addition of 100 μM glutamate in comparison to both the control and the NpHR group (Figure 21C). To compare further divulge if NpHR's effect was inhibitive, cFOS response in 1 μM TTX was compared to that in NpHR (Figure 21D). NpHR treated groups exhibited significantly more cFOS than those in 1 μM TTX by approximately 4-fold (Figure 21D). While this effect is difficult to interpret, however, I speculate that NpHR activation might have included a subset of inhibitory neurons and then their release from inhibition might have activated a small percentage of non-transduced cells that eventually activated c-FOS. In any instances, the red light seems to exert a response specifically and significantly and thus indicates that the channel is correctly driven. It is plausible that NpHR's excitation spectrum does not optimally coincide with the red LED's emission spectrum and thus NpHR may open partially/shut randomly thereby generating a "rebound' potential (Mattingly et al., 2018; Yizhar, Fenno, Davidson, et al., 2011).

Finally, to assess whether multiple LEDs can be used simultaneously, the Arduino was programmed to give alternating oscillations of blue and red LED activation (Figure 22A). This contraphasic switching between red and blue LEDs was measured again via oscilloscopy (Figure 22A) and verified that the microcontroller is efficient in driving 100 Hz oscillations while switching between blue- and red-LED activation; the base frequency

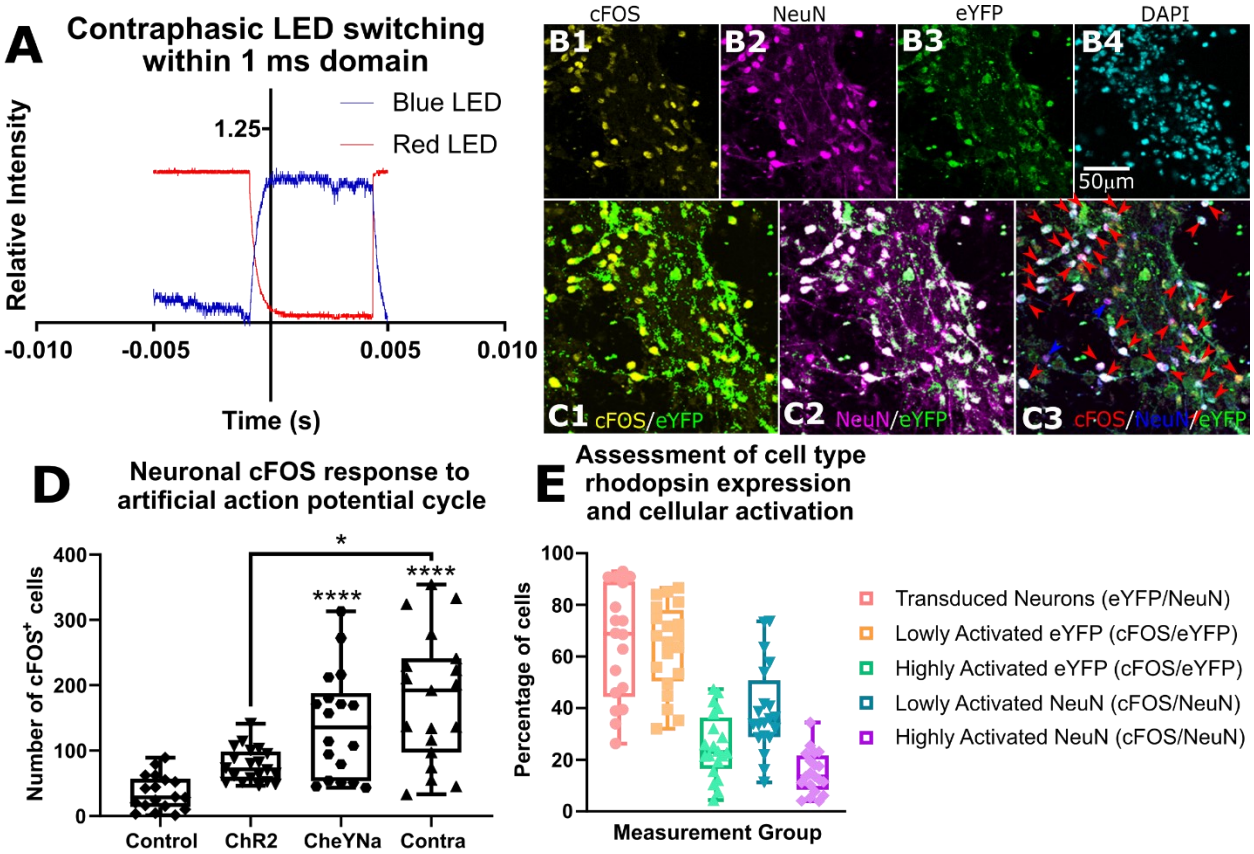

Figure 22. Contraphasic activation of CheYNa-transduced mESC-derived neurons. (A) Oscilloscopic assay for temporal fidelity of contraphasic switching between red and blue LEDs at 100Hz; during 10 ms, the red and blue LEDs inverse states completely and in parallel within 1 ms while maintaining their respective square phase. At DIV 35, optogenetically targeted cells were exposed to 4 light trains pulsed at 100Hz outlined in Fig 11B over the course of 1 hour except utilizing both blue and red LEDS in the contraphasic pattern (A). Cells were either untransduced or expressed the CheYNa construct (B) . Thereafter, cells were fixed and immunostained for cFOS (Col. 1), NeuN (Col. 2), amplified eYFP (Col. 3), and DAPI (Col. 4). Their coexpression was assess-ed by visual analysis in (C1-3) only in CheYNA cells stimulated with contraphasic light; red arrows indicate $cFOS^+/NeuN^+/eYFP^+$ cells (C3). Z-stack mages were acquired via confocal and cFOS images were processed semi-automatedly in each stack with a batch cell counter macro in ImageJ. (D) Compared to the control (No Light) and ChR2, CheYNA-expressing cells stimulated with contraphasic red and blue lights (Contra) expressed more cFOS (+148 cells, +122 cells, respectively). cFOS response was unchanged however between 100Hz blue light in CheYNa and Contra. Analysis was performed with a one-way ANOVA followed by a Kruskal-Wallis post-hoc test. Asterisks above box plots indicate comparison to control whereas asterisks above solid black bars indicate between groups. *p-val<0.05, ****-p-val<0.0001 Error bars representative of 99% CI, N=19. (E) Additional assessment of transduced neurons, cFOS expression lowly expressed across transduced cells, cFOS expression highly expressed across transduced cells, cFOS expression lowly expressed across NeuN-expressing cells, and cFOS expression highly expressed across NeuN-expressing cells. N=18

is highly conserved between cycles and further both waves exhibit a fine degree of delineation during deactivation contrary to the others' respective activation (Figure 22A). After verification that both LEDs could be activated contraphasically and with a microsecond degree precision, I attempted to recapitulate action potentials. CheYNa-transduced cells (Figure 22B-C) were given contraphasic blue and red light. As demonstrated previously (Kleinlogel et al., 2011), the ChR2-eYFP-β-NpHR allows for precision control over membrane potential and in theory has the capacity to artificially moderate an action potential cycle in neurons. Though it is known that neurons will hyperpolarize autonomously, it is also known that their capacity for re-firing is diminished post ChR2-mediated AP possibly to due to an imbalance in expressed inward potassium channels (Aravanis et al., 2007). CheYNa-transduced cells were exposed to 100 Hz of blue-LED oscillations and in contraphase, 100 Hz of red-LED oscillations for 10 minutes, followed by 5 minutes of rest; this pattern was repeated 4 times. I hypothesized that contraphasic exposure of CheYNa-transduced cells would produce an increased cFOS response as the red light would facilitate re-hyperpolarization after depolarization. When compared with no light control as well as ChR2-transduced cells stimulate with 100Hz blue light, dual contraphasic exposure elicited 6.6 times and 2.7 times greater responses (Figure 22D). Furthermore, it is clear from immunocytodetection that almost all transduced neurons have been activated under contraphasic conditions (Figure 22C). Though it cannot be stated completely that more frequent and successful action potentials were generated by contraphasic light, it seems that a constructive interaction is produced which supersedes blue light alone in monomeric ChR2 (Figure 22D). These results augment the performance value of the device, in that dual activation of discreetly excited channelrhodopsins is supported by the incorporated LEDs and microprocessor.

CHAPTER V: Optogenetically targeted activation of mESC-derived neurons for the purpose of future experiments (Discussion)

I first validated mESC-derived neurons with a battery of functional maturity assessments including live Ca^{2+} signaling, cFOS response to glutamate, glutamine, bicuculline, and TTX, electrophysiological patch clamp recordings with the help of Gianluca Pietra, and microfluidic chamber transsynaptic activation. Like previous reports (Barth et al., 2014; Streckfuss-Bömeke et al., 2009; Tong et al., 2010), I found that neurons derived from mESC populations could differentiate into functional neurons if grown until ~DIV 35 with corresponding media and supplement changes along the maturation process. This included incorporating 20 ng/ml of BDNF and 500 μM of ascorbic acid from DIV 11 until the end of the experiment and supplementing 500 nm Retinoic Acid starting from DIV22-25 depending on the state of projections in culture. Both BDNF and retinoic acid have been demonstrated as contributory to the upregulation of voltage-gated sodium channels and functional maturity from development to adult neurons (Diss et al., 2008; Leng et al., 2009). Furthermore, it is known that *in vitro* models risk increased ROS generation because of their xenobiological environment (Halliwell & Whiteman, 2004). This is counteracted in part by antioxidative compounds in the N-2 supplement to promote mitochondrial integrity, but they are absent at DIV 11 when N-2 is removed to promote differentiation, thus requiring additional pro-mitochondrial supplement. With the addition of these three molecules, I noticed a significant increase in cell culture health, neurite outgrowth, and ultimately an increase in voltage gated sodium inward sodium current at DIV 35 compared to those cultures BDNF or Retinoic Acid (none was observed). Having further demonstrated that Ca^{2+} signals could be modulated by 1 μM TTX addition, that 100 μM glutamate or 20 μM bicuculline could elicit an increase in cFOS, and that approximately 60% of patched cells exhibit inward sodium currents, I inferred that my mouse neuronal cultures were functional as demonstrate previously (Tong et al., 2010) and were suitable for optogenetic stimulation.

The OPAL provides a platform on which mESC-derived neurons may be stimulated to express cFOS under physiological conditions

In comparison with their counterparts (Elena et al., 2016; Gerhardt et al., 2016; Repina et al., 2020), the OPAL offers several unique advantages which commercial devices and previous open-source devices do not. The three overlapping advantages include: (1) the ability to directly program virtually any desired pattern of LED switching frequency thereby adaptably accommodating to diverse ranges biologically based needs; (2) a triad of LEDs whose individual activations can concatenate, overlap, or deactivate with respect to the others' activation and attenuating performance; and (3) the device requires low power, minimal cooling, and operates wirelessly thereby providing a safe, easily integrable, and scalable tool for established laboratory settings. The design is compact and ergonomic, minimizing the cost of materials and potentially maximizing experimental throughput efficiency. Because of its size and its lack of external cables, several to tens of OPAL devices could execute different light paradigms or many individual experiments simultaneously. This gives a unique advantage compared to the Axion system (Clements et al., 2016) as only one interface may perform one unique experiment at one time unless many interfaces are present and operating individually. Furthermore, the OPAL is battery-operated and requires a common 9V battery to perform up to 24 hours contiguously in the on state in the incubator. This allows long term, continuous cellular experiments disturbing the OPAL or culture infrastructure. In comparison to those open-source devices found in the literature (Gerhardt et al., 2016; Repina et al., 2020), the OPAL has been directly shown to stimulate transduced neuronal populations with a variety of complex signaling patterns (Figure 18D, Figure 22D) which are only limited by the programming skills of the user. Furthermore, the OPAL can stimulate dual-expressed channelrhodopsins (Figure 22C-D) with discreet excitation spectra, a novelty upon which has been speculated but not yet shown in *in vitro* optogenetic literature. It should be noted that Figure 22E demonstrates that not all CheYNa-transduced cells express cFOS at a high level after stimulation. Furthermore, an even smaller number of $NeuN^{+}$ cells express cFos at both low (signal threshold in 8-bit images set to 20) and at high levels (threshold = 60). This may account for the variability in samples as well (Figures 18-22) that perhaps not all cells are neuronal, however, removal of

statistical outliers does not affect significance in the overall effect in any of the groups analyzed. It may instead be more reasonable to consider that cFOS expressing cells may be neurons but not expressing NeuN as NeuN expression is not present in all mature neurons (Ambrogini et al., 2004). NeuN is upregulated in immature neurons but its constitutive expression after maturation is present only in a subset of neurons (Gusel'nikova & Korzhevskiy, 2015). Speculatively, a combination of other neuronal markers or transitioning channelrhodopsins to neuronal specific promoters (Syn, CamKII, for example) would serve to deconvolute this result and would demonstrate if there is off-target activation or if there is a cell-type specific result that has been acquired.

As studies begin to take a multiplexed approach with channelrhodopsins, it will be necessary to optically partition available "channels" to stimulate differentially optogenetically targeted cell populations coinhabiting the same well, for example, co-culture of PV^+ interneurons expressing ChRimson and $CamKIIa^+$ projection neurons expressing gTaChR. Discussed earlier in the introduction, a majority of available optogenetic devices lack integrated recording ability. Limited by the deficit of an integrated multiple electrode array (MEA), the OPAL does not support real time field potential acquisition from activated neuronal populations and is reliant on genetic or proteinic upregulation of canonical activation path-related factors, like cFOS. In theory, by introducing a third-party MEA system to the optogenetic circuit, it could be feasible to simultaneously record from *in vitro* cultures while inducing light patterns. It can be asserted that in some ways, assaying pancultural transcription or translation is a more direct and robust approach as MEA recordings can exhibit low signal-to-noise ratio (Obien et al., 2015). Furthermore, if a channelrhodopsin protein is not sufficiently expressed either from limited cell-type composition or weak non-constitutive promoter, then the noise can only be exacerbated. This is further amplified by the ever-growing cruciality of cell-types when discussing contributory roles in neuronal circuitry or networks (Yuste et al., 2020) and contemporarily it is not possible to individuate cell types from their field potential dynamics alone via MEA as individual neuronal fields converge rapidly (J. Müller et al., 2015). Ultimately, this precludes the same outcome in that the user must respect both the limitations of the OPAL and the target question, regarding methods of detection. For the time

being, the OPAL is a robust method to stimulate general populations within a mixed-type neuronal culture to study network-related dynamics.

Future advancements and prototypical drawbacks of the OPAL

Prospectively, short-term developments of the OPAL include a user-friendly GUI whereby researchers may simply "draw" their experiments on a virtual representation of the platform grid. Upgrading the interface from cold script in Arduino to more "intuitive" design would greatly increase the scope of users. Additionally, compartmentalizing the circuitry to a PCB would shorten time of assembly as it would eliminate the need to solder LED connections. Longer-term prospects include widening the array of LEDs, scaling grid sizes for larger or smaller culture plates (between 6 and 96 wells) for generalized photobiological applications requiring robust sample quantity or high-throughput single-cell assessment. Finally, incorporation of MEA and/or CMOS detectors per individual well to allow for real-time monitoring, acquisition of population signal, and/or fluorescent reporter dynamics.

Tentatively, this platform could also be used to assess activity-mediated post translational modifications of dynamic, disordered proteins within the context of neurodegenerative models, neurogenesis models in human iPSC-derived neurons, or with cancer cell lines as a diagnostic tool for personalized medicines. More generally, it could be applied to investigate chloride signaling in developmental models, photobiological studies in prokaryotic models, light-mediated protein degradation or uncaging, rapid assessment of novel channelrhodopsins a priori *in vivo* investigations, and high throughput study of signaling dependent pathways. Based on the results presented above regarding NpHR cultures, however, I cannot declare definitively that NpHR, an "orange"-wavelength-activated channelrhodopsin, is compatible with the OPAL. Speculatively, when expressed, a continuously opened chloride gate could non-specifically inhibit glutamatergic/GABAergic cells or activate transient, chloride-sensitive neural progenitor (Alfonsa et al., 2015). This protocol estimates ~8% GABAergic neuron culture composition around DIV 20 (Bertacchi, Pandolfini, et al., 2015) though BIC

stimulation induces cFOS expression in culture. Given that the cells in these experiments remain an additional two weeks, it may be possible that the GABAergic population increased. An increase in GABAergic cell population and ubiquitous expression of NpHR under the EF-1a promoter would further explain why the red-LED conditions induce cFOS like BIC. However, the total number of GABAergic neurons were not quantified at this stage and it is more plausible that NpHR's excitation spectrum does not optimally coincide with the red LED's emission spectrum. Thus NpHR may not shuttle chloride ions continuously, thereby generating a "rebound' potential, an action potential generated autonomously during depolarization from negative potentials with a value less than -70 mV (Mattingly et al., 2018; Yizhar, Fenno, Davidson, et al., 2011). Furthermore, it has more recently been demonstrated that constitutive light exposure in optogenetic experiments may alter activation signals varyingly (Owen et al., 2019). And while the results regarding contraphasic blue- and red-light stimulation are congruent with my original hypothesis that a light paradigm mimicking the action potential would elicit higher cFOS response in comparison to ChR2 alone, validating the surmised action potential via electrophysiology would have increased the strength of this statement. Further use of the CheYNa construct for dual light exposure would be benefitted by a more direct assessment with contraphasic light.

I report that the OPAL is very suitable for direct, literarily relevant modes of stimulation. This mode of light-mediated activity in neuronal cultures is cohesive with past literature; blue-light in optogenetically targeted cultures facilitates a large enough membrane current to elicit an action potential, upregulates cFOS within the neuronal networks, and that the cFOS effect is ablated by voltage-gated sodium channel blocker, TTX. Through development of the OPAL, I have aimed to fabricate a device whose light-sources parallel the wide range of commercially available channelrhodopsins while still appealing to higher-order functionality demonstrated in other neurobiological signaling models. Optical data from the light sources and testing a small array of channelrhodopsins within my neuronal models allude that the OPAL is an efficient, fidelitous, and adaptable device that provides new avenues for light-signaling *in vitro* optogenetic neuronal investigations.

Section II: Hippocampal neurogenesis and the dentate gyrus

CHAPTER VI: Introduction to the hippocampus and its role in adult neurogenesis

Overview of the hippocampus

To understand molecular mechanisms in human neuronal compartments, I first undertook establishing a novel model of the human hippocampus. The hippocampus is a duplicitous hemispheric complex most often associated with spatial memory and contextual memory consolidation. It forms a network of circuits in the mature brain, is more classically associated with the temporal lobe and limbic system but has more recently been divulged as a multiplexed integratory processing unit. It receives efferent connections from the lateral entorhinal cortex, medial entorhinal cortex (Rutecki et al., 1989), septum, parahippocampal formation, retrosplinial cortex (Sugar et al., 2011), neocortex (Schwerdtfeger, 1979), ipsi- and contra- lateral amygdala (Yang & Wang, 2017), thalamus, putamen, cingulate bundle, fornix, and contralateral hippocampus (Maller et al., 2019; Witter, 2010) though the fornical and entorhinal cortical pathways are considered the dominant pathways (Gaskin & White, 2013). Infrastructurally, the abundance of reciprocal hippocampocortical networks give rise to the "bit-depth" of episodic memories (Cooper & Ritchey, 2019) as it simultaneously processes incoming spatial information from the entorhinal cortex and emotional information from the amygdala (Gaskin & White, 2013). More historically, the hippocampus is associated with spatial awareness as it hosts "places cells," or neuronal networks associated with orientation in space (O'Keefe, 1976; Thompson & Best, 1990). Together with the entorhinal cortex, the hippocampus integrates these signals to interpret an organism's conformation in space-time (Fyhn et al., 2004) by explicit field rotation of grid cells in the entorhinal cortex (Fyhn et al., 2007). The hippocampus does not only serve as a relay for emotional (Hitti & Siegelbaum, 2014) and spatial information from external regions but is intrinsically wired throughout its layers (M. W. Jones & Mchugh, 2011; Lisman, 1999). These internal connections are argued to sustain internal computation for filtering and processing extraregional inputs (Stepan et al., 2015; Wiebe & Stäubli, 1999) before the signal is forwarded to the subsequent destination (X. Zhang et al., 2020) at least regarding spatial information. Because

its reciprocal pathways are highly integrated within the brain connectome, the hippocampus is imperative to multidimensional memory formation (Gava et al., 2021) and arguably render the region more susceptible to pathological insult, driven internally (Abdelmalik et al., 2005; Q. G. Zhang et al., 2013) or downstream from preceding regions (Cope et al., 2018; Gail Canter et al., 2019) like the entorhinal cortex discussed in the previous section (Andorfer et al., 2003; Hardy & Higgins, 1992). Furthermore, it is a particularly sensitive region to age related deficits reflected not only in cognitive decline but also in the inflexibility of older place cells and their inability to adapt to new environments (Wilson et al., 2004). The hippocampus' sophisticated network of afferent and efferent projections facilitates important spatial information processing after development, but the infrastructure is encoded during embryogenesis.

Hippocampal embryogenesis

Spatial processing and place encoding is not a mammalian uniquity and structures like the hippocampal formation in aviaries or medial pallium in reptiles and teleost (Wullimann & Mueller, 2004) are responsible are responsible for navigation and contextual memory in their respective host. The hippocampus is derived from the medial pallium, an embryonic structure found in most vertebrates which gives rise to the allocortex (Salas et al., 2003). During embryogenesis, the invaginated telencephalon subdivides molecularly into the pallium by Pax6 and Tbr1 and the subpallium by Dlx2 and Nkx2-1 between E9.5-10.5 in mice (Puelles et al., 2000). The pallium is then further subdivided into the cortical hem, the medial pallium, the dorsal pallium, and lateral pallium which forms the ventral pallial border via sustained Dlx2 expression (Qiu et al., 1995). The cerebral cortex and hippocampal or dentate gyrus primordium are encoded within the medial pallium, speculatively in the ventral-medial and dorsal-medial pallium, respectively. These two regions are molecularly demarcated by Emx2 (Pellegrini et al., 1996) but requires conserved Pax6 signaling to further differentiate the dentate gyrus primordium (Kimura et al., 2005). It is commonly known that intraregional signaling moderates development and indeed, a local Wnt reservoir in the cortical hem drives early

hippocampal development until E9.5 in mice (Grove et al., 1998) while contributes to further hippocampal differentiation (Machon et al., 2007). Cortical hem-derived Wnt3a activates canonical b-catenin signaling and is thought to serve as the hippocampal organizer (S. M. K. Lee et al., 2000) though more recent evidence suggests that signaling between the two regions is bilateral and zinc-finger protein-mediated (Rosenthal et al., 2012). Zinc-finger protein families are implicated in hippocampally relevant Wnt actuation as Smad-interacting protein-1 has also been shown to ablate the hippocampus via absent noncanonical Wnt signaling at E12.5 in mice (Miquelajauregui et al., 2007). Regardless of formal hippocampal organizer, it is evident that Wnt signaling is nonetheless necessary to further propagate the hippocampal formation as lymphoid enhancing binding factor 1 and LIM homeobox binding domain proteins, downstream transcription factors of b-catenin pathway, are upregulated at E14.5 and E16.5 in mice (Abellán et al., 2014). Finally, after the critical window of fate locking for the hippocampus, late stages of fetal hippocampus development is regulated by chemokine pathways, specifically through CXCR4 (Lu et al., 2002). A different mechanism seems to control internal layering of the hippocampus however, as excision of vicinal embryonic structures like the cortical hem do not alter layering pattern (Tole & Grove, 2001).

Layering within embryonic hippocampal formation

Within the hippocampal primordium, three epithelial subsections diverge: the ammonic, the primary dentate, and the fimbrial, wherein the ammonic neuroepithelium is vicinal to the cortical hem, the dentate neuroepithelium dorsal to the ammonic, and the fimbrial glioepithelium dorsal to the dentate (Altman & Bayer, 1990c). The ammonic and primary dentate give rise to neurons in the Ammon's horn/Cornu ammonis (Altman & Bayer, 1990b) and Dentate Gyrus and hilus, respectively (Altman & Bayer, 1990a), while the fimbrial instead form glia which support the fimbria-fornix pathway (Barry et al., 2008). Within the cornu ammonis, there exist 3 principal fields: the CA1, CA2, and CA3. All three fields are comprised primarily of pyramidal neurons though their developmental tempo and mature neuronal morphology are varied (Lein et al., 2005). Purportedly, CA3

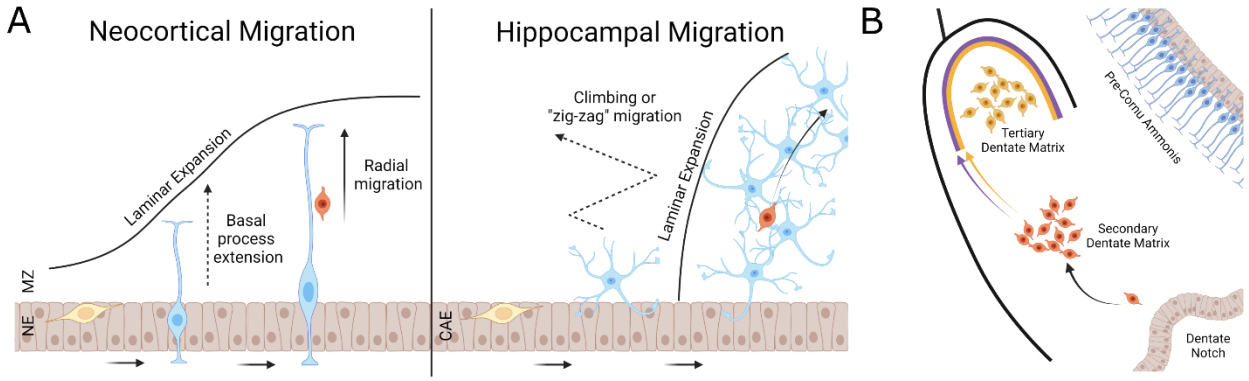

Figure 23. Embryogenic layering of the hippocampus. (A) The neocortex is formed during embryogenesis by radial migration, in which neuroepithelial cells migrate from the subplate by extension of radial processes into the medial zone. Progenitors then undergo direct transit toward target layer and gradually expand outward, giving rise to the diverse lneocortical laminae sequentially. The hippocampus is instead populated by climbing or zigzag migration in which the preliminary expansion stem cells, called 'pioneer cells,' do not directly extend their basal processes but instead somatically tranlocate in a climbing or 'zig zag' conformation. They then populate outwardly, using the previous pioneer cell as an anchor, growing in parallel to the pial surface. The outer shells of both the dentate gyrus and cornu ammonis form like this to create the scaffold for the somatic layer. At later embryonic stages in the cornu ammonis, migratory precursors may travel along this bridge like formation of pioneer cells to populate the inner pyramidal layer and rely on radial migration for this. (B) The dentate gyrus however, undergoes radial migration first during expansion from the dentate notch, where cells enter the secondary dentate matrix and remain for 3-7 days before continuing to the tertiary matrix. Cells not migrating populate the subgranular zone. Cells in the tertiary matrix then migrate first (violet arrow) to populate the outer shell (violet line) of the granule cell layer, then proceed (yellow arrow) to populate the inner shell of the granule cell layer. Cells which migrate late into the tertiary matrix consitute the hilar. Figure adapted from text of Altman & Bayer, 1990a.

precursors undergo radial migration from the ventricular zone to the hippocampal plate whereas CA1 precursors migrate in a zig-zag or “climbing” orientation (Kitazawa et al., 2014) along a horizontal projection (Figure 23). This horizontal projection gives rise to the curvature of the cornu ammonis as the ammonic neuroepithelium deploys precursors along horizontal radial glial projection tracts in an end-point assembling manner (Xu et al., 2014). Interestingly, CA3 precursors are the first to begin migration and are followed by CA1-destined migratory precursors less than 2 days later in rats (Bayer, 1980a) however the incorporation of CA3 precursors into the stratum pyramidale and CA3 endpoint formation are delayed. Both CA1 and CA3 migratory precursors become multipolar, however, CA3 cells born at E12.5 remain in the multipolar cell accumulation zone for up to 4 days, whereas CA1 cells born between E14-E16 tend to migrate gradually and consistently (Nakahira & Yuasa, 2005). Both the delay in CA3 formation and the prolonged pause of multipolar CA3 cells in the multipolar cell zone were thought to temporally match the delay in the dentate gyrus formation (Gaarskjaer, 1985) and later confirmed that CA3 principal neurons are temporally selective in synaptic connections between CA1 or DG (Deguchi et al., 2011). These fields are molecularly distinguishable from each

other, starting from E12.5 in mouse, as the pre-CA3 exclusively expresses kainite receptor, Grik4, and the pre-CA1 expresses POU3F1 (Grove & Tole, 1999) though matured identity assumption begins from opposing subicular/dentate poles and moves gradually inward (Tole et al., 1997).

Development of the dentate gyrus on the other hand, peaks around E16 in mice (Angevine, 1965) which begins as a migratory stream from the dentate notch followed by radial migration at E18 (Nakahira & Yuasa, 2005). A minority of granular cells are generated in the dentate gyrus neuroepithelium and instead the migration from the dentate notch first leads to the establishment of the secondary dentate matrix (Altman & Bayer, 1990a); granular cells that mature early in the secondary matrix later constitute the outer sublayer of the suprapyramidal blade followed by the infrapyramidal blade of the granular cell layer by E18.5 in mice (Seki et al., 2014). From the secondary dentate matrix, precursors begin to express radial glial markers (Eckenhoff & Rakic, 1984; Rickmann et al., 1987; Sievers et al., 1992) and will either progress to form the tertiary dentate matrix or will remain to populate the subgranular zone (Altman & Bayer, 1990a). Once established in the tertiary matrix, radial migrators continue along $Reelin^{+}$ tracts (Stanfield & Cowan, 1979), coordinated to give rise to $NeuroD^{+}/Prox1^{+}$ populations in the granule cell layer and $NeuroD6^{+}$ cells in the hilar (Pleasure et al., 2000). Once the hilar and granule cell layer form, the CA3 terminates development through CXCL12/Cxcr4 signaling in the subpial hilum, finalizing the formation of the subgranular zone and completing embryonic development (G. Li et al., 2009). Ultimately, the CA1, CA2, CA3, dentate gyrus, and hilar become molecularly distinct from each other at endpoint layering (Lein et al., 2004) (Figure 24). Despite extensive study into the development of separate layers, the CA2 remains anomalous in its development (Dudek et al., 2016) though has recently been shown to organize around mossy fibers (Fernandez-Lamo et al., 2019). It also hosts the most diverse hippocampal interneuron population (Botcher et al., 2014) despite its restricted proportion in the striatum pyramidale (Grove & Tole, 1999). Although this completes the current field of embryonic development of the hippocampus, transsynaptic refining and maturity continue in postnatal stages, dependent primarily upon stellate projection neurons in layer II of the medial entorhinal cortex (Donato et al., 2017).

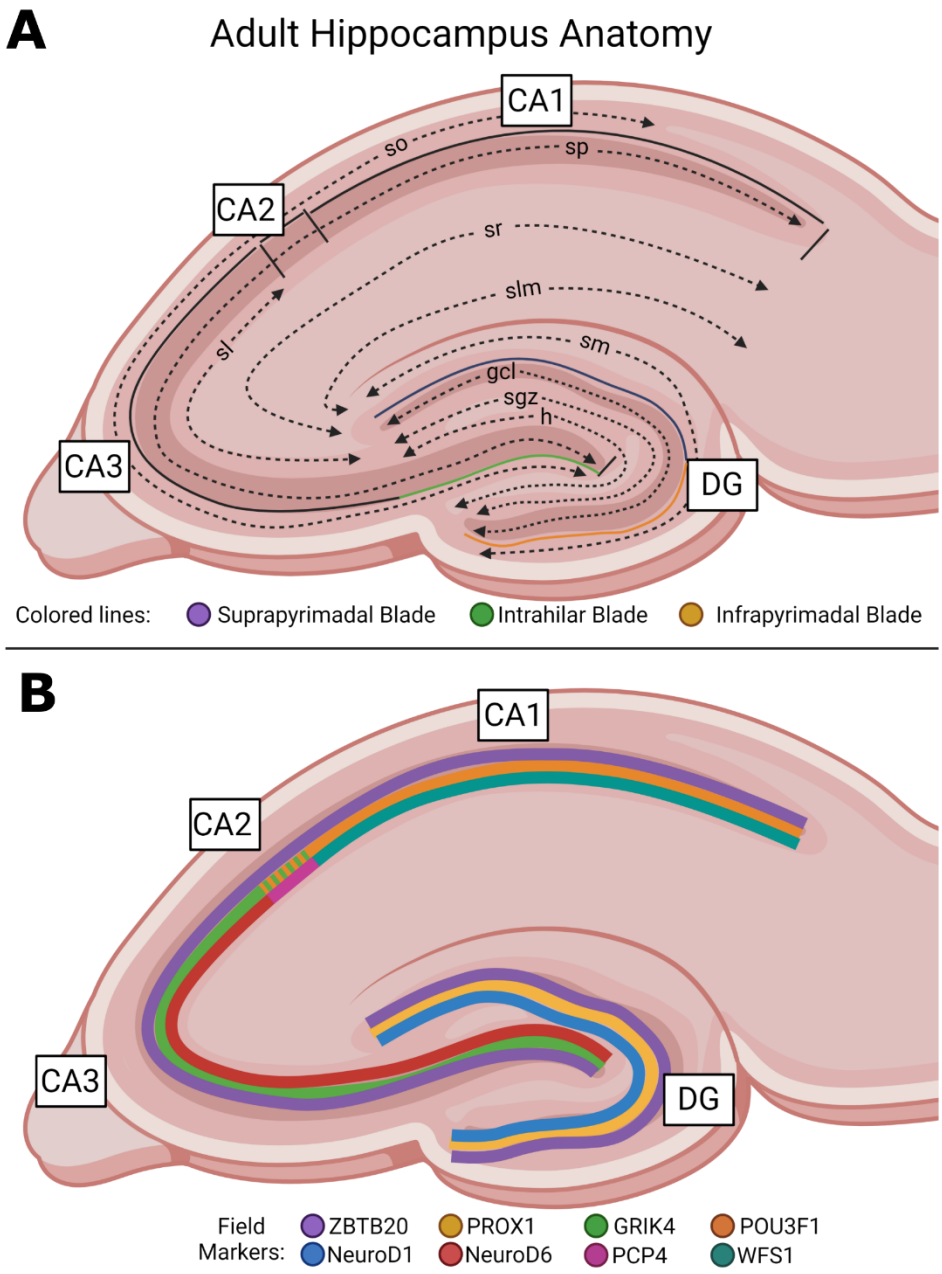

Figure 24. Hippocampal field and layer anatomy in the adult hippocampus. (A) Depiction of the Cornu Ammonis (CA) fields 1,2, and 3 as well as the Dentate Gyrus (DG) and the somatic layers that comprise their anatomy. For developmental refrence, the suprapyramidal, intrahilar, and infrapyramidal blades have been labeled in the legend. Abbreviations for layers are as follows: stratum oriens (so), stratum pyramidale (sp), stratum radiatum (sr), stratum luciderm (sl), stratum lacunosm moleculare (slm), stratum moleculare (sm), granular cell layer (gcl), subgranular zone (sgz), and hilar (h). The pink, unlabeled boundary between the sm and slm represent the hippocampal fissure. (B) Molecular identifiers of postnatal hippocampal regions, as defined by previous literature. Colored bands do not necessarily represent individual layers depicted in A but instead correspond to the hippocampal field in which they extend. ZBTB20 extends pan-hippocampally as depicted from Mitchelmore et al., 2002, Nielsen et al., 2007, Nielsen et al., 2010, and Nielsen et al., 2014. The figure is otherwise adapted from Grove et al., 1999, Tole and Grove, 2000, Sarkar et al., 2018, and Dudek et al., 2014.

Parahippocampal implications for hippocampal development

The hippocampus, or hippocampal formation, is constituted not only by the cornu ammonis and dentate gyrus but also conventionally includes the medial entorhinal cortex, lateral entorhinal cortex the presubiculum, the parasubiculum, and the subiculum (Figure 25)(Bayer, 1980b). Whether each region is derived from the hippocampal neuroepithelium is not clear. Speculatively, the greater subiculum is derived from a

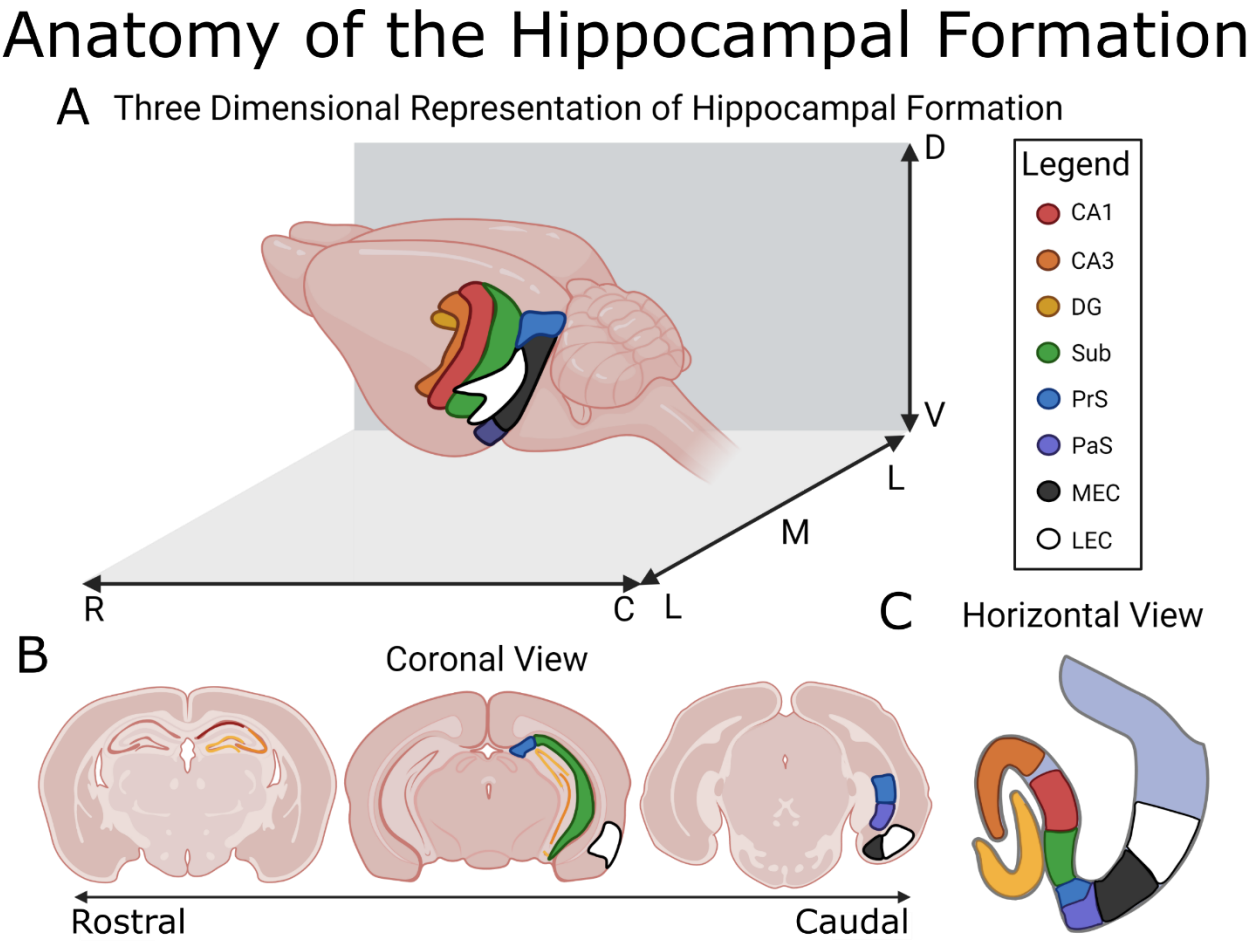

Figure 25. Spatial representation of the regions in the hippocampus. (A) Three dimensional (Rostral (R) <> Caudal (C), (Lateral (L) <> Medial (M) <> Lateral, and Dorsal (D) <> Ventral (V)) rendering of the hippocampal formation fields, locations are ventral to the outer neocortex. Hidden borders indicate representative depth in comparison to the other layers. (B) Coronal section representation of the HF fields in reference to their rostral-caudal position. The full CA and DG fields are visible more rostrally whereas the entorhinal cortex and subicullar fields are more visible in caudal sections. (C) A horizontal or axial cut across the HF regions to demonstrate their approximate proximity to each other. Figure adapated using the Allen Brain Atlas, *Hippocampal Formation* by Cappaert, Van Strien, and Witter, and *Atlas of the Developing Mouse Brain 2nd edition*, by Paxinos, Watson, Kassem, and Halliday 2020. Legend indicates region corresponding to color: CA1 (Cornu Ammonis 1), CA3 (Cornu Ammonis 3), DG (Dentate Gyrus), Sub (Subicullum), PrS (Presubicullum), PaS (Parasubicullum), MEC (Medial Entorhinal Cortex), LEC (Lateral Entorhinal Cortex).

neuroepithelium contiguous with the ammonic neuroepithelium but with regards to the entorhinal cortex, the epithelial origin is not known (Bayer, 1980b). However, the entorhinal cortex is paleocortical and programmatically develops radially albeit in "sandwich" or inverted orientation compared to that of the neocortex (Y. Liu et al., 2019). Instead the possibility exists that both arguments hold validity and evidence alludes that multiple neuroepithelia contribute to the formation of the entorhinal cortex (Ramsden et al., 2015) though this remains to be fully explored. Extracortical lamination is not the only implication of hippocampal development as is well known that the subgranular zone, the adult neurogenic niche of the hippocampus is formed in parallel and because of dentate gyrus formation (Amaral et al., 2007). The full extent of subgranular niche maintenance is not known but recently and intriguingly, neural stem cells (NSCs) that contribute to embryogenic neurogenesis are molecularly distinct from adult NSCs. Furthermore, they are fated differently via Hopx signaling during early development, indicative that adult hippocampal neurogenesis is programmed in fetal stages (Berg et al., 2019). While Hopx has been demonstrated as a DNA-binding protein necessary for cardiac myocyte differentiation (F. Chen et al., 2002), it's function in neural tissue remains largely unknown. Besides serving as molecular identifier between subventricular zone (SVZ) and subgranular zone (SGZ) radial glia (RG) (D. Li et al., 2015), Berg et al 2019 suggests that Hopx maintains chromatin accessibility by maintaining self-renewal-related transcription factors including Zbtb18 and Bcl6 (Berg et al., 2019). As adult neurogenesis and hippocampal neural progenitor self-renewal is a prominent field in hippocampal investigations and a facet explored here within, this thesis proceeds to introduce the field as it stands.

Adult hippocampal neurogenesis

While not all species of animals develop a hippocampus, most exhibit an orthologous compartment dedicated to spatial and working memory processing (Salas et al., 2003), as this phenomenon assumedly requires newborn neurons (Altman, 1962; Altman & Das, 1965, 1969). The prior studies from Altman and Das demonstrate the earliest findings of adult neurogenesis in the brain, prolonged hippocampal neurogenesis

itself has been studied extensively since the observation of newborn neurons in the canary vocal center (Alvarez-Buylla & Nottebohm, 1988; Goldman & Nottebohm, 1983). Neurogenesis is not unique throughout the animal kingdom, as it is fundamental to both vertebrate and invertebrate embryogenesis and consequently the development of the nervous system (Ramón y Cajal, 1930). The true novelty of the hippocampus compared to most other brain regions is its ability to maintain neurogenesis past fetal development and well into adulthood. While the exact driver and function of neurogenesis is not clear (Kitabatake et al., 2007), it is strongly argued that mammalian neurogenesis is a function of memory formation (Schmidt-Hieber et al., 2004) and consolidation postnatally (Alam et al., 2018). It has more recently been implicated considering the neurogenesis' bidirectional relationship with LTP (Bruel-Jungerman et al., 2006; X. Zhao et al., 2003). Adult neurogenesis has been demonstrated as an evolutionarily conserved phenomenon (Harzsch & Dawirs, 1996) and its continuation in the hippocampus pervades many mammalian species including rat (Kuhn et al., 1996), mouse, nonhuman primate (Kornack & Rakic, 1999), and human (Eriksson et al., 1998). Hippocampal neurogenesis in a broader scope has been demonstrated to be a strictly regulated process, however, many environmental and molecular pathways have been demonstrated to actively contribute to adult hippocampal neurogenesis. Environmental and physiological factors include stress (Mirescu et al., 2004), an enriched environment (Kempermann et al., 1997), seizures (Overstreet-Wadiche et al., 2006) , learning , aging (Ben Abdallah et al., 2010; Okamoto et al., 2011; Tozzini et al., 2012), and exercise (Van Praag et al., 2005) though paradoxically, stress and learning have also been associated with downregulated neurogenesis. Molecular influences on neurogenesis include Notch (Ehm et al., 2010; Lugert et al., 2010), Wnt/b-catenin (Lie et al., 2005) via Wnt3a (Yoshinaga et al., 2010), noncanonical Wnt signaling via Wnt5a (Arredondo et al., 2020), Sonichedgehog (Sohyun Ahn & Joyner, 2005; Breunig et al., 2008), VEGF (Cao et al., 2004; Udo et al., 2008), BDNF (Kazim & Iqbal, 2016), FGF (Kang & Hébert, 2015), inflammatory pathways (Chesnokova et al., 2016; Ekdahl et al., 2003), estrogen (Scharfman & MacLusky, 2006; Tanapat et al., 1999), Tau protein (Criado-Marrero et al., 2020; Pallas-Bazarra et al., 2016), astrocytic glutamate release (Guo et al., 2013), BMP signaling (Mira et al., 2010), SoxB family (Ahmed et al., 2009; Matsuda et al., 2012; Ohtsuka et al., 1999), parvalbuminergic GABA

release (Song et al., 2012), IGF-1 (Åberg et al., 2000), and insulin (Mainardi et al., 2015). Furthermore, different cell types influence when and how neural precursors from the subgranular layer migrate to upper layers include astrocytes (Lie et al., 2005), endothelial cells (Leventhal et al., 1999; Palmer et al., 2000), microglia (Reshef et al., 2014), other neural precursors (Wexler et al., 2009), parvalbuminergic inhibitory neurons (Song et al., 2013), cholecystokinin (Cck) inhibitory neurons (Asrican et al., 2020), CA1/CA3 inhibitory projection neurons (Bergami et al., 2015), and neurons within the granular layer of the DG (Qu et al., 2013). Considering that the subgranular zone is bombarded by environmental, paracrine, and cell autonomous cues, it has been proposed that the dentate gyrus's ability to selectively respond to certain signals or a combination of signals is mediated by a yet undetermined algorithmic-like convergent signal integration (T. J. Schwarz et al., 2012). Despite the overwhelming volume of molecular input received by the stem cell niche in the SGZ, the field is cohesive regarding integration mechanisms and the purpose of neuronal renewal for memory formation.

Cellular implications of adult neurogenesis in the mammalian hippocampus

Contemporarily, adult neurogenesis in the SGZ has been segmented into distinct steps, partially echoing those found in SVZ and radial migratory stream (RMS). These steps are not identical, however, as the SGZ does not directly border the lateral ventricles and thus lacks ependymal cells (Clarke & Van Der Kooy, 2011). Physiological differences have also been demonstrated as mechanistically differential regarding adult stem cell maturation in SVZ niche response is temporally and insult-dependent whereas the SGZ seems to induce maturity more constitutively (Sabrina Wang et al., 2000). The overarching maturation process is seemingly stepwise, in which a cell transitions from radial glia to intermediate progenitor to neuroblast to neuron. However, it is more accepted that maturing cells transition through a spectrum of molecular signals, as the overall process of hippocampal adult neurogenesis spans ~4-7 weeks in mice (Jessberger & Kempermann, 2003; van Praag et al., 2002). Neurogenesis starts from quiescent neural stem cell recruitment by tonic GABAergic signaling (Espósito et al., 2005). Maturation of RG neural stem cells (NSCs) is followed sequentially

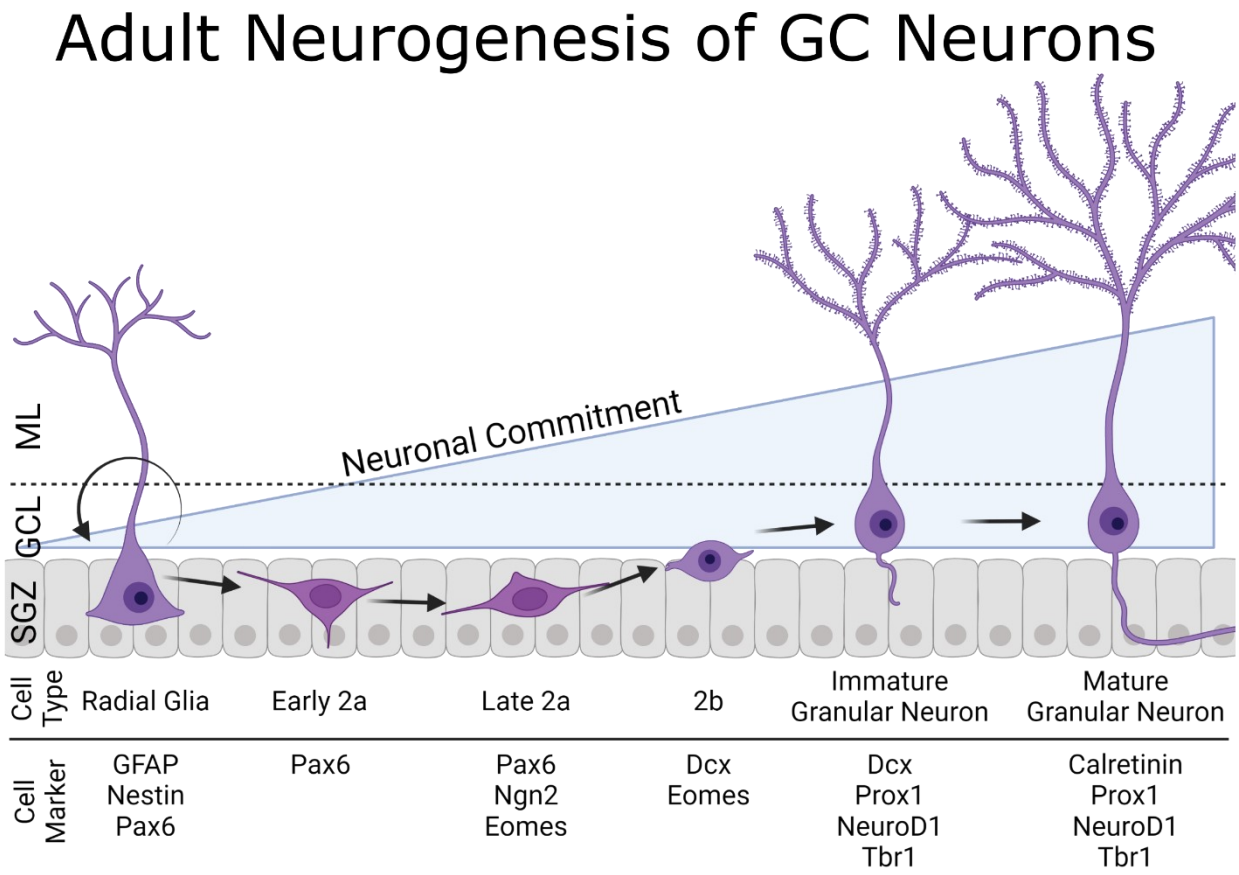

Figure 26. Cellular hippocampal adult neurogenesis. The hippocampus is noted for its neurogenic capacity throughout mammalian lifespan long after embryogenesis to produce granule cell neurons in the dentate gyrus de novo. Cells start as radial glia expressing GFPA, Nestin, and Pax6 and are induced into an asymetrical dividing state producing one radial glia and a sister nonradial precursor, early 2a cell still expressing Pax6. The nonradial precursor proceeds through molecular differentiation marked by Neurogenin2 (Ngn2) and Eomes (or Tbr2) upregulation with minimal morphological changes into a late 2a cell. The 2a cell begins to migrate out of the SGZ and into the granule cell layer (GCL) and is morphologically similar to transient amplifying progentiors in the SVZ. This new stage is "2b," at which they express low levels of immature neuronal marker, Dcx, and Eomes. Cell type 2b is the stage at which cells most likely are fully committed to a neuronal fate. After the soma reaches the GCL, it extends neuronal processes into the dentate molecular layer (ML) and expresses immature neuron marker Dcx, dentate gyrus markers Prox1 and NeuroD1, and axonal elongation-related transcription factor, Tbr1. Further maturation is accompanied by Ca2+ binding protein, Calretinin. Figure adapted from Song et al., 2013.

by 5 identified cell phases through which SGZ RG NSCs or $SOX2^+$/$Nestin^+$/$GFAP^+$ Type I NSCs divide asymmetrically to produce sister cells (Mignone et al., 2004; L. P. Wang et al., 2005). These sister cells include one non-radial precursor NSC (Type II), whose fate will return to a quiescent state RG NSC in the SGZ, and one intermediate progenitor which will integrate into the granule cell layer (Encinas et al., 2006). The intermediate progenitor, distinguished by Tbr2 and MCM2 expression (Bonaguidi et al., 2011), gradually becomes a DCX^+/$Calretinin^+$ neuroblast (Brandt et al., 2003) though there is speculated to exist an intermediate transition-

stage cell type between neuroblast and intermediate progenitor (Encinas et al., 2006; Espósito et al., 2005). Furthermore, the intermediate progenitor populations undergo mass programmed cell death, a mechanism assumed to increase regulatory dimensionality and mediated by microglial populations (Sierra et al., 2010). Surviving neuroblasts migrate further into the granule cell layer but as they transition to $Prox1^{+}$ immature neurons (Iwano et al., 2012), they encounter a second wave of cell death (Tashiro et al., 2007) before fully committing to a mature neuronal stage, marked by $Calbindin^{+}/NeuN^{+}$ cell bodies (Figure 26)(Ambrogini et al., 2004; Kuhn et al., 1996). Purportedly, exit from SGZ cell cycle is more generally marked by upregulation of proopiomelanocortin (POMC) (Overstreet et al., 2004) and is physiologically accompanied by a critical period of enhanced LTP (Snyder et al., 2001). This critical period if further characterized by afferent mossy fiber input (Deshpande et al., 2013) as well as septocholinergic and CA3 projection neurons (Vivar et al., 2012) which in turns contribute to additional synaptic refinement (Adlaf et al., 2017). But what drives transcriptional exit from the symmetrical neural stem cell cycle in the subgranular zone? BTG2 (PC3, Tis21) (Farioli-Vecchioli et al., 2009), ASCL1 (MASH1) (Parras et al., 2004), WNT3a (Lie et al., 2005), DISC1 (Duan et al., 2007), Neurogenin2 (Galichet et al., 2008), NeuroD1 and D6 (Miyata et al., 1999), and POMC (Overstreet et al., 2004) have been identified as strong inducers of cell cycle exit from the NSC niche. However, only BTG2, Neurogenin2, NeuroD, and ASCL1 have been demonstrated as transcriptional regulators. Additionally, while the overexpression of both Neurog2 (S. Li et al., 2015) and NeuroD (Noma et al., 1999) induces cell cycle exit and neuronal maturation, the developmental KO models do not demonstrate ablation of all hippocampal neurons during embryogenesis (Galichet et al., 2008; Miyata et al., 1999). Moreover, BTG2 is demonstrated in a broader function among CNS embryogenesis (Iacopetti et al., 1994) and the SVZ (Malatesta et al., 2000, 2001) whereas ASCL1 drives oligodendrogenesis in the SGZ (Jessberger et al., 2008). More recently, evidence has emerged illuminating a master regulator of the hippocampal formation, ZBTB20 (Nielsen et al., 2014; Rosenthal et al., 2012)

ZBTB20's Transcriptional Role in Neurogenesis

ZBTB20 (alias ZNF288, HOF, DPZF) is a multifaceted transcription factor which harbors both zinc finger binding and BTB/POZ binding domains. As the name implies ZBTB20 expresses both a zinc finger domain and a BTB binding domain indicating its function as a Zn^{2+}-mediated DNA binding protein. It consists of 6 experimentally confirmed tertiary, quasi-helical motifs and 15 messenger RNA variants including 1 non-coding variant in the human transcriptome (W. Zhang et al., 2001). Originally described in 2001, ZBTB20 is a relatively novel transcription factor whose involvement transgresses an array of biological functions. During chondrocytic differentiation, it is surmised to repress SOX9 expression (Zhou et al., 2015) whereas, across several glioblastomal cell lines, ZBTBT20 induces cellular proliferation and division (J. Liu et al., 2018). Furthermore, ZBTB20 knockout has been linked to reduced insulin secretion from pancreatic β cells and global hyperglycemia (Ye Zhang et al., 2012). With respect to the central nervous system, ZBTB20 has been implicated in neocortical embryonic neurogenesis and layering (Tonchev et al., 2016), in neocortical astrocytogensesis (Nagao et al., 2016), and, when mutated, as putatively causative of Primrose syndrome (Stellacci et al., 2018). Primrose syndrome is a developmental syndrome phenotypical of macrocephaly, ossified pinnae, and in later stages movement disorders including Parkinsonism (Primrose, 1982). Furthermore, specific familial mutations in ZBTB20 are

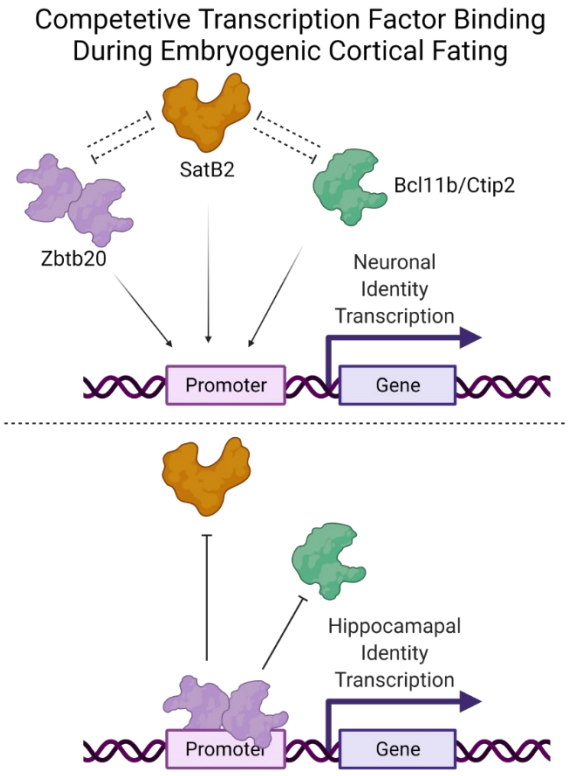

Figure 27. Transcriptional repression of neural stem genes. During embryogenesis of telencephalic derived cortices, several transcription factors compete to directly or indirectly repress genes regulating neural stemness to initiate neuronal differentiation. In the neocortex, the two major transcription factors regulating lamination of neuronal somatic layers are Satb2 and Bcl11b/Ctip2. Satb2 and Bcl11b competitively inhibit each other at the promoter level. In the hippocampus, Zbtb20 also competes for the same binding sites as Satb2 and Bcl11b, including Satb2 and, to some extent, Bcl11b promoters. Zbtb20 dimerizes via the BTB binding domain and typically represses promoter activity of neural stem genes, including the Sox-family. Zbtb20 is thought to also induce some gene expression directly but it has yet to be shown. Figure adapted from text in Nielsen et al., 2014.

concatenated with idiosyncrasies in Primrose syndrome case studies, including congenital hypothyroidism (Mattioli et al., 2016) and dysfunctional callosal projections (Alby et al., 2018). As extensively studied as ZBTB20's role in neocortical development has preceded this thesis, its entire role in human hippocampal development and adult neurogenesis is yet emergent. The zinc finger was originally proposed as a marker for the hippocampus based on a pan-developmental study showing ZBTB20's expression across hippocampal epithelium emergence and by neurons in the dentate plate (Mitchelmore et al., 2002). Zbtb20 in mice was further found to suppress deep-layer pyramidal neuron fating during corticogenesis, its overexpression resulting in decreased ER81, Pou3f2, and Pou3f3, suggesting that Zbtb20 prevents unwanted state transitioning hippocampal-like pyramidal neurons (Nielsen et al., 2007). Within the hippocampus, Zbtb20 knockout in mice demonstrated in fact that CA1 architecture became disrupted and elicited ectopic neocortical gene expression, *Cux2* and *Mef2c* (Nielsen et al., 2010). Following this study, another group demonstrated that an *in vivo* KO model of Zbtb20 failed to generate a functional hippocampal formation, decreased Wnt3a cortical hem expression, and permitted compensatory retrospliniocortical expansion (Rosenthal et al., 2012). These studies provide robust, anatomical evidence that Zbtb20 is an imperative transcription factor in hippocampal development. However, Zbtb20 is not exclusively expressed by the hippocampus and seems constitutively express in other regions vicinal to the lateral ventricles, including the subventricular zone, striatum, and amygdaloid complex. Furthermore, $Zbtb20^{+}$ newborn neurons appear in the olfactory bulb and $Zbtb20^{+}$ glia in the neocortex after fetal development (Doeppner et al., 2019). The first of the two studies to demonstrate that hippocampal Zbtb20's role may be neurogenic indicated that Zbtb20 guides neural progenitors into an identity different than supra-and infra-granular blade cell identities typical of isocortex by suppressing both Satb2 and Bcll11b *in vivo* (Figure 27)(Nielsen et al., 2014). The second study to indicate Zbtb20's role as neurogenic, however, demonstrates that throughout subventricular neurogenesis, $Tbr2^{+}$ newborn neurons coexpress ZBTB20 and that its KO drastically reduces the number of immature (and arguably still-migratory) neurons (Tonchev et al., 2016). While these studies demonstrate that ZBTB20 drives neural progenitors to hippocampal identity during embryogenesis and via a unique but developmentally conserved pathway, they do not elucidate

whether Zbtb20's facilitation throughout adult neurogenesis is mechanistically conserved. Currently lacking from literature is a definitive molecular integration of ZBTB20's downstream effectors, its uniquity in fate locking, and its upstream actuators with respect to differentiation in context of *homo sapiens*.

To fully understand molecular mechanisms of hippocampal adult neurogenesis in humans, however, requires not only *in vitro* models of the hippocampus but also reproducible modeling techniques/protocols that manifest hippocampal molecular signals and the potential to recapitulate the dentate gyrus and subgranular zone. As discussed earlier in this introduction, *in vitro* models are advantageous to isolate and directly manipulate environmental factors while minimizing confounding, influential factors like those found *in vivo*. Despite chemical manipulation of the SGZ niche in rodent models, it is almost impossible to recreate the same studies in human models due to ethical restrictions. Deriving human dentate gyrus neural cells *in* vitro is thus imperative to furthering study human adult neurogenesis. Hippocampal *in vitro* models have been published several times over in the past half decade (Sakaguchi et al., 2015; Sarkar et al., 2018; Terrigno et al., 2018; Diana Xuan Yu et al., 2014). The limitations are either the stem cell model type (mouse embryonic, human embryonic), their mode of differentiation (directed), or the resultant layer (CA3). This thesis thus tangentially defines a culture condition using broadly ethical hiPSCs to differentiate dentate gyrus neural precursors and to maintain their stemness longitudinally to demonstrate transcriptional control of NSC maturation by ZBTB20.

Pathological aggregation, optogenetics, and hippocampal development seem disjointed in their separate fields, however, the three are in fact imminently entwined and exceedingly imperative to accurately convey the molecular underpinnings of neurodegenerative hyperexcitability onset in a human context. To date, most studies relinquish either regional accuracy, human context, physiological stimulation, or a combination of the three. This thesis aims to address facets currently unavailable from the literature to set up future studies for molecular Tau pathogenesis with *in vitro* human parameters.

Chapter VII: Establishment of a small molecule-based approach to derive Dentate Gyrus identity cell cultures from hiPSCs (Methods)

COEISA/COEIRA analysis of scRNA seq dataset

Mouse dentate gyrus single cell dataset acquired from embryonic day 16.5, post-natal day 0, post-natal day 5, and post-natal day 23 (Hochgerner et al., 2018) was analyzed by cell clustering and ranked co-expression of exon and intron analysis (COEIRA) utilizing COTAN package, as detailed previously (Galfrè et al., 2020) .

Lentiviral plasmid construction for ZBTB20 overexpression

Lentiviral plasmid reconstruction was performed starting from pCMV6-ZBTB20 (NM_001164343) (insert A; Origene SC114633) and EF-1a-IRES-Puro (vector; Addgene Plasmid #85132, RRID:Addgene_85132). pCMV6-ZBTB20 was Maxi Prep amplified using XL10-GOLD in LB + 50 mg/l ampicillin overnight followed by extraction with Qiagen Plasmid Maxi kit (Qiagen 12165). Extracted and amplified pCMV6-ZBTB20 was used to excise ZBTB20 ORF with NotI (NEB, R0189), incubated at 37oC for 1 hour, and was purified on 0.8% agarose gel. The ~3 kbp band was isolated, melted, and dsDNA was purified using the Wizard SV Gel and PCR Clean-up System (Promega, A9285). EF-1α-IRES backbone (5 μg) was subsequently and correspondingly opened with NotI overnight at 37oC followed by 1-hour incubation with Calf Intestinal Alkaline Phosphotase (CIP; NEB M0290). Following NEB's T4 ligation protocol, NotI-digested ZBTB20 and backbone were co-incubated for no longer than 35 minutes, transformed into XL10-GOLD E. coli, plated onto agarose + ampicillin plates overnight, and positive colonies were selected for Mini Prep amplification, incubated at 37oC overnight in LB + ampicillin. The following day, pDNA was extracted using the Wizard Plus Minipreps DNA Purification System (Promega A1465) from ampicillin-resistant colonies and were subjected to restriction-enzyme mapping and sequencing. After identifying clones with sense oriented ZBTB20 (EF-1α-ZBTB20-IRES-Puro), a single positive colony was amplified by MaxiPrep in the same way as noted above. Extracted and amplified EF-1a-ZBTB20-IRES-Puro then

served as the subsequent backbone and recipient of mRuby2-WPRE, PCR amplified from pCAG-ChroME-mRuby2-ST (Addgene Plasmid #108902, RRID:Addgene_108902). Using the following primers:

Forward: 5'- CCCGGGTACCATGGTGTCTAAGGGCGAAGAG -3'

Reverse: 5'- GCGCGGTACCGCGGGGAGGCGGCCC -3'

Both forward and reverse primer included Acc65I restriction sites. After PCR amplification of mRuby2-WPRE, amplification products were purified on 0.8% agarose gel by isolating the 1.7 kbp band which was further processed with Promega Wizard Gel and PCR Clean-up kit. Extracted mRuby2-WPRE insert was digested with Acc65I (NEB R0599), incubated at 37oC for 1 hour, and was repurified through Promega Wizard Gel and PCR Clean-up kit. EF-1α-ZBTB20-IRES-Puro backbone (5 μg) was opened with Acc65I overnight at 37oC followed by 1-hour incubation with Calf Inositol Phosphotase (CIP), thereby excising the Puro-WPRE cassette. Following NEB's T4 ligation protocol, Acc65I -digested mRuby2-WPRE and EF-1α-ZBTB20-IRES- were co-incubated for no longer than 35 minutes, transformed into XL10-GOLD E. coli, plated onto agarose + ampicillin plates overnight, and positive colonies were selected for MiniPrep amplification. The following day, pDNA was extracted using the Promega MiniPrep kit from ampicillin-resistant colonies and were subjected to restriction-enzyme mapping and sequencing to identify sense-oriented mRuby2-WPRE, the final plasmid identified as plvEF-1α -ZBTB20-IRES-mRuby2. Plasmids generated were subjected to Western Blot verification after lentiviral packaging.

Lentiviral packaging of ZBTB20 knockdown plasmid and CRISPR KO plasmid

Using in-house generated plvEF-1α-ZBTB20-IRES-mRuby2 and ZBTB20 CRISPR guide RNA 2_pLentiCRISPRv2 (GenScript guide RNA construction services), lentiviruses were prepared using an adapted version of Addgene's protocol (https://www.addgene.org/protocols/lentivirus-production/#). Plasmids were packaged by incubating 2.5 μg/ml psPAX2 (Addgene plasmid #12260, RRID:Addgene_12260) 0.83 μg/ml

pMD2.G (Addgene plasmid #12259, RRID:Addgene_12259), and 3.33 µg/ml of plasmid construct in RT reduced serum Optimem Reduced Serum Medium, GlutaMAX™ Supplement media (ThermoFisher, 51985034) and 0.12 µg/ml linear Polyethyleneimine hydrochloride (Merck, 764965). HEK 293T cells were transfected for 6 hours at 37°C in OptiMEM whereupon the transfection media was removed from the culture and replaced with fresh OptiMEM. Virally active media was collected at 48 hours after transfection and immediately added to cell culture plates. mRuby2 transgenic expression was assayed via live cell monitoring throughout post-transfection incubation on an inverted Leica epifluorescent microscope. ZBTB20 overexpression/knockout was assayed by Western Blot and immunocytochemical detection.

Western blot

HEK 293T cells were transduced with ZBTB20 pKD and HeLa H2B cells were transduced with ZBTB20 pKO for 4 hours in virally active OptiMEM/8 µg/ml polybrene at 37°C. After incubation, virally active medium was removed, inactivated with bleach, and disposed of in a biohazard container. Cells were harvested 3 days after transduction, lysed, and proteins were separated and quantified. ~ 10 mg of protein were electrophoresed through an 8% SDS-PAGE gel for ~1.5 hours. After electrophoresis, the protein gel was transferred to a nitrocellulose membrane for ~1 hour, blocked for an hour in 5% milk/1X TBS-T and then incubated overnight in 1:1000 anti-ZBTB20 (rabbit, A-11122, Invitrogen, RRID:AB_221569) and 1:2,000 anti-RFP (rabbit, 10R-G109A, Fitzgerald, RRID:AB_1285808) in 5%

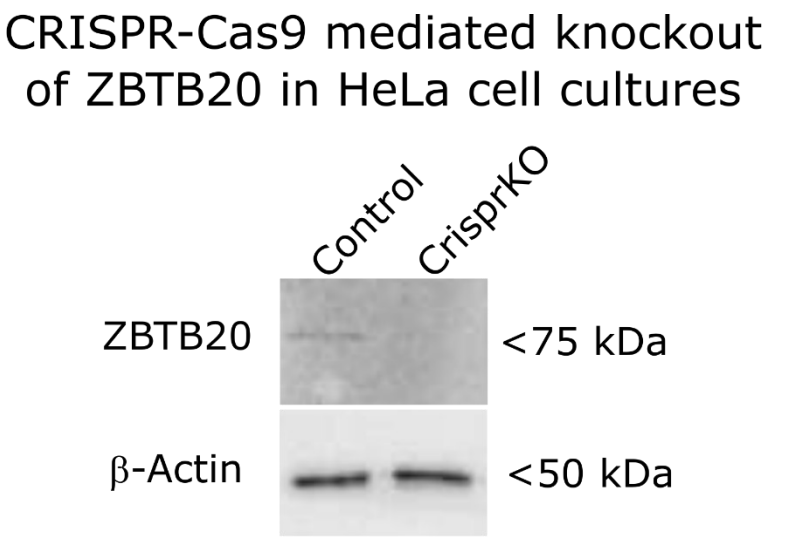

Figure 28. Western blot validation of CRISPR-Cas9 system. HeLa cells were used because of their availability and detectable expression of ZBTB20 in the Cell Atlas of https://www.proteinatlas.org/ . ZBTB20 is noteably ablated by CRISPR-Cas9.

milk/1X TBS-T at 4oC. Membrane was washed 3 times in 1X TBS-T followed by incubation in 1:2000 anti-mouse HRP conjugate (SC-516102, Santa Cruz Biotechnologies, RRID:AB_2687626) and 1:2000 anti-rabbit HRP conjugate (SC-2004, Santa Cruz Biotechnologies, RRID:AB_631746,) in 5% milk/1X TBS-T for 2 hours at RT. Membrane was washed 3 times in 1X TBS-T and then developed in UV-sensitive peroxidase substrate (WBKLS0500, Merck). Images of membrane were acquired utilizing a Bio-Rad Molecular Imager ChemiDoc XRS+ (Bio-Rad) and the successful knockout validated in Figure 28.

Lentiviral transduction of ZBTB20 overexpression and knockout plasmids

Human cells and mouse cells were transduced differently. Mouse cells were transduced via spinoculation during passage at DIV 3 (fourth day of WiBi treatment, sixth day from initial seeding) and DIV 7 (eighth day of WiBi treatment, tenth day from initial seeding). Spinoculation was conducted by resuspending cells in 37^{o}C OptiMEM containing viral particles and 5 µg/ml of polybrene followed by 30-minute centrifugation at 32^{o}C and 800g. Thereafter, cells were immediately resuspended in N2B27 medium and plated on poly-l-ornithine/purified mouse laminin-coated Eppendorf glass-bottom plates at their DIV-respective surface density, noted above. Instead, human cells were incubated at 37^{o}C for 4 hours with virally active OptiMEM/8 µg/ml of polybrene one day after cell seeding onto poly-l-ornithine/purified mouse laminin-coated Eppendorf glass-bottom plates.

Fating hiPSCs for DG neuronal precursor

To fate cells with a hippocampal progenitor identity, I adapted two protocols, one for telencephalic hiPSC differentiation and one for mESC hippocampal differentiation. Starting from hiPSCs (ATCC DYS0100) cells were seeded onto Geltrex™ LDEV-Free Reduced Growth Factor Basement Membrane Matrix (ThermoFisher, A1413202) in Essential 8™ Medium (ThermoFisher A1517001) containing Essential 8™ Medium Supplement

(ThermoFisher A1517-01), 100 U/ml Penicillin-streptomycin, and 2 μM Y-27632 (Cell Guidance Systems SM02-5). Less than 24 hours later, E8 containing Y-27632 was aspirated and fresh E8 media without Y-27632 was added. E8 media was changed daily for another 2 days. Cells were then subjected to neural induction (DIV 0) and incubated in WiBiTi media based in DMEM/F-12 containing 2mM Glutamine, 1 mM Sodium Pyruvate, 100 U/ml Penicillin-streptomycin, 1mM Non-essential amino acids, 0.05mM β-mercaptoethanol, 10 μM 53AH, 10 μM LDN193189 hydrochloride, 1 μM RepSox (SigmaAldrich R0158-5MG), N-2 Supplement 100X, and B-27 Supplement minus Vitamin A 50X. WiBiTi was changed daily until DIV 10 where cells were passaged and reseeded in N2B27 media containing Y-27632 at a density of 200,000 cells/cm2 on poly-l-ornithine and Laminin iMatrix-511silk E8 (511 human laminin, Amsbio AMS.892 021) coated plastic. Less than 24 hours later, N2B27 containing Y-27632 was aspirated and fresh WiBiTi media without Y-27632 was added. Cells were maintained in WiBiTi for another 4 days until DIV 15, where the media was changed to N2B27. The following day, DIV 16, cells were then cultured for an additional 6 days (DIV 21) in CH27 media, N2B27 media supplemented with 3 μM CHIR99021 (SigmaAldrich SML1046-5MG). At DIV 21 cells reach confluency and required another passage in CH27 media supplemented with Y-27632 and onto poly-l-ornithine/511 human laminin coated plastic at a density of 200,000 cells/cm2. Less than 24 hours later, CH27 containing Y-27632 was aspirated and fresh CH27 media without Y-27632 was added. Media was changed daily with fresh CH27 until DIV 28 wherein cells were passaged for longitudinally maintaining the huDG NSC niche, their final reseeding, frozen in N2B27 containing Y-27632 and 10% DMSO, fixed for immunocytodetection, or allowed to grow another 6 days in N2B27 media for qRT-PCR harvesting.

Maintaining huHC NSC niche

Starting from DIV 28, huDG NSCs were passaged and reseeded in N2B27 media containing Y-27632 at a density of 100,000 cells/cm2 on poly-l-ornithine/511 human laminin coated plastic. Less than 24 hours later, CH27 containing Y-27632 was aspirated and fresh CH27 media without Y-27632 was added. CH27 media was

changed daily for 2 weeks from the reseeding date (DIV 42) whereupon cells were passaged again in an identical manner until DIV 200. Approximate cell counts were recorded per passage by Bürker technique and subtracted from the total number of cells plated at the previous passage, then taken the $\log_2$ of the differential ($\log_2$(most recent passage cell count number - previous passage cell count number)).

Differentiating huHC neuronal precursors

Neural precursors, regardless of age, do not differentiate on 511 human laminin and attempted differentiation resulted in cell detachment and death. When ready to differentiate, either endogenously or by NOTCH inhibitor, DAPT, huDG NSCs were seeded onto poly-l-ornithine/purified mouse laminin coated plates. For immunocytodetection purposes, cells were seeded onto Eppendorf biofilm-bottom plates as they did not survive differentiation on Eppendorf glass-bottom plates without a layer of mESC-derived hippocampus neurons, derived using the protocol from Terrigno et al, 2018. Cells were also seeded in a density correspondent to their age and purpose i.e., for RNAseq, DIV 28 cells were plated at 200,000 cells/cm2 and DIV160 cells were plated at 400,000 cells/cm2. After passaging/thawing, cell suspensions were centrifuged at 200 g for 4 minutes and the cell pellet resuspended in CH27 supplemented with Y-27632. Less than 24 hours later, CH27 containing Y-27632 was aspirated and fresh CH27 media without Y-27632 was added. Media was changed daily with fresh CH27 until cells reached 90% confluency (after ~10 days) whereupon media was changed to Dentate Gyrus Differentiation (DGD) media, containing DMEM/F-12 2mM Glutamine, 1 mM Sodium Pyruvate, 100 U/ml Penicillin-streptomycin, 0.05mM β-mercaptoethanol, N-2 Supplement (100X) B-27 Supplement (50X) (with Vitamin A, ThermoFisher 125870-01), 20 ng/ml Recombinant human BDNF (NBP2-52006, Novus Biologicals), and 0.5 mM Ascorbate (A92902, Sigma Aldrich). Experimental differentiation media included +3 μM CHIR99021 (DGDC), +12.5 μM DAPT (DGDD, Sigma Aldrich D5942-5MG), or both (DGDCD).

Immunocytodetection of human cells in vitro

Cells were fixed in 2% PFA warmed to 37oC. Media added the preceding day was aspirated and PFA solution added instead to the cell chambers, incubated at RT for 15 minutes, followed by aspiration and 3 RT 1XPBS wash, 10' each. Cells were then permeabilized and blocked in 3%FCS/3%BSA (Blocking) + 0.2% Triton at RT for 1 hour. The permeabilization buffer was then aspirated and replaced with primary antibody solution in Blocking containing the corresponding dilution in the table below. Primary solution was incubated at 4oC between ranges from overnight (for cytoskeletal/membrane proteins) up to 72 hours (for nuclear antigens). Primary antibody solution was removed, and cells were washed 3 times with RT 1XPBS. Secondary antibody solution was supplemented with corresponding anti-(host) secondary antibodies in Blocking, diluted at 1:500 (v:v), and cells were incubated for ~1.5 hours at RT. Secondary antibody solution was removed, and cells were washed 3 times with RT 1XPBS. If Hoechst was used, it was added to the last 10' PBS wash. After the final PBS wash, all PBS was aspirated, and cells were mounted in Aqua/Poly-mount and allowed to cure before confocal acquisition. Images were produced on a Leica SP2 Confocal Microscope by acquiring z-stack images 10-15 optical slices thick, each slice ~1 μm in thickness. Images were reconstructed using FIJI/ImageJ and analyzed using a series of in-house scripts published previously. In brief, the scripts allowed for semi-supervised, automated quantification of either signal intensity, cell number, or neural cell processes.

- For signal intensity, experimental TIFF files were extracted automatedly from their respective microscope file, converted from Z-stack to Z-projection, and were then processed automatedly through "Measure" function on ImageJ, to include the entire range of image measurements
- For cell counting, experimental TIFF files were extracted automatedly from their respective microscope file and were processed through a pipeline which first set the threshold of the individual image using "Set Threshold" function followed by cell counting using "Analyze Particle" function. Thresholds were set manually to prevent variability generated in the "Automatic Threshold" function, however, each experiment differed in exact threshold as

some parameters could not be replicated between experiments i.e. different batch of antibodies, temperature of microscope room, necessary bit-depth of acquisition. Thresholds for cell counting were set to only include cells strongly expressing the target protein or nuclear stain. Likewise, exclusion parameters in "Analyze Particles" were set to exclude:

  - non-rounded objects in the 'Circularity' parameter
  - Debris-like and large-clumped objects in the 'Size (pixel^2)' ranged parameter
  - Objects outside of frame by enabling 'Exclude on Edges' parameter

- For neural cell processes and estimation of fiber lengths, experimental TIFF files were extracted automatedly from their respective microscope file, converted from Z-stack to Z-projection, and processed through a second automated pipeline. The second pipeline converted the image to a black and white 8-bit image, converted nonzero pixels above a defined threshold to binary intensity signals (0/255), deconvolved to a minimal frame (1 pixel width) using the 'Skeletonize' function, and the number of total pixels quantified. The total number of pixels were then converted to μm using the scale of the experimental settings to estimate total fiber lengths in the region of interest.

Table 5: primary and secondary antibodies used in this section:

Antibody	Host	Dilution	Company	Catalog No	RRID
ZBTB20	Rat	1:200	BD Biosciences	565453	AB_2739244
ZBTB20	Rabbit	1:500	Novus	NBP1-84146	AB_11013683
MAP2	Chicken	1:6000	Novus	NB300-213	AB_2138178
MAP2 (A-4)	Mouse	1:100	Santa Cruz	SC-74421	AB_1126215
GFP	Chicken	1:1000	Aves	GFP-1020	AB_10000240
Cherry	Rat	1:2000	Invitrogen	M11217	AB_2536611
FOXG1	Rabbit	1:500	Abcam	ab18259	AB_732415
SATB2	Mouse	1:200	Abcam	ab51502	AB_882455
CTIP2	Rabbit	1:1000	Abcam	ab28448	AB_1140055
Ki67	Chicken	1:1000	EnCor	CPCA-Ki-67	AB_2637049
Nestin	Mouse	1:500	Santa Cruz	SC23927	AB_627994
DCX	Rabbit	1:6000	Abcam	ab18723	AB_732011
Human Nuclei	Mouse	1:500	Merck	MAB1281	AB_94090
Human NCAM	Mouse	1:500	Santa Cruz	SC-106	AB_627128

PSD-95	Rabbit	1:500	Abcam	ab18258	AB_444362
Synaptophysin	Guinea Pig	1:1000	Synaptic Systems	101-004	AB_1210382
PAX6	Rabbit	1:1000	Covance	PRB278P	AB_291612
TUJIII	Rabbit	1:1000	Covance	MRB435P	AB_663339
NeuN	Guinea Pig	1:500	Millipore	ABN90	AB_11205592
AlexaFluor 405, goat anti-mouse	Goat	1:500	Invitrogen	A48255	AB_1963128
AlexaFluor 405, goat anti-rabbit	Goat	1:500	Invitrogen	A48254	AB_1963129
AlexaFluor 488, goat anti-rabbit	Goat	1:500	Invitrogen	A32731	AB_2633280
AlexaFluor 488, goat anti-guinea pig	Goat	1:500	Invitrogen	A-11073	AB_2534117
AlexaFluor 488, goat anti-chicken	Goat	1:500	Invitrogen	A32931	AB_2762843
AlexaFluor 488, goat anti-mouse	Goat	1:500	Invitrogen	A32723	AB_2633275
AlexaFluor 546, goat anti-chicken	Goat	1:500	Invitrogen	A-11040	AB_2534097
AlexaFluor 546, goat anti-rabbit	Goat	1:500	Invitrogen	A-11035	AB_143051
AlexaFluor 546, goat anti-rat	Goat	1:500	Invitrogen	A-11081	AB_141738
AlexaFluor 633, goat anti-guinea pig	Goat	1:500	Invitrogen	A-21105	AB_2535757
AlexaFluor 633, goat anti-mouse	Goat	1:500	Invitrogen	A-21052	AB_2535719
AlexaFluor 633, goat anti-rabbit	Goat	1:500	Invitrogen	A-21070	AB_2535731

RNA extraction

All *in vitro* samples used for transcriptomic assays were harvested by 5', 37^{o}C trypsinization after which was inactivated with inactivated Fetal Bovine Serum (Euroclone ECS0180L). Detached cells were homogenously suspended in solution, collected in microcentrifuge tubes and pelleted at 200 g for 5'. After centrifugation, the supernatant was aspirated, and the cell pellet was disrupted and processed using NucleoSpin® RNA kit (Machery-Nagel, 740955.250). RNA concentration was measured using a NanoDrop™ Lite Spectrophotometer (ThermoFisher ND-LITE).

qRT-PCR analysis

RNA extracted from *in vitro* samples were processed using Reverse Transcriptase Core Kit 300 (Eurogentec RT-RTCK-03). Approximately 200 ng of RNA was reverse transcribed into cDNA for qRT-PCR analysis. SensiFAST SYBR mix (12 μl, BioLine BIO-98020) and cDNA (8 μl) were combined in tubes and quantified using Qiagen 72-Well Rotorgene with the protocol previously published. All take-off cycles were normalized to their sample's respective βACT take off-cycle.

Table 6: Primers used in this section.

Gene	Forward Primer	Reverse Primer
ACTB	CTGGAACGGTGAAGGTGACA	AAGGGACTTCCTGTAACAATGCA
BTG1	TCTCCAAGTTTCTCCGCACC	GGGTCAACCCAGAGTGTGAG
BTG2	GGGTAACGCTGTCTTGTGGA	TGGGGTCCATCTTGTGGTTG
CCNE2	TAGCTGGTCTGGCGAGGTTT	ACAGGTGGCCAACAATTCCT
CDK6	GCAGGGAAAGAAAAGTGCAATGA	TCCTCGAAGCGAAGTCCTCA
CDKN1A	CCGTCTCAGTGTTGAGCCTT	CCTGGAGCTGAGAGGGTACT
CDKN1B	CGTCGGGGTCTGTGTCTTTT	CTCCCGTTAGACACTCGCAC
CDKN2C	CAATAAACGTGGGGAGGGCT	AGCAAGGGAAAAGCCAAGGA
E2F1	AAACAAGGCCCGATCGATGT	GGTGGGGAAAGGCTGATGAA
EMX1	TGACGGTTCCAGTCCGAAGT	CCAAGGACAGGTGAGCATCC
EMX2	CGACTCCGTTCCACTCTCG	TGGCTTGATGATTGGTCGCT
FOXG1	AGGAGGGCGAGAAGAAGAAC	TCACGAAGCACTTGTTGAGG
GDNF-R	ATCAGTGGAGCACATTCCCA	AGCATTCCGTAGCTGTGCTT
HOXB4	GGGCCCCGGAAAAATCTATCTG	GTCTTCTCCTCGGCAGAGG
HOXB9	AAAAAGCGCTGTCCCTACACC	AGGAGTCTGGCCACTTCGTG
LEF1	CTTTCTCCACCCATCCCGAG	GTGAGGATGGGTAGGGTTGC
LHX1	ACACCAGTGGACCTACCCTT	GGGACAGGTGGTTTCCGTAG
LHX2	CCAACTGTGACGTCCGTCTT	AGTTGTTCCTCGGTCCACAC
LHX5	CCGGGAAGCAACTACGACTT	ATCATGTCGGTGAACCTGGG
LHX9	CTGGCCCTGCCTTACTTCAA	CTGAATTTGGCTCGTGCGTT
LMO1	GAGACGGCCACGAGATTCC	CTGGCAACGACACAGCTTTC
LMO3	CTGTGCTTACTGAACGGCCT	TCCCGTTACACCAAAGAGCC
LMO4	CCTCAAGCACTGCTGCGTAT	CCCCATTAGAGCCGGGTTTT
NEUROD1	CCTTCGTTCAGACGCTTTGC	CCATCAAAGGAAGGGCTGGT
NEUROD6	TGCGAGGACCAGAAGCAAAT	AAGTTGTCCAGAGCGTCGTT
NEUROG1	AGTGACCTATCCGGCTTCCT	TCAAGTTGTGCATGCGGTTG
NKX2.1	AGCACACGACTCCGTTCTCA	CCCTCCATGCCCACTTTCTT
PAX6	GTGTCCAACGGATGTGTGAG	CTAGCCAGGTTGCGAAGAAC

PROX1	GAGGGTGGGAAAGGGGTTTT	TCAAACGGCACTGAGCTTGT
RLN	AAGCAGCTACCAAGCCTCTG	TTGTTTGCGAGTGAGGACGA
SATB2	CTTCTTCCCTGCCCGGTATC	AAAACGCACAGGGACCTTGA
SIX3	GTCCTACAGATGCCCACTCC	TCTATGGGCCTTTTGGCGTC
WNT7b	CGGTCGCTCAACCGGG	GGCTAGGCCAGGAATCTTGTT
WNT8a	GTCCCAAGGCCTATCTGACC	CACTCCTCGATGCCACTCTG
WNT8b	GAGGCTGCAGTGACAATGTG	TTCCAGGGCATCGACAAAC
ZBTB20	AAAGAGCGCGAGGAGACAAA	ATGTTCATTGGGGCAGGGAG

RNAseq of human cells

RNA-seq libraries were prepared with the SMART-Seq® HT PLUS Kit (Takara) as described in manufacturer's instructions and processed on a NovaSeq machine (Illumina), obtaining between 20-35M reads per sample. Transcripts were pseudo aligned using Salmon (REF:10.1038/nmeth.4197) in mapping-based mode (with its default "--validateMappings" flag). A decoy-aware version of the Ensembl mouse transcriptome (mm10; refgenomes.databio.org) was used as a reference. RNA-seq analysis was carried out using the R package NOISeq. Raw counts were normalized with the Trimmed Mean of M values (TMM) method. Low-count filtering was performed with the CPM method, using cpm=1 as threshold. PCA exploration was carried out to confirm that the experimental samples were clustered according to the experimental design (see Supplementary Figure “X”). Differential expression was calculated by the NOISeqBIO method and a significance threshold of q=0.95 was applied. RNA-seq data from Allen Atlas (REF) were compared to hiPSCs data upon scaling of both datasets to percent and by applying the hclust (distance) and prcomp R packages.

Table 7: Hippocampal markers table used for clustering (HIP Markers):

Transcript ID	Gene	Description
ENST00000379951	*LEF1*	lymphoid enhancer binding factor 1

ENST00000446480	*LHX2*	LIM homeobox 2
ENST00000261731	*LHX5*	LIM homeobox 5
ENST00000561173	*LHX9*	LIM homeobox 9
ENST00000616247	*LMO3*	LIM domain only 3
ENST00000370542	*LMO4*	LIM domain only 4
ENST00000435016	*PROX1*	prospero homeobox 1
ENST00000343737	*WNT8B*	Wnt family member 8B
ENST00000313071	*FOXG1*	forkhead box G1
ENST00000442245	*EMX2*	empty spiracles homeobox 2
ENST00000455099	*PAX6*	paired box 6
ENST00000295206	*EN1*	engrailed homeobox 1
ENST00000637191	*EGR2*	early growth response 2
ENST00000339475	*OTX2*	orthodenticle homeobox 2
ENST00000345514	*BCL11B*	BAF chromatin remodeling complex subunit B
ENST00000417098	*SATB2*	SATB homeobox 2
ENST00000425244	*CUX1*	cut like homeobox 1
ENST00000475839	*FEZF2*	FEZ family zinc finger 2
ENST00000481110	*FGFR3*	fibroblast growth factor receptor 3
ENST00000374561	*ID3*	inhibitor of DNA binding 3, HLH protein
ENST00000393785	*ZBTB20*	zinc finger and BTB domain containing 20
ENST00000468911	*DCX*	doublecortin
ENST00000389554	*TBR1*	T-box, brain 1
ENST00000449599	*EOMES*	eomesodermin
ENST00000325404	*SOX2*	SRY-box 2
ENST00000370536	*SOX3*	SRY-box 3
ENST00000322002	*SOX11*	SRY-box 11
ENST00000378453	*HES5*	hes family bHLH transcription factor 5
ENST00000313341	*NEUROG2*	neurogenin 2
ENST00000314744	*NEUROG1*	neurogenin 1
ENST00000295108	*NEUROD1*	neuronal differentiation 1
ENST00000346562	*NPAS3*	neuronal PAS domain protein 3
ENST00000353267	*CREB1*	cAMP responsive element binding protein 1
ENST00000375271	*PTCH1*	patched 1
ENST00000343882	*FOXO3*	forkhead box O3
ENST00000318789	*FOXP1*	forkhead box P1
ENST00000350908	*FOXP2*	forkhead box P2
ENST00000503800	*GSX2*	GS homeobox 2
ENST00000234198	*DLX2*	distal-less homeobox 2
ENST00000354822	*NKX2-1*	NK2 homeobox 1
ENST00000511384	*ISL1*	ISL LIM homeobox 1
ENST00000517373	*EBF1*	EBF transcription factor 1

ENST00000629706	*TCF7L2*	transcription factor 7 like 2
ENST00000647447	*NR2F1*	nuclear receptor subfamily 2 group F member 1
ENST00000258106	*EMX1*	empty spiracles homeobox 1
ENST00000260653	*SIX3*	SIX homeobox 3
ENST00000320185	*FGF8*	fibroblast growth factor 8
ENST00000256640	*WNT2B*	Wnt family member 2B
ENST00000284523	*WNT3A*	Wnt family member 3A
ENST00000285018	*WNT7A*	Wnt family member 7A
ENST00000339464	*WNT7B*	Wnt family member 7B
ENST00000287934	*FZD1*	frizzled class receptor 1
ENST00000315323	*FZD2*	frizzled class receptor 2
ENST00000286201	*FZD7*	frizzled class receptor 7
ENST00000523546	*FZD3*	frizzled class receptor 3
ENST00000295417	*FZD5*	frizzled class receptor 5
ENST00000374694	*FZD8*	frizzled class receptor 8
ENST00000344575	*FZD9*	frizzled class receptor 9
ENST00000539839	*FZD10*	frizzled class receptor 10

Transplantation of huDG neuronal precursors

Human hippocampal neural stem cells were cultivated either from DIV 28 or DIV 160, transduced with lentiviral vector mGFP the day following seeding and were expanded until DIV 39 or DIV 169, respectively. Cells were treated with 12.5 mM DAPT and 3mM CHIR99021 24 hours prior to transplantation. At DIV 40 or DIV 170, cells were dissociated with 1X Accutase or 25 min, centrifuged at 180 g for 4 minutes, and resuspended in fetal bovine serum. Cells were then transplanted at 5×10^5 cells/ml into the right hemisphere's dentate gyrus as previously described (Terrigno et al., 2018). After 90 days *in vivo*, mice were sacrificed and cross sections of hippocampus were stained with anti-Vglut1 (mouse, 1:1000), anti-PSD-95 (rabbit, 1:500), and anti-GFP (chicken, 1:500). Z-stack images were made using a Zeiss confocal microscope with Airy Scan resolution.

CHAPTER VIII: Extrinsic and intrinsic signaling factors contribute to human hippocampal neurogenesis *in vitro* (Results)

Neural progenitors derived from hiPSCs with dentate gyrus identity

To study hippocampal neurogenesis an ZBTB20 in a human context, I prioritized validating ZBTB20 expression *in vivo*. I relied on the Braincloud (Figure 29A; no longer open-source) (Colantuoni et al., 2011) and Allen Brain Institute's Brainspan (Figure 29B) (Miller et al., 2014) datasets for regional expression of *ZBTB20* transcript. The Braincloud confirmed that *ZBTB20* is upregulated in the early embryonic human prefrontal cortex and rapidly downregulated by 20 pcw throughout lifespan (Figure 29A). Brainspan regional datasets instead showed a relatively strong upregulation of *ZBTB20* in embryogenesis followed by a stable upregulation compared to the frontal cortex, primary visual cortex, primary motor cortex, striatum, and amygdala (Figure 1B).

After validating that *ZBTB20* is constitutively expressed in the human hippocampus, it was necessary to understand how ZBTB20 behaves in different hippocampal cell-type populations over time. Single cell RNA-seq provides this information, however, a human dataset encompassing embryonic to late postnatal

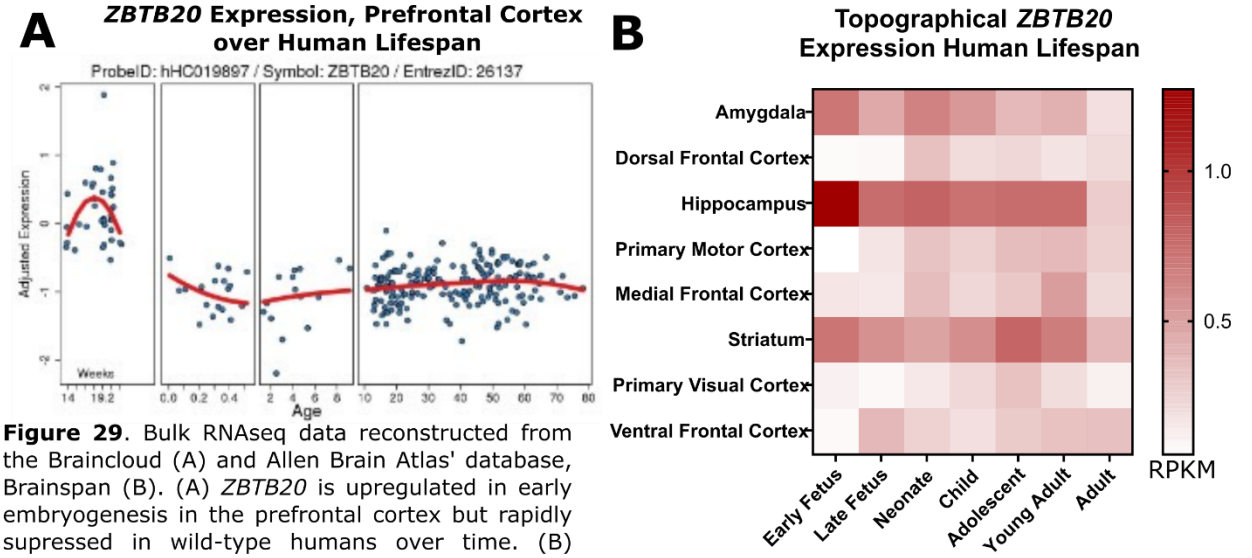

Figure 29. Bulk RNAseq data reconstructed from the Braincloud (A) and Allen Brain Atlas' database, Brainspan (B). (A) *ZBTB20* is upregulated in early embryogenesis in the prefrontal cortex but rapidly supressed in wild-type humans over time. (B) Acquisition begins from 12pcw and contuinues until 40 years of age. Scale is in RPKM. It is evident that the Hippocampus expresses the highest *ZBTB20* transcript across all acquired cerebral regions throughout total human lifespan; expression depicted as Reads Per Kilobase of transcript, per Million mapped reads (RPKM)

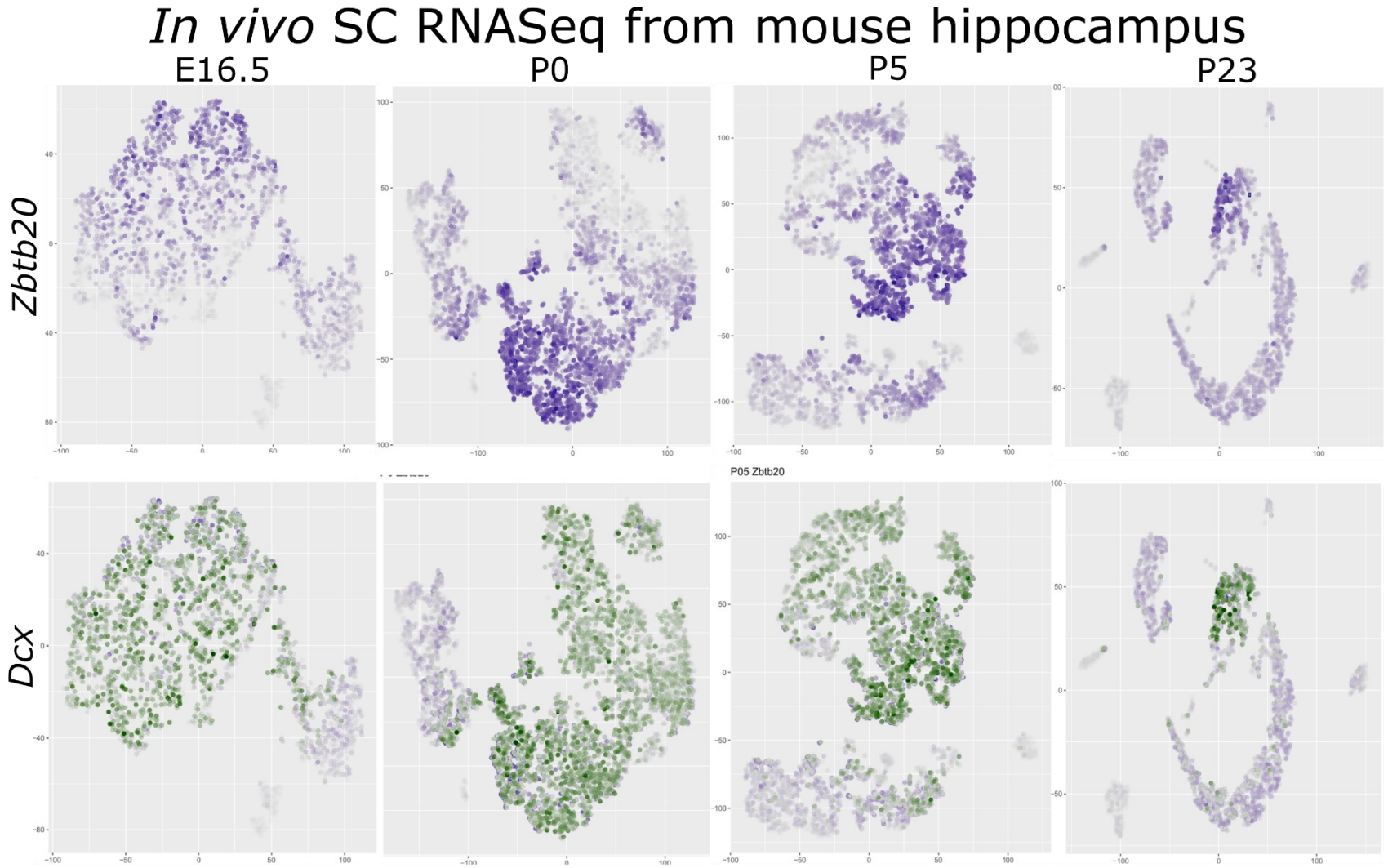

Figure 30. Single cell RNA sequencing of in vivo mouse hippocampus over distinct developmental timepoints. Mined from Hochgerner et al, 2018, single cell transcripts from mouse hippocampus at embryonic day 16.5 (E16.5), post-natal day 0 (P0), postnatal-day 5 (P5), and post-natal day 23 (P23) were analyzed by tSNE spatial distribution of gene read count density per cell. Clustering of *Zbtb20*$^{+}$ and *Dcx*$^{+}$ populations overlap and in a gradient along the differentiation axis from neural stem cell populations to neuronal populations, though not all *Dcx*$^{+}$ cells coexpress *Zbtb20* at early stages. Samples derived from P23 instead seem to strongly coexpress *Zbtb20* and *Dcx* in the same cells. Scale bars indicative of relative normalized expression.

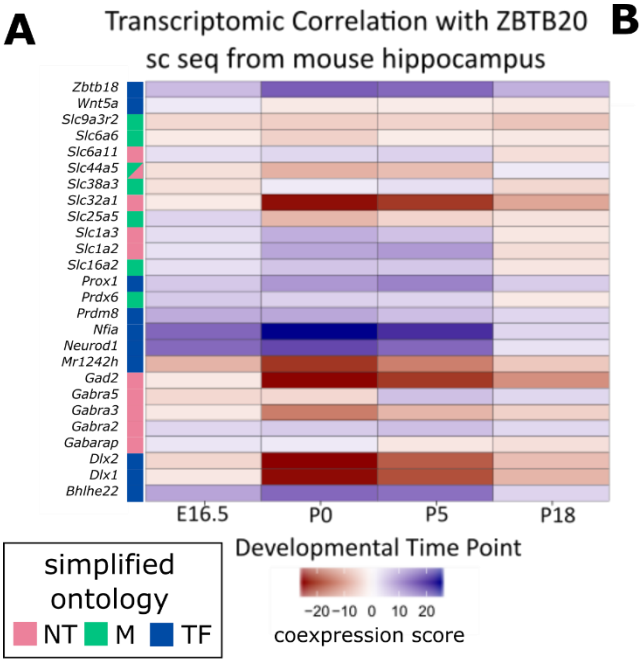

B

Gene	Function
Zbtb18	Transcription Repressor
Wnt5a	Noncanonical Wnt/JNK pathway
Slc9a3r2	Sodium/Hydrogen exchange
Slc6a6	Taurine transporter
Slc6a11	GABA uptake
Slc44a5	Choline Transporter
Slc38a3	Sodium-coupled neutral amino acid transporter
Slc32a1	Vesicular inhibitory amino acid transporter
Slc25a5	ADP/ATP translocase
Slc1a3	Sodium-dependent excitatory amino aid transporter
Slc1a2	Sodium-dependent excitatory amino aid transporter
Slc16a2	Monocarboxylate transporter 8
Prox1	Hippocampal fating
Prdx6	Peroxiredoxin
Prdm8	PR-domain containing zinc finger
Nfia	Nuclear Factor I A, transcription factor
Neurod1	Granule cell fating
Mr124-2h	Inhibitor of astrocyte activation
Gad2	Glutamate Decarboxylase/GAD65
Gabra5	Gamma-Aminobutyric Acid Type A Receptor Subunit Alpha5
Gabra3	Gamma-Aminobutyric Acid Type A Receptor Subunit Alpha3
Gabra2	Gamma-Aminobutyric Acid Type A Receptor Subunit Alpha2
Gabarap	Ubiquitin-like modifier in intracellular transport of GABA(A) receptors
Dlx2	interneuron fating
Dlx1	interneuron fating
Bhlhe22	oligodendrocyte fating

Figure 31. Ranked COEISA of genes coexpressed with *Zbtb20* from *in vivo* SC RNASeq dataset. (A) Truncated COEISA ranking of genes whose expression most strongly correlates with *Zbtb20*, most strongly correlated or anti-correlated. Gene coexpression with *Zbtb20* is mostly conserved throughout early development, with the exception of *Prox1*, *NeuroD1*, and Gad65 (*Gad2*).The simplified ontology (SO) to the left of gene names describes the primary function of each gene as either involved in neurotransmission (pink, NT), metabolism (green, M), or transcription factor (blue, TF) *Zbtb20* is positively correlated with other transcription factors and anticorrelated with GABA-ergic related genes. (B) Table of truncated ranked genes indicating primary function.

developmental stages have yet to publicly release. As mice are accepted for modeling human phenomena in basic biological research, I analyzed SC-seq of mouse hippocampal data sets at timepoints E16.5, P0, P5, and P23 (Figure 30) (Hochgerner et al., 2018) with the support of Silvia Galfré. I chose to analyze first the coexpression of *Zbtb20* and *Dcx*, the gold standard marker for neurogenic activity (Couillard-Despres et al., 2005). *Zbtb20* expression appears coincidental with *Dcx* expression in cell population in a gradient-like manner independent of time but with strongest coexpression at P23 thus suggesting Zbtb20's role in hippocampal neurogenesis. I then decided to rank the genes most strongly co-expressed with Zbtb20 and analyze their GO enrichment. As common methods of scRNA-seq analysis are not precise in predicting the coexpression of gene pairs in single cell I adopted the novel COTAN, which allows better prediction by assigning probability values of gene pair coexpression (Galfrè et al., 2020). Ranked COEISA analysis found that several transcription factors were strongly correlated with *Zbtbt20* including granule neuron marker, *NeuroD1* across all timepoints (Figure

Coexpression of ZBTB20 along neuronal differentiation axis

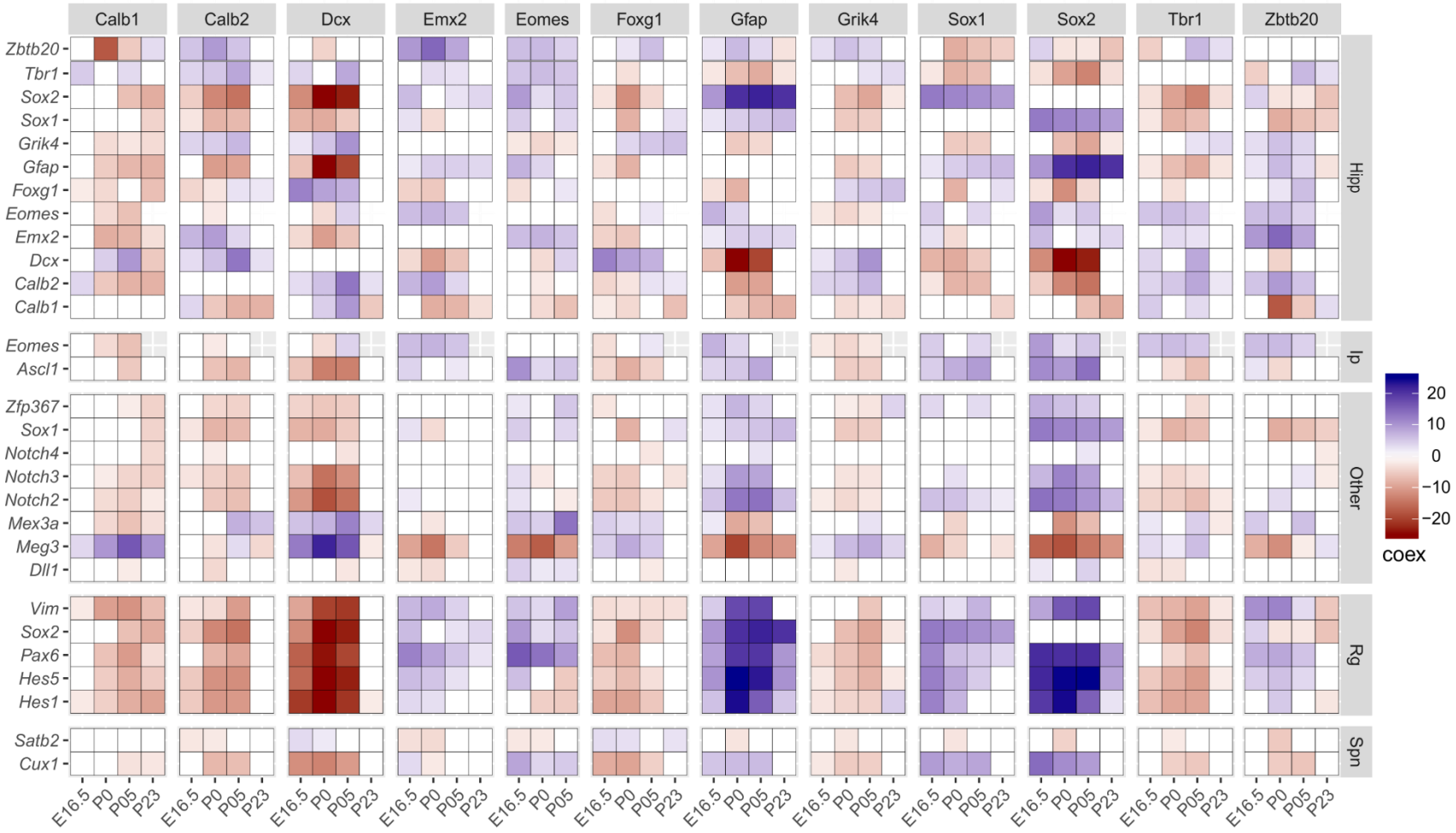

Figure 32. Coexpression of *Zbtb20* along discreet neurogenic populations. Ranked COEISA analysis across longitudinal hippocampus SC RNASeq dataset revealed several correlations historically documented including radial NSC coexpression between *Gfap, Sox2, Notch, Hes1*, and *Hes5*; Nonradial NSC (IP) coexpression of *Eomes* and *Ascl1*; Intermediate progenitor coexpression of *Dcx, Tbr1, Calb2, Grik4,* and *Mex3a.* In Rg, *Zbtb20* messenger instead is most correlated with *Vim*, *Hes5* but anticorrelated with *Sox2*; In IP, *Zbtb20* is correlated with *Eomes* but not *Ascl1* after P0; in hippocampal neurogenesis-associated markers (Hipp), *Zbtb20* is correlated with other markers, including *Calb2* but not *Sox1*.

31). Conversely, inhibitory neuron genes were anti-correlated with *Zbtb20* (Figure 31) with the exception of *Gabara2*, GABA receptor α subunit expressed by neural progenitors (Quadrato et al., 2014). I next extrapolated these findings to general cell types along the differentiation axis (Figure 32) and found that *Zbtb20* was correlated with hippocampal radial glia (Rg), Type II neural precursors (Np), and intermediate progenitors (Ip). Furthermore, it is evident that *Zbtb20* is not strongly associated with *Sox1*$^+$/*Sox2*$^+$ neural stem cells or radial glia but may instead upregulate as a function of cell cycle exit. Zbtb20 has been demonstrated in several mouse models to play a critical role in hippocampal development (Rosenthal et al., 2012; Tonchev et al., 2016) and in particular that it plays sustained function in adult CA1 synapses (Ripamonti et al., 2020). From mined data of wild-type mouse and human hippocampal transcriptional data, it was apparent that *Zbtb20*'s expression is a function of neuronal differentiation in the mouse hippocampus.

Through public datasets, I sought to establish a protocol in which neural precursor cells with dentate gyrus identity could be established to pursue my hypotheses regarding ZBTB20 in a neurogenic context. To differentiate neurons *in vitro*, I performed a handful of conventional protocols used to neuronally differentiate stem cells, including DMEM/F12 media supplemented with N-2 and B-27 (Figure 33A), 500 nM Retinoic Acid (Figure 33B), BMP + TGFβ inhibition (Figure 33C) (Y. Shi, Kirwan, Smith, et al., 2012), and WNT + BMP + TGFβ inhibition (Figure 33D) (Y. Shi, Kirwan, & Livesey, 2012). The two protocols from Shi et al 2012 induced both Nestin (Figure 33C1, 33D1) and FOXG1 (Figure 33C5, 33D5) while downregulating OCT3/4. Next, BMP/TGFβ inhibition (BiTi) and WNT/BMP/TGFβ inhibition (WiBiTi) were assayed for transcriptomic differences as neural progenitors at DIV 10, 14, 17, and 21via qRT PCR (Figure 34). Most transcripts were similar between the two treatments except telencephalic marker, *FOXG1*, which was doubled in relative expression in WiBiTi compared BiTi. For this, I chose to induce telencephalic progenitor differentiation using WiBiTi (Y. Shi, Kirwan, & Livesey, 2012) in step with CHIR 99021. Over the course of 33 days from hiPSC neural induction (DIV 0) until their harvesting at neural precursor stage (DIV 33). WNT, BMP, and TGFβ inhibitors were removed at DIV 14, when *FOXG1* already peaked expression, and GSK3β was inhibited from either DIV 12 for a duration of either 8 (CD12d8) or 12 days (CD12d12), DIV 16 for a duration of either 8 (CD16d8) or 12 days (CD16d12), DIV 20 for a

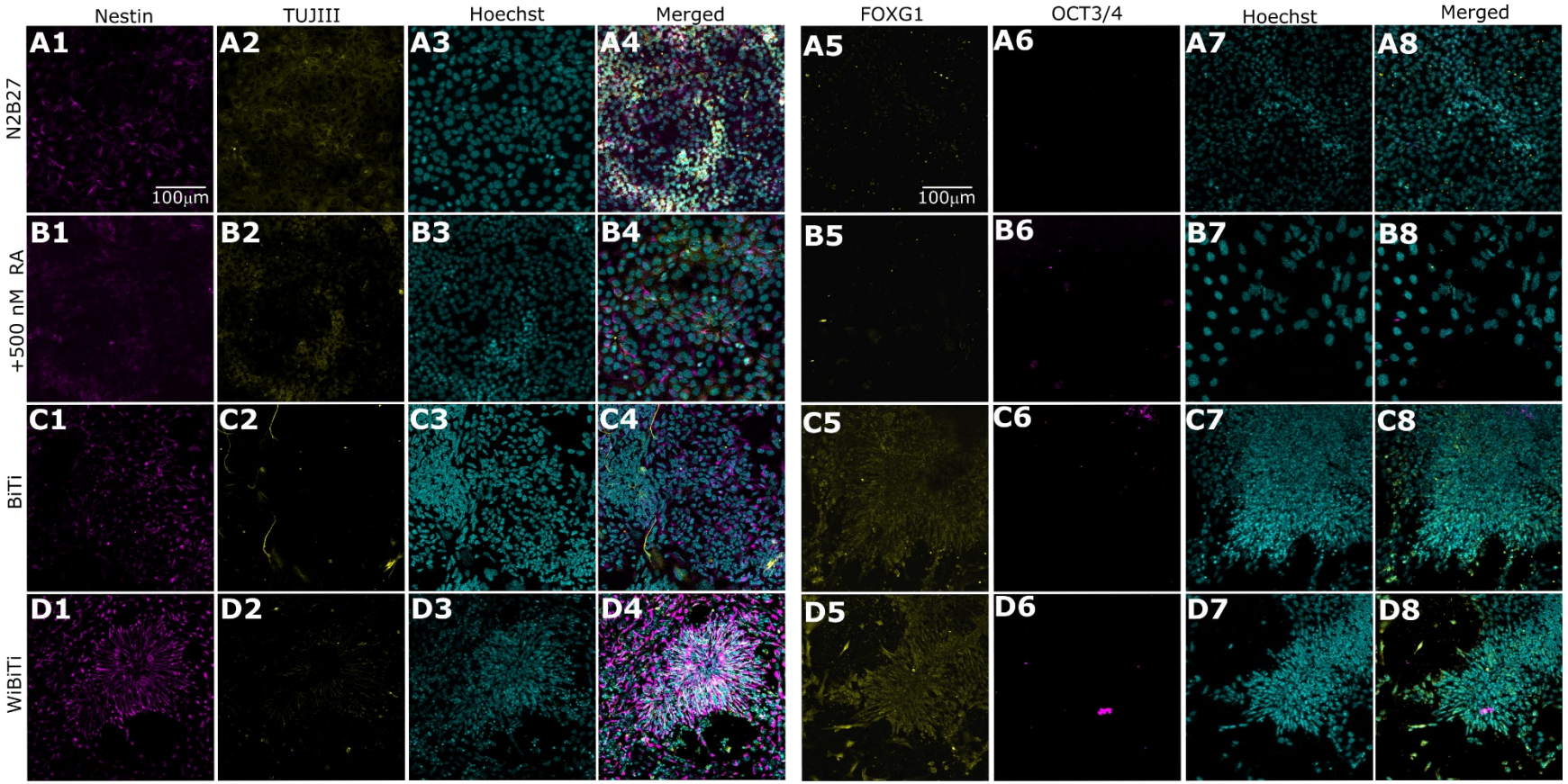

Figure 33. Immunocytochemical detection of pro-neural and stem cell genes in differentiating hiPSC cultures at DIV 12. Cells were treated with conventional differentiation protocols including minimal insulin-containing media (N2B27, row A), 500nM Retinoic acid (RA, Row B), BMP and TGFβ inhibition (BiTi, Row C), or WNT, BMP, and TGFβ inhibtion (WiBiTi,Row D). Cells were fixed and stained with Nestin (Col. 1), bIII-tubulin (TUJIII, Col. 2), and Hoechst (Col. 3) and visually assessed for their coexpression (Col. 4). Sister cells were stained instead with pro-telencephalic transcription factor, FOXG1 (Col. 5), stem cell marker OCT3/4 (Col. 6), Hoechst (Col. 7), and visually assessed for their coexpression (Col. 8). (A) Nestin and bIII-tubulin were expressed slightly in N2B27 cultures and were absent of FOXG1 and OCT3/4. (B) RA treated cells were absent of Nestin, βIII-tubulin, FOXG1, and OCTR3/4. (C) BiTi treated cells expressed Nestin, bIII-tubulin, slight FOXG1, and no OCT3/4.(D) WiBiTi treated cells expressed Nestin, βIII-tubulin, slight FOXG1, and no OCT3/4.

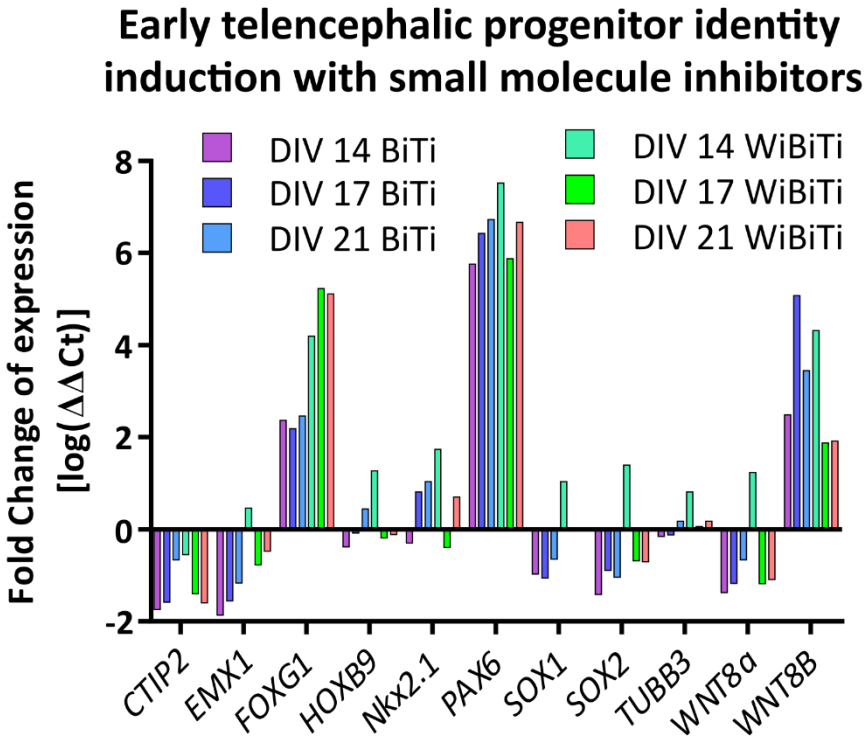

Figure 34. qRT-PCR validation of cortical identity transcripts at DIV 14, 17, and 22 between BiTi and WiBiTi neural induction groups. Proneural, telencephalic, and rostral nervous system markers were assayed for major differences in expression between the two cortical fating protocols including *CTIP2, EMX1, FOXG1, HOXB9, Nkx2.1, PAX6, SOX1, SOX2, TUBB3, WNT8a*, and *WNT8b*. *FOXG1* transcript doubles in WiBiTi treated groups compared to BiTi treated groups while most other genes remain similar between both treatments. N=1, fold change scale, $\log_2 \Delta\Delta Ct$

duration of either 8 (CD20d8) or 12 days (CD20d12), or DIV 24 for a duration of either 8 (CD24d8) or 12 days (CD24d8) (Figure 35A). I then assessed by qRT-PCR several key messengers known to upregulate in DG NPCs including *EMX2*, *FOXG1*, *PROX1*, *WNT8a*, and *ZBTB20* (Figure 35B). *PROX1*, *WNT8a*, and *ZBTB20* were upregulated significantly in CD16d12 treated cells. To assess whether these progenitors' identity was similar to *in vivo* human, CD16d12 was harvested at DIV28 for RNASeq and compared to brain regions from the Allen Brain Atlas (ABA) (Miller et al., 2014) at 12 pcw, the earliest embryonic age for which replicates of each clustered against several brain regions were available. I chose hippocampus (HIP) and three brain regions with different Anterior/Posterior and Dorsal/Ventral identity: cerebral (primary auditory) cortex (AC1) Striatum (STR) and Cerebellum (CB) (from the ABA (Figure 35C). To perform the comparison between cultures and brain regions, I restricted my analysis to 59 markers of early hippocampal development selected form the literature (HIP Markers Table, methods) (Abellán et al., 2014; Cembrowski, Bachman, et al., 2016; Cembrowski, Wang, et al., 2016; Grove et al., 1998; Grove & Tole, 1999; S. M. K. Lee et al., 2000; Lein et al., 2004; Overstreet et al., 2004; Diana X. Yu et al., 2014; C. Zhao et al., 2006).

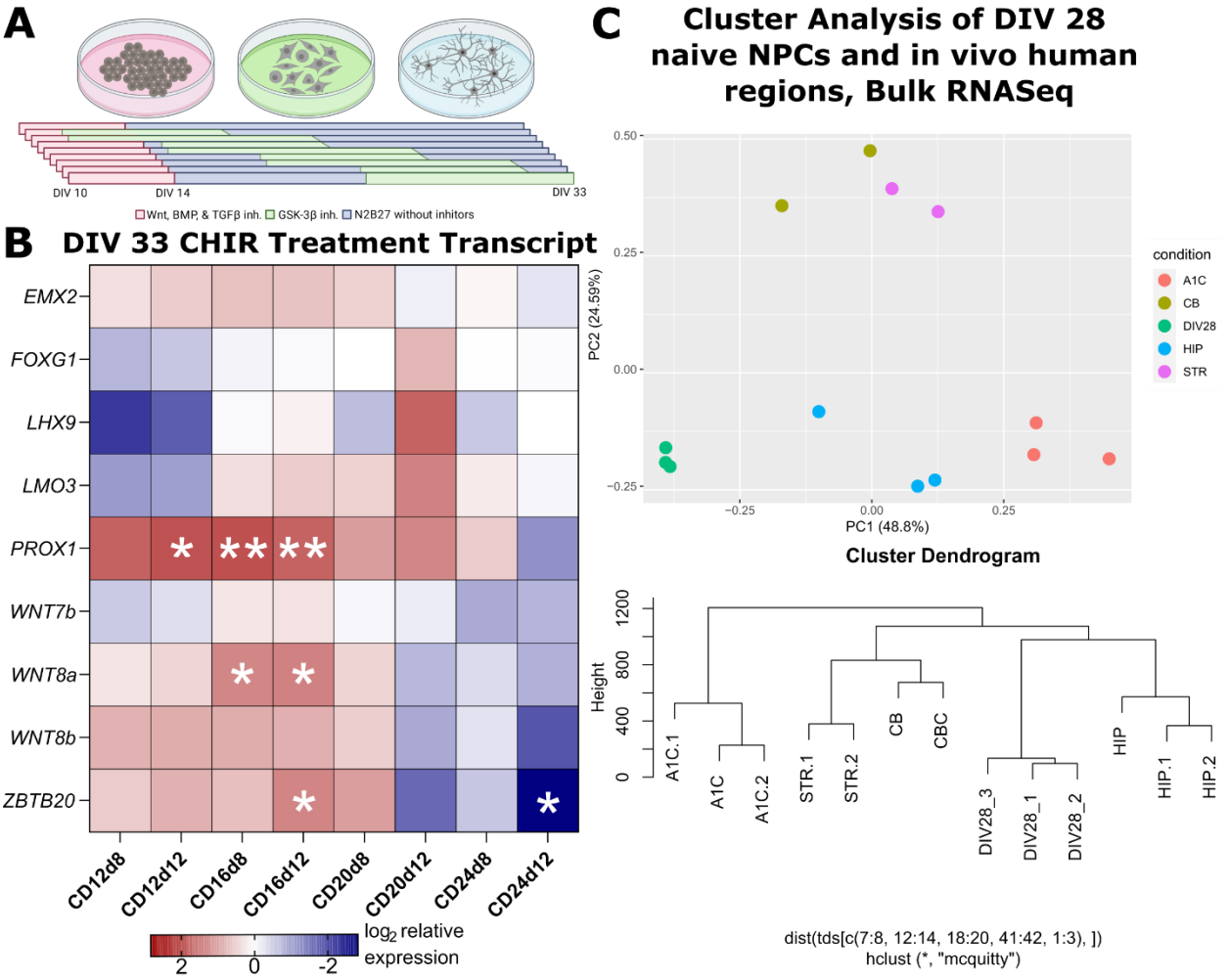

Figure 35. Transcriptomic validation of CHIR treatments. (A) experimental schematic outlining timing of inhibitor addition and withdrawal starting from DIV 10 until final harvest at DIV 33. (B) qRT-PCR panel of treatments from (A) validating expression of hippocampal markers including *EMX2, FOXG1, LXH9, LMO3, PROX1, WNT7b, WNT8a, WNT8b, ZBTB20*. *PROX1*, *WNT8a*, and *ZBTB20* were positively and significantly upregulated in comparison to WiBiTi control in CD16d12. Treatment names correspond to CHIR given at DIV for a duration of time in days e.g. CD12d8 = CHIR from DIV 12 lasting 8 days. All samples were normalized to DIV 33 WiBiTi samples, *-p-val<0.05, **-p-val<0.01, analyszed by Two-Way ANOVA using Sidak-Holm correction. (C) PCA cluster analysis using Bulk RNASeq from DIV 28 naive progenitors in comparison to ABA regions including dorsal thalamus (DTH12), Hippocampus (HIP12, and primary visual cortex (V1C12) at 12 pcw. DIV 28 progenitors cluster most closely to hippocampus, N=3

The first 2 components of PCA account for most of the gene expression variance (PC1=48,8%,PC2=24,59%) and indicate the hippocampus as most like CD16d12 cells. The treatment used to derive CD16d12 cells thus became the candidate protocol for hippocampal differentiation and are hereafter referred to as DIV 28 cells. This observation was also confirmed by hierarchical clustering analysis (Figure 35C). PCA analysis demonstrated that DIV 28 cells clustered most closely to 12 pcw hippocampal RNA. WiBiTi (Figure 36A) and CD16d12 (Figure 36B) were subsequently immunostained for Nestin, ZBTB20, and Hoechst to assay nuclear ZBTB20 expression.

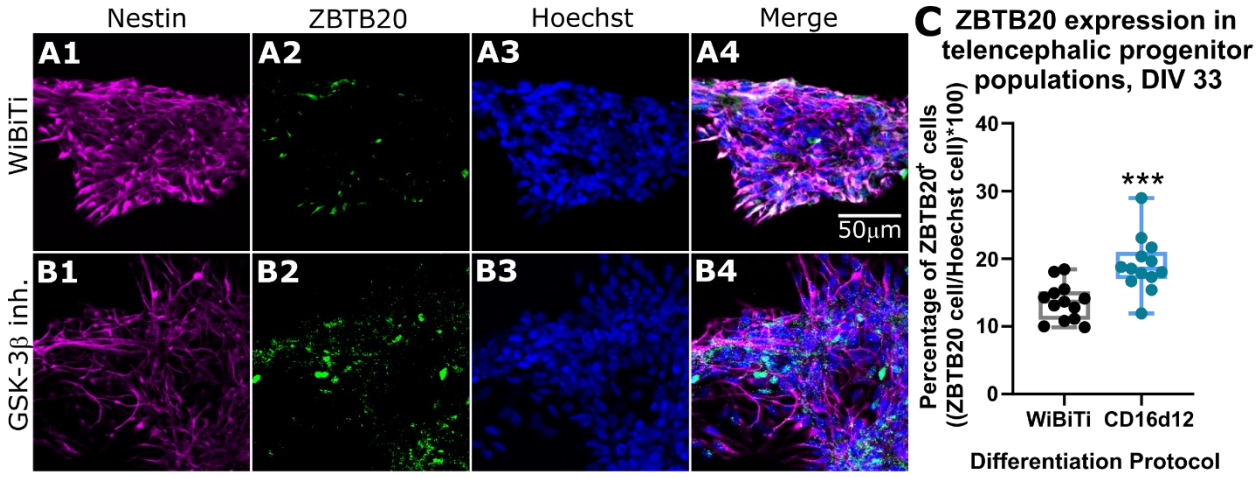

Figure 36. Nuclear ZBTB20 expresion in telencephalic neural progenitors. (A) WiBiTi cells were compared to (B) CD16d12 cells at DIV 33. Cells were immunostained for Nestin (Col. 1), ZBTB20 (Col. 2), Hoechst (Col. 3) in the same culture (Col. 4). ZBTB20$^+$ and Hoechst$^+$ cells were counted using an in-house designed ImageJ macro for batch cell counting each image of each technical replicate. (C) Total number of ZBTB20$^+$ cells were then divided by total number of Hoechst$^+$ cells for their respective z-stack origin and percentages were analyzed by Mann-Whitney nonparametric test. GSK-3β inh. increased by ~6% from WiBiTi; error bars indicate 99% CI; ***-p-val<0.001, N=13

Cells neuralized by GSK-3β inhibition exhibited increased ZBTB20 in NSC populations (Figure 36C). In parallel to CHIR experiments, hiPSCs were neuralized using Wnt3a, a protocol for CA3/DG differentiation published previously (Figure 37) (Sarkar et al., 2018; Diana Xuan Yu et al., 2014). However, when compared WiBiTi (Figure 37A) and CD16d12 (Figure 37B), Wnt3a-treated cells (Figure 37C) no hippocampal markers changed from WiBiTi and were significantly downregulated compared to CD16d12, most strikingly, ZBTB20 protein (Figure 37D) and mRNA (Figure 37E). CD16d12 was thus chosen as the candidate for optimal hippocampal neuralization, and cells were further spontaneously differentiated to assess maturing neuronal markers (Figure 38). When grown on purified mouse laminin, WiBiTi progenitors and CHIR-treated progenitors differentiated and upregulated several maturing neuronal markers including βIII-tubulin, DCX, and MAP2 (A-F, Rows 1 and 2) while maintaining pallial identity markers PAX6 and FOXG1 (Figure 38, C3-F3). However, cells growing longer than DIV 60 detached from the substrate and required more than purified mouse laminin. Two alternatives were required to prolong their attachment to the substrate: coculture with mESC-derived neurons using the Terrigno et all 2018 protocol and substituting glass for a novel, fluorescent-light-permissible biofilm. Using the protocol from Terrigno et al 2018, I established a mouse and human hippocampal co-culture in which human NPCs spontaneously differentiated until DIV 70 (Figure 39A). Spontaneously differentiating human cells

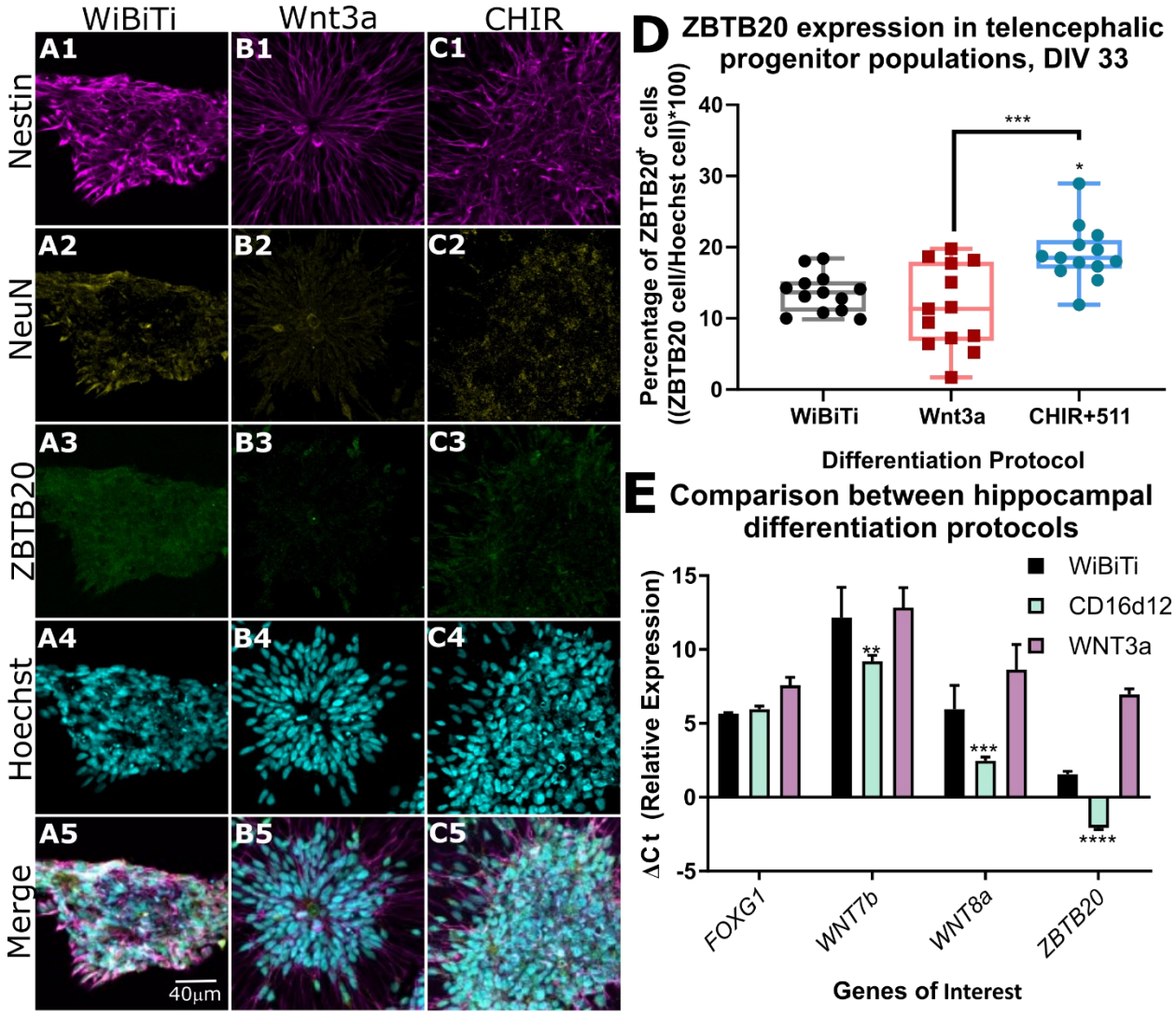

Figure 37. Wnt3a does not induce ZBTB20 expression as efficiently as CHIR99021. (A) WiBiTi, (B) Wnt3a-treated, and (C) CD16d12 cells were immunostained for Nestin (Row 1), NeuN (Row 2), ZBTB20 (Row 3), and Hoechst (Row 4) and were arranged for their coexpression (Row 5). ZBTB20^{+} and Hoechst^{+} cells were counted using an in-house designed ImageJ macro for batch cell counting each image of each technical replicate. (D) Total number of ZBTB20^{+} cells were then divided by total number of Hoechst^{+} cells for their respective z-stack origin and percentages were analyzed by One-way ANOVA and Kruskal-Wallis nonparametric post-hoc test. Cells treated with Wnt3a were unchanged compared to WiBiTi and expressed significantly fewer ZBTB20^{+} cells than CD16d12, -8%. Error bars indicate 99% CI; *-p-val<0.05, ***-p-val<0.001, N=13. (E) qRT-PCR analysis of WiBiTi, Wnt3a, and CD16d12 cells assaying the relative expression (DCt) of *FOXG1, WNT7b, WNT8a*, and *ZBTB20* mRNA expression at DIV 33. Expression was analyzed by Two-Way ANOVA and demonstrated robust changes between CD16d12 and Wnt3a treated cells in *WNT7b, WNT8a*, and *ZBTB20*. Error bars indicate 99% CI; **-p-val<0.01, ****-p-val<0.0001, N=3

expressed maturing neuronal markers (Figure 39B-C) while maintaining some proliferative capacity (Figure 39B2) as well as ZBTB20 expression (Figure 39C3). To expound upon neuronal differentiation promotion in mESC-derived neuronal cultures, I repeated the experiment but instead this time lentivirally overexpressing

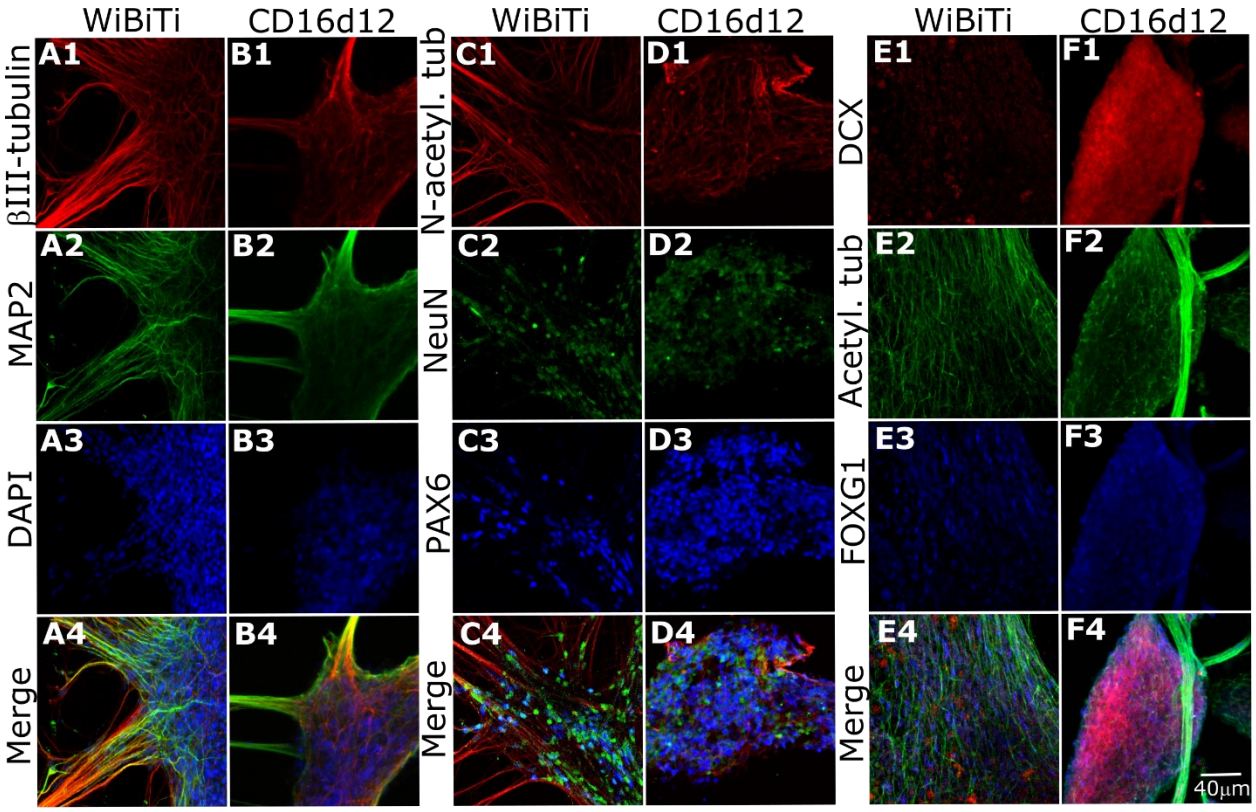

Figure 38. Spontaneous neuronal differentiation in pallial progenitor groups. WiBiTi (A, C, E) and CD16d12 (B, D, F) were immunostained for neurocytoskeletal and pallial-identity transcription factors. Immunogens include βIII-tubulin (A1, B1), MAP2 (A2, B2), DAPI (A3, B3) and their coexpression (A4, B4); N-terminus acetylated tubulin (N-acetyl. tub, C1, D1), NeuN (C2, D2), PAX6 (C3, D3), and their coexpression (C4, D4); DCX (E1, F1), Acetylated tubulin (Acetyl. tub, E2, F2), FOXG1 (E3, F3) and their coexpression (E4, F4).

membrane-bound GFP while treating hNPCs with DAPT and CHIR 1 day prior to replating at DIV 28 (Figure 39D-F). $mGFP^+$ human cells appeared to express less DCX (Figure 39D1) and less Ki67 (Figure 39D2) than their spontaneously differentiated counterparts. Furthermore, these DAPT differentiated cultures expressed matured neuronal markers including $MAP2^+/ZBTB20^+/FOXG1^+$ human cells like those reported in Sakaguchi et al 2015 (Figure 39E) as well as synaptic maturation with mouse neurons (Figure 39F). Having demonstrated that these progenitors share molecular identities like those *in vivo* and temporally traverse the neuronal differentiation axis to express neurocytoskeletal and synaptic markers, I next investigated how ZBTB20 expression is modulated in my model.

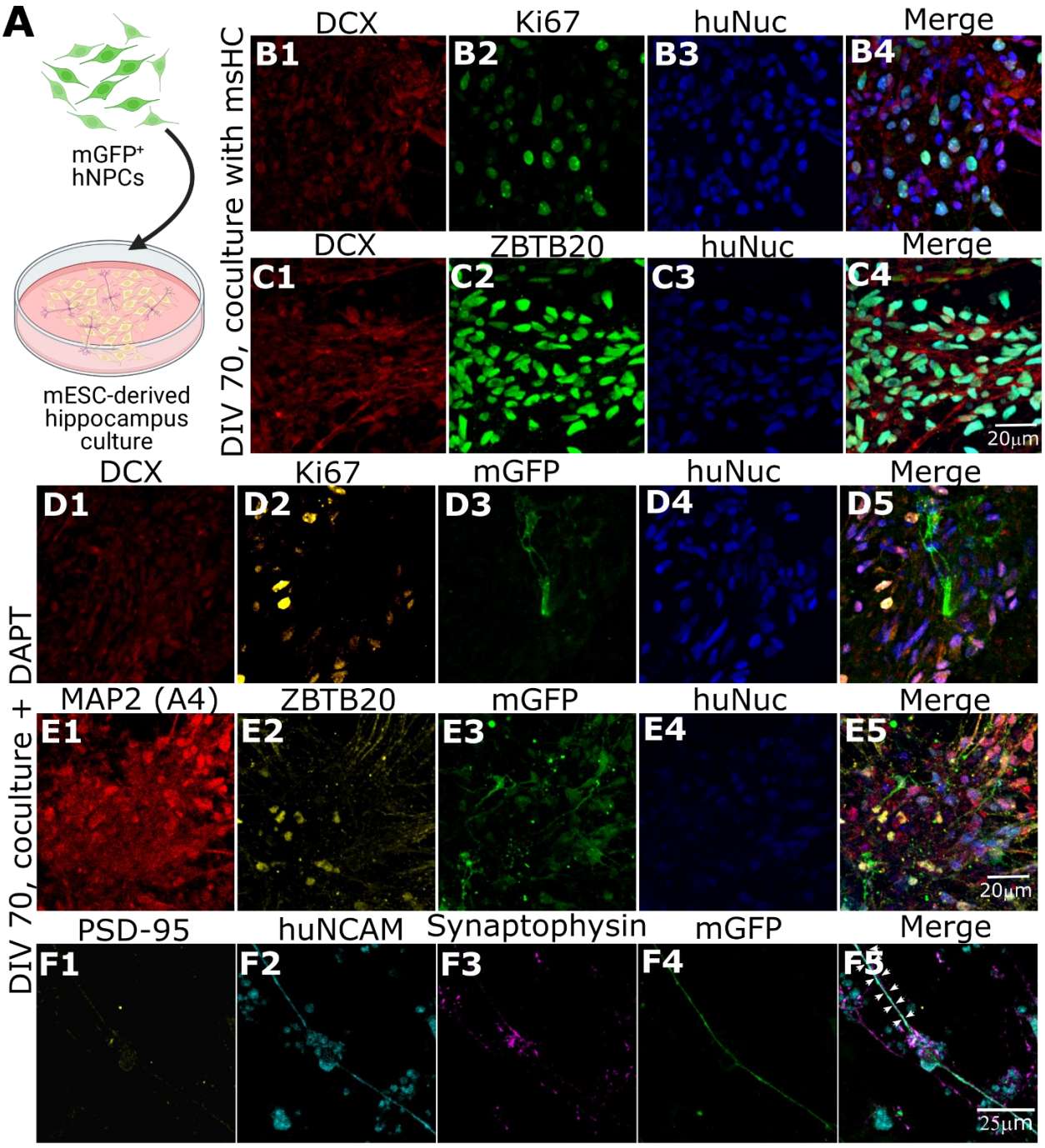

Figure 39. Differentiation of hippocampal neural precursors on mouse hippocampal coculture. (A) Human hippocampal neural precursors were cocultured with mESC-derived hippocampus cultures as (B, C) wild-type or (D-F) transduced with mGFP and treated with DAPT 24 hours prior to reseeding. After 40 days in culture, cells were fixed and immunostained for DCX (B1), Ki67 (B2), human Nuclear antigen (huNuc, B3) and their coexpression (B4); DCX (C1), ZTB20 (C2) huNuc (C3), and their coexpression (C4); DCX (D1), Ki67 (D2), unamplified mGFP (D3), human Nuclear antigen (huNuc, D4) and their coexpression (D5); MAP2 (A4) (E1), ZBTB20 (E2), amplified mGFP (E3), huNuc (E4), and their coexpression (E5); and PSD-95 (F1), human NCAM (huNCAM, F2), synaptophysin (F3), amplified mGFP (F4), and their coexpression (F5). White arrows in F5 indicate overlap between mouse synaptophysin^{+} fiber and human mGFP^{+}/PSD95^{+} fiber

huHC neural progenitors differentiate as a function of ZBTB20

After understanding whether DG-like NPCs could effectively be fated through small molecule programming, I wanted to further understand the role of ZBTB20. ZBTB20's role in human seems ambiguous as it is described as potentiating glioblastoma (J. Liu et al., 2018), inducing astrocytogenesis in the neocortex (Doeppner et al., 2019; Nagao et al., 2016), but whose mutation is contended as pleiotropic for Primrose Syndrome (Alby et al., 2018; Cordeddu et al., 2014; Mattioli et al., 2016; Stellacci et al., 2018), a familial macrocephaly. To uncover ZBTB20's role in human hippocampal development within the context of my hiPSC-derived neural progenitors, I indirectly inhibited NOTCH using γ-secretase inhibitor, DAPT, in progenitor cultures on mouse laminin for 48 hours, either alone or in the co-presence of CHIR (Figure 40). After another 48 hours from the treatments (CHIR-/DAPT- [control, Figure 40A], CHIR+/DAPT- [+GSK-3β inh. Figure 40B], CHIR-/DAPT+ [+NOTCH inh. Figure 40C], CHIR+/DAPT+ [Dual inh. Figure 40D]) I fixed and stained for Nestin (Figure 40A1-D1), NeuN (Figure 40A2-D2), ZBTB20 (Figure 40A3-D3), and Hoechst nuclei (Figure 40A4-D4, merge Figure 40A5-D5) and counted cells expressing high ZBTB20 or NeuN automatedly. I found that 2 days after the treatment, ZBTB20 was most upregulated in CHIR+/DAPT+ cultures, followed by CHIR+/DAPT- culture (Figure 40E). Interestingly, CHIR-/DAPT+ cultures did not elicit a heightened ZBTB20 response in comparison to control cultures (Figure 40E). However, only CHIR+/DAPT- treatment was sufficient to elicit high NeuN expression significantly (Figure 40F). Furthermore, ZBTB20's trend was concomitant with $NeuN^+$ trend. I performed Spearman correlation tests between ZBTB20 and NeuN individual images and found that the average R^2 value between the two was most significantly increased in CHIR+/DAPT+ group (Figure 40G). Given these pieces of data, I next wanted to understand if dual inhibited groups were maturing faster than CHIR-/DAPT+ cultures, as NeuN did not increase in response to DAPT. To test this, I repeated the experiments (CHIR-/DAPT- [control Figure 41A], CHIR+/DAPT- [+GSK-3β inh Figure 41B], CHIR-/DAPT+ [+NOTCH inh. Figure 41C], CHIR+/DAPT+ [Dual inh. Figure 41D]) but stained with DCX (Figure 41, Col. 1), MAP2 (Figure 41, Col.2), Hoechst (Figure 41 Col. 3). I employed a batch fiber length ImageJ macro to estimate the total length of DCX^+ and $MAP2^+$ fibers after treatment. I found that both DAPT+ treatments induced DCX outgrowth (Figure 41E) and MAP2

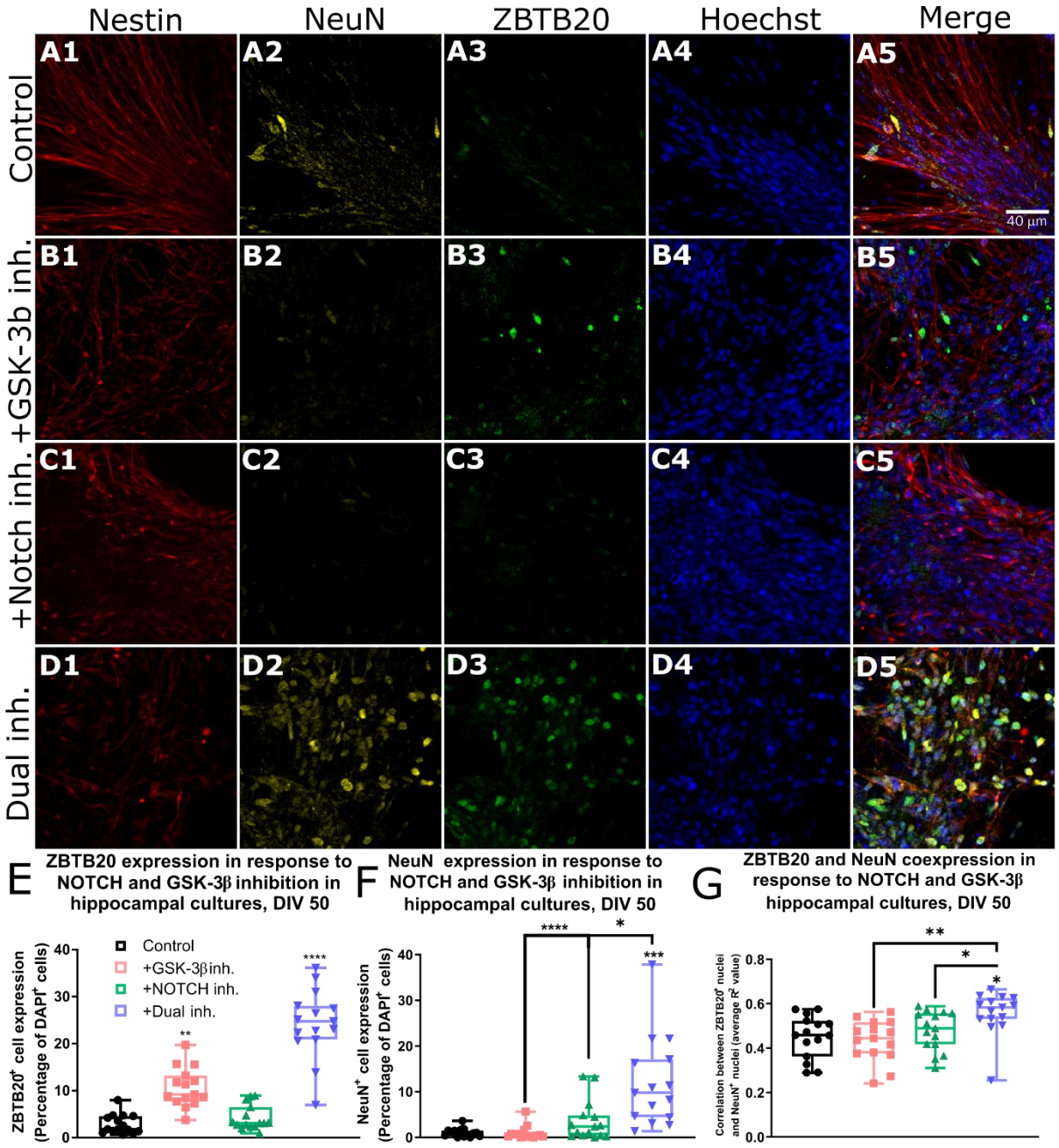

Figure 40. Differentiation of hippocampal neural progenitors by NOTCH inhibition. Naive progenitors were plated on mouse laminin and treated at DIV 46 for two days in either minimal media (Control, A), with 3µM CHIR 99021 alone (+GSK-3β inh., B), with 12.5µM DAPT alone (+Notch inh.), or with simultaneous 3µM CHIR 99021 and 12.5µM DAPT (Dual inh., D). Inhibitors were removed after two days and cells were maintained in minimal media for another two days before fixation. Cells were immunostained with Nestin (Col. 1), NeuN (Col. 2), ZBTB20 (Col. 3), and Hoecsht (Col. 4) and portrayed as their coexpression (Coll. 5). Z-stack mages were acquired via confocal and ZBTB20 and NeuN expressing cells were counted semi-automatedly in each stack with in-house batch cell counter macro in ImageJ. (E) Significant increases in ZBTB20 expressing cells in GSK-3β inh. and Dual inh. were observed compared to control (+5%, +20% respectively). (F) Significant increases in NeuN expressing cells were observed in Dual inh. compared to all groups (+9%). (G) Average Pearson Correlation between ZBTB20 and NeuN .tif images. Significant increases in overlapping signal were observed in Dual inh. compared to all groups (+0.2 R2 value). Statistical analyses were performed by One-Way ANOVA, post-hoc Kruskal-Wallis test; asterisks above plotted values indicate comparison against control whereas above solid black bars indicate between groups; error bars indicate 99% CI *-p-val<0.05, **-p-val<0.01, ***-p-val<0.001, ****-p-val<0.0001

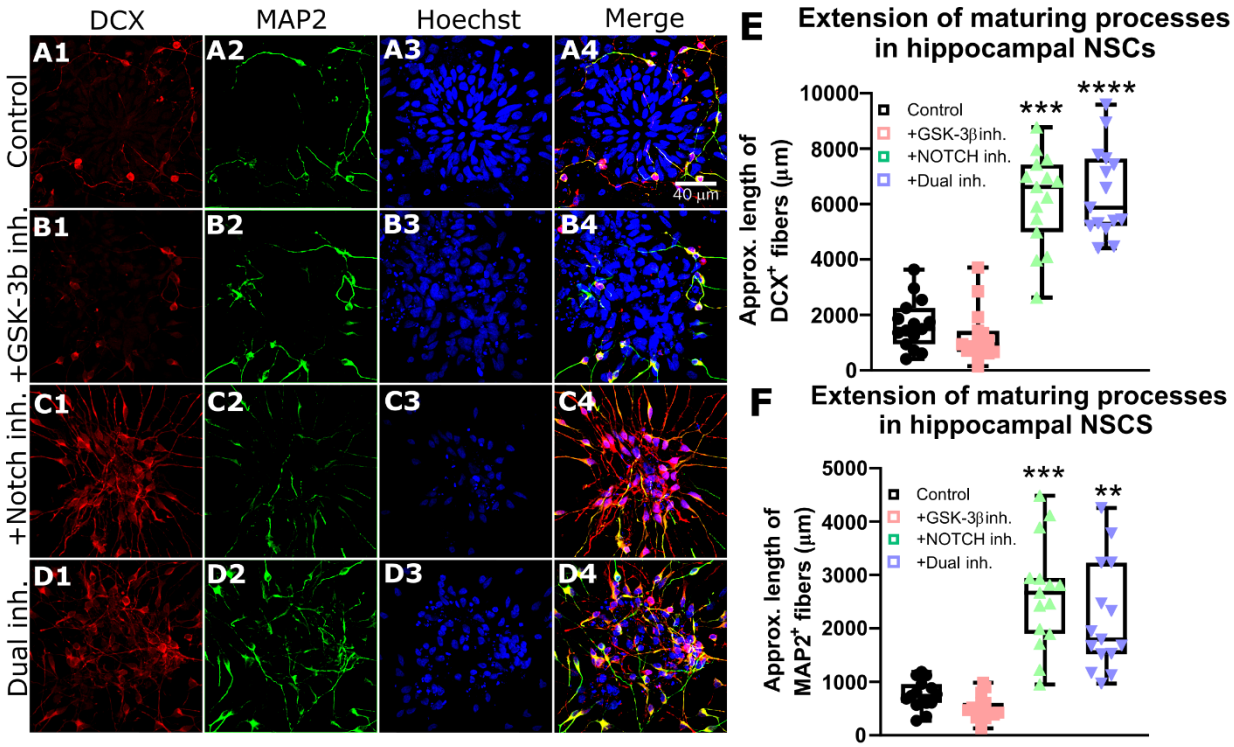

Figure 41. Differentiation of hippocampal neural progenitors by NOTCH inhibition-Neurocytoskeleton. Naive progenitors were plated on mouse laminin and treated at DIV 46 for two days in either minimal media (Control, A), with 3μM CHIR 99021 alone (+GSK-3β inh., B), with 12.5μM DAPT alone (+Notch inh.), or with simultaneous 3μM CHIR 99021 and 12.5μM DAPT (Dual inh., D). Inhibitors were removed after two days and cells were maintained in minimal media for another two days before fixation. Cells were immunostained with DCX (Col. 1), MAP2 (Col. 2), Hoechst (Col. 3), and their coexpression (Col. 4). Z-stack mages were acquired via confocal and DCX and MAP2 fiber were estimated semi-automatedly in each stack with in-house batch fiber measurement macro in ImageJ. (E) Significant increases in DCX^+ fibers were observed in both +Notch Inh. and Dual inh. compared to control (+5000μm, +4200μm respectively). (F) Significant increases in $MAP2^+$ fibers were observed in both +Notch Inh. and Dual inh. compared to control (+2000μm, +1050μm respectively). Statistical analyses were performed by One-Way ANOVA, post-hoc Kruskal-Wallis test; error bars indicate 99% CI; asterisks above plotted values indicate comparison against control; **-p-val<0.01, ***-p-val<0.001, ****-p-val<0.0001

outgrowth (Figure 41F) compared to their respective controls. To understand if the nuclear appearance of ZBTB20 was predictive of maturing neuronal populations like I had inferred from Figure 30, I performed a linear regression analysis between $ZBTB20^+$ nuclei and either DCX fiber length (Figure 42A) or MAP2 fiber length (Figure 42B) and found a correlation with DCX but not MAP2 (Figure 42). I speculate that cells with lengthened DCX and MAP2 fibers belong to two different populations of cells in earlier (DCX elongation) and later (MAP2 elongation) step of neuronal differentiation, respectively, and that ZBTB20 appearance precedes late maturation.

Finally, to understand ZBTB20's function in naïve progenitors, I knocked out ZBTB20 by CRISPRCas9 knockout system by lentiviral transducing hippocampal cells at DIV 29 using the construct provided by Genscript (see methods). Expression KO efficiency was evaluated by first transducing the virus in HeLa cells and validating ZBTB20's absence by Western Blot. To cross-reference the data obtained by CRISPRCas9 -mediated knockout I also knocked down ZBTB20's function (ZKD) by transducing in the same culture conditions induced a dominant negative with ZBTB20^{BTB-}

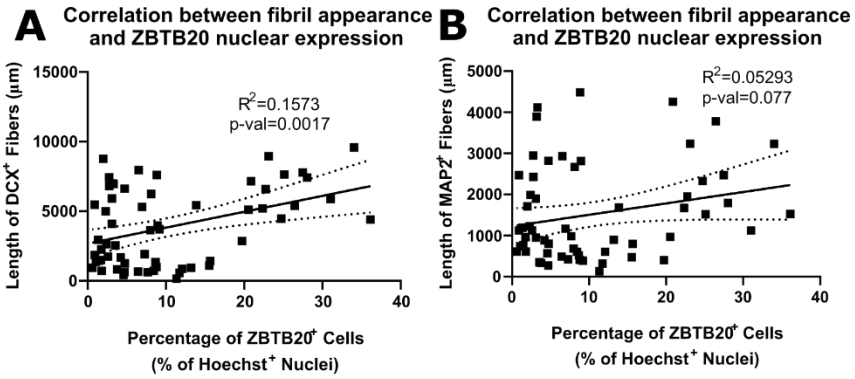

Figure 42. Correlation between ZBTB20 and neurocytoskeletal markers. Correlational models were established to investigate the relationship observed from in vivo SC RNASeq clustering data in Fig 9 (A) A weak but significant relationship was observed between percentage of ZBTB20^{+} cells (acquired from Fig 12) and DCX fiber length (acquired from Fig 13; p-val=0.0017). (B) No correlation was observed between percentage of ZBTB20^{+} cells (acquired from Fig 12) and MAP2 fiber length (acquired from Fig 13). Statistical analyses were performed by constructing a linear regression model of all DIV 50 treatment replicates using a power threshold of 80%; variance plotted as dotted lines N=60

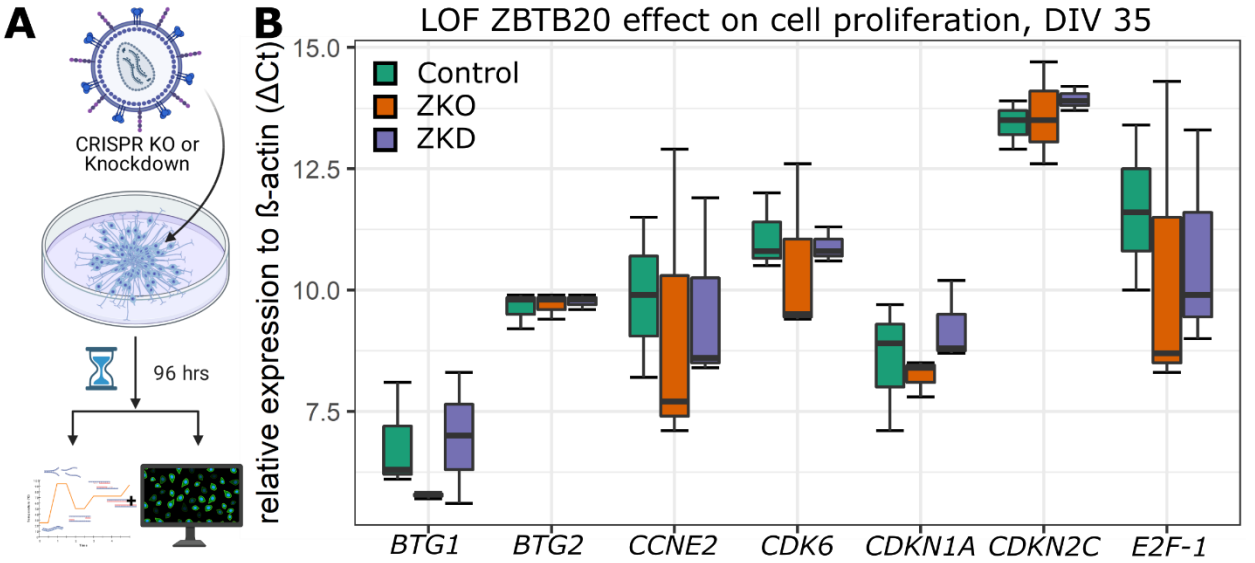

Figure 43. Functional loss of ZBTB20 and downstream differentiation markers. (A) Schematic of experiments, DIV 31 cell were either untransduced (Control), or transduced with either ZBTB20^{BTB-} (ZKD,) or CRISPR KO of ZBTB20 (ZKO); 96 hours later, cells were analyzed by qRT-PCR. (B) No significant changes were observed between any groups within their respective gene comparisons. Data shown as DCt calculated by [Gene of Interest take off cycle] - [β-actin take off cycle] per indidvidual sample. Analysis was made using Two-Way ANOVA. error bars depict 99% CI, N=3

overexpression lentiviral construct lacking the BTB dimerization domain (Origene reference SC114633, see methods) (Figure 43A). qRT-PCR analysis of cell cycling genes, however, demonstrated no differences in cell cycle regulators assessed (Figure 43B). Having demonstrated that that ZBTB20 may be inactive in regulating continuance of symmetrical divisions of human dentate gyrus progenitors at this timepoint *in vitro*, I next sought to assay their propensity for continued cell cycle divisions.

Specific laminar substrate and constitutive GSK-3β inhibition prolongs proliferation of hDG-like progenitors

Hippocampal neurogenesis is sustained across many species' lifespans, long after exit from embryogenesis and early development (Altman & Das, 1965). Both in embryonic and adult neurogenesis, laminins play a crucial role in neural stem cell maintenance and differential transition to neurons (Hyysalo et al., 2017; Nascimento et al., 2018; Yamagishi et al., 2021) . To model prolonged neurogenesis, I theorized that the laminin substrate must actively be involved in maintaining the neural stem niche but that removal from that niche should stimulate cell cycle exit (Figure 44A). Focusing on major laminins (Figure 44B) , With the support of Luca Pandolfini, I first assessed mouse spatial transcriptomic data of laminin alpha chain messenger, *Lama*, expression from SPATiAL Transcriptomic and 10X Genomics. Discreet cross-sections of mouse cortex tissue were bound to 2-D Poly-T mRNA capture probes chips and processed via cDNA amplification and sequencing, allowing spatial analysis of the superficial cells of target tissue encoded by the location on the chip (https://spatialtranscriptomics.com/workflow/). Most *Lama* isoforms were expressed in a salt and pepper pattern across the coronal cortical reconstruction however *Lama5* was condensed near the dentate gyrus (Figure 44C). To assay laminin-mediated survivability, I plated DIV 28 naïve progenitors on glass coated with poly-l-ornithine and one of the following recombinant laminin substrates: 511 (Figure 45A), purified mouse laminin (Figure 45B), 111 (Figure 45C), 121 (Figure 45D), 332 (Figure 45E), and 411 (Figure 45F). After 4 days *in*

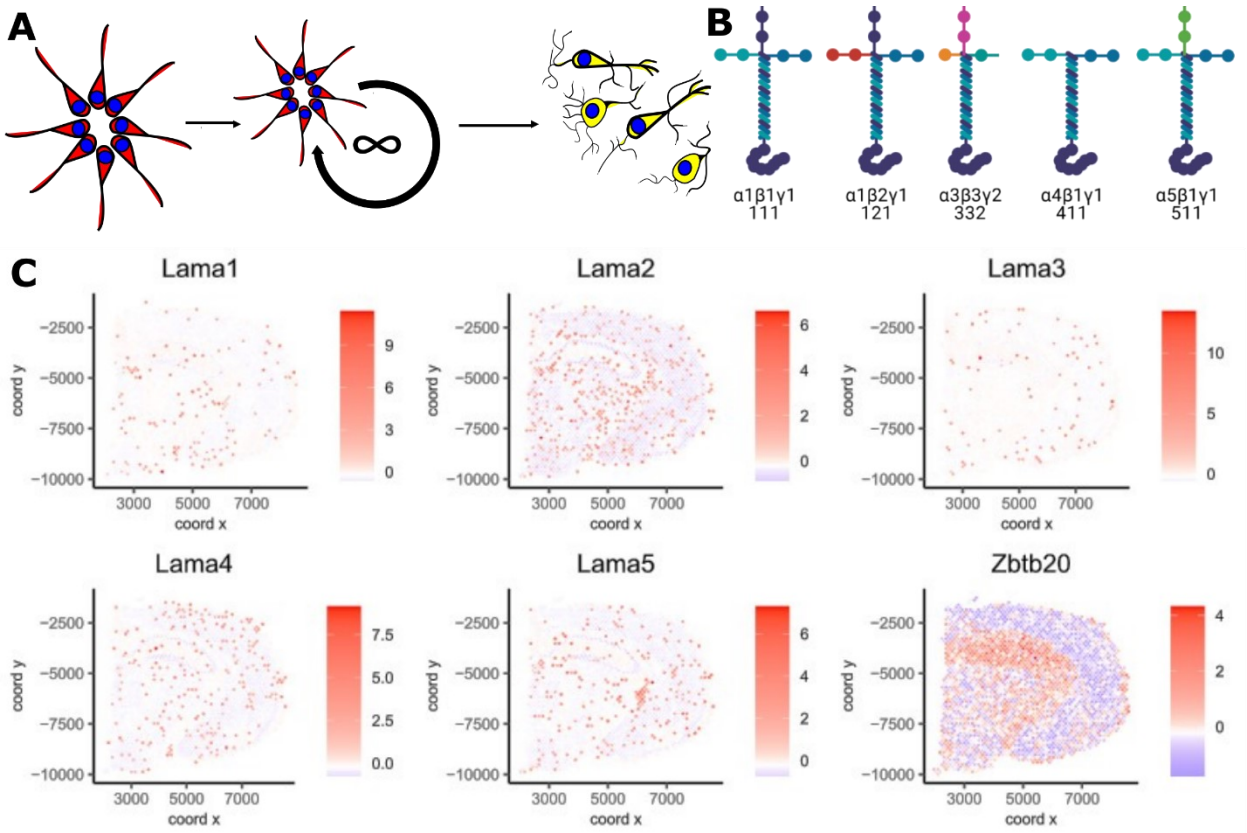

Figure 44. Investigation of laminin in its maintenance in neural stemness. (A) Neural stem cells in the subgranular neurogenic niche self-replicate throughout mammalian lifespan while supplying the granule cell layer of the Dentate Gyrus with neurons. The following experiments and observation investigate the underlying molecular prerequisites for sustaining neurogenesis in vitro. (B) Laminin isoforms used in this thesis and their structural representation. (C) *Lama* (α-chain of laminin) spatial expression across the adult mouse brain using SPATiAL transcriptomic chips, reconstructed from open data provided by SPATiAL proect, subsect of 10X Genomics. Most *Lama* mRNA are expressed salt-and-pepper with the exception of *Lama5* sequestered near the dentate gyrus. Scale bars indicate RPKM

vitro in minimal media, these cells exhibited markedly different phenotypes. During culture, cells plated on laminins 111 and 411 died en masse. Chromatin condensation was assayed via Hoechst staining and epifluorescent microscopy; the average nuclear area, a parameter of pyknosis and cell viability if DNA fragmentation is present (Kroemer et al., 2009), was greatest in cells plated on 511 laminin compared to 111 and 411. Furthermore, membrane blebbing increased in cells plated on 111 and 411 compared to 511 isoforms, as well. These experiments were repeated with CHIR (Figure 46A-F) and assayed via ICD for Nestin (Figure 46 Row 1), βIII-tubulin (Figure 46 Row 2), and Hoechst nuclei (Figure 46 Row 3). Nestin^{+} fibers were upregulated in 511 compared to 111, 332, 411, and trended greater than msl, however, 121 also exhibited lengthened Nestin fibers but only compared to 111 and 332 (Figure 46G). Analysis of βIII-tubulin fiber length

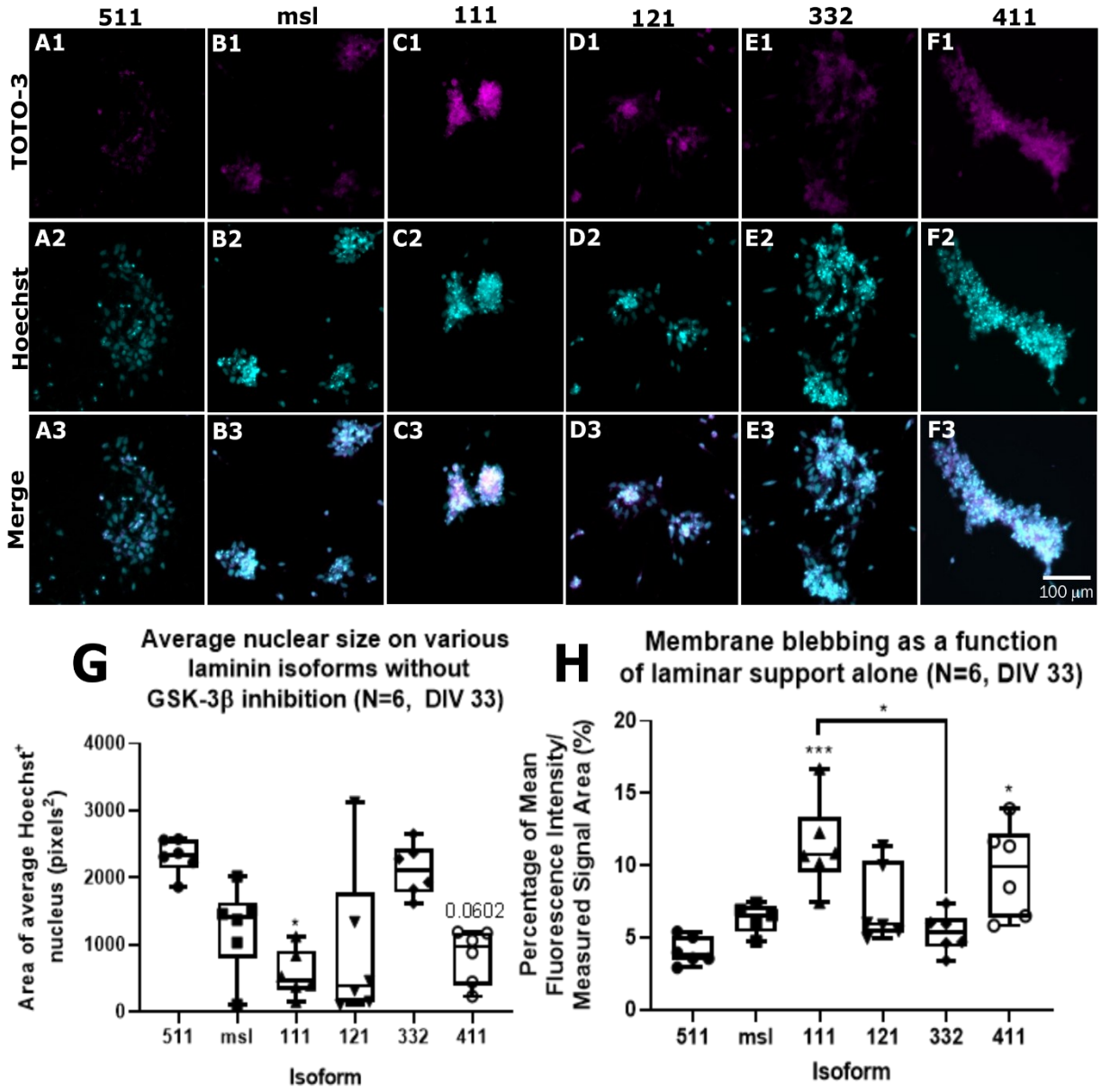

Figure 45. Laminar isoforms and their inherent maintenance of cell health. DIV 28 progenitors were plated on laminin isoforms 511 (A), conventional purified mouse laminin (msl, B), 111 (C), 121 (D), 332 (E), 411 (F) and maintained in minimal media for 5 days before fixation. Cells were histostained pre-permeabilization with DNA intercalant, TOTO-3 (Row 1), post-permeabilization with Hoechst (Row 2), and merged (Row 3). Epifluorescent images were acquired, TOTO-3 was measured by mean fluorescence intensity and Hoechst+ nuclei were processed semi-automatedly in each stack with in-house batch cell counter and summarizer macro in ImageJ. (G) Average area of nuclei of cells plated on various isoforms, 511 supported largest of area of nuclei and significantly compared to 111 (+2150 pixels). (H) Permeabilization of membrane in culture conditions by proxy of TOTO-3. 511 prevents membrane blebbing inherently, demonstrating the least fluorescent signal of TOTO-3 per nuclear area, and significantly compared to 111 (+7%) and 411 (+7%). 332 demonstrated slightly more blebbing but only significantly compared to 111 (+5%). One-way ANOVA analyses and post-hoc Kruskal-Wallis tests were performed using average nuclear area and signal percentage over total area of nuclei; asterisks above box plots indicate comparison against control whereas above solid black bars indicate between groups; error bars indicate 99% CI. *-p-val<0.05, ***-p-val<0.001, N=6

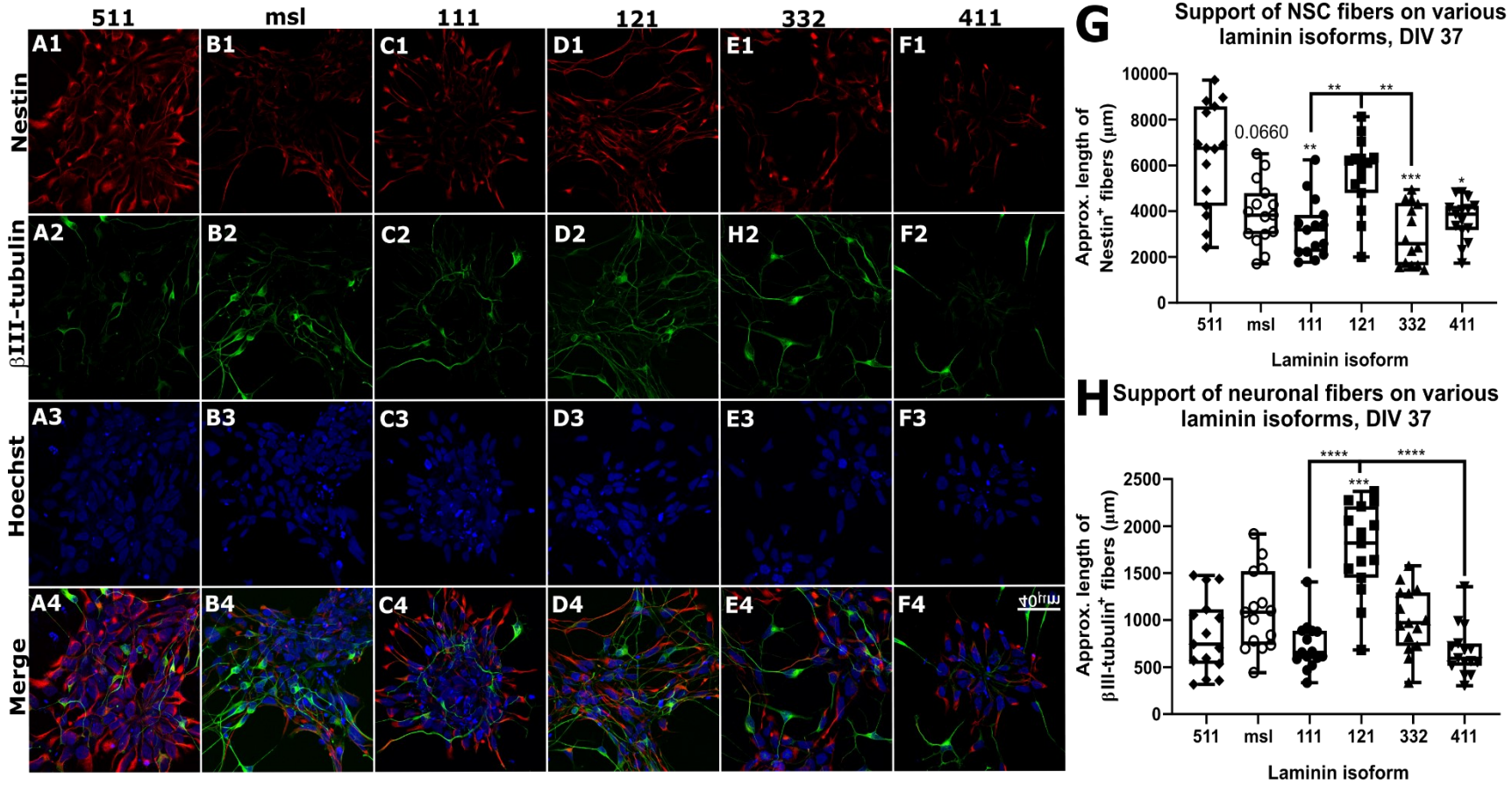

Figure 46. Propagation of hippocampal NSCs on different laminin isoforms. From DIV 28, NPCs were plated on laminin isoforms 511 (A), conventional purified mouse laminin (msl, B), 111 (C), 121 (D), 332 (E), 411 (F) and maintained in minimal media + CHIR for 9 days before fixation at DIV 37. Cells were immunostained for Nestin (Row 1), βIII-tubulin (Row 2), and Hoecsht (Row 3), coexpression (Row 4). Z-stack mages were acquired via confocal and Nestin and βIII-tubulin images were processed semi-automatedly in each stack with in-house batch fiber measurement macro in ImageJ. (G) In comparison to 511, Nestin was downregulated in all other isoforms, except 121, and signficantly in comparison to 111 (-4100 μm), 332 (-4500 μm), and 411 (-3000 μm). 121 maintained Nestin+ fibers in comparison to both 111 (+2700 μm) and 332 (+3100 μm). (H) In comparison to 511, only 121 exhibited upregulated βIII-tubulin (+1000 μm). 121 also exhibited higher expression compared to 111 (+1150 μm) and 411 (+1250 μm). Both (G) and (H) were analyzed with one-way ANOVA analyses and post-hoc Kruskal-Wallis tests; asterisks above box plots indicate comparison against control whereas above solid black bars indicate between groups; error bars represent 99% CI. *-p-val<0.05, **-p-val<0.01, ***-p-val<0.001, ****-p-val<0.0001; N=15

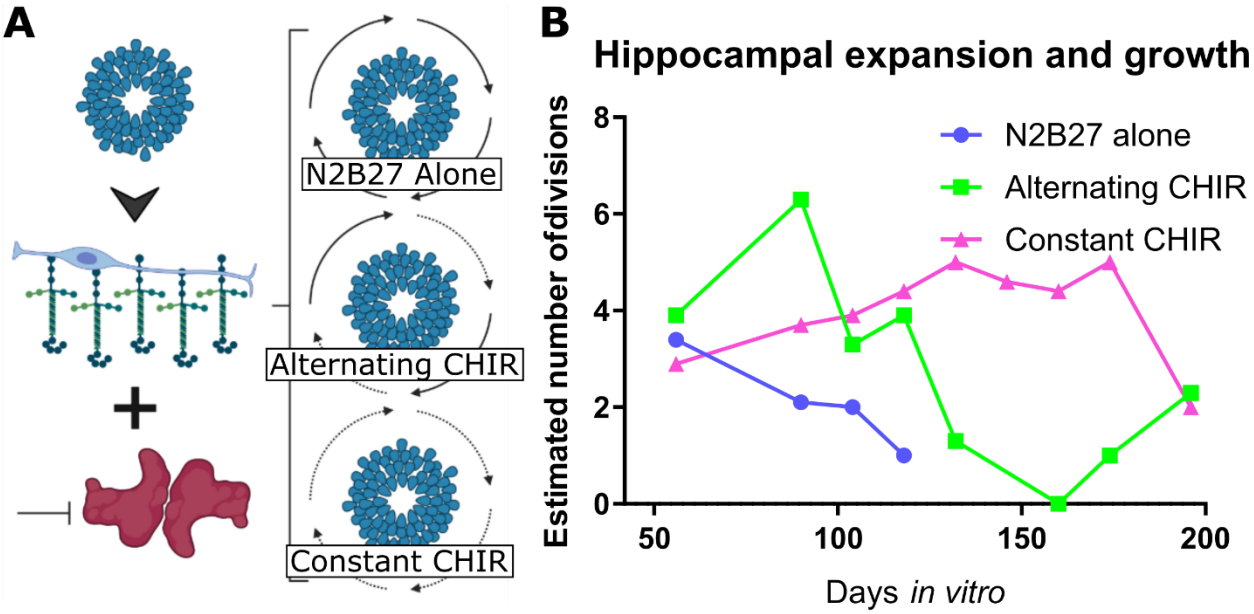

Figure 47. Expansion of hippocampal neural stem cells on 511 laminin. (A) Neural stem cells (blue rosette) were plated on 511 laminin and treated with temporally varying GSK-3β inhibition patterns and passaged every 14 days to assay the second requisite for neural stem maintenance. Patterns included minimal media in all passages (N2B27 alone), minimal media one passage followed by minimal media + CHIR99021 in the subsequent passage (Alternating CHIR), or minimal media + CHIR99021 in all passages (Constant CHIR). (B) Cells were counted at each passage by Burker technique and subtracted from the total number of cells plated at the previous passage, then taken the $\log_2$ of the differential ($\log_2$(most recent passage cell count number - previous passage cell count number)). N2B27 cells decreased growth rate from the initial split and stopped at ~DIV 120, Alternating CHIR exhibited a burst in growth (6 divisions) by DIV 90 but rapidly negatively accelerated until DIV 150, Constant CHIR gradually increased in estimated log divisions until ~DIV 180 then decreased to 2 at DIV 200.

instead demonstrated that βIII-tubulin fibers were significantly lengthened in 121 compared to 511, as well as 111 and 411 (Figure 46H). Overall it was evident 511 was the most optimal substrate for expanding hippocampal neural stem cells as the data further corresponds with previous findings (Ahmed et al., 2009; Doe, 2008; Hyysalo et al., 2017).

I thus used 511 to expand the niche of hippocampal NSCs over the course of 230 days *in vitro*. Passaging every 14 days, I established 3 separate niches to understand the minimal requirements necessary for longitudinal expansion of hippocampal NSCs. The niches always included 511 and cells were either cultivated in N2B27 alone, N2B27 + CHIR in alternating passages, and N2B27 + constitutive CHIR (Figure 47A). At every passage (~14 days), cells were counted, and replated onto 511 laminins at equivalent surface densities. Estimated number of divisions from cell counts pointed that CHIR, cells exhausted their replicative ability over time, CHIR in alternating passages resulted in a large burst of proliferation at ~DIV90 followed by an abrupt

destabilization, and constant CHIR instead seemed to provide the most stable growth pattern (Figure 47B). To understand the proliferative capacity of constant CHIR cells, I quantified DCX (Figure 48 Row 1), ZBTB20 (Figure 48 Row 2), Ki67 (Figure 48 Row 3), and Hoechst (Figure 48, Row 4) at DIV 40 (Figure 48A), 100 (Figure 48B), 170 (Figure 48C), and 240 (Figure 48D). No significant differences emerged between any DIV group though the mean population density seemed to trend negatively (-10%, Figure 49A). Furthermore, interphasic cell count with Ki67 images showed no significant changes despite time spent *in vitro* (Figure 49B). DCX^{+} fibers, however, were shorter at DIV 240 compared to DIV 40 (Figure 49C). $ZBTB20^{+}$ positive cells did not change significantly between any DIV groups (Figure 49D). Finally, while some signs of pyknosis appear prevalent in the DIV240 culture, no further cell death assays or measurements were attempted as the cultures at this time expanded more rapidly than preceding DIVs.. Having longitudinally expanded human hippocampal NSCs on isolated 511 laminin, I next investigated laminar-dependent differentiation (Figure 50A). First, cells were either plated at DIV 21 on 511 laminin (Figure 50B), in progenitor maintenance conditions (PMC, 511, +CHIR, Figure 50C), or spontaneous differentiation conditions (SDC, msl, -CHIR Figure 50D) and were analyzed by ICD for Nestin (Figure 50 Col. 1), NeuN (Figure 50 Col. 2), ZBTB20 (Figure 50 Col. 3), and Hoechst+ nuclei (Figure 50 Col. 4) coexpression

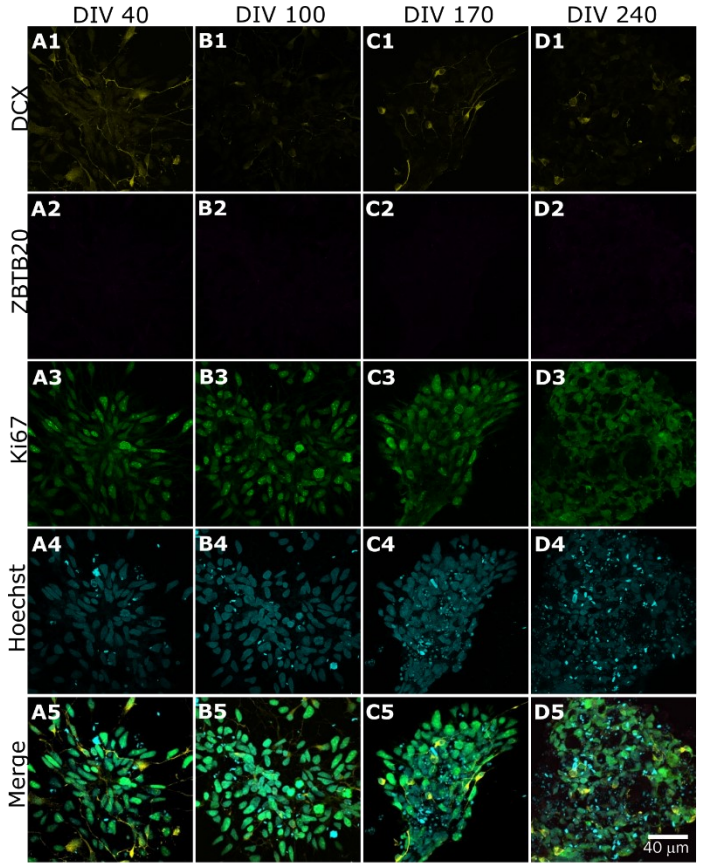

Figure 48. Effect on proliferative and differentiation by longitudinal expansion on 511 laminin and in constant CHIR 99021 for ~1 year. Over the course of 240 days *in vitro*, hippocampal NSCs were assayed at DIV 40 (A), DIV 100 (B), DIV 170 (C) and DIV 240 (D) for their proliferative capacity and potential for spontaneous exit from symmetrical divisions. Cells were immunostained with DCX (Row 1), ZBTB20 (Row 2), Ki67 (Row 3),and Hoechst (Row 4) for their coexpession at their respective timepoint (Row 5). Z-stack mages were acquired via confocal and images were processed semi-automatedly in each stack with respective macros in ImageJ for analysis shown in Fig 22.

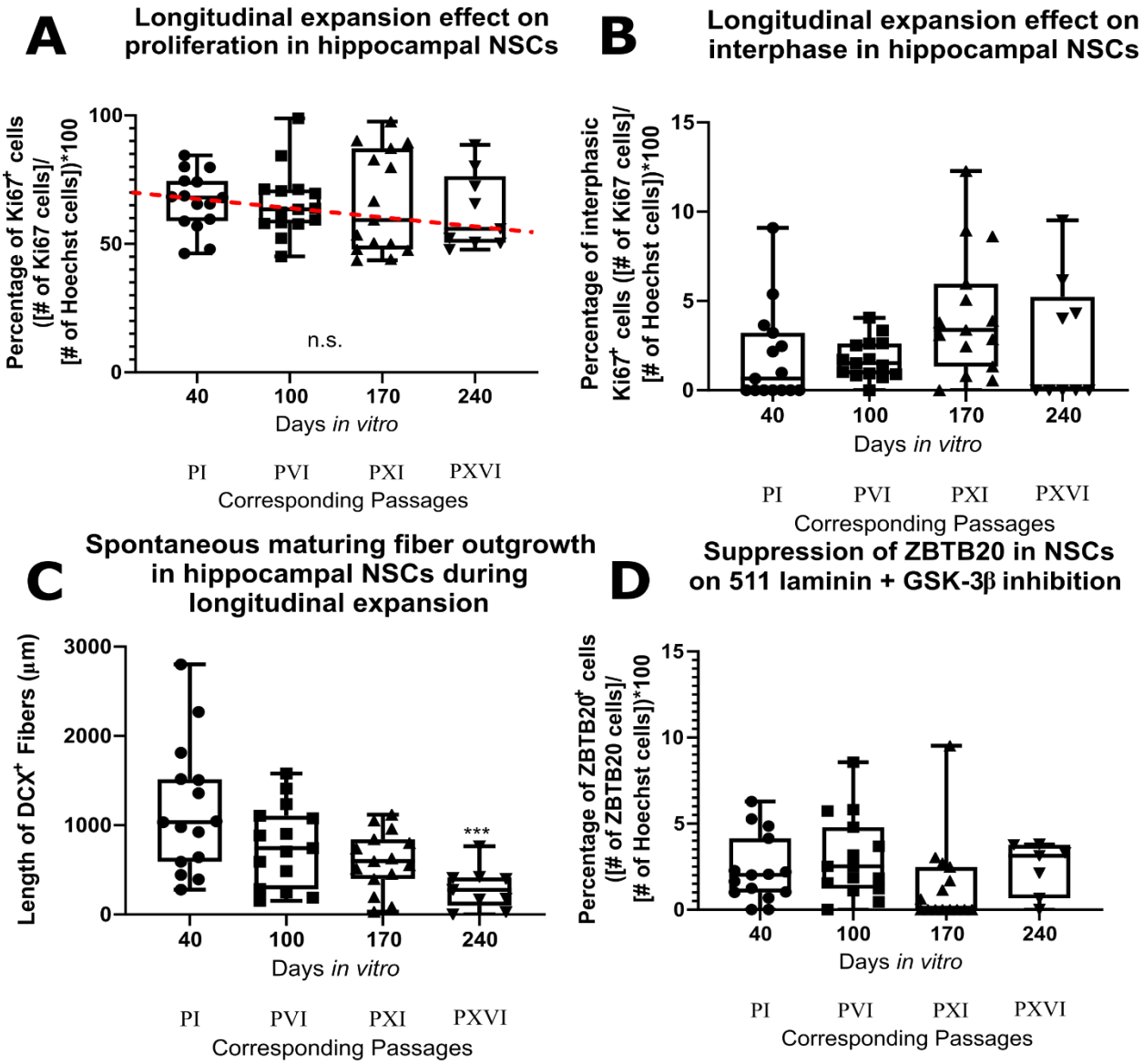

Figure 49. Analysis of proliferation and differentiation by longitudinal expansion on 511 laminin and in constant CHIR 99021. The following analyses were performed using the confocal images acquired in Fig 21. (A) No significant changes were observed in percentage Ki67^{+} cells despite time in vitro, red dashed line intersects through group means (DIV 40 ~70; DIV 240 ~60%). (B) Analysis of interphasic Ki67^{+} cells indicated no further changes in mitotic capacity across longitudinal expansion (~2.5%). (C) No increases in DCX fiber length were observed, only a decrease at DIV240 compared to DIV 40 (-600 mm). (D) No significant changes were observed in the proportion of ZBTB20^{+} nuclei over time and did not upregulate (0-4%). All analyses were performed with a one-way ANOVA followed by a Kruskal-Wallis post-hoc test. Error bars represent 99% CI. ***-p-val<0.001; N=15

(Figure 50 Col. 5). Nestin expression was slightly upregulated in DIV 90 PMC cultures compared to DIV 33 naïve progenitors but instead significantly downregulated in DIV 90 SDC cultures compared to both naïve and PMC progenitors (Figure 50E). A strong increase in ZBTB20 in SDC cultures was also observed in comparison to both

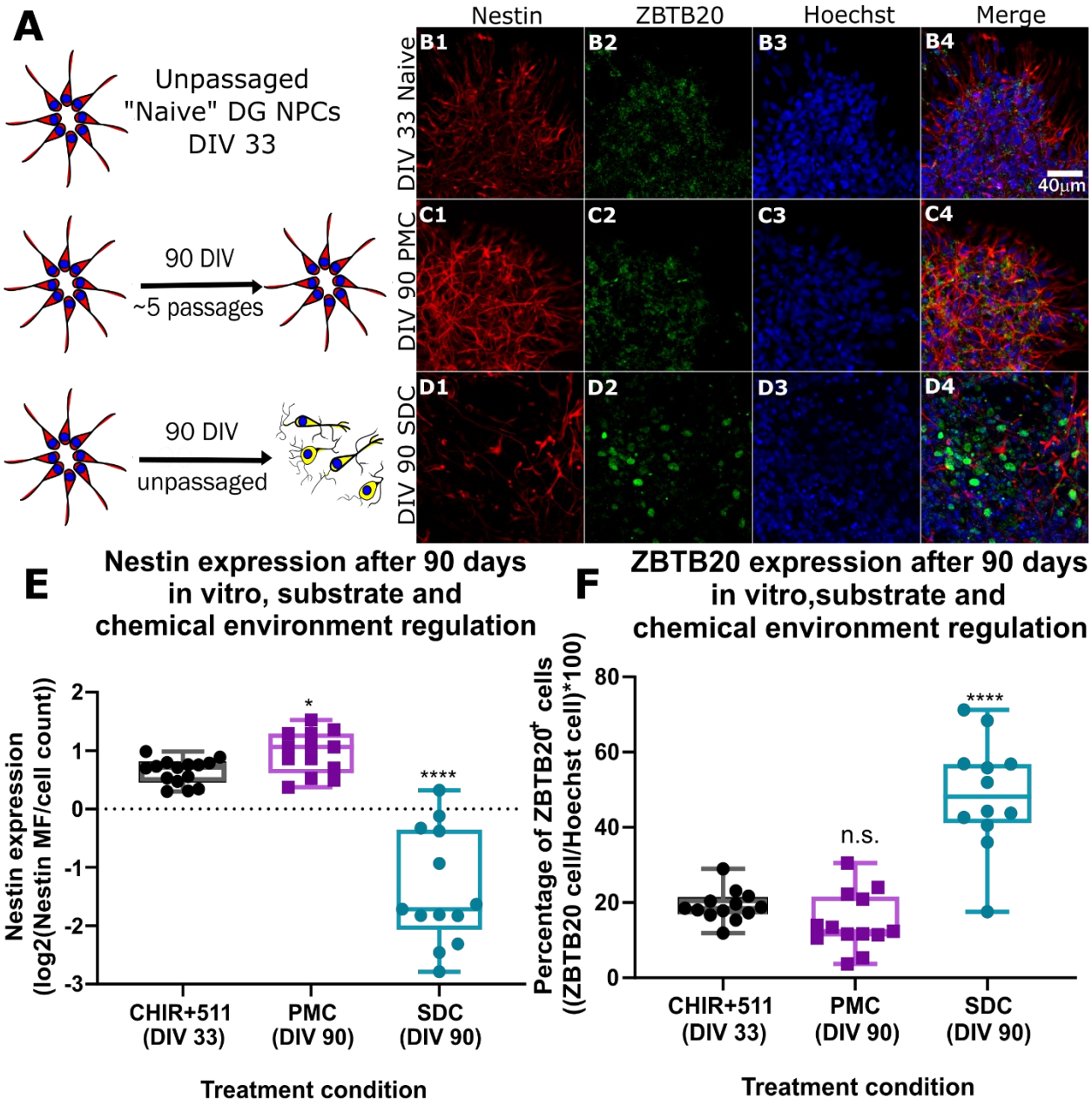

Figure 50. Neural stem cells grown on 511 laminin do not differentiate despite time in vitro. (A) Schematic overview of experiment, three groups of cells, DIV 33 naive progenitors (B, Naive), NSCs grown in progenitor maintenance conditions (PMC, on 511 laminin and in 3μM CHIR) until DIV 90 (C), and NSC grown in spontaneous differentiation conditions (SDC, on mslam and in minimal media) until DIV 90 (D). Cells were fixed and immunostained for Nestin (Col. 1), ZBTB20 (Col. 2), and Hoechst (Col. 3) to assay their coexpression (Col. 4). Z-stack mages were acquired via confocal and images were processed semi-automatedly in each stack with in-house batch fluorescence measurement (Nestin) and batch cell counter macros (ZBTB20, Hoechst) in ImageJ. (E) Nestin fluorescence signal was normalized to Hoecsht^{+} cell count and logarithmically transformed to give a relative Nestin expression score. Nestin in was significantly downregulated in SDC group compared to Naive (-2.7). (F) Percentage of ZBTB20^{+} cells was unchanged between Naive and PMC (~19.5%) but significantly doubled at DIV 90 in SDC cells (+26%). Groups were analyzed with one-way ANOVA analyses and post-hoc Kruskal-Wallis tests; asterisks above box plots indicate comparison against control; error bar represent 99% CI. *-p-val<0.05, ****-p-val<0.0001; N=12

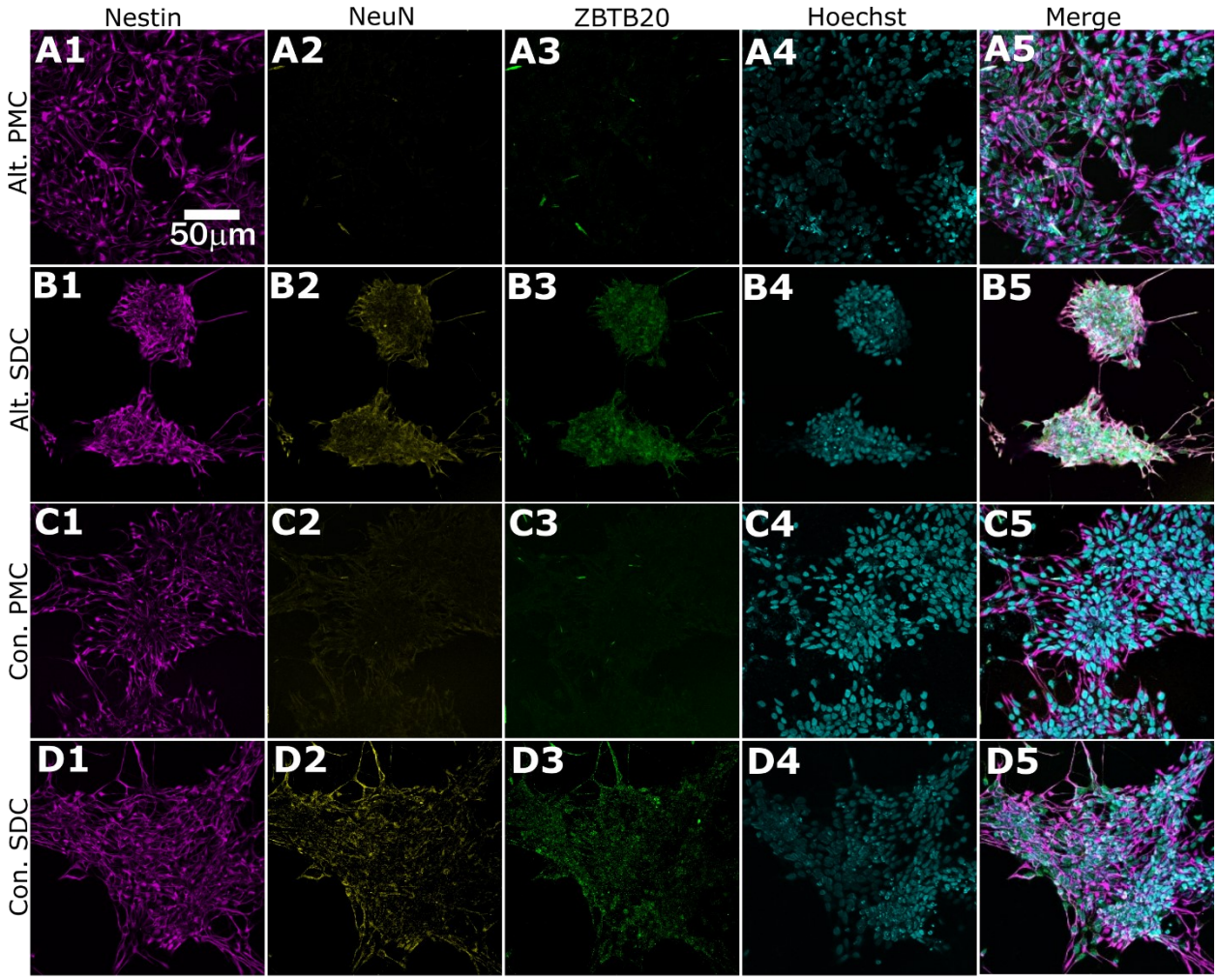

Figure 51. Neural stem cells expanded under prolonged GSK-3β retain neurogenesic capacity despite surviving 511-expanded cells. At DIV 102, after N2B27 alone cells from Fig 20 ceased growing, NSCs from the Alternating CHIR group were grown in PMC (Alt. PMC, A) or SDC (Alt. SDC, B); likewise NSCs from Constant CHIR group were grown were grown in PMC (Con. PMC, C) or SDC (Con. SDC, D). At DIV 110, cells were fixed and immunostained for Nestin (Col. 1), NeuN (Col. 2), ZBTB20 (Col. 3), and Hoechst (Col. 4) for their coexpression (Col. 5). Z-stack mages were acquired via confocal and images were processed semi-automatedly in each stack with in-house batch fluorescence measurement macro in ImageJ. Resultant values were analyzed in Figure 25.

naïve and PMC cultures (Figure 50F). To further investigate differing progenitor pools from Figure 47A, cells from the alternating group (Alt) were cultured on either PMC (Figure 51A) or SDC (Figure 51B) and cells from the constitutive CHIR group (Con) on either PMC (Figure 51C) or SDC (Figure 51D), ICD sampling for Nestin(Figure 51 Col. 1), NeuN (Figure 51 Col. 2), ZBTB20 (Figure 51 Col. 3), and Hoechst+ nuclei (Figure 51 Col. 4) and their coexpression (Figure 51 Col. 5). A decrease in Nestin between Alt. PMC compared to Alt. SDC cells was observed but in contrast, Con. SDC cultures demonstrated an upregulation in Nestin compared to PMC (Figure 52A). NeuN signal did not change between Alt PMC and SDC whereas there was a significant

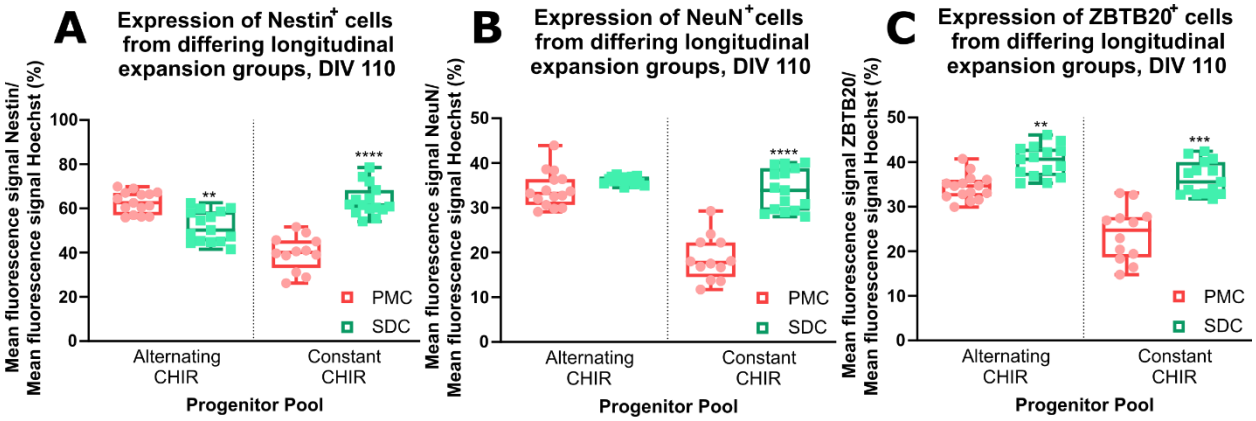

Figure 52. Analysis of NSC pools and their preserved capacity for neurogenesis. ICD images from Fig. 24 were analyzed by fluorescent signal and normalized to Hoechst channel signal and converted to a percentage. Cells from alternating and constant groups from Fig. 20 were started from DIV 102 and were either kept on 511 and in CHIR (PMC) or allowed to differentiate on msl in media lacking CHIR until DIV 110. (A) Nestin signal decreased signifcantly in Alt. SDC compared to Alt. PMC (-12%). Instead, Nestin signal increased significantly in Con. SDC compared to Con. PMC (+19%). (B) NeuN signal was unchanged Alt. SDC compared to Alt. PMC. Instead, NeuN signal increased significantly in Con. SDC compared to Con. PMC (+15%). (C) ZBTB20 signal was significantly increased in Alt. SDC compared to Alt. PMC (+6%) and was also increased significantly in Con. SDC compared to Con. PMC (+8%). Groups were analyzed with one-way ANOVA analyses and post-hoc Kruskal-Wallis tests but were only performed between each group's respective PMC and SDC; asterisks above box plots indicate comparison to respective progenitor pool's PMC group; error bars indicate 99% CI. **-p-val<0.01, ***-p-val<0.001, ****-p-val<0.0001; N=15

increase between Con. PMC and SDC (Figure 52B). Finally, ZBTB20 signal from these 4 culture conditions increased significantly regardless of progenitor pool population from PMC to SDC though the magnitude of change was greater between Con. Groups than Alt. groups (Figure 52C). After delineation laminin effect on differentiation, I assessed if Con. NSCs grown ~6 months from the naïve origin could still differentiate by changing substrate. DIV 160 NSCs were plated onto either 511 or (Figure 53A) or msl (Figure 53B), sustaining both groups in CHIR for 10 days followed by epifluorescence microscopy for βIII-tubulin (Figure 53 Col. 1), Ki67 (Figure 53 Col. 2), and Hoechst (Figure 53 Col. 3), and their coexpression (Figure 53 Col. 4). The singular change in laminin at this culture age was enough to support differentiation despite CHIR presence in the media, first in that Ki67 was downregulated ~2 fold on msl (Figure 53C) and secondly that βIII-tubulin upregulated on msl instead (Figure 53D). These results substantiate that laminin is critical in maintaining NSCs and further allude that DIV 160 cells were still capable of differentiating. In determining that my hippocampal NSCs could still differentiate after 160 days *in vitro*, I proceeded to replicate the experiments performed in Figs. 12-13.

Human hippocampal progenitors differentiate into neurons despite time in vitro

Zbtb20 is constitutively expressed in the rat and mouse adult hippocampus (Nielsen et al., 2014) and is directly implicated in synaptic maintenance in the mouse CA1 (Nielsen et al., 2010; Ren et al., 2012; Ripamonti et al., 2020). Given its importance in embryonic hippocampal neurogenesis, I anticipated that ZBTB20's function in cell cycle exit in hiPSC-derived hippocampal NSC cultures should be conserved regardless of time. To assess this, I first replicated the NOTCH inhibition experiment performed earlier (Figures 40-42). I observed first that these progenitors did not survive when removed from CHIR and thus were only able to show CHIR+/DAPT- (Figure 54A) and CHIR+/DAPT+ (Figure 54B) cultures. Cell cultures were assayed by ICD for Nestin (Figure 54 Col. 1), NeuN (Figure 54 Col. 2), ZBTB20 (Figure 54 Col. 3), Hoechst+ nuclei (Figure 54 Col. 4), and their coexpression (Figure 54 Col. 5). Including the 4 experimental groups with the same treatment paradigms from DIV 50, ZBTB20 was upregulated

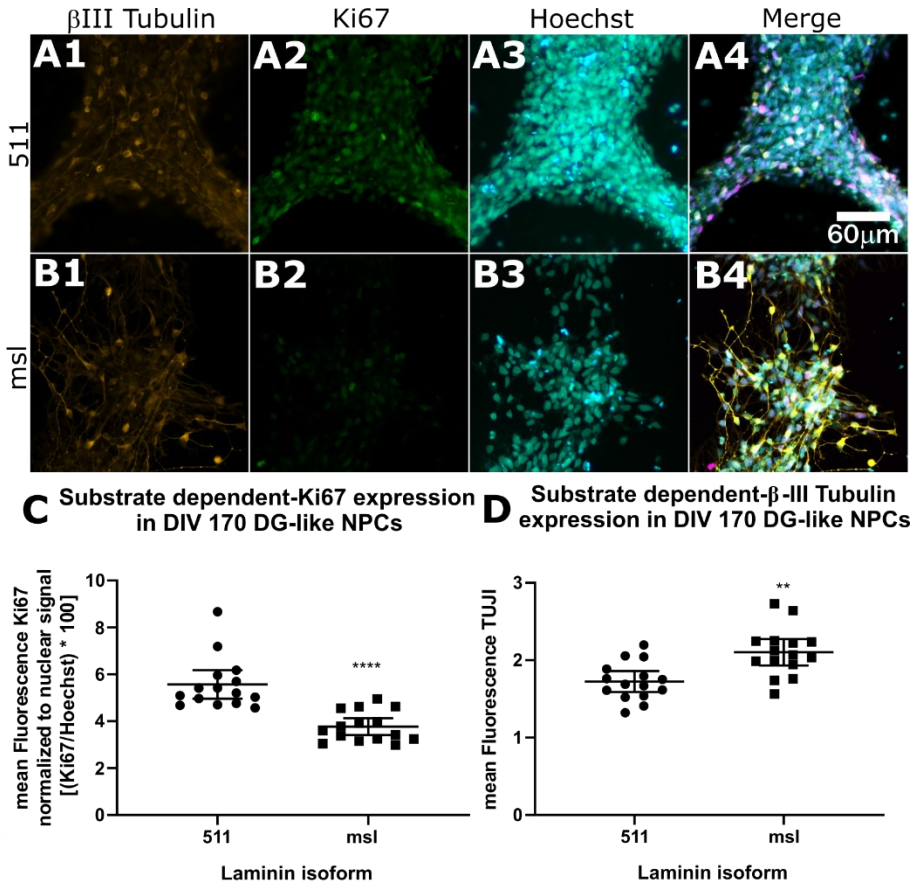

Figure 53. Retention of neurogenesis after ~6 month-long in vitro expansion. At DIV 160, hippocampal NSCs from constant CHIR group were plated on either 511 (A) or msl (B) and kept in 3μM CHIR 99021 for 10 days, after which cultures were fixed and immunostained for βIII-tubulin (Col. 1), Ki67 (Col. 2), and Hoechst (Col. 3) for their coexpression (Col. 4). Cultures were imaged with an epifluorescent microscope and images were processed using a semi-automated batch fluorescence measurement macro in ImageJ. (C) Ki67 signal decreased signifcantly in msl-plated cells compared to 511-plated cells (-1.7%). (D) βIII-tubulin increased signifcantly in msl-plated cells compared to 511-plated cells (+0.4 AU). Groups were analyzed with nonparametric t-test; asterisks above box plots indicate comparison against 511 **-p-val<0.01, ****-p-val<0.0001; N=15

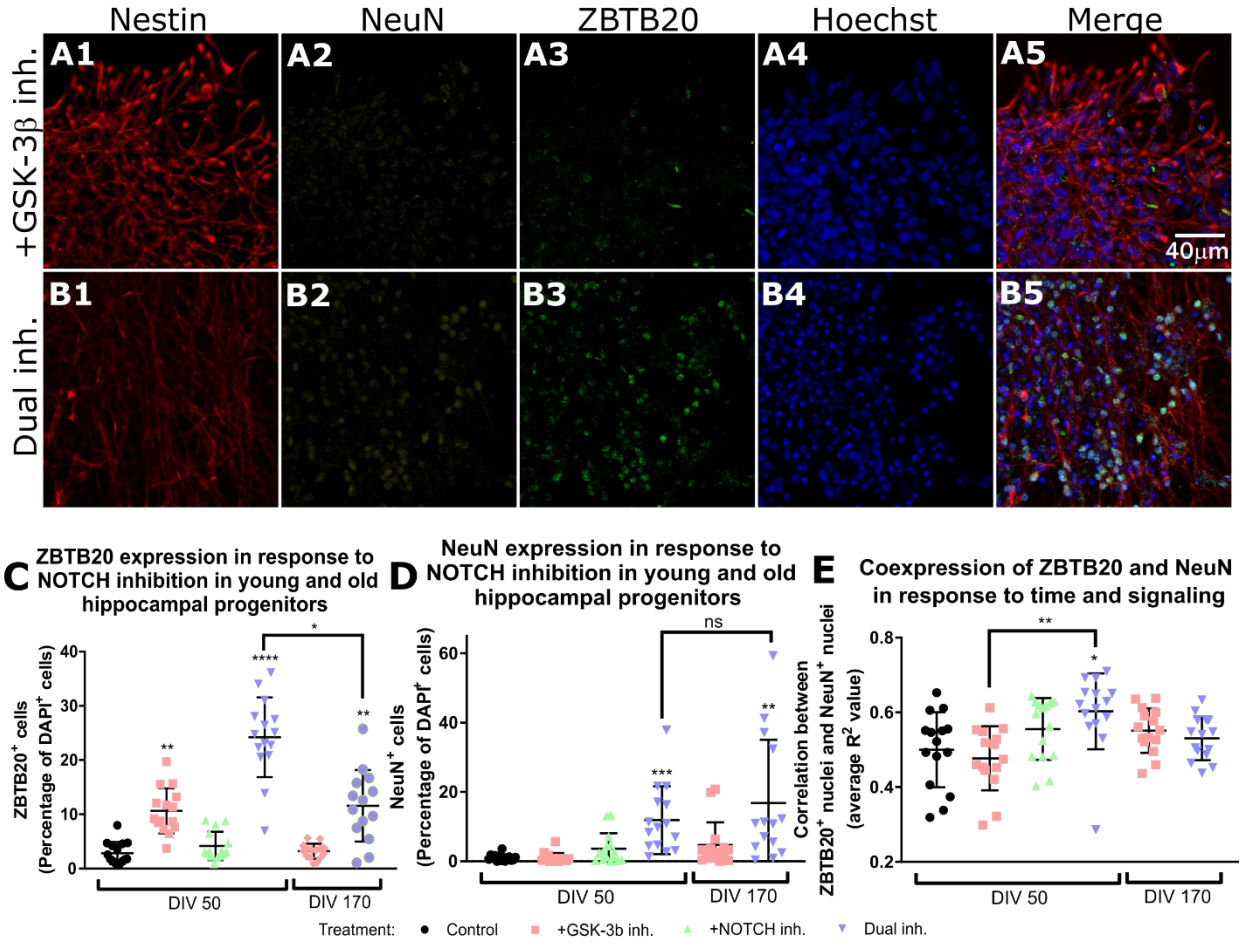

Figure 54. Conservation of ZBTB20 upregulation in older hippocampal NSCs. DIV 160 progenitors were plated on mouse laminin and treated at DIV 166 for two days in either minimal media with 3μM CHIR 99021 alone (+GSK-3β inh., A) or with simultaneous 3μM CHIR 99021 and 12.5μM DAPT (Dual inh., B). Inhibitors were removed after two days and cells were maintained in minimal media for another two days before fixation. Cells were immunostained with Nestin (Col. 1), NeuN (Col. 2), ZBTB20 (Col. 3), and Hoecsht (Col. 4) and portrayed as their coexpression (Coll. 5). Z-stack mages were acquired via confocal and ZBTB20 and NeuN expressing cells were counted semi-automatedly in each stack with in-house batch cell counter macro in ImageJ. (C) Significant increases in ZBTB20 expressing cells in DIV 170 Dual inh. were observed compared to DIV 50 control (+7%). This effect was not as large as their DIV 50 counterpart (-13%). (D) Significant increases in NeuN expressing cells were observed in DIV 170 Dual inh. were observed compared to DIV 50 control (+16%). No significant differences were observed in NeuN upregulation between DIV 50 and DIV 170 Dual inh. groups. (E) Average Pearson Correlation between ZBTB20 and NeuN .tif images. No significant changes were observed between any DIV 170 groups compared to any other group. Statistical analyses were performed by One-Way ANOVA, post-hoc Kruskal-Wallis test; asterisks above plotted values indicate comparison against control whereas above solid black bars indicate between groups; error bar represent 99% CI. *-p-val<0.05, **-p-val<0.01, ***-p-val<0.001, ****-p-val<0.0001

nuclearly in response to CHIR+/DAPT+ treatment at DIV 170 though not to the same extent as DIV 50 CHIR+/DAPT+ treatment (Figure 54C). Furthermore, an increase in NeuN+ cells at DIV 180 was observed in CHIR+/DAPT+ cultures in comparison to the DIV 50 control (Figure 54D) though the correlation between NeuN and ZBTB20 was not conserved between treatment matched DIV 180 compared to DIV50 (Figure 54E).

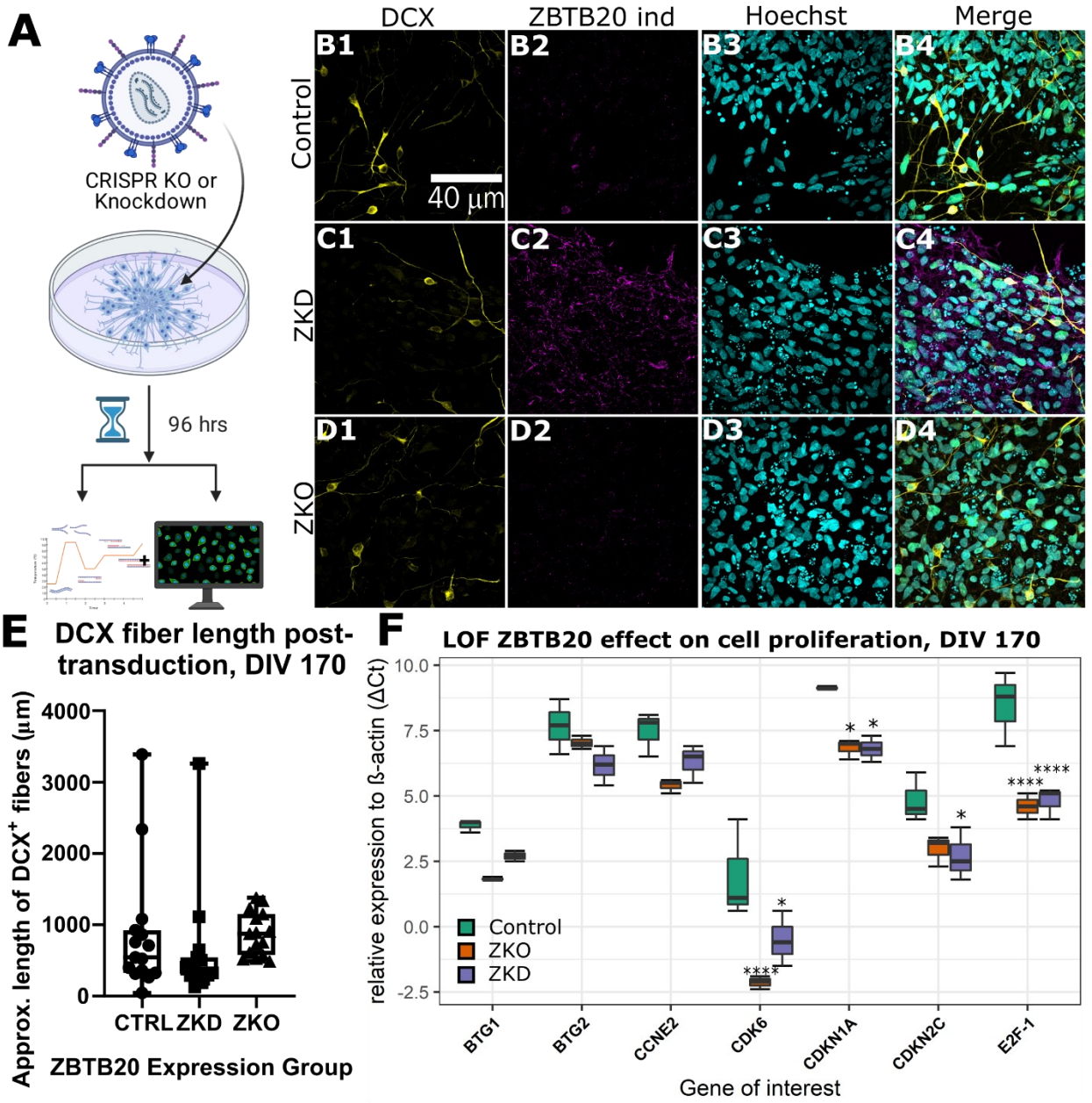

Figure 55. Differentiation and proliferation mediated by loss-of-function ZBTB20 in hippocampal NSCs at DIV 170.(A) Like the experiment in Fig 16A, DIV 160 cells were maintained on msl and in CHIR until DIV 166 at which point cells either remained untransduced (Control, B), were transduced with ZBTB20^{BTB-} overexpression plasmid (ZKD, C), or were transduced with CRISPR-Cas9 ZBTB20 knockout plasmid (ZKO, D). Cells were immunostained were targeted for DCX (Col. 1), plasmid expression signal (ZB ind, Col. 2; anti-ZBTB20 for Control and ZKO, anti-Cherry for ZKD), Hoechst (Col. 3), and their coexpression (Col. 4). Z-stack mages were acquired via confocal and DCX images were processed semi-automatedly in each stack with in-house batch fiber measurement macro in ImageJ (E) No differences were observed between viral experimental groups; error bars depict 99% CI, N=15 (F) ZKO decreased ΔCt of *CDK6*, *CDKN1A*, and *E2F-1* compared to control (-3.6, -3.0, -3.8, respectively) whereas ZKO decreased ΔCt of *CDK6*, *CDKN1A*, *CDKN2C*, and *E2F-1* compared to control (-1.6, -3.1, -1.5, -3.7, respectively). Data shown as ΔCt calculated by [Gene of Interest take off cycle] - [β-actin take off cycle] per indidvidual sample. Analysis was made using Two-Way ANOVA. asterisks above plotted values indicate comparison against control; *-p-val<0.05, ***-p-val<0.001, ****-p-val<0.0001, error bars depict 99% CI, N=3

Altogether, these results confirm that despite the time *in vitro*, albeit 6 months, these "aged" NPCs still behave in some neurogenic capacity that is deviated only in magnitude as opposed to overall trend. Utilizing the same paradigm presented (Figure 55A), I either performed ZBTB20 functional silencing treatments in DIV160 NSCs (Figure 55B) and transduced them either with ZKD (Figure 55C) or ZKO (Figure 55D) and assayed for DCX (Figure 55 Col.1), ZBTB20 viral indicator (Figure 55 Col.2), Hoechst (Figure 55 Col.3), as well as their coexpression (Figure 55 Col.4). DCX was downregulated between ZKD and ZKO but overall unchanged significantly compared to the untransduced control (Figure 55D). RNA expression by qRT-PCR of these cells further demonstrated that ZKO upregulated *CDK6* strongly compared to the control as well as *CDKN1A* and *E2F-1* and that ZKD upregulated these same genes, but also *CDKN2C* though did not upregulate *CDK6* to the same extent as ZKO (Figure 55E).

Molecular nature of young and old cultures and role of Wnt signaling in DG NPC maturation

After probing early and late cultures for physiological ZBTB20 response and cell cycle maintenance of hippocampal neural precursors, I proceeded to investigate the transcriptomic changes in WNT- and NOTCH-related pathways in the experiments reported earlier. CHIR treatment significantly changed the expression of 3330 genes (1518 up-regulated and 1812 down-regulated) (Figure 56A). Go analysis of genes with changed expression highlighted highly significant enrichment of terms related to neuronal differentiation (Figure 56B). Moreover, the hippocampal differentiation protocol preferentially induced genes of hippocampal embryonic identity at DIV28, with few exceptions (Figure 56C). These results, together with the PCA comparison of DIV28 cells and 12pcw brain regions, reinforce the idea that Wnt signaling re-activation after DIV12 is crucial to establish a hippocampal identity of telencephalic neural cells.

I sought to understand the role of WNT signaling in later phases of the culture protocol and the nature of differentiating cells at different times. First, I compared cultures maintained under high WNT signaling until DIV50 with DIV50 cultures in which WNT signaling was suspended at DIV28. M/D plot in Figure 57A shows 220 RNA species that significantly changed their expression between the two culture conditions. To evaluate this

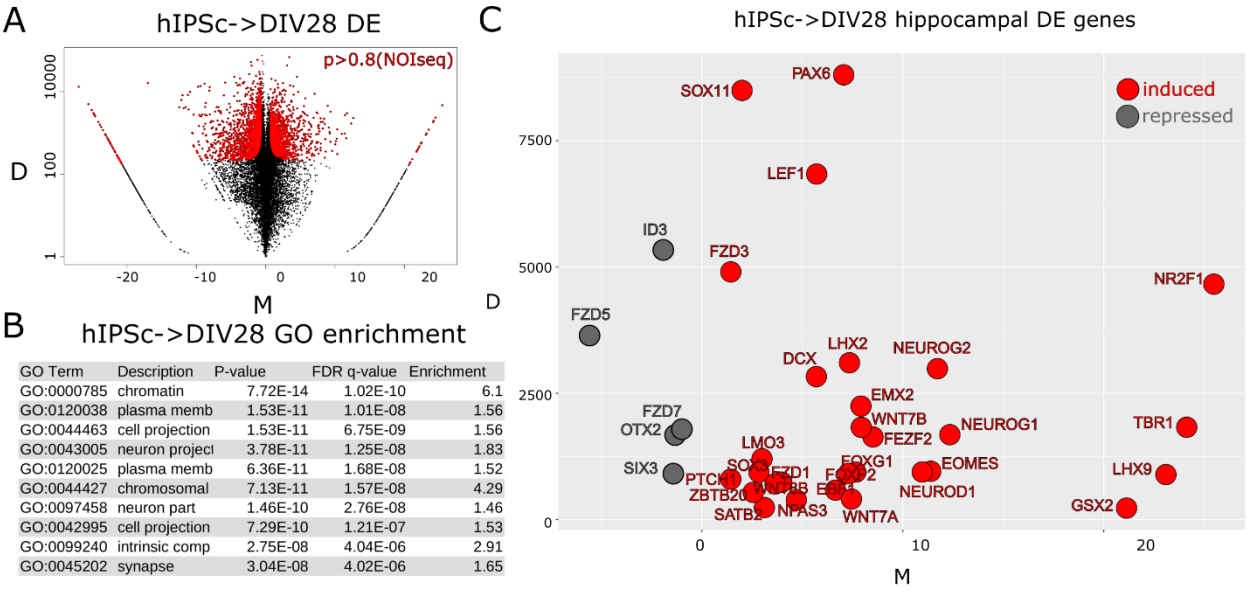

GO Term	Description	P-value	FDR q-value	Enrichment
GO:0000785	chromatin	7.72E-14	1.02E-10	6.1
GO:0120038	plasma memb	1.53E-11	1.01E-08	1.56
GO:0044463	cell projection	1.53E-11	6.75E-09	1.56
GO:0043005	neuron projecl	3.78E-11	1.25E-08	1.83
GO:0120025	plasma memb	6.36E-11	1.68E-08	1.52
GO:0044427	chromosomal	7.13E-11	1.57E-08	4.29
GO:0097458	neuron part	1.46E-10	2.76E-08	1.46
GO:0042995	cell projection	7.29E-10	1.21E-07	1.53
GO:0099240	intrinsic comp	2.75E-08	4.04E-06	2.91
GO:0045202	synapse	3.04E-08	4.02E-06	1.65

Figure 56. Induction of a hippocampal identity in hiPSCs. A, mean-difference (MD) plot of differentially expressed (DE) genes between hiPSC and DIV28 cell cultures. Red dots report the MD distribution of significantly DE genes (NOIseq, p>0.8). B, GO cell component enrichment of DE genes shown in A as computed by Gorilla (Eden et al, 2009, https://doi.org/10.1186/1471-2105-10-48). C, MD distribution of DE genes of hippocampal signature (59 genes). Genes of the signature not shown in the plot were not differentially expressed or were filtered out for low expression. D= $\log_2$ differential expression, M= average read counts.

expression change rate, I compared it though the rate exerted by the Notch antagonism with DAPT treatment form DIV 43 to DIV50. Figures 57B, C show that 368 and 435 mRNA species significantly changed their expression when treating with DAPT cells grown with high WNT signaling and cell with WNT signaling suspended, respectively. GO term analysis indicates that the mRNA species significantly increased by DAPT in both WNT-induced and WNT-depleted cultures are dramatically enriched for cell component terms of neuronal differentiation, with slightly higher enrichment for WNT-depleted cells. The PCA in Figure 57D shows that the highest variability of expression described by component 1 (68,24%) is represented by DAPT-induced changes while the second component (19,53%) accounts for changes due to WNT. Nonetheless, gene variability described by the second component is much higher between cultures with no DAPT treatment than cultures with DAPT treatments. I thus reasoned that part of the gene expression change induced by WNT depletion could be ascribed to a neuronal differentiative drive. Indeed, the intersection analysis of the mRNA species which expression is significantly changed among the treatments (Figure 57E) shows that more than half of the mRNAs significantly affected by WNT treatment (n=117) are common to DAPT-dependent mRNAs. However,

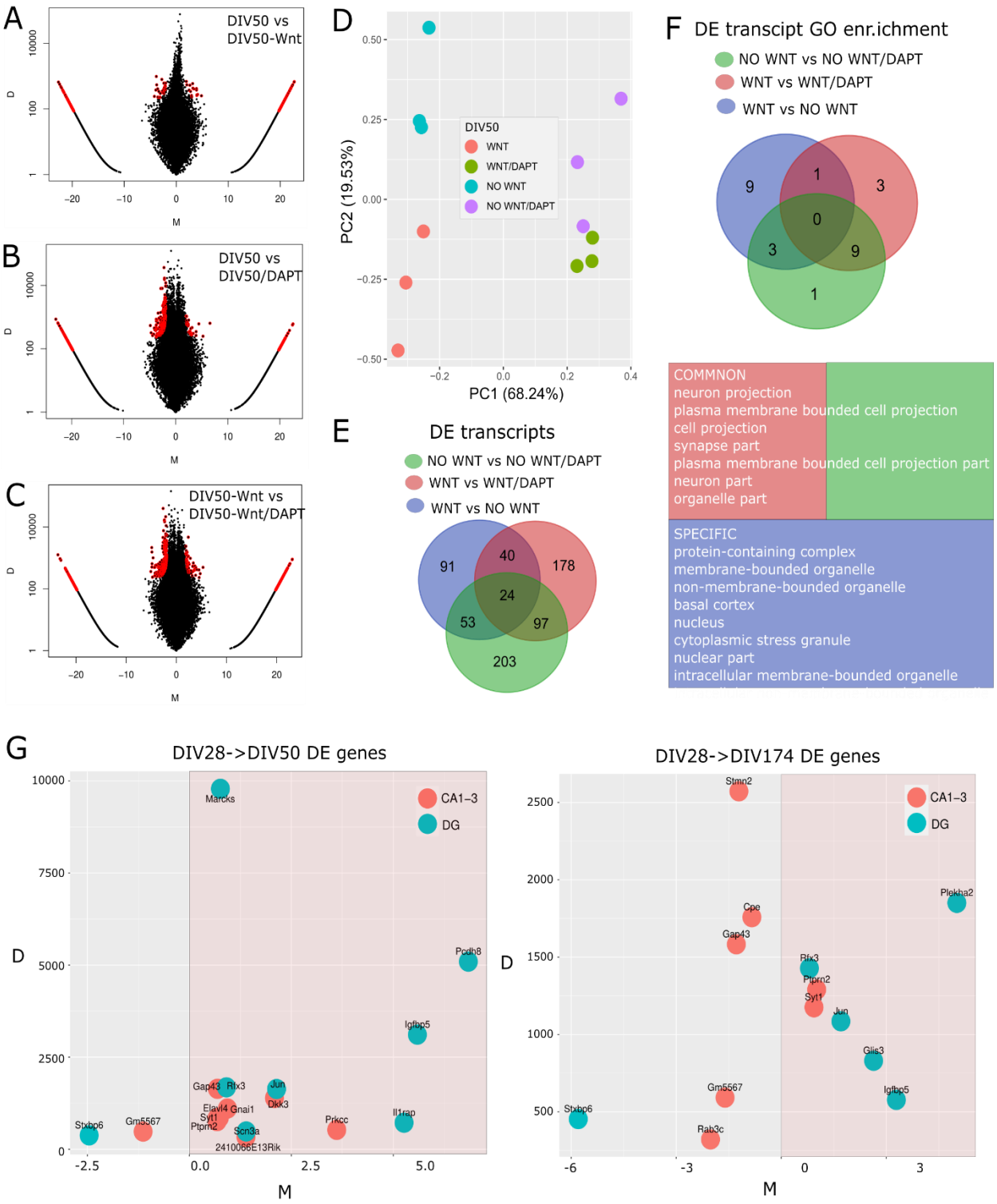

Figure 57. WNT signaling support the differentiation of DG and CA1-3 hippocampal layers. (A-C) MD plots of gene DE between different cell culture conditions and times. (D), PCA of global gene expression change among different culture conditions at DIV50. (E,F) Venn Diagram of GO terms enriched in DE genes in cultures at DIV50. (G) MD plots of the DE genes belonging to the gene signatures of DG and CA1-3 cell identity of mouse hippocampus (Cembrowski et al, 2016, https://doi.org/10.7554/eLife.14997). Pink area indicates upregulate genes. D= log2 differential expression, M= average read counts.

A

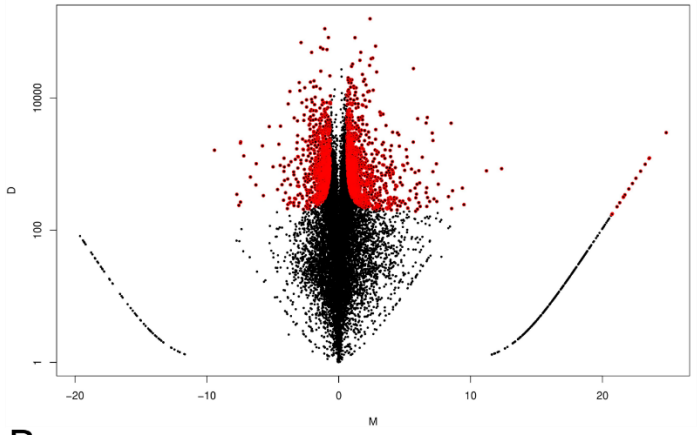

B

DIV50->DIV174 GO term enrichment

GO Term PROCESS	Description	P-value
GO:0043170	macromolecule metabolic process	5.33E-09
GO:0006357	regulation of transcription by RNA polymerase II	2.74E-08
GO:0043412	macromolecule modification	1.4E-07
GO:0019538	protein metabolic process	1.75E-07
GO:0031326	regulation of cellular biosynthetic process	1.84E-07
GO:0051254	positive regulation of RNA metabolic process	2.53E-07
GO:0044238	primary metabolic process	2.74E-07
GO:0045935	positive regulation of nucleobase-containing compound metabolic process	2.84E-07
GO:0006807	nitrogen compound metabolic process	3.59E-07
GO:0044260	cellular macromolecule metabolic process	3.66E-07
GO:0045944	positive regulation of transcription by RNA polymerase II	3.77E-07
GO:0051252	regulation of RNA metabolic process	5E-07
GO:0010557	positive regulation of macromolecule biosynthetic process	7.01E-07
GO:0009891	positive regulation of biosynthetic process	8.9E-07
GO:0031323	regulation of cellular metabolic process	9.4E-07
GO:2000112	regulation of cellular macromolecule biosynthetic process	9.68E-07
GO:1902680	positive regulation of RNA biosynthetic process	9.82E-07
GO:0045893	positive regulation of transcription, DNA-templated	9.82E-07
GO:1903508	positive regulation of nucleic acid-templated transcription	9.82E-07

GO Term FUNCTION	Description	P-value
GO:0016706	oxidoreductase activity, acting on paired donors, with incorporation or reduc	1.69E-06
GO:0051213	dioxygenase activity	2.85E-06
GO:0000977	RNA polymerase II regulatory region sequence-specific DNA binding	1.43E-05
GO:0001012	RNA polymerase II regulatory region DNA binding	1.43E-05
GO:0003676	nucleic acid binding	1.54E-05
GO:0140110	transcription regulator activity	1.58E-05
GO:0003700	DNA-binding transcription factor activity	1.6E-05
GO:0140096	catalytic activity, acting on a protein	1.82E-05
GO:0000981	DNA-binding transcription factor activity, RNA polymerase II-specific	3.15E-05
GO:0000976	transcription regulatory region sequence-specific DNA binding	3.74E-05
GO:0044212	transcription regulatory region DNA binding	4.15E-05
GO:0001067	regulatory region nucleic acid binding	4.54E-05
GO:0000978	RNA polymerase II proximal promoter sequence-specific DNA binding	6.07E-05
GO:0000987	proximal promoter sequence-specific DNA binding	9.5E-05

GO Term COMPONEI	Description	P-value
GO:0044428	nuclear part	2.4E-05
GO:0044424	intracellular part	0.00015
GO:0001750	photoreceptor outer segment	0.000183
GO:0043229	intracellular organelle	0.000476
GO:0000785	chromatin	0.000586

Figure 58. Hippocampal cell maturation upon continuous WNT signaling. A, MD plot od DE genes at the progression from DIV50 to DIV174.D= $\log_2$ differential expression, M= average read counts. B, Enrichment of GO terms of DE genes in A.

GO term enrichment analysis indicates that 9 out of the 13 GO categories of transcripts that are differentially expressed upon differential WNT treatments (WNT vs NO WNT) are not shared with the two DAPT-differentially treated cultures (WNT vs WNT/DAPT, NO WNT vs NO WNT/DAPT), while the two latter share 9 out of the 13 most enriched GO terms (Figure 57F). Overall, these data indicate that prolonged WNT signaling supports a peculiar gene expression profile unrelated to mere neuronal differentiation.

I then analyzed the expression change of a panel of genes specific for DG or CA1-3 identity (Cembrowski, Wang, et al., 2016). MD plot in Figure 57G shows that DIV50 cells upregulate most of both DG and CA1-3 markers differentially expressed upon maturation from DIV28 and DAPT treatment, indicating that these cultures can differentiate into all the different hippocampal mature neuronal cell types. Conversely, DAPT-treated DIV174 cells downregulate most of the CA1-3 markers compared to DIV28 cells, while inducing the expression of most DG genes. I speculate that late cultures behave as mature hippocampus that keep on producing granule DG cells but fail generating new CA1-3 neurons. Eventually, I analyzed the

nature of genes differentially expressed between DIV50 and DIV174. Figure 58A shows a MD plot of the 843 upregulated and 1140 downregulated genes from DIV50 to DIV174 (NOIseq analysis, p>0.8). A list of the highest enriched terms of GO is reported in Figure 58B. The analysis highlights metabolic and chromatin reorganization processes, including upregulation of transcription factor activity, RNAPII-mediated and non-RNAPII-mediated, suggesting that these cells undergo an aging-like process *in vitro* but do not change their regional fate over time. Most notably among upregulated gene networks in late DIV cultures are known late-stage embryogenic/early post-natal granular cell neurogenic transcription factor *PAX6* (Maekawa et al., 2005), clock and hippocampal-maintenance specific genes *TRIB3* and *BHLHE40* (Hamilton et al., 2018; Lorenzi et al., 2018), and birth-related solute carrier genes *SLC6A6* and *SLC7A5*, regulating taurine transport for cell maturation and differentiation (Desforges et al., 2013; Lang et al., 1998) and gestational cellular insulin response modulation (Scalise et al., 2018), respectively. I then transitioned my studies to more physiological investigation of these cells' behavior at different time points *in vitro* and *in vivo*.

Human hippocampal neurons behave like neurons and integrate into in vivo hippocampus

Finally, human hippocampal NSCs were assayed for neurogenesis in physiological manners, both with the OPAL and by transplanting NSCs *in vivo* using methods previously described (Terrigno et al., 2018). Cells at DIV 28 were transduced with ChR2 under the synaptophysin promoter and were treated with DAPT/CHIR at DIV 29, followed by reseeding at DIV 30 onto mESC-derived hippocampal neuron cultures. After 40 days *in vitro*, cells were exposed to the same 1-hr light paradigm of 100Hz blue-LED trains as in Section 1, Figure 11 using the OPAL. Experimental groups of no light (Figure 59A), no light + TTX (Figure 59B), 100Hz blue light (Figure 59C), and 100HZ blue light + TTX (Figure 59D) were assessed for cFOS expression in human nuclei. cFOS in human nuclei was significantly upregulated in cultures exposed to 100Hz blue light compared to no light control (0 Hz, Figure 59E). However, TTX only partially blockaded this effect as it was not significantly

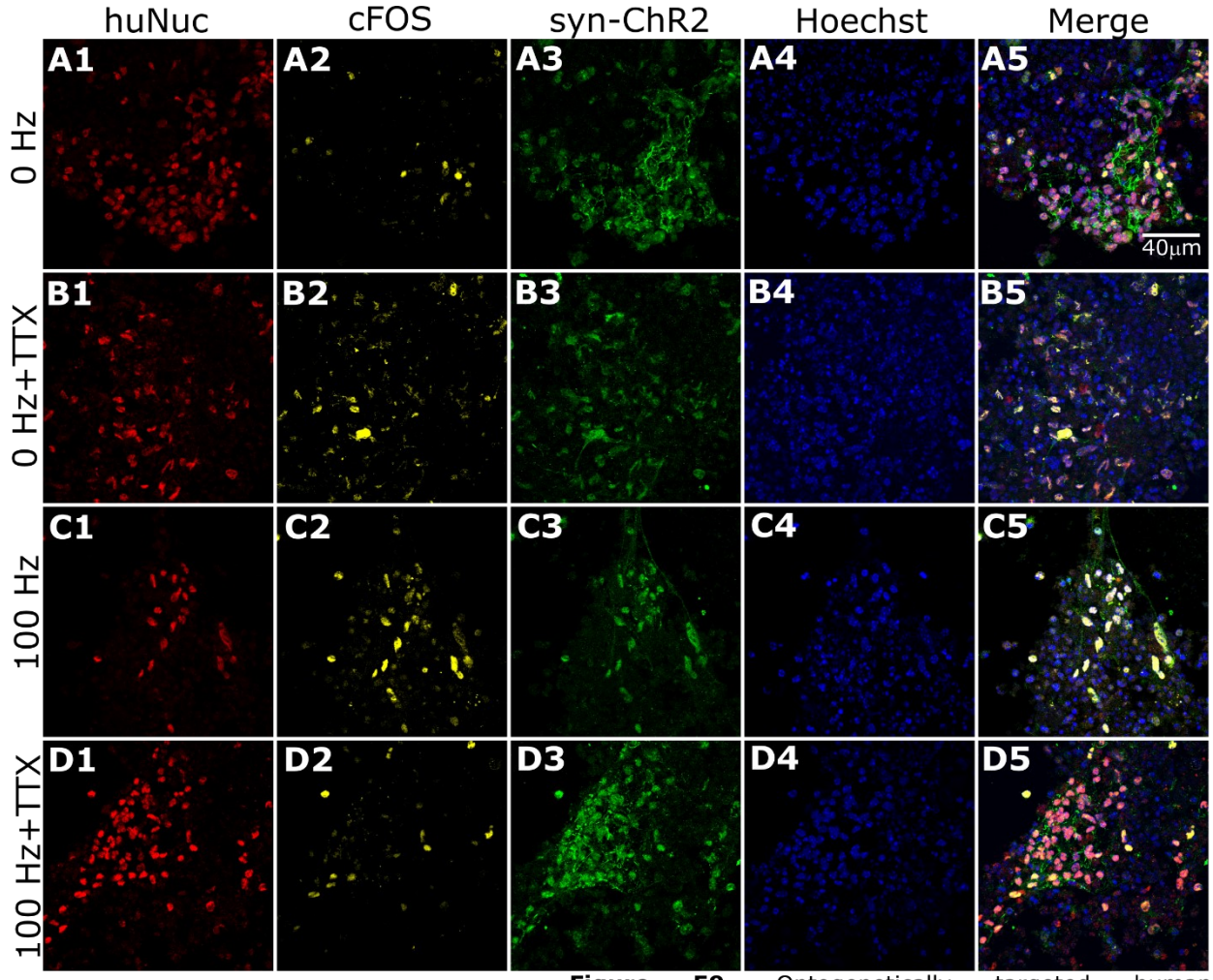

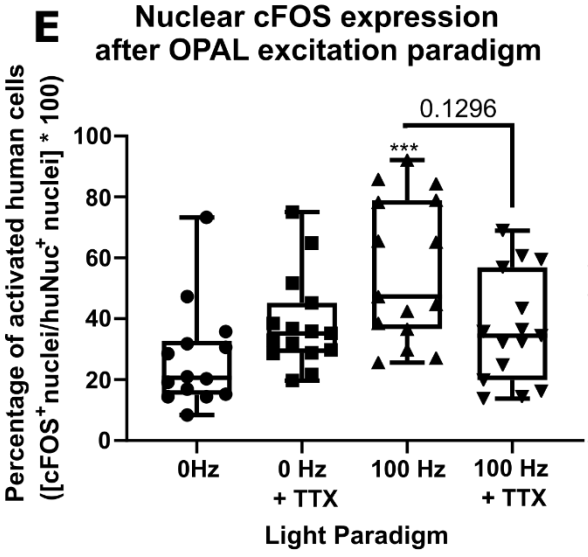

Figure 59. Optogenetically targeted human hippocampal neurons are activated by light stimulation paradigms at DIV 70. Cells were transduced with Syn-ChR2 at DIV 28, treated with 25μM DAPT and 3μM CHIR99021 at DIV 29, split and replated onto mESC-derived neurons at DIV 30 where they continued to grow for 40 days. At DIV 70, cells were exposed to the same light paradigms introduced in the optogenetics chapter, wherein cells were given trains of 100 Hz light for 10 min followed by 5 min, repeated 4 times for a total of 1 hour. Paradigms included no light (A), no light + 1μM TTX (B), 100Hz paradigm (C), or 100Hz paradigm + 1μM TTX (D). Thereafter, cells were fixed and immunostained for human nuclei (Col. 1), cFOS (Col. 2), ChR2-eGFP (Col. 3), and Hoechst (Col. 4) for their coexpression (Col. 5). Z-stack images were acquired via confocal; huNuc and cFOS expressing cells were counted semi-automatedly in each stack with in-house batch cell counter macro in ImageJ. (E) total cFOS cell count was divided by total huNuc cell count and converted to percentage. Cells exposed to 100Hz light-trains expressed signifcantly more cFOS than those of no light control (+25%). Statistical analyses were performed by One-Way ANOVA, post-hoc Kruskal-Wallis test; asterisks above plotted values indicate comparison against control whereas above solid black bars indicate between groups; error bars represent 99% CI. ***-p-val<0.001, N=15

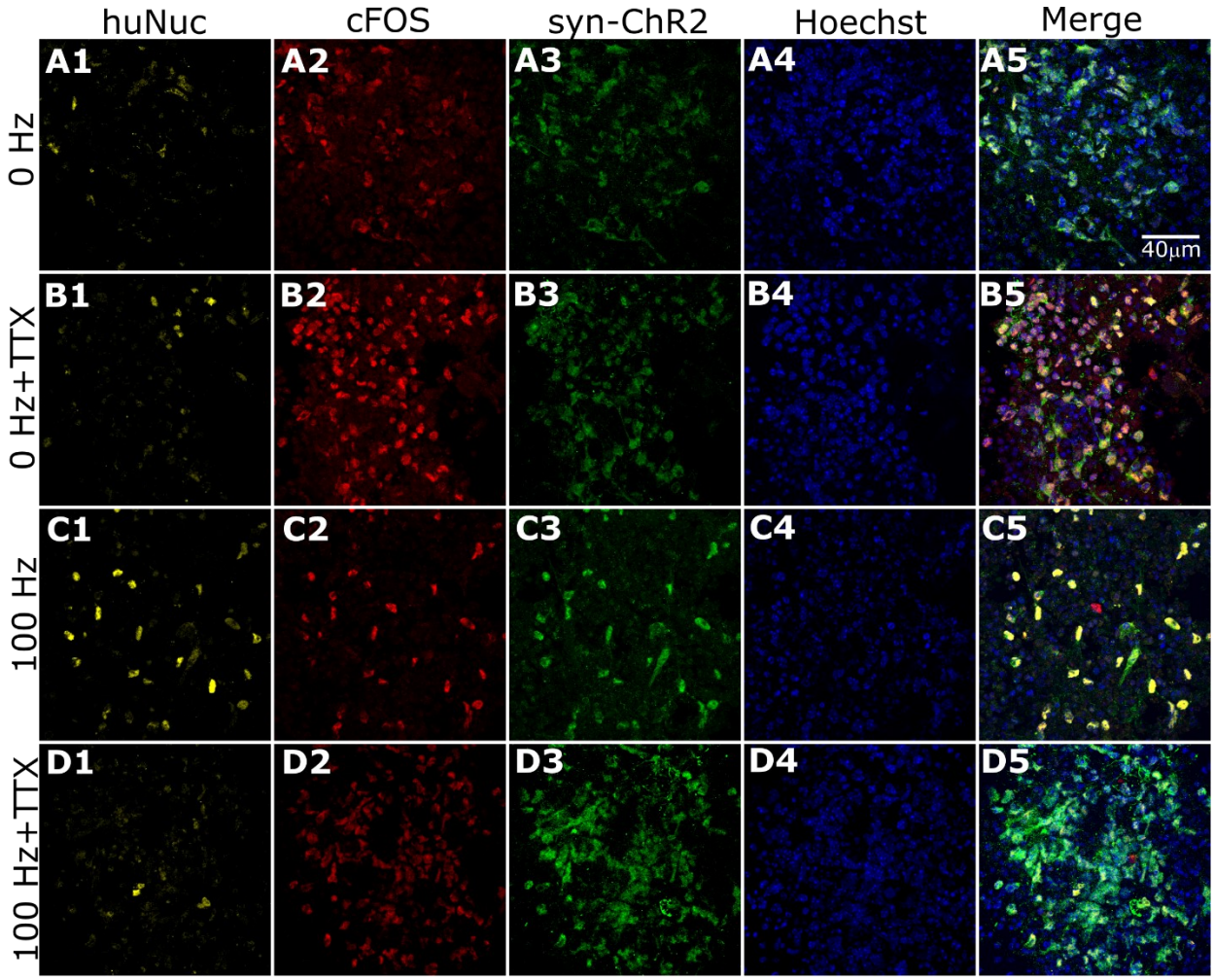

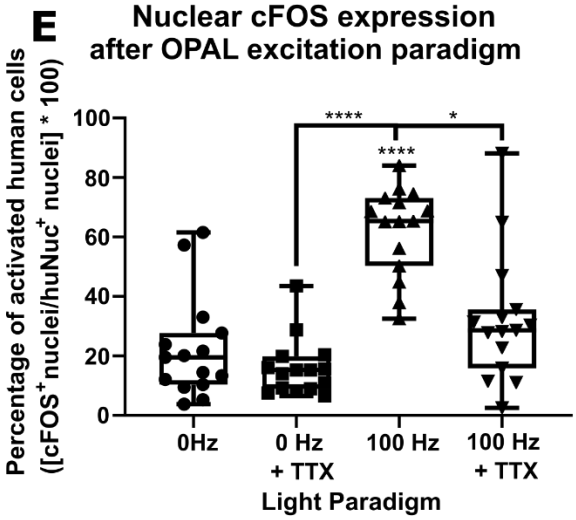

Figure 60. Optogenetically targeted human hippocampal neurons are activated by light stimulation paradigms at DIV 210. Cells were transduced with Syn-ChR2 at DIV 168, treated with 12.5μM DAPT and 3μM CHIR99021 at DIV 169, split and replated onto mESC-derived neurons at DIV 170 where they continued to grow for 40 days. At DIV 210, cells were exposed to the same light paradigms introduced in the optogenetics chapter, wherein cells were given trains of 100 Hz light for 10 min followed by 5 min, repeated 4 times for a total of 1 hour. Paradigms included no light (A), no light + 1μM TTX (B), 100Hz paradigm (C), or 100Hz paradigm + 1μM TTX (D). Thereafter, cells were fixed and immunostained for human nuclei (Col. 1), cFOS (Col. 2), ChR2-eGFP (Col. 3), and Hoechst (Col. 4) for their coexpression (Col. 5). Z-stack images were acquired via confocal; huNuc and cFOS expressing cells were counted semi-automatedly in each stack with in-house batch cell counter macro in ImageJ. (E) total cFOS cell count was divided by total huNuc cell count and converted to percentage. Cells exposed to 100Hz light-trains expressed signifcantly more cFOS than those of no light control (+45%) and 0Hz + TTX (+48%). cFOS increase was not observed in 100Hz treated cultures incubated with TTX (-36%). Statistical analyses were performed by One-Way ANOVA, post-hoc Kruskal-Wallis test; asterisks above plotted values indicate comparison against control whereas above solid black bars indicate between groups; error bars represent 99% CI. *-p-val<0.05, ****-p-val<0.0001, N=15

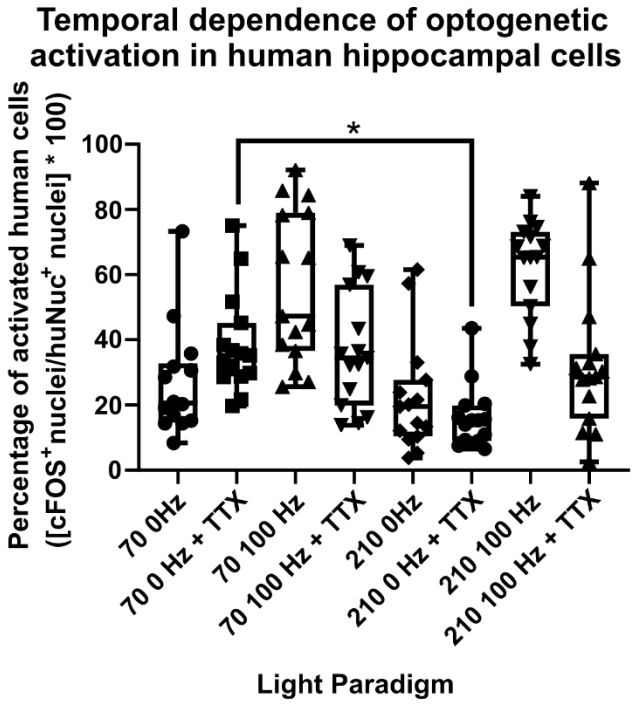

Figure 61. Age differences with respect to light patterning and cFOS activation. DIV 70 cells from Fig 32 and DIV 210 cells from Fig 33 were compared for differences between all groups. No signifcant differences were observed between 100Hz treatments, however, addition of TTX at DIV 70 elicited a larger cFOS response than at DIV 210. Statistical analyses were performed by One-Way ANOVA, post-hoc Kruskal-Wallis test; asterisks above plotted values indicate comparison against control whereas above solid black bars indicate between groups; error bars represent 99% CI. *-p-val<0.05, N=15

downregulated in 100Hz + TTX group and trended decreasingly (Figure 59E). This experiment was repeated with DIV 160 NSCs grown until DIV 210 on hippocampal mouse neurons (no light (Figure 60A), no light + TTX (Figure 60B), 100Hz blue light (Figure 60C), and 100HZ blue light + TTX (Figure 60D)) and assessed for cFOS response in human nuclei. Human cells at DIV 210 were cFOS inducible by 100 Hz blue light compared to no light control (0 Hz, Figure 60E) and this response was significantly prevented by TTX in the 100Hz + TTX treatment group (Figure 60E). While the percentage of $cFOS^+$ human nuclei were unchanged between DIV 70 and DV 210 treated were not significantly different from each other, the 0HZ + TTX DIV 70 group was significantly higher percentage than DIV 210 (Figure 61). This suggests that there are a higher population of neural progenitors yet in the DIV 70 group compared to the DIV 210 group, as hyperpolarization has been attributed to increase proliferation and Ca^{2+} influx in neural stem cells (Lancaster, 2019; Vitali et al., 2018).

Assessment of *in vitro* phenomena transitioned to assessment of human hippocampal NSC differentiation behavior *in vivo*. Starting from either naïve or DIV 160 NSC populations, cells were transduced with mGFP lentiviral vector, expanded, and treated with DAPT/CHIR 24 hours prior to transplantation into wild-type mice dentate gyrus (Figure 62A). After ~3 months *in vivo*, cell survival and integration were assessed in the DIV 130 cells by confocal analysis of human fibers in the DG (Figure 62B) and CA3 (Figure 62C).

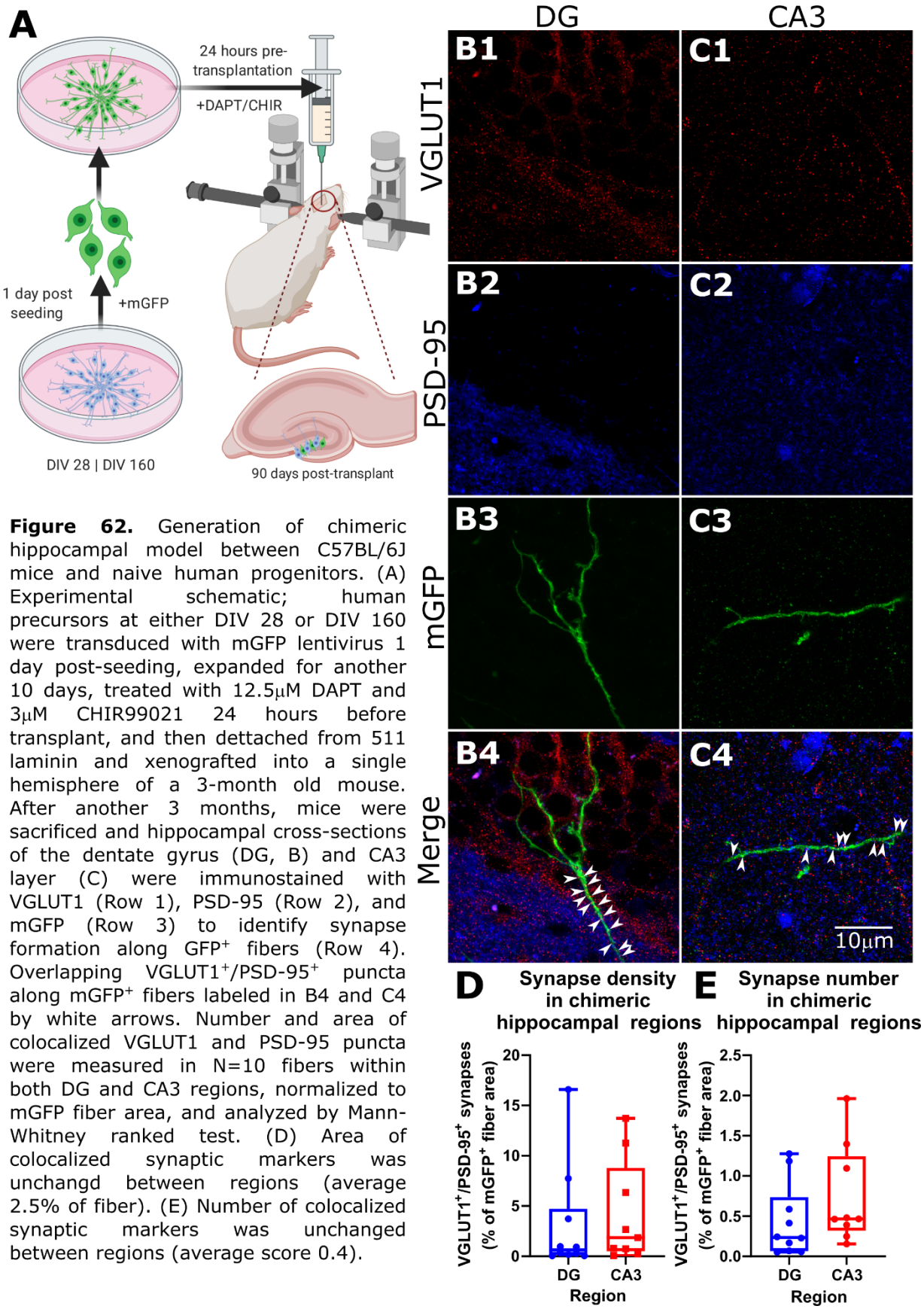

Figure 62. Generation of chimeric hippocampal model between C57BL/6J mice and naive human progenitors. (A) Experimental schematic; human precursors at either DIV 28 or DIV 160 were transduced with mGFP lentivirus 1 day post-seeding, expanded for another 10 days, treated with 12.5μM DAPT and 3μM CHIR99021 24 hours before transplant, and then dettached from 511 laminin and xenografted into a single hemisphere of a 3-month old mouse. After another 3 months, mice were sacrificed and hippocampal cross-sections of the dentate gyrus (DG, B) and CA3 layer (C) were immunostained with VGLUT1 (Row 1), PSD-95 (Row 2), and mGFP (Row 3) to identify synapse formation along GFP^+ fibers (Row 4). Overlapping $VGLUT1^+/PSD\text{-}95^+$ puncta along $mGFP^+$ fibers labeled in B4 and C4 by white arrows. Number and area of colocalized VGLUT1 and PSD-95 puncta were measured in N=10 fibers within both DG and CA3 regions, normalized to mGFP fiber area, and analyzed by Mann-Whitney ranked test. (D) Area of colocalized synaptic markers was unchangd between regions (average 2.5% of fiber). (E) Number of colocalized synaptic markers was unchanged between regions (average score 0.4).

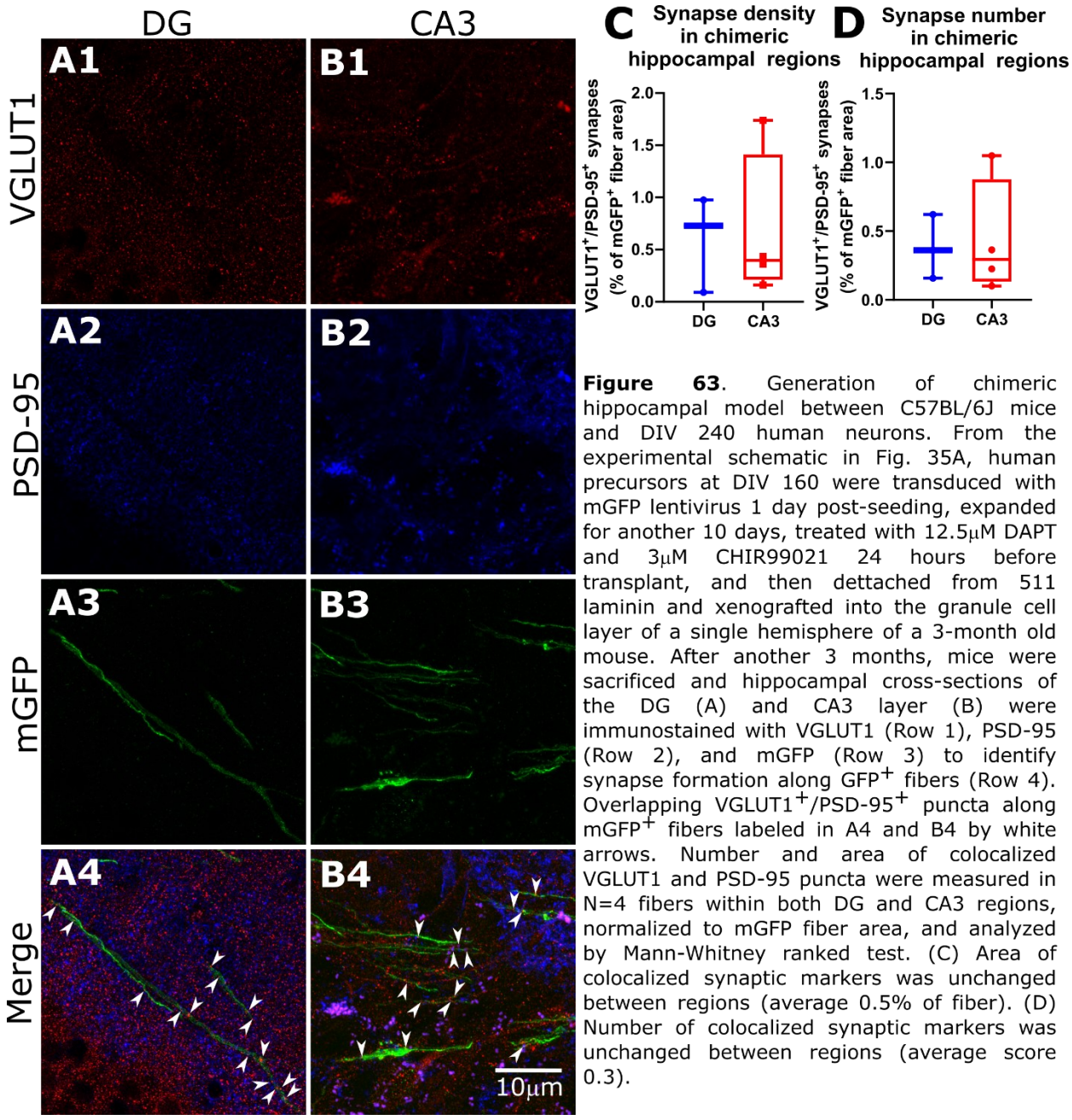

Figure 63. Generation of chimeric hippocampal model between C57BL/6J mice and DIV 240 human neurons. From the experimental schematic in Fig. 35A, human precursors at DIV 160 were transduced with mGFP lentivirus 1 day post-seeding, expanded for another 10 days, treated with 12.5μM DAPT and 3μM CHIR99021 24 hours before transplant, and then dettached from 511 laminin and xenografted into the granule cell layer of a single hemisphere of a 3-month old mouse. After another 3 months, mice were sacrificed and hippocampal cross-sections of the DG (A) and CA3 layer (B) were immunostained with VGLUT1 (Row 1), PSD-95 (Row 2), and mGFP (Row 3) to identify synapse formation along GFP^+ fibers (Row 4). Overlapping $VGLUT1^+/PSD\text{-}95^+$ puncta along $mGFP^+$ fibers labeled in A4 and B4 by white arrows. Number and area of colocalized VGLUT1 and PSD-95 puncta were measured in N=4 fibers within both DG and CA3 regions, normalized to mGFP fiber area, and analyzed by Mann-Whitney ranked test. (C) Area of colocalized synaptic markers was unchanged between regions (average 0.5% of fiber). (D) Number of colocalized synaptic markers was unchanged between regions (average score 0.3).

$VGLUT1^+/Psd\text{-}95^+$ synapses (white arrows, Figure 62B4, C4) formed between the $mGFP^+$ human fibers and mouse host were analyzed and between groups no difference was found in change along mGFP area (Figure 62D), or number of synapses formed (Figure 62E). Human neuronal fibers were also assessed at DIV 260 for synaptic integration in the DG (Figure 63A) and CA3 (Figure 63B) and similarly to those naïve cells transplanted, $VGLUT1^+/Psd\text{-}95^+$ synapses formed along $mGFP^+$ fibers (white arrows, Figure 63A4, B4). Significant changes were neither observed in synaptic area between regions (Figure 63C) nor in synaptic number (Figure 63D). A

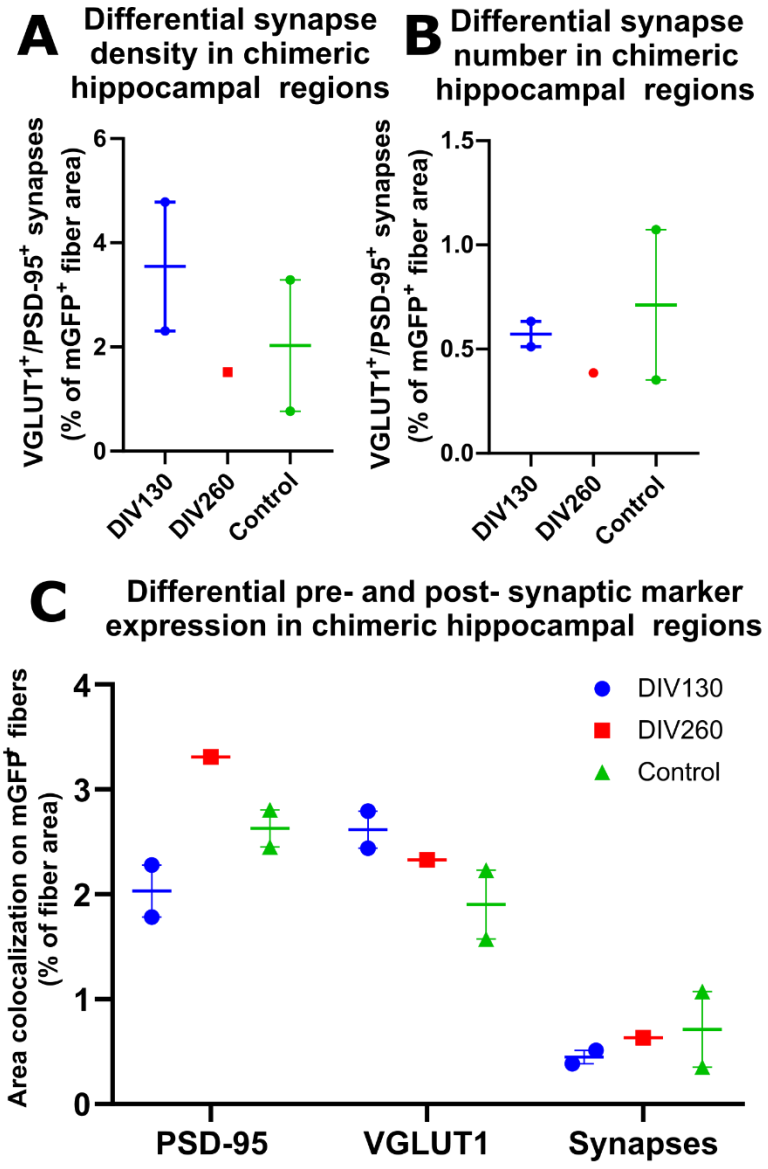

Figure 64. Preliminary analysis of differential synaptic expression in DIV 130 (N=2) and DIV 260 (N=1) compared to age-mathced CHR2-eGFP transgenic mouse (Control, N=2). Fiber counts from Fig 35 and Fig 36 were averaged and analyzed and plotted as average quantification per mouse of origin. (A) Area of colocalized synaptic markers is unchanged between groups though additional sample replicates may demonstrate an increase at DIV 130 compared to the transgenic control. (B) Number of colocalized synaptic markers is unchanged between groups and with additional replicates, may remain unchanged. (C) Individual synaptic markers plotted as percentage of GFP^+ fibers; wild-type PSD-95 juxtaposed against GFP^+ fibers is highest at DIV260, VGLUT1 along GFP^+ fibers instead seems highest at DIV 130, however, total synapses seems unchanged between groups.

preliminary analysis of averaged fibers per mouse host was conducted to understand trend in synaptic formations between time points. This analysis included transgenic, ChR2-eYFP mice whose fibers were labeled with Vglut1 and Psd-95 (Control). Considering the low sample number, statistical significance could not be assessed, however, area of synapses in hippocampal regions appeared unchanged between the three groups (Figure 64A). Likewise, the number of synapses along GFP^+ fibers was unchanged between DIV 130, DIV 260, and the transgenic control (Figure 64B). The individual synaptic markers themselves appeared unchanged as well, though Psd-95 count seemed higher at DIV 260 (Figure 37C). These results are promising as they suggest that further development

of this system may elaborate no changes in synaptic formation propensity despite time *in vitro* and that they are in fact stemming from a hippocampal pseudo embryonic origin.

CHAPTER IX: hiPSC-derived hippocampal neural stem cells provide a robust model to study human hippocampal neurogenesis (Discussion)

The hippocampus is a neurogenic anomaly both in embryonic development and in sustained adult neurogenesis. It and its proximal lateral afferent pathways are responsible for multilayered environmental input processing and learning with associated detriment in cognitive neurodegnerations in humans. Both its position as the crux of learning and its susceptibility to degeneration make it an imperative region of study. But because the hippocampus is a deep-seated compartment within the cerebral cortex and ethical limitations prevent widespread study of human development, studying human hippocampal development and neurogenesis has been limited. Several *in vitro* approaches have sought to rectify this inaccessibility using stem cell-derived models, though these protocols rely either on direct reprograming (Diana Xuan Yu et al., 2014), human ESCs (Sakaguchi et al., 2015), or extracellular signaling induced by rapidly degraded proteins (Sarkar et al., 2018). Here, I demonstrate a human induced pluripotent stem cell model of the dentate gyrus induced using GSK-3β inhibitor. Furthermore, this model is capable of sustained neurogenesis for over 6 months *in vitro* by constitutive utilization of the same inhibitor and purified laminin isoform $\alpha5\beta1\gamma1$, 511.

Human induced pluripotent stem cells are differentiable toward a dentate gyrus identity in vitro

Prior to initiating human *in vitro* experiments to investigate ZBTB20, I examined open-source human bulk RNAseq datasets from Braincloud and Allen Brain Atlas' Brainspan. I first confirmed previous literature findings use prefrontal cortex data from Braincloud that in fact while *ZBTB20* is upregulated during critical neurogenesis stages in the dorsal telencephalon, that rapidly downregulates halfway through gestation and remains downregulated in the prefrontal cortex through lifespan remainder. To visualize how *ZBTB20* messenger behaves in other regions, I next examined and reconstructed regional data from *ZBTB20* expression across 8 different regions including the hippocampus. In comparison to all available regions, the hippocampus

demonstrates the highest embryonic expression of *ZBTB20* and sustains its expression throughout adulthood. Furthermore, *ZBTB20* is upregulated alongside other hippocampal markers in human like *EMX2* and *PROX1* at embryonic stages. *ZBTB20* was thus correlated with other developmental hippocampus markers and demonstrated sustained, longitudinal expression over human lifespan. I anticipated that in deriving human hippocampus, *ZBTB20* served as a robust developmental marker for hiPSC fating.

Before undertaking hippocampal neural precursor differentiation, however, it was necessary to establish a reliable protocol to derive dorsal pallial epithelium from hiPSCs. I referred to the adaptation of past protocols (Bertacchi, Lupo, et al., 2015; Bertacchi, Pandolfini, et al., 2015) as well as commonly accepted isocortical protocols (Y. Shi, Kirwan, & Livesey, 2012; Y. Shi, Kirwan, Smith, et al., 2012; Sposito et al., 2015) to generate neural precursors utilizing minimal media, 500 nM retinoic acid, dual inhibition of BMP and TGFβ, or triple inhibition of WNT, BMP, and TGFβ. I assessed cells by qRT PCR and ICD by DIV 10 to understand population identity, observing that BiTi and WiBiTi produced canonical neural rosettes as opposed to the carpet of $Nestin^{-}$ cells produced in minimal media and with RA. I next assayed a small transcriptomic panel of representative pallial genes between BiTi and WiBiTi between DIV 3-21 and found that while most of the same candidate genes were upregulated, the most notable difference I observed between the two groups was a doubling of FOXG1 in the WiBiTi group between DIV 14-21. Considering this is generally accepted as a strong marker for ventral telencephalic epithelium (Martynoga et al., 2005) I used WiBiTi to initiate neural induction of hiPSCs. I also tested the protocol in parallel with Wnt3a, a molecular signal associated with the cortical hem (Grove et al., 1998) and utilized previously to differentiate hESC derived from dentate gyrus neural epithelium to dentate gyrus neuronal identity (Diana Xuan Yu et al., 2014) as well as hiPSC to CA3 neuronal identity (Sarkar et al., 2018). I observed that Wnt3a treatment instead downregulated *ZBTB20* messenger by DIV 33 and within the small panel most mRNA was like that of WiBiTi. I next adapted two more protocols utilizing CHIR to differentiate hippocampal neurons from ESCs (Sakaguchi et al., 2015; Terrigno et al., 2018) and found that indirect b-catenin pathway activation has an optimal time frame of hippocampal fating post-WiBiTi induction. Inhibiting GSK-3β from DIV 16 for 12 days demonstrated the highest upregulation in dentate gyrus markers

including *ZBTB20*, *EMX2*, and *PROX1* while maintaining *FOXG1* expression. The common protocol for generating dopaminergic striatal projection neurons uses CHIR as well to fate cells (Lukovic et al., 2017) and indeed if telencephalic ventralization is shortened and replaced with CHIR instead, an abrupt decrease in *FOXG1* and *EMX2* transcript is observed, further solidifying the importance of when morphogenic fate molecules are introduced to culture. Furthermore, I was able to demonstrate that ZBTB20 upregulates nuclearly and in a higher of percentage of cells compared to the WiBiTi control as anticipated (Tonchev et al., 2016). Moreover, nuclear ZBTB20 was underregulated in the Wnt3a treated group compared to the CHIR treated group. While this does not necessarily indicate that Wnt3a is an inappropriate molecule for deriving hippocampal-identity neurons from hiPSCs, it does not present conclusive evidence that Wnt3a is uniformly required for fating all the hippocampal neuroepithelium. I offer that it is possible the treatment was ineffective, given that I used a recombinant mouse Wnt3a, however, when aligning the sequences of mouse Wnt3a to homo sapiens Wnt3a and Wnt3a precursor, I observed a 97% conservation between mouse Wnt3a and both human orthologs, with ~99% functional conservation between both mature forms. Overall, inducing a hippocampal identity with CHIR in neural precursors establishes a culture that is molecularly like literary observations.

It is commonly accepted that the hippocampus and cortex host similar cell types and undergo layering in a shared transcription factor dependent manner (Gaspard et al., 2008). The molecular difference explaining how and why these two regions laminate in physiologically different manners is not completely understood, however. Altman and Bayer demonstrated that many of the first neural progenitors provide the working scaffold for subsequent layering of the cornu ammonis and granule blades. Early pioneer progenitors are referred to as “climbers” which expand outward in a zig-zag conformation as opposed to radial glia commonly found in the neocortex which expand outwardly through direct transit (Altman & Bayer, 1990b, 1990a, 1990c). Intriguingly, all early-born pioneer progenitors comprising the outer shells of the cornu ammonis and the dentate gyrus express nuclear Zbtb20 (Mitchelmore et al., 2002) serving to suppress Ctip2 and Satb2 and thereby suppressing neocortical fating pathways (Nielsen et al., 2014). Indeed, it can be first inferred that

hiPSCs maintain this pattern of embryonic ZBTB20 expression when regarding both transcriptomic analysis and ICD of DIV 50 cells. At this DIV, cells not only upregulate ZBTB20 under NOTCH inhibition and WNT upregulation, they also express markers associated both with CA and DG fields. This difference becomes more pronounced when considering the same treatment at DIV 170, wherein the number of $ZBTB20^{+}$ cells decreases and the molecular identity shifts toward a DG field identity. This would imply a novel function for ZBTB20 in that it is crucial for establishing the outer boundaries of the hippocampal field in earlier embryogenic stages but later is only necessary to populate the DG.

While Zbtb20 is yet expressed in astrocytes in the neocortex to contribute to layering (Tonchev et al., 2016), its overexpression instead results in ectopic hippocampal-like layering (Nielsen et al., 2007). Applying the assumption that the neocortex evolved from the hippocampus (Hofman, 2014; Rakic, 2009) may assist in connecting the redundancy of ZBTB20 in the human neocortex and the persistence of its expression in the hippocampus as a trade-off between computational advantages in increased lamination compared to memory generation *de novo* in the hippocampus. Because Zbtb20 is so critical to hippocampal identity and boundary establishment prior to the formation of hippocampal layers at E10 in mice (Rosenthal et al., 2012), I demonstrated through transcriptomics not only how similar my cells are to *in vivo* human hippocampus but also how molecularly different they are from neocortical subregions thereby scratching the surface of the molecular network that contributes to the bifurcation of regional and laminar identity in human corticogenesis.

After verifying that neural precursors could be fated with a hippocampal identity, I next assessed how these cells matured in comparison to to neural prcursors fated with a neocortical identity (WiBiTi-treated cells). At DIV 60, CD16d12 and WiBiTi differentiated cells seemed to express similar neural cytoskeletal, regional transcription factor, and synaptic markers indifferently from culture conditions. An increase in DCX^{+} cell bodies seemed to be present in CHIR-derived cultures in comparison to WiBiTi-derived cultures, however this was only observed by eye. It was discovered however that CHIR treated cells did not adhere well to glass coated with p-l-ornithine/mouse laminin and instead needed to be plated on either a carpet of mESC-derived hippocampal cells (from Terrigno et al 2018) or on light/gas-permissible membrane called biofilm. To continue to assay my

culture more deeply, I transduced cells with mGFP, forced their differentiation with indirect NOTCH inhibitor, DAPT, and replated transduced cells onto mouse cultures. I noticed that human nuclei costained with DCX and ZBTB20 in both groups, that Ki67 seemed to downregulate in the DAPT group, and as expected only in DAPT treated groups were I able to replicate $ZBTB20^{+}/FOXG1^{+}/MAP2^{+}$ neurons, like those derived *in vitro* from embryonic dentate gyrus primordium tissue from Sakaguchi et al 2015. Furthermore, the human neurons seemed to establish synaptic connections with the mouse neurons. Altogether, the results imply that CHIR is an efficient molecule to fate telencephalic progenitor cultures for DG neuronal identity. Considering the ZBTB20 signal was much stronger in older cultures as opposed to naïve cultures at DIV 33, I further pressed ZBTB20 in its role in differentiation.

ZBTB20 expression coincides with maturation of young differentiating DG neural precursors in vitro but does not regulate cell cycle

To understand first if ZBTB20 plays a role in neurogenesis, I analyzed another open-source dataset of single cell RNAseq in mouse hippocampus from embryonic to early postnatal stages. I first checked if Zbtb20 was upregulated across all cells and intriguingly, from E18.5 through P23, it is not and instead is most strongly expressed in clusters of differentiated neurons. More intriguingly, regardless of time point analyzed, Zbtb20 seemed to upregulate in populations expressing Dcx, suggesting that Zbtb20 is consistently functioning as a chaperone to neurogenesis in the hippocampus. Expounding upon this data, I performed a ranked correlation analysis to determine which genes demonstrated the strongest relationship to Zbtb20, regardless of direction. This analysis showed that Zbtb20 was most positively correlated with genes associated to differentiation like Bhlh genes, including granule cell specific NeuroD1, and was negatively correlated to genes expressed by radial neural stem cells, particularly GABA receptor subunits. Zbtb20 thus seems to be a crucial signal in embryonic generation of hippocampal neurons but would also appear to play a further sustained role in adult neurogenesis.

Using my hiPSC-hippocampus model, I investigated the potential of ZBTB20 to upregulate during differentiation from neural progenitor to immature neuron. I employed NOTCH inhibitor, DAPT, to induce

differentiation in my neural precursor cultures and analyzed Nestin, NeuN, and ZBTB20 expression by ICD 2 days after ending DAPT treatment. ZBTB20 was most upregulated in dual inhibition by DAPT and CHIR, followed by CHIR treatment alone, and strikingly unchanged compared to DAPT treatment alone. NeuN was simultaneously significantly upregulated in dual inhibition treatments and seemed to remain at baseline in all other groups. Taken by itself, it seems that both Notch inhibition and b-catenin pathway activation are obligatory for the maturation of these cells. To further investigate this point, I repeated the experiments and measured maturing cytoskeletal outgrowth by DCX and MAP2. Both DAPT experiments induced DCX and MAP2 outgrowth to the same extent in comparison to minimal media and CHIR treatment alone. I further established the relationship between DCX and ZBTB20 as well as MAP2 and ZBTB20 and found that DCX was significantly correlated with ZBTB20 appearance whereas MAP2 was uncorrelated with ZBTB20. These data reconfirm that ZBTB20 upregulates in the nucleus at early neuronal differentiation stages. Previous findings have suggested that NeuN does not ubiquitously detect all neurons (Gusel'nikova & Korzhevskiy, 2015; Kumar & Buckmaster, 2007) and in fact in the mouse hippocampus, deletion of NeuN/Rbfox3 results primarily in altered dentate gyrus synapses but not in a loss of neurons (H. Y. Wang et al., 2015). Furthermore, Rbfox1, an ortholog of NeuN, has been demonstrated as crucial in efferent connection establishment (Wamsley et al., 2018) suggesting that the Rbfox family may play a role upstream of synaptic connections and not necessarily in neuronal identity. Furthermore, NeuN is not constitutively upregulated during neurogenesis and exhibits an "off period" during neuroblast stages (Ambrogini et al., 2004; Gusel'nikova & Korzhevskiy, 2015). Despite NeuN's discreetly phasic nature, I postulate that ZBTB20 does in fact upregulate as cells progress along the differentiation axis but that simultaneous inhibition of NOTCH and GSK-3β are the minimal extrinsic signaling requirements to elicit ZBTB20 nuclear expression in maturing human hippocampal neurons.

Having demonstrated that ZBTB20 is integral in the neural stem cell-maturation pathway during pseudo-embryonic stages, I next evaluated ZBTB20's functional role in these cultures. From DIV 31, I either knocked-out by CRISPR or negative-dominant ZBTB20 and assessed a small panel of cell cycling related genes. These results suggest that ZBTB20 does not facilitate neurogenic exit at early stages but a deeper investigation

into precise cell type emergence would be very beneficial for understanding ZBTB20's overall role, given its competitive nature in mouse with Ctip2, Satb2, CoupTF1, and Fezf2 (Nielsen et al., 2014) as well as its role in archicortical organization (Rosenthal et al., 2012). It is plausible that either these cells were assayed at an inconsequential timepoint as many D-cyclin-related genes have been demonstrated as redundant in driving proliferation during early-to-mid gestational periods (Kozar et al., 2004).

Culture substrate, Laminin α5β1γ1, lengthens symmetrical divisions in vitro independent of time and maintains neural precursor populations

In demonstrating that ZBTB20 is inactive in regulating cell cycle during early human hippocampal neurogenesis, I next investigated if these hippocampal neural precursors could be expanded past terminal spontaneous differentiation timepoint. Laminins are a crucial basement protein family in the developing cortical subplate (Hunter et al., 1992; Long et al., 2019) and have been more recently shown to sustain neurogenesis in the SVZ through fractone bulb expression of the a5 subunit (Nascimento et al., 2018). Furthermore, I mined another open-source repository harboring spatial transcriptomics of adult mouse cortex and reconstructed the data to display a sagittal recreation. I found that while most LAMA subunits are expressed in a salt-and-pepper manner, LAMA5 seems to be sequestered in a ZBTB20-void that most likely corresponds to enrichment in the dentate gyrus/subrganular zone. Utilizing a panel of previously assessed laminins (Hyysalo et al., 2017), I demonstrated that laminin isoform α5β1γ1 is protective against membrane blebbing and preferentially sustains Nestin$^+$ fibril outgrowth over βIII-tubulin$^+$ fibers in comparison to the other laminar isoforms. Intriguingly, 121 demonstrated the second highest Nestin expression, however, concomitantly expressed highest βIII-tubulin while its paralog, 111, suppressed βIII tubulin. Neuronal outgrowth may be attributed to LAMB, the beta subunit of laminin (Leventhal et al., 1999), as 521 has also been demonstrated to support MAP2 and TBR1 expression (Hyvärinen et al., 2019), however investigations into laminar regulation of neurocytoskeleton are limited. Once I procedurally demonstrated that 511 laminin

was optimal for supporting neural stem cells, I then proceeded to expand neural progenitor populations maintained on 511 laminin.

As LAMA5 is a crucial substrate for regulating neurogenesis in the subventricular niche (Nascimento et al., 2018) and based on my results regarding NSC promotion by 511, I proceeded to expand my neural progenitor niche on 511 but in three distinct conditions: CHIR, alternating CHIR between passages, and constant CHIR. I found that 511 does not intrinsically support sustained cell division and instead that constant CHIR gives a more stable expansion than its alternating counterpart. This was further supported by demonstrating constitutively repressed ZBTB20 and DCX expression for over 200 days *in vitro* with constant CHIR treatment. It is surprising that hippocampal neural stem cell niche maintenance is requisite of only a purified laminin isoform and constant GSK-3β inhibition. However, CHIR99021 has most frequently been used in stem cell expansion protocols as it promotes proliferation and maintains stemness (P. Li et al., 2008) while simultaneously offering a nontoxic yet highly specific GSK-3β inhibitor compared to molecular analogs (Naujok et al., 2014). GSK-3β inhibition is also ubiquitously involved across several adult stem cell niches (Racaud-Sultan & Vergnolle, 2021) including hematopoietic (Holmes et al., 2008). To assess this point of NSC niche laminar sustainment, I attempted to derive the niche on the conventional substrate of purified mouse laminin, however, I found that ZBTB20 was neither expressed strongly as messenger nor in the nucleus compared to cells grown on 511.

To delve further into the niche, I next assayed DIV 90 cells maintained on PMC, DIV 90 cells on SDC, and naïve DIV 33 cells for ZBTB20 and Nestin. DIV 90 PMC cells expressed Nestin and ZBTB20 akin to their naïve predecessors whereas DIV 90 SDC cells expressed increase ZBTB20 and decreased Nestin compared to both groups. Next, I examined Nestin, ZBTB20, and NeuN within alternating and constant CHIR niche pools at DIV 110, a time past typical hiPSC-derived neuronal differentiation endpoint (~DIV 100). I found that the constant group upregulated all markers when transitioned to SDC and instead that the alternating group downregulated Nestin. The implications of this experiment suggest firstly that cells kept in the niche can differentiate past the commonly accepted time that hiPSCs differentiate into mature neurons. Secondly that the Nestin results of the

alternating group imply that these cells might be farther progressed along the differentiation axis than their counterparts treated with constant chir. Counterintuitively however, this does not change the magnitude at which these markers are expressed between alternating and constant groups, only the differential from their respective PMC condition.

With regards to the niche and laminar regulation, I examined one final aspect regarding progenitors expanded well past DIV 90 and the potential for older progenitors to still express neuronal cytoskeletal markers. At DIV 160, I plated hippocampal neural progenitors onto either 511 or mouse laminin but maintained CHIR in both conditions for 10 days after which Ki67 and βIII-tubulin were assayed. Cells grown on mouse laminin exhibited decreased Ki67 expression but upregulated βIII-tubulin expression compared to those grown on 511, suggesting that these neural stem cells maintain their ability to differentiate despite longitudinal expansion *in vitro*. Furthermore, this suggests that cells migrating out of the niche may transition from a molecularly specific annex to a more general laminar basement during maturation. Altogether, my results indicate that hippocampal neural precursors can be maintained in the stem cell niche with 511 laminin and CHIR, for at least 240 days *in vitro*, and can further be differentiated by simply transitioning the cells to conventional laminar substrates.

ZBTB20 expression coincides with maturation of older differentiating DG neural precursors in vitro and regulates cell cycling genes

After elucidating that hiPSC-derived hippocampal progenitors can remain under longitudinal GSK-3β inhibition and retain their neurogenic properties, I next assessed if these cells retain their propensity to express nuclear ZBTB20. I repeated the experiments I analyzed with DIV 50 cells, starting from DIV 174 instead and assaying CHIR and DAPT in their differentiation. First, I observed that cells did not survive with CHIR withdrawal and so only $CHIR^{+}/DAPT^{-}$ and $CHIR^{+}/DAPT^{+}$ could be analyzed appropriately. Second, I found that dual inhibition was still able to elicit a 2-fold increase of nuclear ZBTB20 by DIV 180 compared to DIV 50 control and DIV 180 CHIR treatment alone. This was followed by a subsequent increase in $NeuN^{+}$ cells as well, however,

the average correlation between NeuN and ZBTB20 was not increased significantly from the DIV 50 control. Excitingly, this indicates that ZBTB20 is phenomenologically conserved in older cells despite the "aging" routine, yet downstream of NOTCH pathway inhibition. However, as expected, the efficiency of ZBTB20 response is decreased from its younger counterparts by almost 2-fold, suggesting that these cells do not retain all their differentiable capacity. When I repeated the viral construct experiments with older progenitors, I found a marked phenomenological switch unobserved at DIV 35 in that most D-cyclin related genes assayed were upregulated, most notably *CDK6*, a major G1 phase regulator intrinsic to regulating symmetrical NSC divisions in adult hippocampal neurogenesis (Beukelaers et al., 2011). Furthermore, both viral constructs downregulate DCX compared to their untransduced control group. These results, when considered in terms of the results acquired from DIV 35, suggest that there is a functional switch for ZBTB20 with respect to time and that maturing hippocampal NSCs are regulated by ZBTB20 in humans. Plausibly, this switch may be temporally biphasic, suggesting different functions correspondent to developmental progression. A similar zinc finger and transcription factor, Bcl11b, is known to exhibit both cell fating properties in early developmental stages (Arlotta et al., 2008) as well as synaptic maintenance in post-developmental neurons (R. Simon et al., 2016). A deeper insight into the molecular mechanism of ZBTB20 would be highly beneficial to parse its time-dependent functions.

Hippocampal neural precursor pseudodevelopment in vitro is similar to embryonic hippocampal development by RNA-Seq Analysis

Considering ZBTB20 upregulation is decreased between DIV 50 and 174 DAPT induced neurons, the next cellular aspect to investigate was their molecular profiles via bulk RNA sequencing. Principal component and differential expression analyses of transcriptomic data on my cells treated with CHIR, DAPT, or both demonstrated a crucial role in WNT signaling in hippocampal neural stem cell maturation. Canonical WNT signaling through Wnt3a has been long established as necessary for the developing hippocampus (S. M. K. Lee et al., 2000) and that its downstream effect on layering induces molecularly segmented layers between the

granule cell layer, CA1, CA2, and CA3 (Grove & Tole, 1999). Intriguingly, when comparing DIV 50 and DIV 174 transcriptomic profiles to DIV 28 naïve progenitors by PCA, DIV50 groups expressed both markers for dentate gyrus and CA1-CA3 whereas DIV 174 selectively expressed markers associated with the dentate gyrus. Hippocampal layers develop embryonically *in vivo* by first populating the cornu ammonis from E 12.5-E16.5 mice and then the dentate gyrus and intra-hilar CA3 blade from E14.5-P0 (Altman & Bayer, 1990b, 1990a, 1990c). Furthermore, an enrichment in metabolic and chromatin remodeling GO functions related to clock GRNs or late-embryonic stage granule cell emergence was observed. These results imply that these cells do not undergo accelerated aging *in vitro* but instead recapitulate molecular events of embryonic hippocampal layering over the course of a pseudo gestation period equivalent to time *in vivo*. Furthermore, these results are very promising and suggest that longitudinal neurogenesis studies replicating the SGZ *in vitro* may be possible by extending their time in culture, a particularly enticing facet for memory, aging, and pathology studies in a human context.

Differentiating DG neural precursors mature physiologically in vitro and in vivo

The next set of experiments were designed to assay functionally relevant aspects of my hippocampal cultures. Utilizing the OPAL once again, I plated $CHIR^{+}/DAPT^{+}$ treated naïve and older neural precursors transduced with ChR2 under the synaptophysin promoter onto mouse hippocampal cultures. After 40 days *in vitro*, I repeated the original experiments I performed with mESC-derived isocortical neurons, giving 4 x 15-minute cycles of 100 Hz blue light for 10 minutes followed by a dark pause for 5 minutes. In parallel, I performed the same paradigm but with 1 μM TTX for the hour-long treatment. With the conclusion of the stimulation, I stained for human nuclei and cFOS and found that in the 100Hz condition, both young and old neurons exhibited a marked increase in $cFOS^{+}/huNuc^{+}$ nuclei compared to their controls. Most interestingly, cells at DIV 210 exhibited a significant increase in $cFOS^{+}/huNuc^{+}$ nuclei compared to 0 Hz, 0 Hz +TTX, and 100 Hz + TTX whereas cells at DIV 70 exhibited a slight but insignificant increase with both TTX treatments. These results

suggest that older progenitors may be more primed than younger progenitors to become functionally active and moreover, at DIV 70 there are still immature precursors within the culture. To complete my exploration into the neurogenic capacity of my hippocampal neural stem cell niche, I transplanted NSCs into wild type mouse dentate gyrus to establish a chimeric model.

The last experiment I performed with the imperative skillset of Matteo Caleo, Claudia Alia, and Verediana Massa, and involved xenografting both naïve and older progenitors into wild type mice to assay their synaptic integration in *in vivo* dentate gyrus. Cells were lentivirally transduced with mGFP and treated with CHIR and DAPT prior to the transplantation to induce differentiation in the event neural precursors were not coaxed within the host dentate gyrus. After three months *in* vivo, mice were fixed, and cross-sections were stained with VGLUT1 and PSD-95 to identify pre and post synaptic puncta between $mGFP^+$ human fibers and mouse post-synaptic domains. Not only did both naïve and older hippocampal neural progenitors survive within the dentate gyrus, but projections had been established across the hilar toward the CA3, the natural synaptic target of adult-born granule DG neurons (Vivar et al., 2012; C. Zhao et al., 2006). Furthermore, along these GFP^+ projections, I observe $VGLUT1^+$/$PSD\text{-}95^+$ puncta, indicating that the human cells had formed architectural synapses within the mouse host No differences between naïve, older, and transgenic control synapses were identified. My chimeric model demonstrates several key aspects about my cells generated *in vitro*. As has been demonstrated throughout the literature, the hippocampus is a tightly regulated neuronal niche and cells that do not molecularly mirror target layers are severely inhibited in their post-xenograft integration (Quattrocolo et al., 2017; Terrigno et al., 2018). I infer thus that the integration of both DCX^+ cells in the SGZ and human fiber projections stemming from the GCL toward the CA3 confirm that these cells are not only morphologically neuronal but also molecularly like DG precursors and neurons. Secondly, my experiments compound my earlier findings that these neurons form synaptic architecture though this further demonstrates that they are most likely biologically relevant and not aberrant synaptic expression. Third, these data suggest that older neural precursors, while fewer in surviving number post-xenograft, do not establish fewer synaptic connections than their naïve counterparts. This implies, like in rodent neurogenesis studies,

that while older neural precursors must survive programmatic cell death (Ryu et al., 2016) their integration into the circuit is unchanged. To criticize my chimeric *in vivo* model, despite assaying cFOS response using the OPAL, I did not assess electrophysiological function of present synapses and thus can only speculate on their synaptic morphology. A beneficial follow-up to the present study would include increasing the number of animals transplanted with heterochronic progenitors to assay changes in synapse densities and to bolster the investigation of neuronal function by transducing ChR2 into neural precursors and recording afferent field potential changes via multiunit in the CA1 and CA3.

Human iPSCs offer a powerful tool to model human hippocampal development and may be utilized in future patient-derived stem cell therapies

During rodent embryonic neurogenesis, Zbtb20 appears in neurons maturing from the ammonic neuroepithelium and dentate notch but is absent from cortical progenitors and radial glia (Mitchelmore et al., 2002) and acts as a functional competitor of Ctip2 and Satb2 during hippocampal layering, presumably fating neural precursors for specific field identity (Nielsen et al., 2014). Using my hiPSC-derived precursors, I sought to demonstrate the conservation of this phenomenon in human. Integrating the observations from these datasets with a recent open-source single cell transcriptomic mouse data set, it was evident that Zbtb20 is constitutively expressed from E18.5-P23 in mice and concordant with the literature, is absent $Sox2^{+}$ radial glia from P0 onward but whose mRNA seems to upregulate while passing through the differentiation axis. This observation was again conserved across all 4 acquired time points, implying that Zbtb20 mRNA may upregulate in radial NSCs exiting the cell cycle. When I again forced differentiation of DG NSCs at early DIV, I observed that upregulated ZBTB20 nuclear expression required co-inhibition of GSK-3β. Intuitively, co-inhibition of NOTCH and GSK-3β should demonstrate conflicting results given NOTCH/b-catenin pathways overlap (Peignon et al., 2011). However, as the WNT/b-catenin pathway is upregulated under GSK-3β inhibition (Naujok et al., 2014), as the hippocampus develops under direct Wnt signaling (Grove et al., 1998), and that DAPT inhibit γ-secretase instead of NOTCH receptor, it stands to reason that concomitant blockade of Notch activation in parallel with

upregulated canonical Wnt signaling generates hippocampal identity neurons. This is further confirmed by the fact that the hippocampus endogenously inhibits GSK-3β via canonical Wnt pathway to induce dendritic morphogenesis in embryonic primary hippocampus cultures (Ramos-Fernández et al., 2019). Indeed, the correlation between DCX and ZBTB20 along with the finding that dual inhibition elicited the most robust ZBTB20 response implies that an endogenous Wnt signal is necessary to drive human neuronal fate in the hippocampus.

Reassessment of hiPSC-derived hippocampal model: summary and literary integration of presented findings

Where the previous sections regarded each experiment and its individual finding in chronological order, this section reassesses the experiments in terms of larger scope and links the findings together based on relevance and previous literature. Overall, in the context of the current literature on ZBTB20 and human hippocampal development, this thesis has observed and described several conclusions:

1. Several hippocampal models exist for *in vitro* study of the human hippocampus (Sakaguchi et al., 2015; Sarkar et al., 2018; Diana Xuan Yu et al., 2014), however, this exists as a novel approach to generate pan-hippocampal field identity cultures as demonstrated by increased $ZBTB20^{+}$ cell number and mRNA at DIV33 alongside comparison to *in vivo* brain regions using RNA-seq. Furthermore, temporally "purified" cultures of dentate gyrus may be generated with laminin 511 by sustaining symmetrical neurogenesis. It has been demonstrated in rodent hippocampus that CA fields develop at the same time as the DG but terminate a majority of field development 2-3 days earlier than the DG (Altman & Bayer, 1990b, 1990c). Moreover, in rodents, nonhuman primates, and human, neurogenesis persists in the SGZ of the DG long after hippocampal field maturation (Ming & Song, 2011; Overstreet-Wadiche & Westbrook, 2006). RNA-seq of our cultures demonstrated that older cultures that were expanded on laminin 511 exhibit this same

behavior, in that differentiating cells at DIV 50 express molecularly similar profiles to the CA3 and DG but are more similar to only the DG at DIV 180. This is not the first report of conserved embryogenic mechanisms in stem cell-derived neuronal culture models (Moodley et al., 2013; Morgani et al., 2018; Muguruma et al., 2010; Zhu & Huangfu, 2013) but is a significant contribution as a non-organoidal model for studying hippocampal field development and molecular bifurcation of CA and DG layers over time.

2. Laminins have been minimally investigated in neurogenesis and the hippocampus. Several studies demonstrate that either they are crucial for NSCs in the neuroepithelium (Leventhal et al., 1999), maintenance of neuronal cells *in vitro* (Doi et al., 2014; Hyysalo et al., 2017), or maintain NSCs at fractone bulbs in the SVZ (Kerever et al., 2007; Nascimento et al., 2018). I originally anticipated that utilizing laminin 511 would mimic the adult SGZ niche and would model adult neurogenesis *in vitro*. I instead found that 511 more likely mimics the dentate epithelium and the secondary dentate matrix in which NSCs continue to symmetrically divide to populate the granule cell layer (Altman & Bayer, 1990a). These findings are novel in that extended use of 511 and CHIR 99021 has drastically different effects on hippocampal-fated NSC maintenance in comparison to other laminins with similar matrix structures (Hyysalo et al., 2017) or purified mouse laminin commonly found in *in vitro* protocols (Bertacchi, Pandolfini, et al., 2015; Martins et al., 2021; Pandolfini et al., 2016; Y. Shi, Kirwan, & Livesey, 2012; Terrigno et al., 2018). Most likely, this implies a novel finding that the alpha 5 and beta 1 chain of laminin are lateral to sustained b-catenin signaling in maintaining hippocampal NSC populations by suppressing differentiation in embryonic niches.
3. ZBTB20 has been observed to upregulate in CA and DG outer fields in early human embryogenesis similar to mouse and rat (Nielsen et al., 2014). I observed an increase in $ZBTB20^{+}$ cells in a mixed CA3/DG culture system and a decrease in $ZBTB20^{+}$ cell number between DIV 50 and DIV 180 after dual inhibition of NOTCH and GSK-3b. Taken together with the hippocampal field-comparison RNA-seq data, this implies that ZBTB20 may become more specific to DG and granule cell

maturation later in embryogenesis as other transcription factors fate the pyramidal cell layer, like Ctip2 in the CA1 (Ruth Simon et al., 2012). Furthermore, this is supported by the differential gene analysis between DIV28 and DIV 174 cell cultures demonstrating an upregulation of mitochondrial/aging related gene networks, indicating that these cells express circadian and longitudinal time keeping genes in an "aging" context. This model exhibits strong similarities to *in vivo* phenomena, as is characteristic of pluripotent stem cell models (Gordon et al., 2021).Indeed, this ample may be used to study discreet timepoints during human hippocampal neurogenesis and contributes to the growing body of literature that hiPSCs provide a robust tool to study human embryogenic mechanisms for neurodevelopment.

4. Another aspect this thesis sought to uncover was the functional role of ZBTB20, considering that the transcription factor is constitutively expressed throughout rodent (Mitchelmore et al., 2002; Nielsen et al., 2007) and, according our analysis of the Allen Brain Atlas, human lifespans. Several studies demonstrated that Zbtb20 is crucial for hippocampal organization during embryogenesis (Rosenthal et al., 2012), competes with cortical transcription factors, Ctip2 and Satb2, in repressing neural stem-related genes (Nielsen et al., 2014), and is crucial to memory formation in the CA1 (Ren et al., 2012) most likely by a SUMOylation-dependent mechanism (Ripamonti et al., 2020). However, Zbtb20 has been shown both upregulated in proliferating glioblastoma (J. Liu et al., 2018) and in differentiation of wild-type olfactory bulb progenitors during embryogenesis (Doeppner et al., 2019). The following aspects regarding ZBTB20's role will be broken into subdivided conclusions to substitute paragraph breaks in the retained outline format:
    a. To understand first if Zbtb20 is related to proliferation or differentiation in hippocampal development, a Single Cell RNA-seq dataset of the developing mouse hippocampus was analyzed. Analysis revealed that *Zbtb20* was upregulated gradually as hippocampal neural stem cells proceeded through differentiation steps, providing substantial insight into the anticipated role of ZBTB20 in a human context based on previous human hippocampal

findings (Nielsen et al., 2014). Indeed, we observed that ZBTB20^{+} cell number and DCX fiber length correlated in DIV 50 cells, similarly to mouse SC RNA-seq dataset. However, ZBTB20 expression was dependent on WNT upregulation/b-catenin pathway activation at DIV 50 and that NOTCH inhibition alone was not sufficient to drive ZBTB20 expression. This implies another novel aspect for ZBTB20 and embryonic hippocampal neurogenesis in that ZBTB20 is downstream of activated WNT and is more strongly expressed at the protein-level under simultaneous NOTCH signaling inhibition (Figure 65). Intuitively, both WNT signaling and differentiation may be crucial in establishing CA and DG hippocampal fields in early human embryogenesis, as Zbtb20 has been associated with pioneer cells in mouse hippocampus (Mitchelmore et al., 2002). Furthermore, ZBTB20 may be responsible for generating cortico-specific cell types at the same timepoint, as suggested by differential expressed gene analysis showing GO enriched membrane and membrane receptor between NOTCH-inhibited and dual inhibited cells at the same timepoint as well as increased NeuN expression in dual inhibited cells. Interestingly, while ZBTB20 was co-expressed with neuroblast/immature neuronal marker, DCX, its knockout was not associated with increased mRNA for cell cycling-related genes. Given that earlier day *in vitro* most likely represent earlier periods of gestation, it is plausible that functional knockout of ZBTB20 does not affect cell cycling genes as cell cycling genes may be redundant during early gestation, as demonstrated in combined knockout of CDK1, CDK4, and CDK6 in mouse embryogenesis (Kozar et al., 2004). Thus, ZBTB20's role is likely to fate hippocampal NSCs toward a specific identity in human hippocampal embryogenesis but the appearance of neuronal markers like DCX may be more coincidental with general maturation as opposed to ZBTB20-mediated differentiation, considering that DCX and MAP2 were upregulated in both NOTCH inhibited and dual NOTCH/GSK-3b inhibited culture groups (Figure 66A). It may be possible that ZBTB20 knockout at this timepoint is

then redundant and that NSC cultures will instead continue to mature but with a different neuronal fate. This is supported in that Zbtb20 knockout in mice ablates the hippocampus but the retrosplinial cortex invades the hippocampal region in a compensatory mechanism (Rosenthal et al., 2012). It is further plausible that ZBTB20 knockout may ease competition with other transcription factors at earlier days *in vitro* and allow Satb2 and Ctip2 less molecular competition for neural stem related binding sites (Nielsen et al., 2014). The remaining transcription factors may still induce terminal differentiation despite ZBTB20 knockout.

b. ZBTB20 is a marker for differentiated neurons in the hippocampus (Mitchelmore et al., 2002; Nielsen et al., 2007; Sarkar et al., 2018), however, as several experiments conducted herein demonstrate that it is not only downstream of NOTCH and WNT activation but is also repressed by 511 laminin longitudinally. In determining that 511 represses neural differentiation, three further experiments were conducted. The first demonstrated that ZBTB20 upregulates in hippocampal neural cells after 90 days of neural induction on mouse laminin but remains lowly expressed in DIV 33 cultures as well as in cultures maintained for 90 days on 511. The second demonstrated that despite 100 days proliferating on laminin 511, ZBTB20 still upregulated when NSCs were transferred to mouse laminin. The third experiment demonstrated that 511 maintained ZBTB20 at a low expression despite more than 240 days *in vitro*. These experiments demonstrate yet another novel finding that it has a conserved, time-independent role in the hippocampus. This role would imply ZBTB20 as a marker of differentiating hippocampal Type II NSCs and whose expression is upregulated gradient-wise with progressive stages of differentiation. While this claim is still preliminary, further experiments based on past studies elaborating neurogenic cell stages (Doetsch et al., 1999; Ming & Song, 2011; Overstreet-Wadiche & Westbrook, 2006) coincidental with ZBTB20 expression level that would strengthen this

assertion are discussed in the following section, “Future perspectives.” Regardless, this represents a crucial first step in elaborating ZBTB20’s mechanistic role in the human hippocampus and provides preliminary insight into how ZBTB20 contributes to the development of the hippocampal anatomy and cytoarchitecture.

c. Finally, this thesis made one final novel finding regarding ZBTB20’s mechanistic role during hippocampal neurogenesis to distinguish time-dependency. Dual inhibition of NOTCH and GSK-3β still induces $ZBTB20^{+}$ cell number and $NeuN^{+}$ cell number, in comparison to GSK-3β inhibition alone at DIV 180 and the DIV 50 uninhibited control. ZBTB20 at DIV 180 was not upregulated to the same extent as in the DIV 50 dual inhibited group, it demonstrates a novelty that ZBTB20’s role as a marker of differentiating hippocampal neurons is conserved regardless of age (Figure 66B). Previous literature does not explicitly distinguish this feature of ZBTB20, despite demonstrating that Zbtb20 is expressed constitutively throughout the hippocampus during mouse and rat lifespan (Mitchelmore et al., 2002; Nielsen et al., 2007, 2014, 2010). Furthermore, ZBTB20’s role at this DIV switches to regulate cell cycle, as both the knockout and knockdown of ZBTB20 increase cell cycling genes at DIV 170. This increase demonstrates a significant finding, suggesting that at later stages in embryogenesis, ZBTB20 may more actively facilitate cell cycle exit as it has been shown previously to suppress SOX-family genes in non-neuronal chondrocytes (Zhou et al., 2015) and neocortical astrocytes (Nagao et al., 2016). Further investigation of this aspect is necessary however and is likewise discussed in the following “Future perspectives” section.

d. To summate, the overall finding of point 4 is that ZBTB20 may behave in a time-dependent manner that spans from embryogenesis to late adulthood in humans. Based on the literature and the findings herein, it is possible that ZBTB20 is conserved as a marker of neuronal differentiation across human lifespan but still multiphasic with regards to age

and stage of differentiation. The original hypothesis anticipated that ZBTB20's function would remain conserved throughout the modeled embryogenic hippocampus model as a facilitator of neurogenic differentiation, the somewhat-contradictory results indicate even more compelling implications for ZBTB20's role in the hippocampus. To elaborate: (1) In early embryogenesis or the first trimester, ZBTB20 may be key to fating pioneer cells and establishing the outer shells of the cornu ammonnis and dentate gyrus (Mitchelmore et al., 2002; Nielsen et al., 2010; Rosenthal et al., 2012) . These findings may be extrapolated to include human as we found ZBTB20 expression in maturing neurons of mixed cornu ammonis/dentate gyrus identity cultures at an early timepoint *in vitro*, DIV 50. (2) As the cultures aged *in vitro*, they still expressed ZBTB20 when differentiation was induced by dual NOTCH and GSK-3b inhibition but expressed markers more specific to dentate gyrus than cornu ammonis, suggesting that ZBTB20 may specify neurons in the dentate gyrus at later stages in embryogenesis. Furthermore, ZBTB20 may also take on a role mediating cell cycle regulation, as its knockout at DIV 170 induced upregulation of several cell cycling genes including *CDK6*, *CDKN1A*, and *EF1A*. This is a major finding suggesting a time-dependent phase switch for ZBTB20 wherein at later embryonic stages, ZBTB20 may assert a more active role in mediating cell cycle exit in hippocampal NSCs. Two more roles for ZBTB20 that were unable to be assessed with this model but that were discussed earlier in the introduction include (3) ZBTB20-mediated cell cycle exit during adult neurogenesis, as suggested by the mouse SC RNA-seq analysis, extrapolation of ZBTB20-knockout experiments, and SOX-family repression by ZBTB20 in adult, non-neural dividing cells (Zhou et al., 2015); and (4) the plausibility of activity-dependent ZBTB20 recruitment at synapses in mature neurons in the adult hippocampus (K. A. Jones et al., 2018; Ren et al., 2012; Ripamonti et al., 2020).

5. The final novelty of this study demonstrates a previously unreported finding, that hiPSCs may be differentiated into physiological neurons with a dentate gyrus identity. Previous protocols demonstrate either: hiPSC differentiation to CA3-identity (Sarkar et al., 2018), hESC differentiation to functional dentate gyrus identity (Sakaguchi et al., 2015), or hiPSC differentiation to functional neocortical identity (Y. Shi, Kirwan, Smith, et al., 2012; Xie et al., 2018). The hypothesis intended to demonstrate that cells generated in this protocol are neuronal by utilizing the OPAL to assay optogenetically targeted hippocampal cells and transplantation of GFP-tagged hippocampal cells into mouse hippocampus. First, that if the protocol generates neurons, then the differentiated cells should upregulate cFOS when exposed to blue light. Second, that if the protocol generates hippocampal neurons, then the cells should not only survive in a chimeric hippocampal model but extend processes into the host tissue and establish synapses, as demonstrated in heterotopic cell-cortex transplant experiments (Quattrocolo et al., 2017; Terrigno et al., 2018). Several experiments were conducted to demonstrate upregulation of neuronal markers (βIII-tubulin, DCX, MAP2), hippocampal markers (ZBTB20, *EMX2*, *PROX1*), and GO analysis of RNA-Seq data to demonstrate that DIV 28 cells are molecularly different from hiPSCs. However, a common criticism of stem cell-derived neuronal model studies is the physiological relevance of neuronal cells generated (Bardy et al., 2016; Wernig et al., 2004) despite neuronal marker expression. Both facets of the hypothesis were confirmed, though, in generating functional neurons that extended synaptic processes when transplanted *in vivo*. Furthermore, hippocampal cells expressing ChR2 under the synaptophysin promoter generated from DIV 28 and DIV 160 NSCs upregulated cFOS when exposed to blue-light in a 100Hz duty-cycle paradigm, though cells at the later DIV were more sensitive to TTX, possibly due to transient NSC population in the earlier DIV cultures (R. Chen & Chung, 2014). These results are further supported by synaptic integration post-xenotransplantation of hippocampal cells generated from DIV 28 and DIV 160 into mouse dentate gyrus. As previous studies demonstrated that neuronal cells of a specific identity do not integrate

into heterotopic brain regions, this further confirmed that not only do these cells survive in the dentate gyrus but they extend into the CA3 downstream and establish synaptic protein junctions with host neurons in the CA3. Despite exhaustive studies detailing xenografting of hiPSC-derived neural cells into mouse cortex (Espuny-Camacho et al., 2013), rat striatum (Fjodorova & Li, 2018), or mouse cerebellum (Shuyan Wang et al., 2015), hESC-derived neural cells into mouse cortex (Denham et al., 2012; Michelsen et al., 2015; Wernig et al., 2004), or striatum (Arber et al., 2015), and human embryonic NSCs into the mouse dentate gyrus (Clarke & Van Der Kooy, 2011), this newly describes transplanting iPSC-derived hippocampal NSCs from different age groups into mouse dentate gyrus with successful synaptic integration at both early and late timepoints. Both timepoints is imperative to the model as it demonstrates that these NSCs are fated with identities that are undeniably similar to the dentate gyrus and provide a platform for neurophysiological studies *in vivo* within the context of human cells (discussed further in "Future perspectives").

Future perspectives

This thesis introduces a novel role of ZBTB20 strongly suggesting it as a marker for hippocampal neural stem cells exiting cell cycle in a human context and further divulges that hiPSCs fated for hippocampal neuronal identity share common developmental timing in cornu ammonis and dentate gyrus formation. However, while the hypotheses anticipate that ZBTB20's function would be conserved across both representative time points in this embryogenic hippocampal model, my results instead support the hypothesis that ZBTB20's role in embryonic hippocampogenesis is time dependent. ZBTB20 was demonstrated as a marker of differentiating neuronal cells at both early and later timepoints, however, in functional experiments ZBTB20 knockout increased cell cycle-related genes in older cultures. This study was concluded supporting the hypothesis that this protocol fates hiPSCs as both functionally neurogenic and hippocampal in origin. Experimental results, though, are compelling to explore mechanisms of ZBTB20 and laminin 511 more thoroughly to develop the

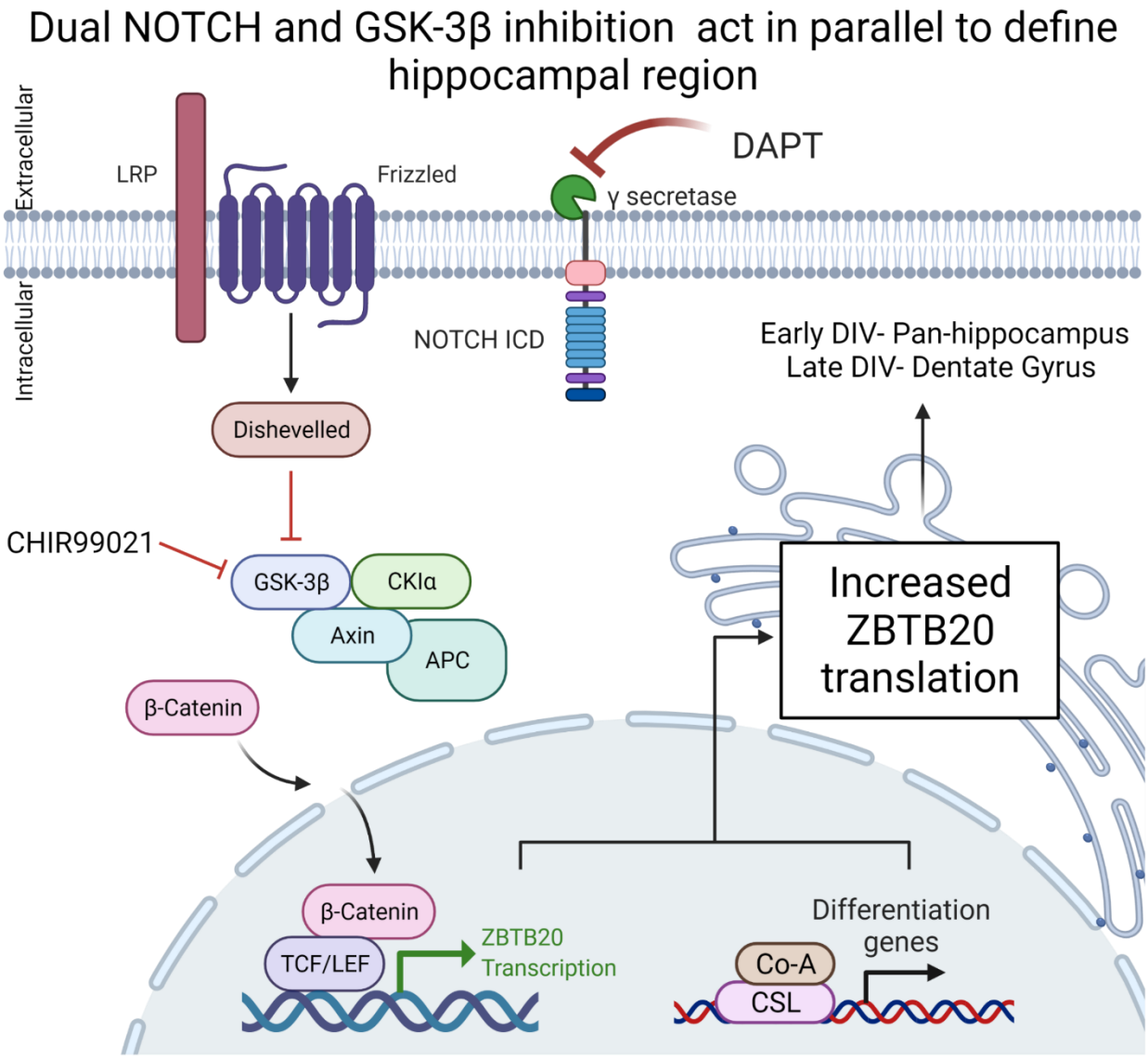

Figure 65. Proposed mechanism for simultaneous WNT activation and NOTCH inhibition are imperative establishing hippocampal field boundaries. Adjusted Wnt mechanism to include inhibited NOTCH signaling by DAPT depicting that β-catenin most likely drives ZBTB20 mRNA expression as demonstrated in DIV28 and DIV 33 fating experiments and that the messenger is recruited for translation after differentiation signals, like NOTCH pathway inhibition. Both of these contribute to a robust ZBTB20 expression response at the translational level that was unobserved in either NOTCH inhbition or WNT activation alone. Potential time-dependent cellular effects are depicted in Figure 66.

model as well as to drive the model toward use in clinical therapy for cognitive dementia. This section will address each point made in the previous section and will detail future experiments that would strengthen the investigation.

First, previous studies have shown that specific laminin isoforms like 121, 511, and 521 intrinsically maintain neural cells *in vitro* (Hyysalo et al., 2017; Sasaki et al., 2010). Hyysalo et al. 2017 explicitly

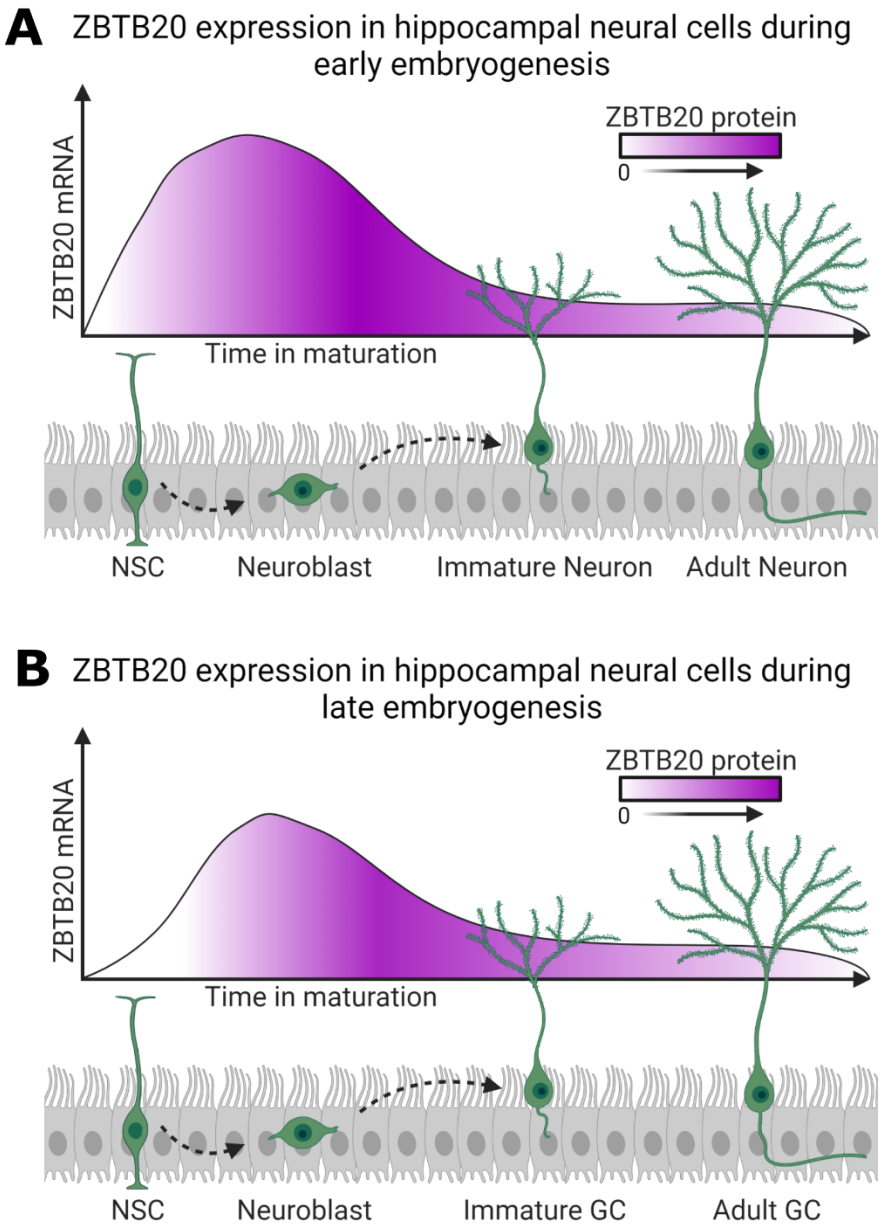

Figure 66. Schematic of ZBTB20 expression during neuronal differentiation from timepoint experiments. (A) Both ZBTB20 mRNA and protein increase as a function of neurogenic differentiation in the human hippocampus, though its mRNA most likely primes NSCs for expression in neuroblasts to fate the hippocampal pioneer cells and thus early born neurons in early embryonic stages. (B) Likewise, during during later embryonic stages, ZBTB20 mRNA and protein upregulate during differentiation, however, not to equivalent levels as during earlier stages. Furthermore, this change is accompanied by a switch in ZBTB20 function in that ZBTB20 plays a more active role in cell cycle regulation at the NSC stages. This suggests that ZBTB20 has a biphhasic nature during human embryonic hippocampogenesis in which it serves to fate NSCs derived from both the ammonic and dentate epithelia but after the outer shells of both the CA and DG have been established, switches to regulating cell cycle exit for progenitors derived only from the dentate epithelium.

demonstrated compelling integrin-signaling pathway changes by RNA-Seq. Repeating the laminin experiments at DIV 28 to investigate laminin 511 and CHIR dependent mechanisms by RNA-Seq would expand significantly which gene networks are responsible for maintaining neural stem cell identity via 511-activated integrin pathways. Furthermore, utilizing 511 laminin with a NOTCH agonist to compare against CHIR-dependent proliferation mechanisms would be enormous in deconvolving overlapping NOTCH/b-catenin signaling pathways in a human hippocampal development context. This may expand the utility of the model's embryonic-conserved nature

to further elucidate how the subgranular zone is molecularly specified in a suitable model of the embryonic dentate gyrus.

To more thoroughly investigate ZBTB20's temporally dynamic mechanisms, future experiments include ZBTB20 overexpression at both timepoints (DIV 50 and DIV 180) to understand if ZBTB20 gain-of-function has the opposite effect to the loss-of-function experiments. Additionally, starting viral experiments at DIV 15, the culture timepoint immediately following dual SMAD inhibition, and comparing over-expression or knockout of ZBTB20 to CHIR-treated cultures would provide more detailed insight into how ZBTB20 fates the hippocampus and if it acts independently from other transcription factors or molecular interactors. Incorporating RNA-Seq on viral experiments at all timepoints as well would demonstrate which ontological processes and functions ZBTB20 affects at different stages and would provide evidence for the molecular basis of ZBTB20's action. To expand on transcription-factor relevant mechanisms, DNA Methylation analysis/ATAC-Seq at all timepoints with viral vectors would reveal where in the chromatin ZBTB20 is responsible for inactivating at different steps of human embryonic hippocampogenesis. ATAC-Seq provides a powerful platform, especially in neurodevelopment, to probe chromatin states and accessible genes over developmental stages (Di Bella et al., 2021). As zinc finger families have ambivalent functions in contributing to the opening or closing of chromatin in a maturation-stage dependent manner (Cassandri et al., 2017), it would be imperative to understand if ZBTB20's mechanisms unilaterally inactivate specific chromatin sites or if it plays a bidirectional role in chromatin accessibility. Because of the expense related to ATAC-Seq however, and because ZBTB20 itself is not considered a direct chromatin remodeler (W. Zhang et al., 2001), it would be more beneficial to perform CHIP-Seq analysis of at least ZBTB20 but may include SATB2, and/or CTIP2 at different time points using viral vectors. This would assist to understand if compensatory, competition-dependent mechanisms take place at earlier timepoints in culture age in defining hippocampal fields. As the three transcription factors are in competition in rodent hippocampus (Nielsen et al., 2014), it would be a major benefit to understand promoter binding mechanisms at different timepoints to understand first if the three also compete to inhibit each other but also if ZBTB20 binds to SOX-family promoters (Nagao et al., 2016; Zhou et al., 2015) in the hippocampus as well.

The final experiment regarding ZBTB20's mechanism would characterize ZBTB20 appearance in conjunction with neuronal differentiation stage specific markers under previously published paradigms (Ge et al., 2008; Lugert et al., 2010; Ming & Song, 2011). This would most likely be performed in a controlled, short-term timepoint analysis by inducing maturation with DAPT and harvesting cells every 4-6 hours over the course of 2-3 days to correlate ZBTB20 expression levels with demarcated maturation stages. This could further be repeated with a transient overexpression of ZBTB20 to analyze by qRT-PCR genes under immediate control of ZBTB20.

Lastly, to expand on the functional and clinical relevance with regards to the chimeric model, several follow-up projects are able to be envisioned to probe physiological process integration of human hippocampal NSCs. Among these include support experiments utilizing electrophysiology on differentiated human neurons, whether by patch clamp techniques similar to those demonstrated in Section I and previously in hiPSC-derived cortical neurons (Y. Shi, Kirwan, Smith, et al., 2012), or by growing neurons directly onto MEA-enabled cell cultures (Obien et al., 2015), or by transplantation of optogenetically targeted neurons with multi-electrode in downstream, monosynaptic-affected targets *in vivo* i.e. stimulating in the dentate gyrus with blue light and recording post-synaptic potential changes in the CA3. Functionally characterizing either membrane potential or local field potential dynamics of terminally differentiated human hippocampal neurons is imperative to supporting that these cells are functional neurons and to transition into potential pre-clinical studies elaborated upon in the following paragraph.

The chimeric mouse hippocampal model suits three further projects to investigate human dentate gyrus neurons more accessibly in a physiological *in vivo* environment. The first project will assess whether transplanted cells functionally integrate into the host mouse hippocampal network. The experimental schematic presented in Figure 62 would be repeated with optogenetically targeted NSCs from both young and old progenitors. After approximately 3-4 months *in vivo*, cells would be exposed to blue light with a fiberoptic explant to stimulate human cells and local field potentials would be recorded the CA3. This would provide unparalleled insight to the capacity of functional synaptogenesis by these cells and would provide a robust

foundation for the following projects, which are more "distant future." The second project would investigate age-related learning model *in vivo* with chimeric dentate gyrus to demonstrate neurogenic capacity and its relevance to memory consolidation. Learning and memory declines in the aging hippocampus in tandem with declining neurogenesis capacity (Berdugo-Vega et al., 2020; Kempermann et al., 2002; Lester et al., 2017; Wilson et al., 2004). Restoration of learning and memory retention has been demonstrated previously (Villeda et al., 2014) but in transplanting hematopoietic stem cells into the dentate gyrus. Transplanting DG-specific hippocampal cells, and from differently aged culture groups, would provide insight into whether this effect is cell autonomous or dictated by the wider "aging molecular environment" (Baumgart et al., 2014) of the aged mammalian hippocampus. The follow-up experimental design would reincorporate Zbtb20 as the paradigmatic focus, utilizing the conditional Zbtb20-KO mouse utilized to demonstrate Zbtb20's function in CA1-dependent learning (Ren et al., 2012). Zbtb20-KO mouse would be assessed for neurogenic capacity like EdU incorporation, PCNA/Ki67/Dcx staining, or low-titer virus injection. This would be accompanied by behavioral assessment to first understand the relationship between working memory and altered neurogenesis, but to further investigate if ZBTB20-KO-mediated memory impairment is rescued by transplantation of wild-type human DG neurons *in vivo*.

The third *in vivo* chimeric project would be a preclinical study in rescuing behavioral deficits and neurodegenerative pathophysiology in an Alzheimer's disease mouse model. Alzheimer's disease is hallmarked by neurofibrillary tangles comprised of ectopic TAU (Regalado-Reyes et al., 2019) and amyloid-beta (Mucke et al., 2000), decreased neurogenic capacity (Hu et al., 2013), and detrimental changes to learning and social behavior (Atwood & Bowen, 2015). TAU has been linked to driving premature exit from symmetrical neurogenesis (Criado-Marrero et al., 2020; Llorens-Martin et al., 2012; Pallas-Bazarra et al., 2016) whereas optogenetic stimulation of the dentate gyrus has alleviated memory impairment in an Alzheimer's disease mouse model (Perusini et al., 2017). Despite optogenetic progress in alleviating human neurological disorders (Sahel et al., 2021), the hippocampus presents some complications for long-term optogenetic therapy due to its medial ventral location. Instead the field of Parkinson's disease has seen improved human patient motor-

defecits after dopaminergic striatum-fated NSC transplantation (Lindvall et al., 1990). These studies persist and have demonstrated that patient-derived iPSCs offer a feasible and ethical route forward in treating neurodegenerations. This dentate gyrus model could potentially be used in a similar schematic (Fjodorova & Li, 2018) wherein a preclinical study utilizing Alzheimer's disease rodent models are xenografted with hiPSC-derived DG cells using this protocol and assessed for learning and behavioral improvements with the ultimate goal to transition to human clinical therapy for a wider spectrum of cognitive impairment.

These perspectives are just a handful of examples and avenues that may further explored with this hippocampus model. The advantageous scope of this model boasts many opportunities to ethically and accessibly explore different facets of the hippocampus. Furthermore, future incorporations for this model may provide a beneficial route as a treatment for cognition decline-related neurodegenerations.

Conclusion

For the past 40 years, stem cell models have provided crucial insight into molecular development regarding their derivative species. In this thesis, I proffer a modest addition to the current knowledge of stem cell integration within the field of neuroscience. I have demonstrated that mouse ESC-derived neurons behave physiologically when transduced with optogenetic constructs, opening an entire avenue to reliably study activity-dependent molecular pathways in specific regions or under inhibitive conditions. Simultaneously, this brought a novel device for photobiological applications which demonstrates higher degrees of control and adaptability for light-based experimental paradigms. I further demonstrated the human iPSCs provide an unparalleled starting point for differentiating hippocampal identity neural stem cells and further elucidated that laminin is a key component in maintaining neural stemness over the course of almost a full year. Using this aspect of laminar stem sustainment, I was able to investigate preliminary aspects of ZBTB20 behavior in a wild-type human context in that its tangent to the human hippocampal neuronal differentiation axis seems to be downstream of NOTCH inhibition and conserved from rodents. These hippocampal neural precursors could be further xenografted into 3-month-old wild-type mouse hippocampus and integrate into the existing hippocampal architecture, regardless of time spent proliferating *in vitro*. Speculatively, the chimeric model could offer novel insights into sustained neurogenesis by *ex vivo* niche expansion, physiology of memory in youth and aging given my results from OPAL multiplexed with human neurons, or even as a potential stem-cell based therapy approaches in pre-clinical cognitive pathology models. To conclude, my models thus far have provided substantial answers regarding molecular maintenance of the subgranular niche, the potential facets of ZBTB20's role in hippocampal neurogenesis, and the neurogenic nature of hippocampal neural stem cells while simultaneously creating daunting yet exhilarating scientific opportunities for the future.

References

Abdelmalik, P. A., Burnham, W. M. I., & Carlen, P. L. (2005). Increased seizure susceptibility of the hippocampus compared with the neocortex of the immature mouse brain in vitro. *Epilepsia*, *46*(3), 356–366. https://doi.org/10.1111/j.0013-9580.2005.34204.x

Abellán, A., Desfilis, E., & Medina, L. (2014). Combinatorial expression of Lef1, Lhx2, Lhx5, Lhx9, Lmo3, Lmo4, and Prox1 helps to identify comparable subdivisions in the developing hippocampal formation of mouse and chicken. *Frontiers in Neuroanatomy*, *8*(JULY), 1–22. https://doi.org/10.3389/fnana.2014.00059

Åberg, M. A. I., Åberg, N. D., Hedbäcker, H., Oscarsson, J., & Eriksson, P. S. (2000). Peripheral infusion of IGF-I selectively induces neurogenesis in the adult rat hippocampus. *Journal of Neuroscience*, *20*(8), 2896–2903. https://doi.org/10.1523/jneurosci.20-08-02896.2000

Adamson, M. C., Dennis, C., Delaney, S., Christiansen, J., Monkley, S., Kozak, C. A., & Wainwright, B. (1994). Isolation and Genetic Mapping of Two Novel Members of the Murine Wnt Gene Family, Wnt11 and Wnt12, and the Mapping of Wnt5a and Wnt7a. *Genomics*, *24*(1), 9–13. https://doi.org/10.1006/geno.1994.1575

Adlaf, E. W., Vaden, R. J., Niver, A. J., Manuel, A. F., Onyilo, V. C., Araujo, M. T., Dieni, C. V., Vo, H. T., King, G. D., Wadiche, J. I., & Overstreet-Wadiche, L. (2017). Adult-born neurons modify excitatory synaptic transmission to existing neurons. *ELife*, *6*, 1–25. https://doi.org/10.7554/eLife.19886

Ahmed, S., Gan, H. T., Chen, S. L., Poonepalli, A., Ramasamy, S., Tay, Y., Tham, M., & Yuan, H. Y. (2009). Transcription factors and neural stem cell self-renewal, growth and differentiation. *Cell Adhesion and Migration*, *3*(4), 412–424. https://doi.org/10.4161/cam.3.4.8803

Ahn, Sandra, Kim, T. G., Kim, K. S., & Chung, S. (2016). Differentiation of human pluripotent stem cells into Medial Ganglionic Eminence vs. Caudal Ganglionic Eminence cells. *Methods*, *101*, 103–112.

https://doi.org/10.1016/j.ymeth.2015.09.009

Ahn, Sohyun, & Joyner, A. L. (2005). In vivo analysis of quiescent adult neural stem cells responding to Sonic hedgehog. *Nature*, *437*(7060), 894–897. https://doi.org/10.1038/nature03994

Alam, M. J., Kitamura, T., Saitoh, Y., Ohkawa, N., Kondo, T., & Inokuchi, K. (2018). Adult neurogenesis conserves hippocampal memory capacity. *Journal of Neuroscience*, *38*(31), 6854–6863. https://doi.org/10.1523/JNEUROSCI.2976-17.2018

Alby, C., Boutaud, L., Bessières, B., Serre, V., Rio, M., Cormier-Daire, V., de Oliveira, J., Ichkou, A., Mouthon, L., Gordon, C. T., Bonnière, M., Mechler, C., Nitschke, P., Bole, C., Lyonnet, S., Bahi-Buisson, N., Boddaert, N., Colleaux, L., Roth, P., … Thomas, S. (2018). Novel de novo ZBTB20 mutations in three cases with Primrose syndrome and constant corpus callosum anomalies. *American Journal of Medical Genetics, Part A*, *176*(5), 1091–1098. https://doi.org/10.1002/ajmg.a.38684

Alenina, N., Bashammakh, S., & Bader, M. (2006). Specification and differentiation of serotonergic neurons. *Stem Cell Reviews*, *2*(1), 5–10. https://doi.org/10.1385/SCR:2:1:5

Alfonsa, H., Merricks, E. M., Codadu, N. K., Cunningham, M. O., Deisseroth, K., Racca, C., & Trevelyan, A. J. (2015). The Contribution of Raised Intraneuronal Chloride to Epileptic Network Activity. *Journal of Neuroscience*, *35*(20), 7715–7726. https://doi.org/10.1523/jneurosci.4105-14.2015

Altman, J. (1962). Are new neurons formed in the brains of adult mammals? *Science*, *135*(3509), 1127–1128. https://doi.org/10.1126/science.135.3509.1127

Altman, J., & Bayer, S. A. (1990a). Migration and distribution of two populations of hippocampal granule cell precursors during the perinatal and postnatal periods. *Journal of Comparative Neurology*, *301*(3), 365–381. https://doi.org/10.1002/cne.903010304

Altman, J., & Bayer, S. A. (1990b). Prolonged sojourn of developing pyramidal cells in the intermediate zone of the hippocampus and their settling in the stratum pyramidale. *Journal of Comparative*

Neurology, *301*(3), 343–364. https://doi.org/10.1002/cne.903010303

Altman, J., & Bayer, S. A. (1990c). Mosaic organization of the hippocampal neuroepithelium and the multiple germinal sources of dentate granule cells. *The Journal of Comparative Neurology*, *301*(3), 325–342. https://doi.org/10.1002/cne.903010302

Altman, J., & Das, G. D. (1965). Post-natal origin of microneurones in the rat brain. *Nature*, *207*(5000), 953–956. https://doi.org/10.1038/207953a0

Altman, J., & Das, G. D. (1969). Autoradiographic and histological studies of postnatal neurogenesis. IV. Cell proliferation and migration in the anterior forebrain, with special reference to persisting neurogenesis in the olfactory bulb. *The Journal of Comparative Neurology*, *137*(4), 433–457. https://doi.org/10.1002/cne.901370404

Alvarez-Buylla, A., & Nottebohm, F. (1988). Migration of young neurons in adult avian brain. In *Nature* (Vol. 335, Issue 6188, pp. 353–354). https://doi.org/10.1038/335353a0

Amaral, D. G., Scharfman, H. E., & Lavenex, P. (2007). The dentate gyrus: fundamental neuroanatomical organization (dentate gyrus for dummies). *Progress in Brain Research*, *163*, 3–22. https://doi.org/10.1016/S0079-6123(07)63001-5

Ambrogini, P., Lattanzi, D., Ciuffoli, S., Agostini, D., Bertini, L., Stocchi, V., Santi, S., & Cuppini, R. (2004). Morpho-functional characterization of neuronal cells at different stages of maturation in granule cell layer of adult rat dentate gyrus. *Brain Research*, *1017*(1–2), 21–31. https://doi.org/10.1016/j.brainres.2004.05.039

Amiri, A., Coppola, G., Scuderi, S., Wu, F., Roychowdhury, T., Liu, F., Pochareddy, S., Shin, Y., Safi, A., Song, L., Zhu, Y., Sousa, A. M. M., Gerstein, M., Crawford, G. E., Sestan, N., Abyzov, A., & Vaccarino, F. M. (2018). Transcriptome and epigenome landscape of human cortical development modeled in organoids. *Science*, *362*(6420). https://doi.org/10.1126/science.aat6720

Andersen, P., & Lømo, T. (1967). Control of Hippocampal Output by Afferent Volley Frequency. *Progress*

in Brain Research, *27*(C), 400–412. https://doi.org/10.1016/S0079-6123(08)63112-X

Andorfer, C., Kress, Y., Espinoza, M., De Silva, R., Tucker, K. L., Barde, Y. A., Duff, K., & Davies, P. (2003). Hyperphosphorylation and aggregation of tau in mice expressing normal human tau isoforms. *Journal of Neurochemistry*, *86*(3), 582–590. https://doi.org/10.1046/j.1471-4159.2003.01879.x

Andrews-Zwilling, Y., Bien-Ly, N., Xu, Q., Li, G., Bernardo, A., Yoon, S. Y., Zwilling, D., Yan, T. X., Chen, L., & Huang, Y. (2010). Apolipoprotein E4 causes age- and Tau-dependent impairment of GABAergic interneurons, leading to learning and memory deficits in mice. *Journal of Neuroscience*, *30*(41), 13707–13717. https://doi.org/10.1523/JNEUROSCI.4040-10.2010

Angevine, J. B. (1965). Time of neuron origin in the hippocampal region. An autoradiographic study in the mouse. *Experimental Neurology*, *11*(SUPPL.), Suppl 2:1-70. https://doi.org/10.1016/0014-4886(65)90121-4

Antinucci, P., Dumitrescu, A. S., Deleuze, C., Morley, H. J., Leung, K., Hagley, T., Kubo, F., Baier, H., Bianco, I. H., & Wyart, C. (2020). A calibrated optogenetic toolbox of stable zebrafish opsin lines. *BioRxiv*, *9*, 2020.01.13.904185. https://doi.org/10.1101/2020.01.13.904185

Aravanis, A. M., Wang, L. P., Zhang, F., Meltzer, L. A., Mogri, M. Z., Schneider, M. B., & Deisseroth, K. (2007). An optical neural interface: in vivo control of rodent motor cortex with integrated fiberoptic and optogenetic technology. *Journal of Neural Engineering*, *4*(3). https://doi.org/10.1088/1741-2560/4/3/S02

Arber, C., Precious, S. V., Cambray, S., Risner-Janiczek, J. R., Kelly, C., Noakes, Z., Fjodorova, M., Heuer, A., Ungless, M. A., Rodriguez, T. A., Rosser, A. E., Dunnett, S. B., & Li, M. (2015). Activin A directs striatal projection neuron differentiation of human pluripotent stem cells. *Development*, *142*(7), 1375–1386. https://doi.org/10.1242/dev.117093

Ardhanareeswaran, K., Mariani, J., Coppola, G., Abyzov, A., & Vaccarino, F. M. (2017). Human induced pluripotent stem cells for modelling neurodevelopmental disorders. *Nature Reviews Neurology*,

13(5), 265–278. https://doi.org/10.1038/nrneurol.2017.45

Arheden, K., Mandahl, N., Strömbeck, B., Isaksson, M., & Mitelman, F. (1988). Chromosome localization of the human oncogene int1 to 12q13 by in situ hybridization. *Cytogenetic and Genome Research*, *47*(1–2), 86–87. https://doi.org/10.1159/000132513

Arlotta, P., Molyneaux, B. J., Jabaudon, D., Yoshida, Y., & Macklis, J. D. (2008). Ctip2 controls the differentiation of medium spiny neurons and the establishment of the cellular architecture of the striatum. *Journal of Neuroscience*, *28*(3), 622–632. https://doi.org/10.1523/JNEUROSCI.2986-07.2008

Arredondo, S. B., Guerrero, F. G., Herrera-Soto, A., Jensen-Flores, J., Bustamante, D. B., Oñate-Ponce, A., Henny, P., Varas-Godoy, M., Inestrosa, N. C., & Varela-Nallar, L. (2020). Wnt5a promotes differentiation and development of adult-born neurons in the hippocampus by noncanonical Wnt signaling. In *Stem Cells* (Vol. 38, Issue 3, pp. 422–436). https://doi.org/10.1002/stem.3121

Asrican, B., Wooten, J., Li, Y. D., Quintanilla, L., Zhang, F., Wander, C., Bao, H., Yeh, C. Y., Luo, Y. J., Olsen, R., Lim, S. A., Hu, J., Jin, P., & Song, J. (2020). Neuropeptides Modulate Local Astrocytes to Regulate Adult Hippocampal Neural Stem Cells. *Neuron*, *108*(2), 349-366.e6. https://doi.org/10.1016/j.neuron.2020.07.039

Atwood, C. S., & Bowen, R. L. (2015). A Unified Hypothesis of Early- and Late-Onset Alzheimer's Disease Pathogenesis. *Journal of Alzheimer's Disease*, *47*(1), 33–47. https://doi.org/10.3233/JAD-143210

Aulicino, F., Pedone, E., Sottile, F., Lluis, F., Marucci, L., & Cosma, M. P. (2020). Canonical Wnt Pathway Controls mESC Self-Renewal Through Inhibition of Spontaneous Differentiation via β-Catenin/TCF/LEF Functions. In *Stem Cell Reports* (Vol. 15, Issue 3, pp. 646–661). https://doi.org/10.1016/j.stemcr.2020.07.019

Avilion, A. A., Nicolis, S. K., Pevny, L. H., Perez, L., Vivian, N., & Lovell-Badge, R. (2003). Multipotent cell lineages in early mouse development depend on SOX2 function. *Genes and Development*, *17*(1),

126–140. https://doi.org/10.1101/gad.224503

Baker, B. M., & Chen, C. S. (2012). Deconstructing the third dimension-how 3D culture microenvironments alter cellular cues. *Journal of Cell Science*, *125*(13), 3015–3024. https://doi.org/10.1242/jcs.079509

Bardy, C., Van Den Hurk, M., Kakaradov, B., Erwin, J. A., Jaeger, B. N., Hernandez, R. V., Eames, T., Paucar, A. A., Gorris, M., Marchand, C., Jappelli, R., Barron, J., Bryant, A. K., Kellogg, M., Lasken, R. S., Rutten, B. P. F., Steinbusch, H. W. M., Yeo, G. W., & Gage, F. H. (2016). Predicting the functional states of human iPSC-derived neurons with single-cell RNA-seq and electrophysiology. *Molecular Psychiatry*, *21*(11), 1573–1588. https://doi.org/10.1038/mp.2016.158

Barry, G., Piper, M., Lindwall, C., Moldrich, R., Mason, S., Little, E., Sarkar, A., Tole, S., Gronostajski, R. M., & Richardse, L. J. (2008). Specific glial populations regulate hippocampal morphogenesis. *Journal of Neuroscience*, *28*(47), 12328–12340. https://doi.org/10.1523/JNEUROSCI.4000-08.2008

Barth, L., Sütterlin, R., Nenniger, M., & Vogt, K. E. (2014). Functional differentiation of stem cell-derived neurons from different murine backgrounds. *Frontiers in Cellular Neuroscience*, *8*(FEB), 1–7. https://doi.org/10.3389/fncel.2014.00049

Batabyal, S., Cervenka, G., Ha, J. H., Kim, Y. T., Mohanty, S., & Davies, W. I. L. (2015). Broad-band activatable white-opsin. *PLoS ONE*, *10*(9), 1–13. https://doi.org/10.1371/journal.pone.0136958

Baumgart, M., Groth, M., Priebe, S., Savino, A., Testa, G., Dix, A., Ripa, R., Spallotta, F., Gaetano, C., Ori, M., Terzibasi Tozzini, E., Guthke, R., Platzer, M., & Cellerino, A. (2014). RNA-seq of the aging brain in the short-lived fish N. furzeri - conserved pathways and novel genes associated with neurogenesis. *Aging Cell*, *13*(6), 965–974. https://doi.org/10.1111/acel.12257

Bayer, S. A. (1980a). Development of the hippocampal region in the rat I. Neurogenesis examined with 3H-thymidine autoradiography. In *Journal of Comparative Neurology* (Vol. 190, Issue 1, pp. 87–114). https://doi.org/10.1002/cne.901900107

Bayer, S. A. (1980b). Development of the hippocampal region in the rat II. Morphogenesis during embryonic and early postnatal life. *Journal of Comparative Neurology*, *190*(1), 115–134. https://doi.org/10.1002/cne.901900108

Beevers, J. E., Lai, M. C., Collins, E., Booth, H. D. E., Zambon, F., Parkkinen, L., Vowles, J., Cowley, S. A., Wade-Martins, R., & Caffrey, T. M. (2017). MAPT Genetic Variation and Neuronal Maturity Alter Isoform Expression Affecting Axonal Transport in iPSC-Derived Dopamine Neurons. *Stem Cell Reports*, *9*(2), 587–599. https://doi.org/10.1016/j.stemcr.2017.06.005

Ben Abdallah, N. M. B., Slomianka, L., Vyssotski, A. L., & Lipp, H. P. (2010). Early age-related changes in adult hippocampal neurogenesis in C57 mice. *Neurobiology of Aging*, *31*(1), 151–161. https://doi.org/10.1016/j.neurobiolaging.2008.03.002

Berdugo-Vega, G., Arias-Gil, G., López-Fernández, A., Artegiani, B., Wasielewska, J. M., Lee, C.-C., Lippert, M. T., Kempermann, G., Takagaki, K., & Calegari, F. (2020). Increasing neurogenesis refines hippocampal activity rejuvenating navigational learning strategies and contextual memory throughout life. *Nature Communications*, *11*(1), 135. https://doi.org/10.1038/s41467-019-14026-z

Berg, D. A., Su, Y., Jimenez-Cyrus, D., Patel, A., Huang, N., Morizet, D., Lee, S., Shah, R., Ringeling, F. R., Jain, R., Epstein, J. A., Wu, Q. F., Canzar, S., Ming, G. L., Song, H., & Bond, A. M. (2019). A Common Embryonic Origin of Stem Cells Drives Developmental and Adult Neurogenesis. *Cell*, *177*(3), 654-668.e15. https://doi.org/10.1016/j.cell.2019.02.010

Bergami, M., Masserdotti, G., Temprana, S. G., Motori, E., Eriksson, T. M., Göbel, J., Yang, S. M., Conzelmann, K. K., Schinder, A. F., Götz, M., & Berninger, B. (2015). A Critical Period for Experience-Dependent Remodeling of Adult-Born Neuron Connectivity. *Neuron*, *85*(4), 710–717. https://doi.org/10.1016/j.neuron.2015.01.001

Bergstein, I., Eisenberg, L. M., Bhalerao, J., Jenkins, N. A., Copeland, N. G., Osborne, M. P., Bowcock, A. M., & Brown, A. M. C. (1997). Isolation of two novel WNT genes, WNT14 and WNT15, one of which

(WNT15) is closely linked to WNT3 on human chromosome 17q21. *Genomics*, *46*(3), 450–458. https://doi.org/10.1006/geno.1997.5041

Bergström, P., Agholme, L., Nazir, F. H., Satir, T. M., Toombs, J., Wellington, H., Strandberg, J., Bontell, T. O., Kvartsberg, H., Holmström, M., Boreström, C., Simonsson, S., Kunath, T., Lindahl, A., Blennow, K., Hanse, E., Portelius, E., Wray, S., & Zetterberg, H. (2016). Amyloid precursor protein expression and processing are differentially regulated during cortical neuron differentiation. *Scientific Reports*, *6*(1), 29200. https://doi.org/10.1038/srep29200

Berndt, A., Schoenenberger, P., Mattis, J., Tye, K. M., Deisseroth, K., Hegemann, P., & Oertner, T. G. (2011). High-efficiency channelrhodopsins for fast neuronal stimulation at low light levels. *Proceedings of the National Academy of Sciences of the United States of America*, *108*(18), 7595–7600. https://doi.org/10.1073/pnas.1017210108

Bertacchi, M., Lupo, G., Pandolfini, L., Casarosa, S., D'Onofrio, M., Pedersen, R. A., Harris, W. A., & Cremisi, F. (2015). Activin/nodal signaling supports retinal progenitor specification in a narrow time window during pluripotent stem cell neuralization. *Stem Cell Reports*, *5*(4), 532–545. https://doi.org/10.1016/j.stemcr.2015.08.011

Bertacchi, M., Pandolfini, L., D'Onofrio, M., Brandi, R., & Cremisi, F. (2015). The double inhibition of endogenously produced bmp and wnt factors synergistically triggers dorsal telencephalic differentiation of mouse es cells. *Developmental Neurobiology*, *75*(1), 66–79. https://doi.org/10.1002/dneu.22209

Bertacchi, M., Pandolfini, L., Murenu, E., Viegi, A., Capsoni, S., Cellerino, A., Messina, A., Casarosa, S., & Cremisi, F. (2013). The positional identity of mouse ES cell-generated neurons is affected by BMP signaling. *Cellular and Molecular Life Sciences*, *70*(6), 1095–1111. https://doi.org/10.1007/s00018-012-1182-3

Beukelaers, P., Vandenbosch, R., Caron, N., Nguyen, L., Belachew, S., Moonen, G., Kiyokawa, H.,

Barbacid, M., Santamaria, D., & Malgrange, B. (2011). Cdk6-dependent regulation of G1 length controls adult neurogenesis. *Stem Cells*, *29*(4), 713–724. https://doi.org/10.1002/stem.616

Bi, A., Cui, J., Ma, Y.-P. P., Olshevskaya, E., Pu, M., Dizhoor, A. M., & Pan, Z.-H. H. (2006). Ectopic Expression of a Microbial-Type Rhodopsin Restores Visual Responses in Mice with Photoreceptor Degeneration. *Neuron*, *50*(1), 23–33. https://doi.org/10.1016/j.neuron.2006.02.026

Bieszke, J. A., Braun, E. L., Bean, L. E., Kang, S., Natvig, D. O., & Borkovich, K. A. (1999). The nop-1 gene of Neurospora crassa encodes a seven transmembrane helix retinal-binding protein homologous to archaeal rhodopsins. *Proceedings of the National Academy of Sciences of the United States of America*, *96*(14), 8034–8039. https://doi.org/10.1073/pnas.96.14.8034

Bonaguidi, M. A., Wheeler, M. A., Shapiro, J. S., Stadel, R. P., Sun, G. J., Ming, G. L., & Song, H. (2011). In vivo clonal analysis reveals self-renewing and multipotent adult neural stem cell characteristics. *Cell*, *145*(7), 1142–1155. https://doi.org/10.1016/j.cell.2011.05.024

Bone, H. K., Damiano, T., Bartlett, S., Perry, A., Letchford, J., Ripoll, Y. S., Nelson, A. S., & Welham, M. J. (2009). Involvement of GSK-3 in Regulation of Murine Embryonic Stem Cell Self-Renewal Revealed by a Series of Bisindolylmaleimides. *Chemistry and Biology*, *16*(1), 15–27. https://doi.org/10.1016/j.chembiol.2008.11.003

Botcher, N. A., Falck, J. E., Thomson, A. M., & Mercer, A. (2014). Distribution of interneurons in the CA2 region of the rat hippocampus. *Frontiers in Neuroanatomy*, *8*(SEP), 1–16. https://doi.org/10.3389/fnana.2014.00104

Bouillet, P., Oulad-Abdelghani, M., Ward, S. J., Bronner, S., Chambon, P., & Dollé, P. (1996). A new mouse member of the Wnt gene family, mWnt-8, is expressed during early embryogenesis and is ectopically induced by retinoic acid. *Mechanisms of Development*, *58*(1–2), 141–152. https://doi.org/10.1016/S0925-4773(96)00569-2

Boyden, E. S., Zhang, F., Bamberg, E., Nagel, G., & Deisseroth, K. (2005). Millisecond-timescale,

genetically targeted optical control of neural activity. *Nature Neuroscience*, *8*(9), 1263–1268. https://doi.org/10.1038/nn1525

Brack, A. S., Conboy, M. J., Roy, S., Lee, M., Kuo, C. J., Keller, C., & Rando, T. A. (2007). Increased Wnt Signaling During Aging Alters Muscle Stem Cell Fate and Increases Fibrosis. *Science*, *317*(5839), 807–810. https://doi.org/10.1126/science.1144090

Brandt, M. D., Jessberger, S., Steiner, B., Kronenberg, G., Reuter, K., Bick-Sander, A., Von Der Behrens, W., & Kempermann, G. (2003). Transient calretinin expression defines early postmitotic step of neuronal differentiation in adult hippocampal neurogenesis of mice. *Molecular and Cellular Neuroscience*, *24*(3), 603–613. https://doi.org/10.1016/S1044-7431(03)00207-0

Brennand, K. J., Simone, A., Jou, J., Gelboin-Burkhart, C., Tran, N., Sangar, S., Li, Y., Mu, Y., Chen, G., Yu, D., McCarthy, S., Sebat, J., & Gage, F. H. (2011). Modelling schizophrenia using human induced pluripotent stem cells. *Nature*, *473*(7346), 221–225. https://doi.org/10.1038/nature09915

Breunig, J. J., Sarkisian, M. R., Arellano, J. I., Morozov, Y. M., Ayoub, A. E., Sojitra, S., Wang, B., Flavell, R. A., Rakic, P., & Town, T. (2008). Primary cilia regulate hippocampal neurogenesis by mediating sonic hedgehog signaling. *Proceedings of the National Academy of Sciences of the United States of America*, *105*(35), 13127–13132. https://doi.org/10.1073/pnas.0804558105

Brewer, G. J. (1997). Isolation and culture of adult rat hippocampal neurons. *Journal of Neuroscience Methods*, *71*(2), 143–155. https://doi.org/10.1016/S0165-0270(96)00136-7

Brion, J. -P, Smith, C., Couck, A. -M, Gallo, J. -M, & Anderton, B. H. (1993). Developmental Changes in τ Phosphorylation: Fetal τ Is Transiently Phosphorylated in a Manner Similar to Paired Helical Filament-τ Characteristic of Alzheimer's Disease. *Journal of Neurochemistry*, *61*(6), 2071–2080. https://doi.org/10.1111/j.1471-4159.1993.tb07444.x

Bruel-Jungerman, E., Davis, S., Rampon, C., & Laroche, S. (2006). Long-term potentiation enhances neurogenesis in the adult dentate gyrus. *Journal of Neuroscience*, *26*(22), 5888–5893.

https://doi.org/10.1523/JNEUROSCI.0782-06.2006

Bui, T. D., Rankin, J., Smith, K., Huguet, E. L., Ruben, S., Strachan, T., Harris, A. L., & Lindsay, S. (1997). A novel human Wnt gene, WNT10B, maps to 12q13 and is expressed in human breast carcinomas. *Oncogene*, *14*(10), 1249–1253. https://doi.org/10.1038/sj.onc.1200936

Cadigan, K. M., & Nusse, R. (1996). wingless signaling in the Drosophila eye and embryonic epidermis. *Development*, *122*(9), 2801–2812. https://doi.org/10.1242/dev.122.9.2801

Cai, C., & Grabel, L. (2007). Directing the differentiation of embryonic stem cells to neural stem cells. *Developmental Dynamics*, *236*(12), 3255–3266. https://doi.org/10.1002/dvdy.21306

Cajal, S. R. y. (1930). Degeneration and Regeneration of the Nervous System. *Nature*, *125*(3146), 230–231. https://doi.org/10.1038/125230a0

Camp, J. G., Badsha, F., Florio, M., Kanton, S., Gerber, T., Wilsch-Bräuninger, M., Lewitus, E., Sykes, A., Hevers, W., Lancaster, M., Knoblich, J. A., Lachmann, R., Pääbo, S., Huttner, W. B., & Treutlein, B. (2015). Human cerebral organoids recapitulate gene expression programs of fetal neocortex development. *Proceedings of the National Academy of Sciences*, *112*(51), 201520760. https://doi.org/10.1073/pnas.1520760112

Cao, L., Jiao, X., Zuzga, D. S., Liu, Y., Fong, D. M., Young, D., & During, M. J. (2004). VEGF links hippocampal activity with neurogenesis, learning and memory. *Nature Genetics*, *36*(8), 827–835. https://doi.org/10.1038/ng1395

Cassandri, M., Smirnov, A., Novelli, F., Pitolli, C., Agostini, M., Malewicz, M., Melino, G., & Raschellà, G. (2017). Zinc-finger proteins in health and disease. *Cell Death Discovery*, *3*(1). https://doi.org/10.1038/cddiscovery.2017.71

Cembrowski, M. S., Bachman, J. L., Wang, L., Sugino, K., Shields, B. C., & Spruston, N. (2016). Spatial Gene-Expression Gradients Underlie Prominent Heterogeneity of CA1 Pyramidal Neurons. *Neuron*, *89*(2), 351–368. https://doi.org/10.1016/j.neuron.2015.12.013

Cembrowski, M. S., Wang, L., Sugino, K., Shields, B. C., & Spruston, N. (2016). Hipposeq: A comprehensive RNA-seq database of gene expression in hippocampal principal neurons. *ELife*, *5*(APRIL2016), 1–22. https://doi.org/10.7554/eLife.14997

Chambers, I. (2005). Mechanisms and factors in embryonic stem cell self-renewal. *ATTI Della Accademia Nazionale Dei Lincei Rendiconti Lincei Scienze Fisiche E Naturali*, *16*(2), 83–97. https://doi.org/10.1007/BF02904758

Chan, S. K., Kitajima-Ihara, T., Fujii, R., Gotoh, T., Murakami, M., Ihara, K., & Kouyama, T. (2014). Crystal structure of cruxrhodopsin-3 from haloarcula vallismortis. *PLoS ONE*, *9*(9). https://doi.org/10.1371/journal.pone.0108362

Cheffer, A., Flitsch, L. J., Krutenko, T., Röderer, P., Sokhranyaeva, L., Iefremova, V., Hajo, M., Peitz, M., Schwarz, M. K., & Brüstle, O. (2020). Human stem cell-based models for studying autism spectrum disorder-related neuronal dysfunction. *Molecular Autism*, *11*(1), 1–23. https://doi.org/10.1186/s13229-020-00383-w

Chen, F., Kook, H., Milewski, R., Gitler, A. D., Lu, M. M., Li, J., Nazarian, R., Schnepp, R., Jen, K., Biben, C., Runke, G., Mackay, J. P., Novotny, J., Schwartz, R. J., Harvey, R. P., Mullins, M. C., & Epstein, J. A. (2002). Hop is an unusual homeobox gene that modulates cardiac development. *Cell*, *110*(6), 713–723. https://doi.org/10.1016/S0092-8674(02)00932-7

Chen, I. W., Ronzitti, E., Lee, B. R., Daigle, T. L., Dalkara, D., Zeng, H., Emiliani, V., & Papagiakoumou, E. (2019). In Vivo submillisecond two-photon optogenetics with temporally focused patterned light. *Journal of Neuroscience*, *39*(18), 3484–3497. https://doi.org/10.1523/JNEUROSCI.1785-18.2018

Chen, R., & Chung, S. H. (2014). Mechanism of tetrodotoxin block and resistance in sodium channels. *Biochemical and Biophysical Research Communications*, *446*(1), 370–374. https://doi.org/10.1016/j.bbrc.2014.02.115

Cheong, S. K., Strazzeri, J. M., Williams, D. R., & Merigan, W. H. (2018). All-optical recording and

stimulation of retinal neurons in vivo in retinal degeneration mice. *PLoS ONE*, 1–20.

Chesnokova, V., Pechnick, R. N., & Wawrowsky, K. (2016). Chronic peripheral inflammation, hippocampal neurogenesis, and behavior. *Brain, Behavior, and Immunity*, *58*, 1–8. https://doi.org/10.1016/j.bbi.2016.01.017

Chin, M. H., Mason, M. J., Xie, W., Volinia, S., Singer, M., Peterson, C., Ambartsumyan, G., Aimiuwu, O., Richter, L., Zhang, J., Khvorostov, I., Ott, V., Grunstein, M., Lavon, N., Benvenisty, N., Croce, C. M., Clark, A. T., Baxter, T., Pyle, A. D., … Lowry, W. E. (2009). Induced Pluripotent Stem Cells and Embryonic Stem Cells Are Distinguished by Gene Expression Signatures. *Cell Stem Cell*, *5*(1), 111–123. https://doi.org/10.1016/j.stem.2009.06.008

Chin, M. H., Pellegrini, M., Plath, K., & Lowry, W. E. (2010). Molecular analyses of human induced pluripotent stem cells and embryonic stem cells. *Cell Stem Cell*, *7*(2), 263–269. https://doi.org/10.1016/j.stem.2010.06.019

Choi, J., Lee, S., Mallard, W., Clement, K., Tagliazucchi, G. M., Lim, H., Choi, I. Y., Ferrari, F., Tsankov, A. M., Pop, R., Lee, G., Rinn, J. L., Meissner, A., Park, P. J., & Hochedlinger, K. (2015). A comparison of genetically matched cell lines reveals the equivalence of human iPSCs and ESCs. *Nature Biotechnology*, *33*(11), 1173–1181. https://doi.org/10.1038/nbt.3388

Choi, S. H., Kim, Y. H., Quinti, L., Tanzi, R. E., & Kim, D. Y. (2016). 3D culture models of Alzheimer's disease: a road map to a "cure-in-a-dish." *Molecular Neurodegeneration*, *11*(1), 75. https://doi.org/10.1186/s13024-016-0139-7

Chow, B. Y., Han, X., Dobry, A. S., Qian, X., Chuong, A. S., Li, M., Henninger, M. A., Belfort, G. M., Lin, Y., Monahan, P. E., & Boyden, E. S. (2010). High-performance genetically targetable optical neural silencing by light-driven proton pumps. *Nature*, *463*(7277), 98–102. https://doi.org/10.1038/nature08652

Clark, C. C., Cohen, I., Eichstetter, I., Cannizzaro, L. A., McPherson, J. D., Wasmuth, J. J., & Iozzo, R. V.

(1993). Molecular Cloning of the Human Proto-oncogene Wnt-5A and Mapping of the Gene (WNT5A) to Chromosome 3p14-p21. *Genomics*, *18*(2), 249–260. https://doi.org/10.1006/geno.1993.1463

Clarke, L., & Van Der Kooy, D. (2011). The adult mouse dentate gyrus contains populations of committed progenitor cells that are distinct from subependymal zone neural stem cells. *Stem Cells*, *29*(9), 1448–1458. https://doi.org/10.1002/stem.692

Clements, I. P., Millard, D. C., Nicolini, A. M., Preyer, A. J., Grier, R., Heckerling, A., Blum, R. A., Tyler, P., McSweeney, K. M., Lu, Y., Hall, D., & Ross, J. D. (2016). Optogenetic stimulation of multiwell MEA plates for neural and cardiac applications. *Clinical and Translational Neurophotonics; Neural Imaging and Sensing; and Optogenetics and Optical Manipulation*, *9690*, 96902C. https://doi.org/10.1117/12.2213708

Colantuoni, C., Lipska, B. K., Ye, T., Hyde, T. M., Tao, R., Leek, J. T., Colantuoni, E. A., Elkahloun, A. G., Herman, M. M., Weinberger, D. R., & Kleinman, J. E. (2011). Temporal dynamics and genetic control of transcription in the human prefrontal cortex. *Nature*, *478*(7370), 519–523. https://doi.org/10.1038/nature10524

Cooper, R. A., & Ritchey, M. (2019). Cortico-hippocampal network connections support the multidimensional quality of episodic memory. *ELife*, *8*, 1–22. https://doi.org/10.7554/eLife.45591

Cope, T. E., Rittman, T., Borchert, R. J., Jones, P. S., Vatansever, D., Allinson, K., Passamonti, L., Vazquez Rodriguez, P., Bevan-Jones, W. R., O'Brien, J. T., & Rowe, J. B. (2018). Tau burden and the functional connectome in Alzheimer's disease and progressive supranuclear palsy. *Brain*, *141*(2), 550–567. https://doi.org/10.1093/brain/awx347

Cordeddu, V., Redeker, B., Stellacci, E., Jongejan, A., Fragale, A., Bradley, T. E. J., Anselmi, M., Ciolfi, A., Cecchetti, S., Muto, V., Bernardini, L., Azage, M., Carvalho, D. R., Espay, A. J., Male, A., Molin, A. M., Posmyk, R., Battisti, C., Casertano, A., … Hennekam, R. C. (2014). Mutations in ZBTB20 cause

Primrose syndrome. *Nature Genetics*, *46*(8), 815–817. https://doi.org/10.1038/ng.3035

Couillard-Despres, S., Winner, B., Schaubeck, S., Aigner, R., Vroemen, M., Weidner, N., Bogdahn, U., Winkler, J., Kuhn, H. G., & Aigner, L. (2005). Doublecortin expression levels in adult brain reflect neurogenesis. *European Journal of Neuroscience*, *21*(1), 1–14. https://doi.org/10.1111/j.1460-9568.2004.03813.x

Criado-Marrero, M., Sabbagh, J. J., Jones, M. R., Chaput, D., Dickey, C. A., & Blair, L. J. (2020). Hippocampal Neurogenesis Is Enhanced in Adult Tau Deficient Mice. *Cells*, *9*(1), 210. https://doi.org/10.3390/cells9010210

Davidson, K. C., Adams, A. M., Goodson, J. M., McDonald, C. E., Potter, J. C., Berndt, J. D., Biechele, T. L., Taylor, R. J., & Moon, R. T. (2012). Wnt/b-catenin signaling promotes differentiation, not self-renewal, of human embryonic stem cells and is repressed by Oct4. *Proceedings of the National Academy of Sciences*, *109*(12), 4485–4490. https://doi.org/10.1073/pnas.1118777109

Dawydow, A., Gueta, R., Ljaschenko, D., Ullrich, S., Hermann, M., Ehmann, N., Gao, S., Fiala, A., Langenhan, T., Nagel, G., & Kittel, R. J. (2014). Channelrhodopsin-2-XXL, a powerful optogenetic tool for low-light applications. *Proceedings of the National Academy of Sciences of the United States of America*, *111*(38), 13972–13977. https://doi.org/10.1073/pnas.1408269111

de Carvalho, A. L. R. T., Strikoudis, A., Liu, H. Y., Chen, Y. W., Dantas, T. J., Vallee, R. B., Correia-Pinto, J., & Snoeck, H. W. (2019). Glycogen synthase kinase 3 induces multilineage maturation of human pluripotent stem cell-derived lung progenitors in 3D culture. *Development (Cambridge)*, *146*(2). https://doi.org/10.1242/dev.171652

Deguchi, Y., Donato, F., Galimberti, I., Cabuy, E., & Caroni, P. (2011). Temporally matched subpopulations of selectively interconnected principal neurons in the hippocampus. *Nature Neuroscience*, *14*(4), 495–504. https://doi.org/10.1038/nn.2768

Denham, M., Parish, C. L., Leaw, B., Wright, J., Reid, C. A., Petrou, S., Dottori, M., & Thompson, L. H.

(2012). Neurons derived from human embryonic stem cells extend long-distance axonal projections through growth along host white matter tracts after intra-cerebral transplantation. *Frontiers in Cellular Neuroscience*, *6*(MARCH), 1–14. https://doi.org/10.3389/fncel.2012.00011

Desforges, M., Parsons, L., Westwood, M., Sibley, C. P., & Greenwood, S. L. (2013). Taurine transport in human placental trophoblast is important for regulation of cell differentiation and survival. *Cell Death and Disease*, *4*(3). https://doi.org/10.1038/cddis.2013.81

Deshpande, A., Bergami, M., Ghanem, A., Conzelmann, K. K., Lepier, A., Götz, M., & Berninger, B. (2013). Retrograde monosynaptic tracing reveals the temporal evolution of inputs onto new neurons in the adult dentate gyrus and olfactory bulb. *Proceedings of the National Academy of Sciences of the United States of America*, *110*(12). https://doi.org/10.1073/pnas.1218991110

Di Bella, D. J., Habibi, E., Stickels, R. R., Scalia, G., Brown, J., Yadollahpour, P., Yang, S. M., Abbate, C., Biancalani, T., Macosko, E. Z., Chen, F., Regev, A., & Arlotta, P. (2021). Molecular logic of cellular diversification in the mouse cerebral cortex. *Nature*, *595*(June 2020). https://doi.org/10.1038/s41586-021-03670-5

Diss, J. K. J., Calissano, M., Gascoyne, D., Djamgoz, M. B. A., & Latchman, D. S. (2008). Identification and characterization of the promoter region of the Nav1.7 voltage-gated sodium channel gene (SCN9A). *Molecular and Cellular Neuroscience*, *37*(3), 537–547. https://doi.org/10.1016/j.mcn.2007.12.002

Doe, C. Q. (2008). Neural stem cells: Balancing self-renewal with differentiation. *Development*, *135*(9), 1575–1587. https://doi.org/10.1242/dev.014977

Doeppner, T. R., Herz, J., Bähr, M., Tonchev, A. B., & Stoykova, A. (2019). Zbtb20 Regulates Developmental Neurogenesis in the Olfactory Bulb and Gliogenesis After Adult Brain Injury. *Molecular Neurobiology*, *56*(1), 567–582. https://doi.org/10.1007/s12035-018-1104-y

Doetsch, F., Caillé, I., Lim, D. A., García-Verdugo, J. M., & Alvarez-Buylla, A. (1999). Subventricular zone

astrocytes are neural stem cells in the adult mammalian brain. *Cell*, *97*(6), 703–716. https://doi.org/10.1016/s0092-8674(00)80783-7

Doi, D., Samata, B., Katsukawa, M., Kikuchi, T., Morizane, A., Ono, Y., Sekiguchi, K., Nakagawa, M., Parmar, M., & Takahashi, J. (2014). Isolation of human induced pluripotent stem cell-derived dopaminergic progenitors by cell sorting for successful transplantation. *Stem Cell Reports*, *2*(3), 337–350. https://doi.org/10.1016/j.stemcr.2014.01.013

Donato, F., Jacobsen, R. I., Moser, M. B., & Moser, E. I. (2017). Stellate cells drive maturation of the entorhinal-hippocampal circuit. *Science*, *355*(6330). https://doi.org/10.1126/science.aai8178

Duan, X., Chang, J. H., Ge, S., Faulkner, R. L., Kim, J. Y., Kitabatake, Y., Liu, X. bo, Yang, C. H., Jordan, J. D., Ma, D. K., Liu, C. Y., Ganesan, S., Cheng, H. J., Ming, G. li, Lu, B., & Song, H. (2007). Disrupted-In-Schizophrenia 1 Regulates Integration of Newly Generated Neurons in the Adult Brain. *Cell*, *130*(6), 1146–1158. https://doi.org/10.1016/j.cell.2007.07.010

DuBridge, R. B., Tang, P., Hsia, H. C., Leong, P. M., Miller, J. H., & Calos, M. P. (1987). Analysis of mutation in human cells by using an Epstein-Barr virus shuttle system. *Molecular and Cellular Biology*, *7*(1), 379–387. https://doi.org/10.1128/mcb.7.1.379

Dudek, S. M., Alexander, G. M., & Farris, S. (2016). Rediscovering area CA2: Unique properties and functions. *Nature Reviews Neuroscience*, *17*(2), 89–102. https://doi.org/10.1038/nrn.2015.22

Eckenhoff, M. F., & Rakic, P. (1984). Radial organization of the hippocampal dentate gyrus: A Golgi, ultrastructural, and immunocytochemical analysis in the developing rhesus monkey. *Journal of Comparative Neurology*, *223*(1), 1–21. https://doi.org/10.1002/cne.902230102

Ehm, O., Göritz, C., Covic, M., Schäffner, I., Schwarz, T. J., Karaca, E., Kempkes, B., Kremmer, E., Pfrieger, F. W., Espinosa, L., Bigas, A., Giachino, C., Taylor, V., Frisén, J., & Lie, D. C. (2010). RBPJκ-dependent signaling is essential for long-term maintenance of neural stem cells in the adult hippocampus. In *Journal of Neuroscience* (Vol. 30, Issue 41, pp. 13794–13807).

https://doi.org/10.1523/JNEUROSCI.1567-10.2010

Eiraku, M., Watanabe, K., Matsuo-Takasaki, M., Kawada, M., Yonemura, S., Matsumura, M., Wataya, T., Nishiyama, A., Muguruma, K., & Sasai, Y. (2008). Self-Organized Formation of Polarized Cortical Tissues from ESCs and Its Active Manipulation by Extrinsic Signals. *Cell Stem Cell*, *3*(5), 519–532. https://doi.org/10.1016/j.stem.2008.09.002

Eisenhauer, K., Kuhne, J., Ritter, E., Berndt, A., Wolf, S., Freier, E., Bartl, F., Hegemann, P., & Gerwert, K. (2012). In channelrhodopsin-2 Glu-90 is crucial for ion selectivity and is deprotonated during the photocycle. *Journal of Biological Chemistry*, *287*(9), 6904–6911. https://doi.org/10.1074/jbc.M111.327700

Ekdahl, C. T., Claasen, J. H., Bonde, S., Kokaia, Z., & Lindvall, O. (2003). Inflammation is detrimental for neurogenesis in adult brain. *Proceedings of the National Academy of Sciences of the United States of America*, *100*(23), 13632–13637. https://doi.org/10.1073/pnas.2234031100

Elena, D., Isaac, C., Daniel, M., Anthony, N., Stacie, C., Michael, G., James, R., & Niels, F. (2016). Multiwell Optogenetic Stimulation For The Precise Control Of In Vitro Cellular Network Activity - Neural And Cardiac Applications. *Frontiers in Neuroscience*, *10*. https://doi.org/10.3389/conf.fnins.2016.93.00030

Encinas, J. M., Vaahtokari, A., & Enikolopov, G. (2006). Fluoxetine targets early progenitor cells in the adult brain. *Proceedings of the National Academy of Sciences of the United States of America*, *103*(21), 8233–8238. https://doi.org/10.1073/pnas.0601992103

Eriksson, P. S., Perfilieva, E., Björk-Eriksson, T., Alborn, A.-M., Nordborg, C., Peterson, D. A., & Gage, F. H. (1998). Neurogenesis in the adult human hippocampus. *Nature Medicine*, *4*(11), 1313–1317. https://doi.org/10.1038/3305

Espósito, M. S., Piatti, V. C., Laplagne, D. A., Morgenstern, N. A., Ferrari, C. C., Pitossi, F. J., & Schinder, A. F. (2005). Neuronal differentiation in the adult hippocampus recapitulates embryonic

development. *Journal of Neuroscience*, *25*(44), 10074–10086. https://doi.org/10.1523/JNEUROSCI.3114-05.2005

Espuny-Camacho, I., Arranz, A. M., Fiers, M., Snellinx, A., Ando, K., Munck, S., Bonnefont, J., Lambot, L., Corthout, N., Omodho, L., Vanden Eynden, E., Radaelli, E., Tesseur, I., Wray, S., Ebneth, A., Hardy, J., Leroy, K., Brion, J. P., Vanderhaeghen, P., & De Strooper, B. (2017). Hallmarks of Alzheimer's Disease in Stem-Cell-Derived Human Neurons Transplanted into Mouse Brain. *Neuron*, *93*(5), 1066-1081.e8. https://doi.org/10.1016/j.neuron.2017.02.001

Espuny-Camacho, I., Michelsen, K. A., Gall, D., Linaro, D., Hasche, A., Bonnefont, J., Bali, C., Orduz, D., Bilheu, A., Herpoel, A., Lambert, N., Gaspard, N., Péron, S., Schiffmann, S. N., Giugliano, M., Gaillard, A., & Vanderhaeghen, P. (2013). Pyramidal Neurons Derived from Human Pluripotent Stem Cells Integrate Efficiently into Mouse Brain Circuits In Vivo. *Neuron*, *77*(3), 440–456. https://doi.org/10.1016/j.neuron.2012.12.011

Etter, G., van der Veldt, S., Manseau, F., Zarrinkoub, I., Trillaud-Doppia, E., & Williams, S. (2019). Optogenetic gamma stimulation rescues memory impairments in an Alzheimer's disease mouse model. *Nature Communications*, *10*(1), 1–11. https://doi.org/10.1038/s41467-019-13260-9

Farioli-Vecchioli, S., Saraulli, D., Costanzi, M., Leonardi, L., Cinà, I., Micheli, L., Nutini, M., Longone, P., Paul Oh, S., Cestari, V., & Tirone, F. (2009). Impaired terminal differentiation of hippocampal granule neurons and defective contextual memory in PC3/Tis21 knockout mice. *PLoS ONE*, *4*(12). https://doi.org/10.1371/journal.pone.0008339

Fear, M. W., Kelsell, D. P., Spurr, N. K., & Barnes, M. R. (2000). Wnt-16a, a novel Wnt-16 isoform, which shows differential expression in adult human tissues. *Biochemical and Biophysical Research Communications*, *278*(3), 814–820. https://doi.org/10.1006/bbrc.2000.3852

Feldbauer, K., Zimmermann, D., Pintschovius, V., Spitz, J., Bamann, C., & Bamberg, E. (2009). Channelrhodopsin-2 is a leaky proton pump. *Proceedings of the National Academy of Sciences of*

the United States of America, *106*(30), 12317–12322. https://doi.org/10.1073/pnas.0905852106

Fernandez-Lamo, I., Gomez-Dominguez, D., Sanchez-Aguilera, A., Oliva, A., Morales, A. V., Valero, M., Cid, E., Berenyi, A., & Menendez de la Prida, L. (2019). Proximodistal Organization of the CA2 Hippocampal Area. *Cell Reports*, *26*(7), 1734-1746.e6. https://doi.org/10.1016/j.celrep.2019.01.060

Fink, J. J., Robinson, T. M., Germain, N. D., Sirois, C. L., Bolduc, K. A., Ward, A. J., Rigo, F., Chamberlain, S. J., & Levine, E. S. (2017). Disrupted neuronal maturation in Angelman syndrome-derived induced pluripotent stem cells. *Nature Communications*, *8*. https://doi.org/10.1038/ncomms15038

Fjodorova, M., & Li, M. (2018). Robust induction of DARPP32-expressing gabaergic striatal neurons from human pluripotent stem cells. In *Methods in Molecular Biology* (Vol. 1780, pp. 585–605). https://doi.org/10.1007/978-1-4939-7825-0_27

Fjodorova, M., Louessard, M., Li, Z., De La Fuente, D. C., Dyke, E., Brooks, S. P., Perrier, A. L., & Li, M. (2019). CTIP2-Regulated Reduction in PKA-Dependent DARPP32 Phosphorylation in Human Medium Spiny Neurons: Implications for Huntington Disease. *Stem Cell Reports*, *13*(3), 448–457. https://doi.org/10.1016/j.stemcr.2019.07.015

Fjodorova, M., Noakes, Z., & Li, M. (2015). How to make striatal projection neurons. In *Neurogenesis* (Vol. 2, Issue 1). https://doi.org/10.1080/23262133.2015.1100227

Flytzanis, N. C., Bedbrook, C. N., Chiu, H., Engqvist, M. K. M. M., Xiao, C., Chan, K. Y., Sternberg, P. W., Arnold, F. H., & Gradinaru, V. (2014). Archaerhodopsin variants with enhanced voltage-sensitive fluorescence in mammalian and Caenorhabditis elegans neurons. *Nature Communications*, *5*(1), 4894. https://doi.org/10.1038/ncomms5894

Fong, H., Hohenstein, K. A., & Donovan, P. J. (2008). Regulation of Self-Renewal and Pluripotency by Sox2 in Human Embryonic Stem Cells. *Stem Cells*, *26*(8), 1931–1938. https://doi.org/10.1634/stemcells.2007-1002

Förster, D., Maschio, M. D., Laurell, E., & Baier, H. (2017). An optogenetic toolbox for unbiased discovery of functionally connected cells in neural circuits. *Nature Communications*, *8*(116). https://doi.org/10.1038/s41467-017-00160-z

Frega, M., Linda, K., Keller, J. M., Gümüş-Akay, G., Mossink, B., van Rhijn, J. R., Negwer, M., Klein Gunnewiek, T., Foreman, K., Kompier, N., Schoenmaker, C., van den Akker, W., van der Werf, I., Oudakker, A., Zhou, H., Kleefstra, T., Schubert, D., van Bokhoven, H., & Nadif Kasri, N. (2019). Neuronal network dysfunction in a model for Kleefstra syndrome mediated by enhanced NMDAR signaling. *Nature Communications*, *10*(1), 1–15. https://doi.org/10.1038/s41467-019-12947-3

Fyhn, M., Hafting, T., Treves, A., Moser, M. B., & Moser, E. I. (2007). Hippocampal remapping and grid realignment in entorhinal cortex. *Nature*, *446*(7132), 190–194. https://doi.org/10.1038/nature05601

Fyhn, M., Molden, S., Witter, M. P., Moser, E. I., & Moser, M. B. (2004). Spatial representation in the entorhinal cortex. *Science*, *305*(5688), 1258–1264. https://doi.org/10.1126/science.1099901

Gaarskjaer, F. B. (1985). The development of the dentate area and the hippocampal mossy fiber projection of the rat. *Journal of Comparative Neurology*, *241*(2), 154–170. https://doi.org/10.1002/cne.902410204

Gail Canter, R., Huang, W. C., Choi, H., Wang, J., Ashley Watson, L., Yao, C. G., Abdurrob, F., Bousleiman, S. M., Young, J. Z., Bennett, D. A., Delalle, I., Chung, K., & Tsai, L. H. (2019). 3D mapping reveals network-specific amyloid progression and subcortical susceptibility in mice. *Communications Biology*, *2*(1), 1–12. https://doi.org/10.1038/s42003-019-0599-8

Galfrè, S. G., Morandin, F., Pietrosanto, M., Cremisi, F., & Helmer-Citterich, M. (2020). COTAN: Co-expression Table Analysis for scRNA-seq data. *BioRxiv*, 2020.05.11.088062. https://doi.org/10.1101/2020.05.11.088062

Galichet, C., Guillemot, F., & Parras, C. M. (2008). Neurogenin 2 has an essential role in development of

the dentate gyrus. *Development*, *135*(11), 2031–2041. https://doi.org/10.1242/dev.015115

Garita-hernandez, M., Guibbal, L., Toualbi, L., Routet, F., Fouquet, S., Bellow, S., Sahel, J., Goureau, O., & Garita-hernandez, M. (2018). Optogenetic Light Sensors in Human Retinal Organoids. *Frontiers in Neuroscience*, *12*(November), 1–12. https://doi.org/10.3389/fnins.2018.00789

Gaskin, S., & White, N. M. (2013). Parallel processing of information about location in the amygdala, entorhinal cortex and hippocampus. *Hippocampus*, *23*(11), 1075–1083. https://doi.org/10.1002/hipo.22179

Gaspard, N., Bouschet, T., Herpoel, A., Naeije, G., van den Ameele, J., & Vanderhaeghen, P. (2009). Generation of cortical neurons from mouse embryonic stem cells. *Nature Protocols*, *4*(10), 1456–1463. https://doi.org/10.1038/nprot.2009.157

Gaspard, N., Bouschet, T., Hourez, R., Dimidschstein, J., Naeije, G., van den Ameele, J., Espuny-Camacho, I., Herpoel, A., Passante, L., Schiffmann, S. N., Gaillard, A., & Vanderhaeghen, P. (2008). An intrinsic mechanism of corticogenesis from embryonic stem cells. *Nature*, *455*(7211), 351–357. https://doi.org/10.1038/nature07287

Gava, G. P., McHugh, S. B., Lefèvre, L., Lopes-dos-Santos, V., Trouche, S., El-Gaby, M., Schultz, S. R., & Dupret, D. (2021). Integrating new memories into the hippocampal network activity space. *Nature Neuroscience 2021*, *24*(March), 1–5. https://doi.org/10.1038/s41593-021-00804-w

Gavin, B. J., McMahon, J. A., & McMahon, A. P. (1990). Expression of multiple novel Wnt-1/int-1-related genes during fetal and adult mouse development. *Genes and Development*, *4*(12 B), 2319–2332. https://doi.org/10.1101/gad.4.12b.2319

Ge, S., Sailor, K. A., Ming, G., & Song, H. (2008). *Synaptic integration and plasticity of new neurons in the adult hippocampus*. *16*, 3759–3765. https://doi.org/10.1113/jphysiol.2008.155655

Gerhardt, K. P., Olson, E. J., Castillo-Hair, S. M., Hartsough, L. A., Landry, B. P., Ekness, F., Yokoo, R., Gomez, E. J., Ramakrishnan, P., Suh, J., Savage, D. F., & Tabor, J. J. (2016). An open-hardware

platform for optogenetics and photobiology. *Scientific Reports*, *6*(June), 1–13. https://doi.org/10.1038/srep35363

Ghosal, K., & Pimplikar, S. W. (2011). Aging and excitotoxic stress exacerbate neural circuit reorganization in APP intracellular domain (AICD) transgenic mice. *Neurobiology of Aging*, *32*(12), 2320.e1-2320.e9. https://doi.org/10.1016/j.neurobiolaging.2010.04.020

Gillespie, A. K., Jones, E. A., Lin, Y., Carr, J. S., Frank, L. M., Huang, Y., Gillespie, A. K., Jones, E. A., Lin, Y., Karlsson, M. P., Kay, K., & Yoon, S. Y. (2016). Disruption of Slow Gamma Oscillations during Article Apolipoprotein E4 Causes Age-Dependent Disruption of Slow Gamma Oscillations during Hippocampal Sharp-Wave Ripples. *Neuron*, *90*(4), 740–751. https://doi.org/10.1016/j.neuron.2016.04.009

Goedert, M., Jakes, R., Crowther, R. A., Six, J., Lubke, U., Vandermeeren, M., Cras, P., Trojanowski, J. Q., & Lee, V. M. Y. (1993). The abnormal phosphorylation of tau protein at Ser-202 in Alzheimer disease recapitulates phosphorylation during development. *Proceedings of the National Academy of Sciences*, *90*(11), 5066–5070. https://doi.org/10.1073/pnas.90.11.5066

Goldman, S. A., & Nottebohm, F. (1983). Neuronal production, migration, and differentiation in a vocal control nucleus of the adult female canary brain. *Proceedings of the National Academy of Sciences of the United States of America*, *80*(8 I), 2390–2394. https://doi.org/10.1073/pnas.80.8.2390

Gordon, A., Yoon, S. J., Tran, S. S., Makinson, C. D., Park, J. Y., Andersen, J., Valencia, A. M., Horvath, S., Xiao, X., Huguenard, J. R., Pașca, S. P., & Geschwind, D. H. (2021). Long-term maturation of human cortical organoids matches key early postnatal transitions. *Nature Neuroscience*, *24*(3), 331–342. https://doi.org/10.1038/s41593-021-00802-y

Govorunova, E. G., Sineshchekov, O. A., Janz, R., Liu, X., & Spudich, J. L. (2015). Natural light-gated anion channels: A family of microbial rhodopsins for advanced optogenetics. *Science*, *349*(6248), 647–650. https://doi.org/10.1126/science.aaa7484

Govorunova, E. G., Spudich, E. N., Lane, C. E., Sineshchekov, O. A., & Spudich, J. L. (2011). New Channelrhodopsin with a Red-Shifted Spectrum and Rapid Kinetics from Mesostigma viride. *MBIO*, *2*(3), 1–9. https://doi.org/10.1128/mBio.00115-11.Editor

Gradinaru, V., Thompson, K. R., & Deisseroth, K. (2008). eNpHR: A Natronomonas halorhodopsin enhanced for optogenetic applications. *Brain Cell Biology*, *36*(1–4), 129–139. https://doi.org/10.1007/s11068-008-9027-6

Graham, F. L., Smiley, J., Russell, W. C., & Nairn, R. (1977). Characteristics of a human cell line transformed by DNA from human adenovirus type 5. *Journal of General Virology*, *36*(1), 59–72. https://doi.org/10.1099/0022-1317-36-1-59

Greco, T. L., Takada, S., Newhouse, M. M., McMahon, J. A., McMahon, A. P., & Camper, S. A. (1996). Analysis of the vestigial tail mutation demonstrates that Wnt-3a gene dosage regulates mouse axial development. *Genes and Development*, *10*(3), 313–324. https://doi.org/10.1101/gad.10.3.313

Grove, E. A., & Tole, S. (1999). Patterning events and specification signals in the developing hippocampus. *Cerebral Cortex*, *9*(6), 551–561. https://doi.org/10.1093/cercor/9.6.551

Grove, E. A., Tole, S., Limon, J., Yip, L. W., & Ragsdale, C. W. (1998). The hem of the embryonic cerebral cortex is defined by the expression of multiple Wnt genes and is compromised in Gli3-deficient mice. *Development*, *125*(12), 2315–2325.

Gunaydin, L. A., Yizhar, O., Berndt, A., Sohal, V. S., Deisseroth, K., & Hegemann, P. (2010). Ultrafast optogenetic control. *Nature Neuroscience*, *13*(3), 387–392. https://doi.org/10.1038/nn.2495

Guo, Y., Wei, Q., Huang, Y., Xia, W., Zhou, Y., & Wang, S. (2013). Neurochemistry International The effects of astrocytes on differentiation of neural stem cells are influenced by knock-down of the glutamate transporter , GLT-1. *Neurochemistry International*, *63*(5), 498–506. https://doi.org/10.1016/j.neuint.2013.08.003

Gusel'nikova, V. V., & Korzhevskiy, D. E. (2015). NeuN as a neuronal nuclear antigen and neuron

differentiation marker. *Acta Naturae*, *7*(2), 42–47. https://doi.org/10.32607/20758251-2015-7-2-42-47

Halevy, T., Czech, C., & Benvenisty, N. (2015). Molecular mechanisms regulating the defects in fragile x syndrome neurons derived from human pluripotent stem cells. *Stem Cell Reports*, *4*(1), 37–46. https://doi.org/10.1016/j.stemcr.2014.10.015

Halliwell, B., & Whiteman, M. (2004). Measuring reactive species and oxidative damage in vivo and in cell culture: How should you do it and what do the results mean? *British Journal of Pharmacology*, *142*(2), 231–255. https://doi.org/10.1038/sj.bjp.0705776

Hamilton, K. A., Wang, Y., Raefsky, S. M., Berkowitz, S., Spangler, R., Suire, C. N., Camandola, S., Lipsky, R. H., & Mattson, M. P. (2018). Mice lacking the transcriptional regulator Bhlhe40 have enhanced neuronal excitability and impaired synaptic plasticity in the hippocampus. *PLoS ONE*, *13*(5), 1–22. https://doi.org/10.1371/journal.pone.0196223

Han, X., Chow, B. Y., Zhou, H., Klapoetke, N. C., Chuong, A., Rajimehr, R., Yang, A., Baratta, M. V., Winkle, J., Desimone, R., & Boyden, E. S. (2011). A high-light sensitivity optical neural silencer: Development and application to optogenetic control of non-human primate cortex. *Frontiers in Systems Neuroscience*, *5*(APRIL 2011), 1–8. https://doi.org/10.3389/fnsys.2011.00018

Hardy, J. A., & Higgins, G. A. (1992). Alzheimer's Disease: The Amyloid Alzheimer's disease. *Science*, *256*, 184–185.

Harzsch, S., & Dawirs, R. R. (1996). Neurogenesis in the developing crab brain: Postembryonic generation of neurons persists beyond metamorphosis. *Journal of Neurobiology*, *29*(3), 384–398. https://doi.org/10.1002/(SICI)1097-4695(199603)29:3<384::AID-NEU9>3.0.CO;2-5

Hasselmann, J., Coburn, M. A., England, W., Figueroa Velez, D. X., Kiani Shabestari, S., Tu, C. H., McQuade, A., Kolahdouzan, M., Echeverria, K., Claes, C., Nakayama, T., Azevedo, R., Coufal, N. G., Han, C. Z., Cummings, B. J., Davtyan, H., Glass, C. K., Healy, L. M., Gandhi, S. P., … Blurton-Jones, M.

(2019). Development of a Chimeric Model to Study and Manipulate Human Microglia In Vivo. *Neuron*, *103*(6), 1016-1033.e10. https://doi.org/10.1016/j.neuron.2019.07.002

Hayer, A., Shao, L., Chung, M., Joubert, L. M., Yang, H. W., Tsai, F. C., Bisaria, A., Betzig, E., & Meyer, T. (2016). Engulfed cadherin fingers are polarized junctional structures between collectively migrating endothelial cells. *Nature Cell Biology*, *18*(12), 1311–1323. https://doi.org/10.1038/ncb3438

He, X., Tan, C., Wang, F., Wang, Y., Zhou, R., Cui, D., You, W., Zhao, H., Ren, J., & Feng, B. (2016). Knock-in of large reporter genes in human cells via CRISPR/Cas9-induced homology-dependent and independent DNA repair. *Nucleic Acids Research*, *44*(9). https://doi.org/10.1093/nar/gkw064

Hegemann, P., Gärtner, W., & Uhl, R. (1991). All-trans retinal constitutes the functional chromophore in Chlamydomonas rhodopsin. *Biophysical Journal*, *60*(6), 1477–1489. https://doi.org/10.1016/S0006-3495(91)82183-X

Hitti, F. L., & Siegelbaum, S. A. (2014). The hippocampal CA2 region is essential for social memory. *Nature*, *508*(1), 88–92. https://doi.org/10.1038/nature13028

Hochbaum, D. R., Zhao, Y., Farhi, S. L., Klapoetke, N., Werley, C. A., Kapoor, V., Zou, P., Kralj, J. M., MacLaurin, D., Smedemark-Margulies, N., Saulnier, J. L., Boulting, G. L., Straub, C., Cho, Y. K., Melkonian, M., Wong, G. K. S., Harrison, D. J., Murthy, V. N., Sabatini, B. L., … Cohen, A. E. (2014). All-optical electrophysiology in mammalian neurons using engineered microbial rhodopsins. *Nature Methods*, *11*(8), 825–833. https://doi.org/10.1038/NMETH.3000

Hochgerner, H., Zeisel, A., Lönnerberg, P., & Linnarsson, S. (2018). Conserved properties of dentate gyrus neurogenesis across postnatal development revealed by single-cell RNA sequencing. *Nature Neuroscience*, *21*(2), 290–299. https://doi.org/10.1038/s41593-017-0056-2

Hofman, M. A. (2014). Evolution of the human brain: When bigger is better. *Frontiers in Neuroanatomy*, *8*(MAR), 1–12. https://doi.org/10.3389/fnana.2014.00015

Holmes, T., O'Brien, T. A., Knight, R., Lindeman, R., Shen, S., Song, E., Symonds, G., & Dolnikov, A. (2008).

Glycogen Synthase Kinase-3β Inhibition Preserves Hematopoietic Stem Cell Activity and Inhibits Leukemic Cell Growth. *Stem Cells*, *26*(5), 1288–1297. https://doi.org/10.1634/stemcells.2007-0600

Hososhima, S., Yuasa, H., Ishizuka, T., Hoque, M. R., Yamashita, T., Yamanaka, A., Sugano, E., Tomita, H., & Yawo, H. (2015). Near-infrared (NIR) up-conversion optogenetics. *Scientific Reports*, *5*, 1–10. https://doi.org/10.1038/srep16533

Hsieh, J. Y., & Baraban, S. C. (2017). Medial ganglionic eminence progenitors transplanted into hippocampus integrate in a functional and subtype-appropriate manner. *ENeuro*, *4*(2), 1–17. https://doi.org/10.1523/ENEURO.0359-16.2017

Hu, Y. S., Long, N., Pigino, G., Brady, S. T., & Lazarov, O. (2013). Molecular Mechanisms of Environmental Enrichment: Impairments in Akt/GSK3β, Neurotrophin-3 and CREB Signaling. *PLoS ONE*, *8*(5). https://doi.org/10.1371/journal.pone.0064460

Huang, G., Chen, S., Chen, X., Zheng, J., Xu, Z., Doostparast Torshizi, A., Gong, S., Chen, Q., Ma, X., Yu, J., Zhou, L., Qiu, S., Wang, K., & Shi, L. (2019). Uncovering the functional link between SHANK3 deletions and deficiency in neurodevelopment using iPSC-derived human neurons. *Frontiers in Neuroanatomy*, *13*(March). https://doi.org/10.3389/fnana.2019.00023

Huguet, E. L., McMahon, J. A., McMahon, A. P., Bicknell, R., & Harris, A. L. (1994). Differential Expression of Human Wnt Genes 2, 3, 4, and 7B in Human Breast Cell Lines and Normal and Disease States of Human Breast Tissue. *Cancer Research*, *54*(10), 2615–2621.

Hunter, D. D., Llinas, R., Ard, M., Merlie, J. P., & Sanes, J. R. (1992). Expression of S-laminin and laminin in the developing rat central nervous system. In *Journal of Comparative Neurology* (Vol. 323, Issue 2, pp. 238–251). https://doi.org/10.1002/cne.903230208

Husson, S. J., Liewald, J. F., Schultheis, C., Stirman, J. N., Lu, H., & Gottschalk, A. (2012). Microbial Light-Activatable Proton Pumps as Neuronal Inhibitors to Functionally Dissect Neuronal Networks in C . elegans. *PLoS ONE*, *7*(7). https://doi.org/10.1371/journal.pone.0040937

Hyvärinen, T., Hyysalo, A., Kapucu, F. E., Aarnos, L., Vinogradov, A., Eglen, S. J., Ylä-Outinen, L., & Narkilahti, S. (2019). Functional characterization of human pluripotent stem cell-derived cortical networks differentiated on laminin-521 substrate: comparison to rat cortical cultures. *Scientific Reports*, *9*(1), 1–15. https://doi.org/10.1038/s41598-019-53647-8

Hyysalo, A., Ristola, M., Mäkinen, M. E. L., Häyrynen, S., Nykter, M., & Narkilahti, S. (2017). Laminin α5 substrates promote survival, network formation and functional development of human pluripotent stem cell-derived neurons in vitro. *Stem Cell Research*, *24*, 118–127. https://doi.org/10.1016/j.scr.2017.09.002

Iacopetti, P., Barsacchi, G., Tirone, F., Maffei, L., & Cremisi, F. (1994). Developmental expression of PC3 gene is correlated with neuronal cell birthday. *Mechanisms of Development*, *47*(2), 127–137. https://doi.org/10.1016/0925-4773(94)90085-X

Ihara, K., Umemura, T., Katagiri, I., Kitajima-Ihara, T., Sugiyama, Y., Kimura, Y., & Mukohata, Y. (1999). Evolution of the archaeal rhodopsins: Evolution rate changes by gene duplication and functional differentiation. *Journal of Molecular Biology*, *285*(1), 163–174. https://doi.org/10.1006/jmbi.1998.2286

Ikegawa, S., Kumano, Y., Okui, K., Fujiwara, T., Takahashi, E., & Nakamura, Y. (1996). Isolation, characterization and chromosomal assignment of the human WNT7A gene. *Cytogenetic and Genome Research*, *74*(1–2), 149–152. https://doi.org/10.1159/000134404

Iovino, M., Agathou, S., González-Rueda, A., Del Castillo Velasco-Herrera, M., Borroni, B., Alberici, A., Lynch, T., O'Dowd, S., Geti, I., Gaffney, D., Vallier, L., Paulsen, O., Káradóttir, R. T., & Spillantini, M. G. (2015). Early maturation and distinct tau pathology in induced pluripotent stem cell-derived neurons from patients with MAPT mutations. *Brain*, *138*(11), 3345–3359. https://doi.org/10.1093/brain/awv222

Ishizuka, T., Kakuda, M., Araki, R., & Yawo, H. (2006). Kinetic evaluation of photosensitivity in genetically

engineered neurons expressing green algae light-gated channels. *Neuroscience Research*, *54*(2), 85–94. https://doi.org/10.1016/j.neures.2005.10.009

Israel, M. A., Yuan, S. H., Bardy, C., Reyna, S. M., Mu, Y., Herrera, C., Hefferan, M. P., Van Gorp, S., Nazor, K. L., Boscolo, F. S., Carson, C. T., Laurent, L. C., Marsala, M., Gage, F. H., Remes, A. M., Koo, E. H., & Goldstein, L. S. B. (2012). Probing sporadic and familial Alzheimer's disease using induced pluripotent stem cells. *Nature*, *482*(7384), 216–220. https://doi.org/10.1038/nature10821

Iwano, T., Masuda, A., Kiyonari, H., Enomoto, H., & Matsuzaki, F. (2012). Prox1 postmitotically defines dentate gyrus cells by specifying granule cell identity over CA3 pyramidal cell fate in the hippocampus. *Development (Cambridge)*, *139*(16), 3051–3062. https://doi.org/10.1242/dev.080002

Janovjak, H., Szobota, S., Wyart, C., Trauner, D., & Isacoff, E. Y. (2010). A light-gated, potassium-selective glutamate receptor for the optical inhibition of neuronal firing. *Nature Neuroscience*, *13*(8), 1027–1032. https://doi.org/10.1038/nn.2589

Jessberger, S., & Kempermann, G. (2003). Adult-born hippocampal neurons mature into activity-dependent responsiveness. In *European Journal of Neuroscience* (Vol. 18, Issue 10, pp. 2707–2712). https://doi.org/10.1111/j.1460-9568.2003.02986.x

Jessberger, S., Toni, N., Clemenson, G. D., Ray, J., & Gage, F. H. (2008). Directed differentiation of hippocampal stem/progenitor cells in the adult brain. *Nature Neuroscience*, *11*(8), 888–893. https://doi.org/10.1038/nn.2148

Jones, K. A., Luo, Y., Dukes-Rimsky, L., Srivastava, D. P., Koul-Tewari, R., Russell, T. A., Shapiro, L. P., Srivastava, A. K., & Penzes, P. (2018). Neurodevelopmental disorder-associated ZBTB20 gene variants affect dendritic and synaptic structure. *PLoS ONE*, *13*(10), 1–13. https://doi.org/10.1371/journal.pone.0203760

Jones, M. W., & Mchugh, T. J. (2011). Updating hippocampal representations: CA2 joins the circuit.

Trends in Neurosciences, *34*(10), 526–535. https://doi.org/10.1016/j.tins.2011.07.007

Kadowaki, T., Wilder, E., Klingensmith, J., Zachary, K., & Perrimon, N. (1996). The segment polarity gene porcupine encodes a putative multitransmembrane protein involved in Wingless processing. *Genes and Development*, *10*(24), 3116–3128. https://doi.org/10.1101/gad.10.24.3116

Kang, W., & Hébert, J. M. (2015). FGF signaling is necessary for neurogenesis in young mice and sufficient to reverse its decline in old mice. *Journal of Neuroscience*, *35*(28), 10217–10223. https://doi.org/10.1523/JNEUROSCI.1469-15.2015

Katoh, M, Hirai, M., Sugimura, T., & Terada, M. (1996). Cloning, expression and chromosomal localization of Wnt-13, a novel member of the Wnt gene family. *Oncogene*, *13*(4), 873—876. http://europepmc.org/abstract/MED/8761309

Katoh, Masaru. (2017). Canonical and non-canonical WNT signaling in cancer stem cells and their niches: Cellular heterogeneity, omics reprogramming, targeted therapy and tumor plasticity (Review). *International Journal of Oncology*, *51*(5), 1357–1369. https://doi.org/10.3892/ijo.2017.4129

Kazim, S. F., & Iqbal, K. (2016). Neurotrophic factor small-molecule mimetics mediated neuroregeneration and synaptic repair: emerging therapeutic modality for Alzheimer's disease. *Molecular Neurodegeneration*, *11*(1), 50. https://doi.org/10.1186/s13024-016-0119-y

Kempermann, G., Gast, D., & Gage, F. H. (2002). Neuroplasticity in old age: Sustained fivefold induction of hippocampal neurogenesis by long-term environmental enrichment. *Annals of Neurology*, *52*(2), 135–143. https://doi.org/10.1002/ana.10262

Kempermann, G., Kuhn, H. G., & Gage, F. H. (1997). More hippocampal neurons in adult mice living in an enriched environment. *Nature*, *386*(6624), 493–495. https://doi.org/10.1038/386493a0

Kerever, A., Schnack, J., Vellinga, D., Ichikawa, N., Moon, C., Arikawa-Hirasawa, E., Efird, J. T., & Mercier, F. (2007). Novel Extracellular Matrix Structures in the Neural Stem Cell Niche Capture the Neurogenic Factor Fibroblast Growth Factor 2 from the Extracellular Milieu. *Stem Cells*, *25*(9),

2146–2157. https://doi.org/10.1634/stemcells.2007-0082

Kianianmomeni, A., Stehfest, K., Nematollahi, G., Hegemann, P., & Hallmann, A. (2009). Channelrhodopsins of volvox carteri are photochromic proteins that are specifically expressed in somatic cells under control of light, temperature, and the sex inducer. *Plant Physiology*, *151*(1), 347–366. https://doi.org/10.1104/pp.109.143297

Kim, S. H., Kim, M. O., Cho, Y. Y., Yao, K., Kim, D. J., Jeong, C. H., Yu, D. H., Bae, K. B., Cho, E. J., Jung, S. K., Lee, M. H., Chen, H., Kim, J. Y., Bode, A. M., & Dong, Z. (2014). ERK1 phosphorylates Nanog to regulate protein stability and stem cell self-renewal. *Stem Cell Research*, *13*(1), 1–11. https://doi.org/10.1016/j.scr.2014.04.001

Kimura, J., Suda, Y., Kurokawa, D., Hossain, Z. M., Nakamura, M., Takahashi, M., Hara, A., & Aizawa, S. (2005). Emx2 and Pax6 function in cooperation with Otx2 and Otx1 to develop caudal forebrain primordium that includes future archipallium. *Journal of Neuroscience*, *25*(21), 5097–5108. https://doi.org/10.1523/JNEUROSCI.0239-05.2005

Kirikoshi, H., Sekihara, H., & Katoh, M. (2001a). WNT10A and WNT6, clustered in human chromosome 2q35 region with head-to-tail manner, are strongly coexpressed in SW480 cells. *Biochemical and Biophysical Research Communications*, *283*(4), 798–805. https://doi.org/10.1006/bbrc.2001.4855

Kirikoshi, H., Sekihara, H., & Katoh, M. (2001b). Molecular cloning and characterization of human WNT7B. *International Journal of Oncology*, *9*(2), 153–157. https://doi.org/10.3892/ijo.19.4.779

Kirkeby, A., Grealish, S., Wolf, D. A., Nelander, J., Wood, J., Lundblad, M., Lindvall, O., & Parmar, M. (2012). Generation of Regionally Specified Neural Progenitors and Functional Neurons from Human Embryonic Stem Cells under Defined Conditions. *Cell Reports*, *1*(6), 703–714. https://doi.org/10.1016/j.celrep.2012.04.009

Kiskinis, E., Kralj, J. M., Zou, P., Weinstein, E. N., Zhang, H., Tsioras, K., Wiskow, O., Ortega, J. A., Eggan, K., & Cohen, A. E. (2018). All-Optical Electrophysiology for High-Throughput Functional

Characterization of a Human iPSC-Derived Motor Neuron Model of ALS. *Stem Cell Reports*, *10*(6), 1991–2004. https://doi.org/10.1016/j.stemcr.2018.04.020

Kitabatake, Y., Sailor, K. A., Ming, G. li, & Song, H. (2007). Adult Neurogenesis and Hippocampal Memory Function: New Cells, More Plasticity, New Memories? *Neurosurgery Clinics of North America*, *18*(1), 105–113. https://doi.org/10.1016/j.nec.2006.10.008

Kitazawa, A., Kubo, K. I., Hayashi, K., Matsunaga, Y., Ishii, K., & Nakajima, K. (2014). Hippocampal pyramidal neurons switch from a multipolar migration mode to a novel "climbing" migration mode during development. *Journal of Neuroscience*, *34*(4), 1115–1126. https://doi.org/10.1523/JNEUROSCI.2254-13.2014

Klapoetke, N. C., Murata, Y., Kim, S. S., Pulver, S. R., Birdsey-benson, A., Cho, Y. K., Morimoto, T. K., Chuong, A. S., Carpenter, E. J., Tian, Z., Wang, J., Xie, Y., Yan, Z., Zhang, Y., Chow, B. Y., Surek, B., Melkonian, M., Jayaraman, V., Constantine-paton, M., … Boyden, E. S. (2014). Independent optical excitation of distinct neural populations. *Nature Methods*, *11*(3), 338–346. https://doi.org/10.1038/nmeth.2836

Kleinlogel, S., Terpitz, U., Legrum, B., Gökbuget, D., Boyden, E. S., Bamann, C., Wood, P. G., & Bamberg, E. (2011). A gene-fusion strategy for stoichiometric and co-localized expression of light-gated membrane proteins. *Nature Methods*, *8*(12), 1083–1091. https://doi.org/10.1038/nmeth.1766

Kobro-Flatmoen, A., Nagelhus, A., & Witter, M. P. (2016). Reelin-immunoreactive neurons in entorhinal cortex layer II selectively express intracellular amyloid in early Alzheimer's disease. *Neurobiology of Disease*, *93*, 172–183. https://doi.org/10.1016/j.nbd.2016.05.012

Kornack, D. R., & Rakic, P. (1999). Continuation of neurogenesis in the hippocampus of the adult macaque monkey. *Proceedings of the National Academy of Sciences of the United States of America*, *96*(10), 5768–5773. https://doi.org/10.1073/pnas.96.10.5768

Kozar, K., Ciemerych, M. A., Rebel, V. I., Shigematsu, H., Zagozdzon, A., Sicinska, E., Geng, Y., Yu, Q.,

Bhattacharya, S., Bronson, R. T., Akashi, K., & Sicinski, P. (2004). Mouse development and cell proliferation in the absence of D-cyclins. *Cell*, *118*(4), 477–491. https://doi.org/10.1016/j.cell.2004.07.025

Kramer, J., Steinhoff, J., Klinger, M., Fricke, L., & Rohwedel, J. (2006). Cells differentiated from mouse embryonic stem cells via embryoid bodies express renal marker molecules. *Differentiation*, *74*(2–3), 91–104. https://doi.org/10.1111/j.1432-0436.2006.00062.x

Kroemer, G., Galluzzi, L., Vandenabeele, P., Abrams, J., Alnemri, E. S., Baehrecke, E. H., Blagosklonny, M. V., El-Deiry, W. S., Golstein, P., Green, D. R., Hengartner, M., Knight, R. A., Kumar, S., Lipton, S. A., Malorni, W., Nuñez, G., Peter, M. E., Tschopp, J., Yuan, J., … Melino, G. (2009). Classification of cell death: Recommendations of the Nomenclature Committee on Cell Death 2009. *Cell Death and Differentiation*, *16*(1), 3–11. https://doi.org/10.1038/cdd.2008.150

Kuhn, H. G., Dickinson-Anson, H., & Gage, F. H. (1996). Neurogenesis in the dentate gyrus of the adult rat: Age-related decrease of neuronal progenitor proliferation. *Journal of Neuroscience*, *16*(6), 2027–2033. https://doi.org/10.1523/jneurosci.16-06-02027.1996

Kumar, S. S., & Buckmaster, P. S. (2007). Neuron-specific nuclear antigen NeuN is not detectable in gerbil subtantia nigra pars reticulata. *Brain Research*, *1142*(1), 54–60. https://doi.org/10.1016/j.brainres.2007.01.027

Lako, M., Strachan, T., Bullen, P., Wilson, D. I., Robson, S. C., & Lindsay, S. (1998). Isolation, characterisation and embryonic expression of WNT11, a gene which maps to 11q13.5 and has possible roles in the development of skeleton, kidney and lung. *Gene*, *219*(1–2), 101–110. https://doi.org/10.1016/S0378-1119(98)00393-X

Lako, Majlinda, Strachan, T., Curtis, A. R. J., & Lindsay, S. (1996). Isolation and characterization of WNT8B, a novel human Wnt gene that maps to 10q24. *Genomics*, *35*(2), 386–388. https://doi.org/10.1006/geno.1996.0374

Lancaster, M. A. (2019). An Electric Take on Neural Fate and Cortical Development. *Developmental Cell*, *48*(1), 1–2. https://doi.org/10.1016/j.devcel.2018.12.014

Lancaster, M. A., Corsini, N. S., Wolfinger, S., Gustafson, E. H., Phillips, A. W., Burkard, T. R., Otani, T., Livesey, F. J., & Knoblich, J. A. (2017). Guided self-organization and cortical plate formation in human brain organoids. *Nature Biotechnology*, *35*(7), 659–666. https://doi.org/10.1038/nbt.3906

Landucci, E., Brindisi, M., Bianciardi, L., Catania, L. M., Daga, S., Croci, S., Frullanti, E., Fallerini, C., Butini, S., Brogi, S., Furini, S., Melani, R., Molinaro, A., Lorenzetti, F. C., Imperatore, V., Amabile, S., Mariani, J., Mari, F., Ariani, F., … Meloni, I. (2018). iPSC-derived neurons profiling reveals GABAergic circuit disruption and acetylated α-tubulin defect which improves after iHDAC6 treatment in Rett syndrome. In *Experimental Cell Research* (Vol. 368, Issue 2, pp. 225–235). https://doi.org/10.1016/j.yexcr.2018.05.001

Lang, F., Busch, G. L., Ritter, M., Völkl, H., Waldegger, S., Gulbins, E., & Häussinger, D. (1998). Functional significance of cell volume regulatory mechanisms. *Physiological Reviews*, *78*(1), 247–306. https://doi.org/10.1152/physrev.1998.78.1.247

Larson, J., Wong, D., & Lynch, G. (1986). Patterned stimulation at the theta frequency is optimal for the induction of hippocampal long-term potentiation. *Brain Research*, *368*(2), 347–350. https://doi.org/10.1016/0006-8993(86)90579-2

Lattanzi, A., Neri, M., Maderna, C., di Girolamo, I., Martino, S., Orlacchio, A., Amendola, M., Naldini, L., & Gritti, A. (2010). Widespread enzymatic correction of CNS tissues by a single intracerebral injection of therapeutic lentiviral vector in leukodystrophy mouse models. *Human Molecular Genetics*, *19*(11), 2208–2227. https://doi.org/10.1093/hmg/ddq099

Lee, J., Rabbani, C. C., Gao, H., Steinhart, M. R., Woodruff, B. M., Pflum, Z. E., Kim, A., Heller, S., Liu, Y., Shipchandler, T. Z., & Koehler, K. R. (2020). Hair-bearing human skin generated entirely from pluripotent stem cells. *Nature*, *582*(7812), 399–404. https://doi.org/10.1038/s41586-020-2352-3

Lee, S., & Huang, E. J. (2017). Modeling ALS and FTD with iPSC-derived neurons. *Brain Research*, *1656*, 88–97. https://doi.org/10.1016/j.brainres.2015.10.003

Lee, S. M. K., Tole, S., Grove, E., & McMahon, A. P. (2000). A local Wnt-3a signal is required for development of the mammalian hippocampus. *Development*, *127*(3), 457–467.

Lein, E. S., Callaway, E. M., Albright, T. D., & Gage, F. H. (2005). Redefining the boundaries of the hippocampal CA2 subfield in the mouse using gene expression and 3-dimensional reconstruction. *Journal of Comparative Neurology*, *485*(1), 1–10. https://doi.org/10.1002/cne.20426

Lein, E. S., Zhao, X., & Gage, F. H. (2004). Defining a Molecular Atlas of the Hippocampus Using DNA Microarrays and High-Throughput In Situ Hybridization. *Journal of Neuroscience*, *24*(15), 3879–3889. https://doi.org/10.1523/JNEUROSCI.4710-03.2004

Leng, J., Jiang, L., Chen, H., & Zhang, X. (2009). Brain-derived neurotrophic factor and electrophysiological properties of voltage-gated ion channels during neuronal stem cell development. *Brain Research*, *1272*, 14–24. https://doi.org/10.1016/j.brainres.2009.03.048

Lester, A. W., Moffat, S. D., Wiener, J. M., Barnes, C. A., & Wolbers, T. (2017). The Aging Navigational System. *Neuron*, *95*(5), 1019–1035. https://doi.org/10.1016/j.neuron.2017.06.037

Leventhal, C., Rafii, S., Rafii, D., Shahar, A., & Goldman, S. A. (1999). Endothelial trophic support of neuronal production and recruitment from the adult mammalian subependyma. *Molecular and Cellular Neurosciences*, *13*(6), 450–464. https://doi.org/10.1006/mcne.1999.0762

Li, D., Takeda, N., Jain, R., Manderfield, L. J., Liu, F., Li, L., Anderson, S. A., & Epstein, J. A. (2015). Hopx distinguishes hippocampal from lateral ventricle neural stem cells. *Stem Cell Research*, *15*(3), 522–529. https://doi.org/10.1016/j.scr.2015.09.015

Li, G., Kataoka, H., Coughlin, S. R., & Pleasure, S. J. (2009). Identification of a transient subpial neurogenic zone in the developing dentate gyrus and its regulation by Cxcl12 and reelin signaling. *Development*, *136*(2), 327–335. https://doi.org/10.1242/dev.025742

Li, P., Tong, C., Mehrian-Shai, R., Jia, L., Wu, N., Yan, Y., Maxson, R. E., Schulze, E. N., Song, H., Hsieh, C. L., Pera, M. F., & Ying, Q. L. (2008). Germline Competent Embryonic Stem Cells Derived from Rat Blastocysts. *Cell*, *135*(7), 1299–1310. https://doi.org/10.1016/j.cell.2008.12.006

Li, S., Xue, H., Wu, J., Rao, M. S., Kim, D. H., Deng, W., & Liu, Y. (2015). Human Induced Pluripotent Stem Cell NEUROG2 Dual Knockin Reporter Lines Generated by the CRISPR/Cas9 System. *Stem Cells and Development*, *24*(24), 2925–2942. https://doi.org/10.1089/scd.2015.0131

Lie, D. C., Colamarino, S. A., Song, H. J., Désiré, L., Mira, H., Consiglio, A., Lein, E. S., Jessberger, S., Lansford, H., Dearie, A. R., & Gage, F. H. (2005). Wnt signalling regulates adult hippocampal neurogenesis. *Nature*, *437*(7063), 1370–1375. https://doi.org/10.1038/nature04108

Lin, J. Y., Knutsen, P. M., Muller, A., Kleinfeld, D., & Tsien, R. Y. (2013). ReaChR: A red-shifted variant of channelrhodopsin enables deep transcranial optogenetic excitation. *Nature Neuroscience*, *16*(10), 1499–1508. https://doi.org/10.1038/nn.3502

Lin, J. Y., Lin, M. Z., Steinbach, P., & Tsien, R. Y. (2009). Characterization of engineered channelrhodopsin variants with improved properties and kinetics. *Biophysical Journal*, *96*(5), 1803–1814. https://doi.org/10.1016/j.bpj.2008.11.034

Lindvall, O., Brundin, P., Widner, H., Rehncrona, S., Gustavii, B., Frackowiak, R., Leenders, K. L., Sawle, G., Rothwell, J. C., Marsden, C. D., & Björklund, A. (1990). Grafts of fetal dopamine neurons survive and improve motor function in Parkinson's disease. *Science*, *247*(4942), 574–577. https://doi.org/10.1126/science.2105529

Lisman, J. E. (1999). Relating Hippocampal Circuitry to Function. *Neuron*, *22*(2), 233–242. https://doi.org/10.1016/s0896-6273(00)81085-5

Liu, J., Jiang, J., Hui, X., Wang, W., Fang, D., & Ding, L. (2018). Mir-758-5p Suppresses Glioblastoma Proliferation, Migration and Invasion by Targeting ZBTB20. *Cellular Physiology and Biochemistry*, *48*(5), 2074–2083. https://doi.org/10.1159/000492545

Liu, L., Drouet, V., Wu, J. W., Witter, M. P., Small, S. A., Clelland, C., & Duff, K. (2012). Trans-synaptic spread of tau pathology in vivo. *PLoS ONE*, *7*(2), 1–9. https://doi.org/10.1371/journal.pone.0031302

Liu, Xiaodong, Tan, J. P., Schröder, J., Aberkane, A., Ouyang, J. F., Mohenska, M., Lim, S. M., Sun, Y. B. Y., Chen, J., Sun, G., Zhou, Y., Poppe, D., Lister, R., Clark, A. T., Rackham, O. J. L., Zenker, J., & Polo, J. M. (2021). Modelling human blastocysts by reprogramming fibroblasts into iBlastoids. *Nature*, *August 2020*. https://doi.org/10.1038/s41586-021-03372-y

Liu, Xiaosong, Huang, J., Chen, T., Wang, Y., Xin, S., Li, J., Pei, G., & Kang, J. (2008). Yamanaka factors critically regulate the developmental signaling network in mouse embryonic stem cells. *Cell Research*, *18*(12), 1177–1189. https://doi.org/10.1038/cr.2008.309

Liu, Y., Bergmann, T., Lee, J., Pfisterer, U., Handfield, L.-F., Mori, Y., Asenjo-Martinez, A., Lisa-Vargas, I., Seemann, S. E., Hang Lee, J. T., Patikis, N., Peralvo Vidal, J. M., Pihl, M., Rahbek Kornum, B., Dybdahl Thomsen, P., Hyttel, P., Witter, M. P., Khodosevich, K., Gorodkin, J., … Hall, V. J. (2019). Sandwich cortical lamination and single-cell analysis decodes the developing spatial processing system. *BioRxiv*, 738443. https://doi.org/http://dx.doi.org/10.1101/738443

Llorens-Martin, M., Teixeira, C. M., Fuster-Matanzo, A., Jurado-Arjona, J., Borrell, V., Soriano, E., Avila, J., & Hernández, F. (2012). Tau isoform with three microtubule binding domains is a marker of new axons generated from the subgranular zone in the hippocampal dentate gyrus: Implications for alzheimer's disease. *Journal of Alzheimer's Disease*, *29*(4), 921–930. https://doi.org/10.3233/JAD-2012-112057

Long, K. R., Huttner, W. B., & Long, K. R. (2019). *How the extracellular matrix shapes neural development*.

Looger, L. L. (2012). Running in reverse: Rhodopsins sense voltage. *Nature Methods*, *9*(1), 43–44. https://doi.org/10.1038/nmeth.1817

Lorenzi, M., Altmann, A., Gutman, B., Wray, S., Arber, C., Hibar, D. P., Jahanshad, N., Schott, J. M., Alexander, D. C., Thompson, P. M., & Ourselin, S. (2018). Susceptibility of brain atrophy to TRIB3 in Alzheimer's disease, evidence from functional prioritization in imaging genetics. *Proceedings of the National Academy of Sciences of the United States of America*, *115*(12), 3162–3167. https://doi.org/10.1073/pnas.1706100115

Lou, S., Adam, Y., Weinstein, E. N., Williams, E., Williams, K., Parot, V., Kavokine, N., Liberles, S., Madisen, L., Zeng, H., & Cohen, A. E. (2016). Genetically Targeted All-Optical Electrophysiology with a Transgenic Cre-Dependent Optopatch Mouse. *Journal of Neuroscience*, *36*(43), 11059–11073. https://doi.org/10.1523/JNEUROSCI.1582-16.2016

Lu, M., Grove, E. A., & Miller, R. J. (2002). Abnormal development of the hippocampal dentate gyrus in mice lacking the CXCR4 chemokine receptor. *Proceedings of the National Academy of Sciences of the United States of America*, *99*(10), 7090–7095. https://doi.org/10.1073/pnas.092013799

Luciani, M., Gritti, A., & Meneghini, V. (2020). Human iPSC-Based Models for the Development of Therapeutics Targeting Neurodegenerative Lysosomal Storage Diseases. *Frontiers in Molecular Biosciences*, *7*(September), 1–15. https://doi.org/10.3389/fmolb.2020.00224

Lugert, S., Basak, O., Knuckles, P., Haussler, U., Fabel, K., Götz, M., Haas, C. A., Kempermann, G., Taylor, V., & Giachino, C. (2010). Quiescent and active hippocampal neural stem cells with distinct morphologies respond selectively to physiological and pathological stimuli and aging. *Cell Stem Cell*, *6*(5), 445–456. https://doi.org/10.1016/j.stem.2010.03.017

Lukovic, D., Diez Lloret, A., Stojkovic, P., Rodráiguez-Martáinez, D., Perez Arago, M. A., Rodriguez-Jimenez, F. J., Gonzáalez-Rodráiguez, P., López-Barneo, J., Sykova, E., Jendelova, P., Kostic, J., Moreno-Manzano, V., Stojkovic, M., Bhattacharya, S. S., & Erceg, S. (2017). Highly efficient neural conversion of human pluripotent stem cells in adherent and animal-free conditions. *Stem Cells Translational Medicine*, *6*(4), 1217–1226. https://doi.org/10.1002/sctm.16-0371

Machon, O., Backman, M., Machonova, O., Kozmik, Z., Vacik, T., Andersen, L., & Krauss, S. (2007). A dynamic gradient of Wnt signaling controls initiation of neurogenesis in the mammalian cortex and cellular specification in the hippocampus. *Developmental Biology*, *311*(1), 223–237. https://doi.org/10.1016/j.ydbio.2007.08.038

Maekawa, M., Takashima, N., Arai, Y., Nomura, T., Inokuchi, K., Yuasi, S., & Osumi, N. (2005). Pax6 is required for production and maintenance of progenitor cells in postnatal hippocampal neurogenesis. *Genes to Cells*, *10*(10), 1001–1014. https://doi.org/10.1111/j.1365-2443.2005.00893.x

Mainardi, M., Fusco, S., & Grassi, C. (2015). Modulation of hippocampal neural plasticity by glucose-related signaling. *Neural Plasticity*, *2015*. https://doi.org/10.1155/2015/657928

Mainardi, M., Landi, S., Berardi, N., Maffei, L., & Pizzorusso, T. (2009). Reduced Responsiveness to Long-Term Monocular Deprivation of Parvalbumin Neurons Assessed by c-Fos Staining in Rat Visual Cortex. *PLoS ONE*, *4*(2). https://doi.org/10.1371/journal.pone.0004342

Malatesta, P., Götz, M., Barsacchi, G., Price, J., Zoncu, R., & Cremisi, F. (2000). PC3 overexpression affects the pattern of cell division of rat cortical precursors. *Mechanisms of Development*, *90*(1), 17–28. https://doi.org/10.1016/S0925-4773(99)00224-5

Malatesta, P., Sgadò, P., Caneparo, L., Barsacchi, G., & Cremisi, F. (2001). In vivo PC3 overexpression by retroviral vector affects cell differentiation of rat cortical precursors. *Developmental Brain Research*, *128*(2), 181–185. https://doi.org/10.1016/S0165-3806(01)00170-5

Maller, J. J., Welton, T., Middione, M., Callaghan, F. M., Rosenfeld, J. V., & Grieve, S. M. (2019). Revealing the Hippocampal Connectome through Super-Resolution 1150-Direction Diffusion MRI. *Scientific Reports*, *9*(1), 1–13. https://doi.org/10.1038/s41598-018-37905-9

Marchetto, M. C. N., Yeo, G. W., Kainohana, O., Marsala, M., Gage, F. H., & Muotri, A. R. (2009). Transcriptional signature and memory retention of human-induced pluripotent stem cells. *PLoS*

ONE, *4*(9). https://doi.org/10.1371/journal.pone.0007076

Mardinly, A. R., Oldenburg, I. A., Pégard, N. C., Sridharan, S., Lyall, E. H., Chesnov, K., Brohawn, S. G., Waller, L., & Adesnik, H. (2018). Precise multimodal optical control of neural ensemble activity. *Nature Neuroscience*, *21*(6), 881–893. https://doi.org/10.1038/s41593-018-0139-8

Martin, G. R. (1981). Isolation of a pluripotent cell line from early mouse embryos cultured in medium conditioned by teratocarcinoma stem cells. *Proceedings of the National Academy of Sciences of the United States of America*, *78*(12 II), 7634–7638. https://doi.org/10.1073/pnas.78.12.7634

Martins, M., Galfrè, S., Terrigno, M., Pandolfini, L., Appolloni, I., Dunville, K., Marranci, A., Rizzo, M., Mercatanti, A., Poliseno, L., Morandin, F., Pietrosanto, M., Helmer-Citterich, M., Malatesta, P., Vignali, R., & Cremisi, F. (2021). A eutherian-specific microRNA controls the translation of Satb2 in a model of cortical differentiation. *Stem Cell Reports*, *16*. https://doi.org/10.1016/j.stemcr.2021.04.020

Martynoga, B., Morrison, H., Price, D. J., & Mason, J. O. (2005). Foxg1 is required for specification of ventral telencephalon and region-specific regulation of dorsal telencephalic precursor proliferation and apoptosis. *Developmental Biology*, *283*(1), 113–127. https://doi.org/10.1016/j.ydbio.2005.04.005

Matsuda, S., Kuwako, K. ichiro, Okano, H. J., Tsutsumi, S., Aburatani, H., Saga, Y., Matsuzaki, Y., Akaike, A., Sugimoto, H., & Okano, H. (2012). Sox21 promotes hippocampal adult neurogenesis via the transcriptional repression of the Hes5 gene. *Journal of Neuroscience*, *32*(36), 12543–12557. https://doi.org/10.1523/JNEUROSCI.5803-11.2012

Mattingly, M., Weineck, K., Costa, J., & Cooper, R. L. (2018). Hyperpolarization by activation of halorhodopsin results in enhanced synaptic transmission: Neuromuscular junction and CNS circuit. *PLoS ONE*, *13*(7), 1–20. https://doi.org/10.1371/journal.pone.0200107

Mattioli, F., Piton, A., Gérard, B., Superti-Furga, A., Mandel, J. L., & Unger, S. (2016). Novel de novo

mutations in ZBTB20 in Primrose syndrome with congenital hypothyroidism. *American Journal of Medical Genetics, Part A*, *170*(6), 1626–1629. https://doi.org/10.1002/ajmg.a.37645

McGregor, C. E., Irwin, A. M., & English, A. W. (2019). The Val66Met BDNF Polymorphism and Peripheral Nerve Injury: Enhanced Regeneration in Mouse Met-Carriers Is Not Further Improved With Activity-Dependent Treatment. *Neurorehabilitation and Neural Repair*, *33*(6), 407–418. https://doi.org/10.1177/1545968319846131

McMahon, J. A., & McMahon, A. P. (1989). Nucleotide sequence, chromosomal localization and developmental expression of the mouse int-1-related gene. *Development*, *107*(3), 643–650. https://doi.org/10.1242/dev.107.3.643

Medda, X., Mertens, L., Versweyveld, S., Diels, A., Barnham, L., Bretteville, A., Buist, A., Verheyen, A., Royaux, I., Ebneth, A., & Cabrera-Socorro, A. (2016). Development of a Scalable, High-Throughput-Compatible Assay to Detect Tau Aggregates Using iPSC-Derived Cortical Neurons Maintained in a Three-Dimensional Culture Format. *Journal of Biomolecular Screening*, *21*(8), 804–815. https://doi.org/10.1177/1087057116638029

Michelsen, K. A., Acosta-Verdugo, S., Benoit-Marand, M., Espuny-Camacho, I., Gaspard, N., Saha, B., Gaillard, A., & Vanderhaeghen, P. (2015). Area-specific reestablishment of damaged circuits in the adult cerebral cortex by cortical neurons derived from mouse embryonic stem cells. *Neuron*, *85*(5), 982–997. https://doi.org/10.1016/j.neuron.2015.02.001

Mignone, J. L., Kukekov, V., Chiang, A. S., Steindler, D., & Enikolopov, G. (2004). Neural Stem and Progenitor Cells in Nestin-GFP Transgenic Mice. In *Journal of Comparative Neurology* (Vol. 469, Issue 3, pp. 311–324). https://doi.org/10.1002/cne.10964

Millard, D. C., Clements, M., & Ross, J. D. (2017). The CiPA Microelectrode Array Assay with hSC-Derived Cardiomyocytes: Current Protocol, Future Potential. In *Methods in Pharmacology and Toxicology* (pp. 83–107). https://doi.org/10.1007/978-1-4939-6661-5_5

Miller, J. A., Ding, S. L., Sunkin, S. M., Smith, K. A., Ng, L., Szafer, A., Ebbert, A., Riley, Z. L., Royall, J. J., Aiona, K., Arnold, J. M., Bennet, C., Bertagnolli, D., Brouner, K., Butler, S., Caldejon, S., Carey, A., Cuhaciyan, C., Dalley, R. A., … Lein, E. S. (2014). Transcriptional landscape of the prenatal human brain. *Nature*, *508*(7495), 199–206. https://doi.org/10.1038/nature13185

Ming, G. li, & Song, H. (2011). Adult Neurogenesis in the Mammalian Brain: Significant Answers and Significant Questions. *Neuron*, *70*(4), 687–702. https://doi.org/10.1016/j.neuron.2011.05.001

Miquelajauregui, A., Van De Putte, T. De, Polyakov, A., Nityanandam, A., Boppana, S., Seuntjens, E., Karabinos, A., Higashi, Y., Huylebroeck, D., & Tarabykin, V. (2007). Smad-interacting protein-1 (Zfhx1b) acts upstream of Wnt signaling in the mouse hippocampus and controls its formation. *Proceedings of the National Academy of Sciences of the United States of America*, *104*(31), 12919–12924. https://doi.org/10.1073/pnas.0609863104

Mira, H., Andreu, Z., Suh, H., Chichung Lie, D., Jessberger, S., Consiglio, A., Emeterio, J. S., Hortigüela, R., Marqués-Torrejón, M. Á., Nakashima, K., Colak, D., Götz, M., Fariñas, I., & Gage, F. H. (2010). Signaling through BMPR-IA regulates quiescence and long-term activity of neural stem cells in the adult hippocampus. *Cell Stem Cell*, *7*(1), 78–89. https://doi.org/10.1016/j.stem.2010.04.016

Mirescu, C., Peters, J. D., & Gould, E. (2004). Early life experience alters response of adult neurogenesis to stress. *Nature Neuroscience*, *7*(8), 841–846. https://doi.org/10.1038/nn1290

Mitchelmore, C., Kjærulff, K. M., Pedersen, H. C., Nielsen, J. V., Rasmussen, T. E., Fisker, M. F., Finsen, B., Pedersen, K. M., & Jensen, N. A. (2002). Characterization of two novel nuclear BTB/POZ domain zinc finger isoforms. Association with differentiation of hippocampal neurons, cerebellar granule cells, and macroglia. *Journal of Biological Chemistry*, *277*(9), 7598–7609. https://doi.org/10.1074/jbc.M110023200

Mitsui, K., Tokuzawa, Y., Itoh, H., Segawa, K., Murakami, M., Takahashi, K., Maruyama, M., Maeda, M., & Yamanaka, S. (2003). The homeoprotein nanog is required for maintenance of pluripotency in

mouse epiblast and ES cells. *Cell*, *113*(5), 631–642. https://doi.org/10.1016/S0092-8674(03)00393-3

Miura, Y., Li, M. Y., Birey, F., Ikeda, K., Revah, O., Thete, M. V., Park, J. Y., Puno, A., Lee, S. H., Porteus, M. H., & Pașca, S. P. (2020). Generation of human striatal organoids and cortico-striatal assembloids from human pluripotent stem cells. *Nature Biotechnology*, *38*(12), 1421–1430. https://doi.org/10.1038/s41587-020-00763-w

Miyata, T., Maeda, T., & Lee, J. E. (1999). NeuroD is required for differentiation of the granule cells in the cerebellum and hippocampus. *Genes and Development*, *13*(13), 1647–1652. https://doi.org/10.1101/gad.13.13.1647

Moodley, Y., Thompson, P., & Warburton, D. (2013). Stem cells: A recapitulation of development. *Respirology*, *18*(8), 1167–1176. https://doi.org/10.1111/resp.12186

Morgani, S. M., Metzger, J. J., Nichols, J., Siggia, E. D., & Hadjantonakis, A. K. (2018). Micropattern differentiation of mouse pluripotent stem cells recapitulates embryo regionalized cell fate patterning. *ELife*, *7*, 1–35. https://doi.org/10.7554/eLife.32839

Mucke, L., Masliah, E., Yu, G., Mallory, M., & Rockenstein, E. (2000). High-Level Neuronal Expression of Aβ1–42 in Wild-Type..Synaptotoxicity without Plaque Formation.pdf. *J Neurosci*, *20*(11), 4050–4058.

Muguruma, K., Nishiyama, A., Ono, Y., Miyawaki, H., Mizuhara, E., Hori, S., Kakizuka, A., Obata, K., Yanagawa, Y., Hirano, T., & Sasai, Y. (2010). Ontogeny-recapitulating generation and tissue integration of ES cell-derived Purkinje cells. *Nature Neuroscience*, *13*(10), 1171–1180. https://doi.org/10.1038/nn.2638

Mukohata, Y., Sugiyama, Y., Ihara, K., & Yoshida, M. (1988). An Australian halobacterium contains a novel proton pump retinal protein: Archaerhodopsin. *Biochemical and Biophysical Research Communications*, *151*(3), 1339–1345.

Müller, J., Ballini, M., Livi, P., Chen, Y., Radivojevic, M., Shadmani, A., Viswam, V., Jones, I. L., Fiscella, M., Diggelmann, R., Stettler, A., Frey, U., Bakkum, D. J., & Hierlemann, A. (2015). High-resolution CMOS MEA platform to study neurons at subcellular, cellular, and network levels. *Lab on a Chip*, *15*(13), 2767–2780. https://doi.org/10.1039/c5lc00133a

Müller, W. A. (1997). *Cell Differentiation Frequently Is Irreversible and Causes Cell Death; Early Cell Death Can Be Programmed BT - Developmental Biology* (W. A. Müller (ed.); pp. 222–227). Springer New York. https://doi.org/10.1007/978-1-4612-2248-4_11

Mulligan, K. A., & Cheyette, B. N. R. (2012). Wnt signaling in vertebrate neural development and function. *Journal of Neuroimmune Pharmacology*, *7*(4), 774–787. https://doi.org/10.1007/s11481-012-9404-x

Nagao, M., Ogata, T., Sawada, Y., & Gotoh, Y. (2016). Zbtb20 promotes astrocytogenesis during neocortical development. *Nature Communications*, *7*, 1–14. https://doi.org/10.1038/ncomms11102

Nagel, G., Brauner, M., Liewald, J. F., Adeishvili, N., Bamberg, E., & Gottschalk, A. (2005). Light activation of Channelrhodopsin-2 in excitable cells of caenorhabditis elegans triggers rapid behavioral responses. *Current Biology*, *15*(24), 2279–2284. https://doi.org/10.1016/j.cub.2005.11.032

Nagel, G., Ollig, D., Fuhrmann, M., Kateriya, S., Musti, A. M., Bamberg, E., & Hegemann, P. (2002). Channelrhodopsin-1: A light-gated proton channel in green algae. *Science*, *296*(5577), 2395–2398. https://doi.org/10.1126/science.1072068

Nagel, G., Szellas, T., Huhn, W., Kateriya, S., Adeishvili, N., Berthold, P., Ollig, D., Hegemann, P., & Bamberg, E. (2003). Channelrhodopsin-2, a directly light-gated cation-selective membrane Channel. *Pnas*, *100*(24), 13940–13945. https://doi.org/10.1073/pnas.1936192100

Nakahira, E., & Yuasa, S. (2005). Neuronal generation, migration, and differentiation in the mouse hippocampal primoridium as revealed by enhanced green fluorescent protein gene transfer by

means of in utero electroporation. *Journal of Comparative Neurology*, *483*(3), 329–340. https://doi.org/10.1002/cne.20441

Naldini, L., Blömer, U., Gallay, P., Ory, D., Mulligan, R., Gage, F. H., Verma, I. M., & Trono, D. (1996). In vivo gene delivery and stable transduction of nondividing cells by a lentiviral vector. *Science*, *272*(5259), 263–267. https://doi.org/10.1126/science.272.5259.263

Narahashi, T., Moore, J. W., & Scott, W. R. (1964). Tetrodotoxin Blockage of Sodium Conductance Increase in Lobster Giant Axons. *The Journal of General Physiology*, *47*, 965–974.

Nascimento, M. A., Sorokin, L., & Coelho-Sampaio, T. (2018). Fractone bulbs derive from ependymal cells and their laminin composition influence the stem cell niche in the subventricular zone. *Journal of Neuroscience*, *38*(16), 3880–3889. https://doi.org/10.1523/JNEUROSCI.3064-17.2018

Naujok, O., Lentes, J., Diekmann, U., Davenport, C., & Lenzen, S. (2014). Cytotoxicity and activation of the Wnt/beta-catenin pathway in mouse embryonic stem cells treated with four GSK3 inhibitors. *BMC Research Notes*, *7*(1), 1–8. https://doi.org/10.1186/1756-0500-7-273

Ni, Y., Liu, B., Wu, X., Liu, J., Ba, R., & Zhao, C. (2021). FOXG1 Directly Suppresses Wnt5a During the Development of the Hippocampus. *Neuroscience Bulletin*, *37*(3), 298–310. https://doi.org/10.1007/s12264-020-00618-z

Nichols, J., Zevnik, B., Anastassiadis, K., Niwa, H., Klewe-Nebenius, D., Chambers, I., Schöler, H., & Smith, A. (1998). Formation of pluripotent stem cells in the mammalian embryo depends on the POU transcription factor Oct4. *Cell*, *95*(3), 379–391. https://doi.org/10.1016/S0092-8674(00)81769-9

Nielsen, J. V., Nielsen, F. H., Ismail, R., Noraberg, J., & Jensen, N. A. (2007). Hippocampus-like corticoneurogenesis induced by two isoforms of the BTB-zinc finger gene Zbtb20 in mice. *Development*, *134*(6), 1133–1140. https://doi.org/10.1242/dev.000265

Nielsen, J. V., Thomassen, M., Møllgård, K., Noraberg, J., & Jensen, N. A. (2014). Zbtb20 defines a hippocampal neuronal identity through direct repression of genes that control projection neuron

development in the isocortex. *Cerebral Cortex*, *24*(5), 1216–1229. https://doi.org/10.1093/cercor/bhs400

Nielsen, J. V, Blom, J. B., Noraberg, J., & Jensen, N. A. (2010). Zbtb20-Induced CA1 Pyramidal Neuron Development and Area Enlargement in the Cerebral Midline Cortex of Mice. *Cerebral Cortex*, *20*(8), 1904–1914. https://doi.org/10.1093/cercor/bhp261

Niwa, H., Burdon, T., Chambers, I., & Smith, A. (1998). Self-renewal of pluripotent embryonic stem cells is mediated via activation of STAT3. In *Genes and Development* (Vol. 12, Issue 13, pp. 2048–2060). https://doi.org/10.1101/gad.12.13.2048

Noma, T., Yoon, Y. S., & Nakazawa, A. (1999). Overexpression of NeuroD in PC12 cells alters morphology and enhances expression of the adenylate kinase isozyme 1 gene. *Molecular Brain Research*, *67*(1), 53–63. https://doi.org/10.1016/S0169-328X(99)00038-8

Nusse, R., Van Ooyen, A., Cox, D., Fung, Y. K. T., & Varmus, H. (1984). Mode of proviral activation of a putative mammary oncogene (int-1) on mouse chromosome 15. *Nature*, *307*(5947), 131–136. https://doi.org/10.1038/307131a0

O'Keefe, J. (1976). Place units in the hippocampus of the freely moving rat. *Experimental Neurology*, *51*(1), 78–109. https://doi.org/10.1016/0014-4886(76)90055-8

Obien, M. E. J., Deligkaris, K., Bullmann, T., Bakkum, D. J., & Frey, U. (2015). Revealing neuronal function through microelectrode array recordings. *Frontiers in Neuroscience*, *9*(JAN), 423. https://doi.org/10.3389/fnins.2014.00423

Oesterhelt, D., & Stoeckenius, W. (1971). Rhodopsin-like protein from the purple membrane of Halobacterium halobium. *Nature New Biology*, *233*(39), 149–152. https://doi.org/10.1038/newbio233149a0

Ohta, E., Nihira, T., Uchino, A., Imaizumi, Y., Okada, Y., Akamatsu, W., Takahashi, K., Hayakawa, H., Nagai, M., Ohyama, M., Ryo, M., Ogino, M., Murayama, S., Takashima, A., Nishiyama, K., Mizuno,

Y., Mochizuki, H., Obata, F., & Okano, H. (2015). I2020T mutant LRRK2 iPSC-derived neurons in the Sagamihara family exhibit increased Tau phosphorylation through the AKT/GSK-3?? signaling pathway. *Human Molecular Genetics*, *24*(17), 4879–4900. https://doi.org/10.1093/hmg/ddv212

Ohtsuka, T., Ishibashi, M., Gradwohl, G., Nakanishi, S., Guillemot, F., & Kageyama, R. (1999). Hes1 and Hes5 as notch effectors in mammalian neuronal differentiation. *The EMBO Journal*, *18*(8), 2196–2207. https://doi.org/10.1093/emboj/18.8.2196

Okamoto, M., Inoue, K., Iwamura, H., Terashima, K., Soya, H., Asashima, M., & Kuwabara, T. (2011). Reduction in paracrine Wnt3 factors during aging causes impaired adult neurogenesis. *The FASEB Journal*, *25*(10), 3570–3582. https://doi.org/10.1096/fj.11-184697

Ouyang, A., Ng, R., & Yang, S.-T. (2007). Long-Term Culturing of Undifferentiated Embryonic Stem Cells in Conditioned Media and Three-Dimensional Fibrous Matrices Without Extracellular Matrix Coating. *Stem Cells*, *25*(2), 447–454. https://doi.org/10.1634/stemcells.2006-0322

Overstreet-Wadiche, L. S., Bromberg, D. A., Bensen, A. L., & Westbrook, G. L. (2006). Seizures accelerate functional integration of adult-generated granule cells. *The Journal of Neuroscience : The Official Journal of the Society for Neuroscience*, *26*(15), 4095–4103. https://doi.org/10.1523/JNEUROSCI.5508-05.2006

Overstreet-Wadiche, L. S., & Westbrook, G. L. (2006). Functional maturation of adult-generated granule cells. In *Hippocampus* (Vol. 16, Issue 3, pp. 208–215). https://doi.org/10.1002/hipo.20152

Overstreet, L. S., Hentges, S. T., Bumaschny, V. F., Souza, F. S. J. De, Smart, J. L., Santangelo, A. M., Low, M. J., Westbrook, G. L., & Rubinstein, M. (2004). *A Transgenic Marker for Newly Born Granule Cells in Dentate Gyrus*. *23*(13), 3251–3259. https://doi.org/10.1523/JNEUROSCI.5173-03.2004

Owen, S. F., Liu, M. H., & Kreitzer, A. C. (2019). Thermal constraints on in vivo optogenetic manipulations. *Nature Neuroscience*, *22*(7), 1061–1065. https://doi.org/10.1038/s41593-019-0422-3

Pallas-Bazarra, N., Jurado-Arjona, J., Navarrete, M., Esteban, J. A., Hernández, F., Ávila, J., & Llorens-Martín, M. (2016). Novel function of Tau in regulating the effects of external stimuli on adult hippocampal neurogenesis. *The EMBO Journal*, *35*(13), 1417–1436. https://doi.org/10.15252/embj.201593518

Palmer, T. D., Willhoite, A. R., & Gage, F. H. (2000). Vascular niche for adult hippocampal neurogenesis. *Journal of Comparative Neurology*, *425*(4), 479–494. https://doi.org/10.1002/1096-9861(20001002)425:4<479::AID-CNE2>3.0.CO;2-3

Pandolfini, L., Luzi, E., Bressan, D., Ucciferri, N., Bertacchi, M., Brandi, R., Rocchiccioli, S., D'Onofrio, M., & Cremisi, F. (2016). RISC-mediated control of selected chromatin regulators stabilizes ground state pluripotency of mouse embryonic stem cells. *Genome Biology*, *17*(1), 94. https://doi.org/10.1186/s13059-016-0952-x

Park, I. H., Lerou, P. H., Zhao, R., Huo, H., & Daley, G. Q. (2008). Generation of human-induced pluripotent stem cells. *Nature Protocols*, *3*(7), 1180–1186. https://doi.org/10.1038/nprot.2008.92

Park, J. W., Vahidi, B., Taylor, A. M., Rhee, S. W., & Jeon, N. L. (2006). Microfluidic culture platform for neuroscience research. *Nature Protocols*, *1*(4), 2128–2136. https://doi.org/10.1038/nprot.2006.316

Parr, B. A., Shea, M. J., Vassileva, G., & McMahon, A. P. (1993). Mouse Wnt genes exhibit discrete domains of expression in the early embryonic CNS and limb buds. *Development*, *119*(1), 247–261. https://doi.org/10.1242/dev.119.1.247

Parras, C. M., Galli, R., Britz, O., Soares, S., Galichet, C., Battiste, J., Johnson, J. E., Nakafaku, M., Vescovi, A., & Guillemot, F. (2004). Mash1 specifies neurons and oligodendrocytes in the postnatal brain. *EMBO Journal*, *23*(22), 4495–4505. https://doi.org/10.1038/sj.emboj.7600447

Paşca, A. M., Sloan, S. A., Clarke, L. E., Tian, Y., Makinson, C. D., Huber, N., Kim, C. H., Park, J.-Y., O'Rourke, N. A., Nguyen, K. D., Smith, S. J., Huguenard, J. R., Geschwind, D. H., Barres, B. A., &

Paşca, S. P. (2015). Functional cortical neurons and astrocytes from human pluripotent stem cells in 3D culture. *Nature Methods*, *12*(7), 671–678. https://doi.org/10.1038/nmeth.3415

Paşca, S. P., Portmann, T., Voineagu, I., Yazawa, M., Shcheglovitov, A., Paşca, A. M., Cord, B., Palmer, T. D., Chikahisa, S., Nishino, S., Bernstein, J. A., Hallmayer, J., Geschwind, D. H., & Dolmetsch, R. E. (2011). Using iPSC-derived neurons to uncover cellular phenotypes associated with Timothy syndrome. *Nature Medicine*, *17*(12), 1657–1662. https://doi.org/10.1038/nm.2576

Pear, W. S., Nolan, G. P., Scott, M. L., & Baltimore, D. (1993). Production of high-titer helper-free retroviruses by transient transfection. *Proceedings of the National Academy of Sciences of the United States of America*, *90*(18), 8392–8396. https://doi.org/10.1073/pnas.90.18.8392

Pégard, N. C., Mardinly, A. R., Oldenburg, I. A., Sridharan, S., Waller, L., & Adesnik, H. (2017). Three-dimensional scanless holographic optogenetics with temporal focusing (3D-SHOT). *Nature Communications*, *8*(1), 1–14. https://doi.org/10.1038/s41467-017-01031-3

Peignon, G., Durand, A., Cacheux, W., Ayrault, O., Terris, B., Laurent-Puig, P., Shroyer, N. F., Van Seuningen, I., Honjo, T., Perret, C., & Romagnolo, B. (2011). Complex interplay between β-catenin signalling and Notch effectors in intestinal tumorigenesis. *Gut*, *60*(2), 166–176. https://doi.org/10.1136/gut.2009.204719

Pellegrini, M., Mansouri, A., Simeone, A., Boncinelli, E., & Gruss, P. (1996). Dentate gyrus formation requires Emx2. *Development*, *122*(12), 3893–3898.

Perny, M., Ting, C. C., Kleinlogel, S., Senn, P., & Roccio, M. (2017). Generation of otic sensory neurons from mouse embryonic stem cells in 3D culture. *Frontiers in Cellular Neuroscience*, *11*(December), 1–12. https://doi.org/10.3389/fncel.2017.00409

Perusini, J. N., Cajigas, S. A., Cohensedgh, O., Lim, S. C., Pavlova, I. P., Donaldson, Z. R., & Denny, C. A. (2017). Optogenetic stimulation of dentate gyrus engrams restores memory in Alzheimer's disease mice. *Hippocampus*, *27*(10), 1110–1122. https://doi.org/10.1002/hipo.22756

Pleasure, S. J., Collins, A. E., & Lowenstein, D. H. (2000). Unique expression patterns of cell fate molecules delineate sequential stages of dentate gyrus development. *Journal of Neuroscience*, *20*(16), 6095–6105. https://doi.org/10.1523/jneurosci.20-16-06095.2000

Primrose, D. A. (1982). A slowly progressive degenerative condition characterized by mental deficiency, wasting of limb musculature and bone abnormalities, including ossification of the pinnae. *Journal of Mental Deficiency Research*, *26 (Pt 2)*(2), 101–106. https://doi.org/10.1111/j.1365-2788.1982.tb00133.x

Puelles, L., Kuwana, E., Puelles, E., Bulfone, A., Shimamura, K., Keleher, J., Smiga, S., & Rubenstein, J. L. R. (2000). Pallial and subpallial derivatives in the embryonic chick and mouse telencephalon, traced by the expression of the genes Dlx-2, Emx-1, Nkx-2.1, Pax-6, and Tbr-1. *Journal of Comparative Neurology*, *424*(3), 409–438. https://doi.org/10.1002/1096-9861(20000828)424:3<409::AID-CNE3>3.0.CO;2-7

Qian, X., Nguyen, H. N., Song, M. M., Hadiono, C., Ogden, S. C., Hammack, C., Yao, B., Hamersky, G. R., Jacob, F., Zhong, C., Yoon, K. J., Jeang, W., Lin, L., Li, Y., Thakor, J., Berg, D. A., Zhang, C., Kang, E., Chickering, M., … Ming, G. L. (2016). Brain-Region-Specific Organoids Using Mini-bioreactors for Modeling ZIKV Exposure. *Cell*, *165*(5), 1238–1254. https://doi.org/10.1016/j.cell.2016.04.032

Qiu, M., Bulfone, A., Martinez, S., Meneses, J. J., Shimamura, K., Pedersen, R. A., & Rubenstein, J. L. R. (1995). Null mutation of Dlx-2 results in abnormal morphogenesis of proximal first and second branchial arch derivatives and abnormal differentiation in the forebrain. *Genes and Development*, *9*(20), 2523–2538. https://doi.org/10.1101/gad.9.20.2523

Qu, Q., Sun, G., Murai, K., Ye, P., Li, W., Asuelime, G., Cheung, Y.-T., & Shi, Y. (2013). Wnt7a Regulates Multiple Steps of Neurogenesis. *Molecular and Cellular Biology*, *33*(13), 2551–2559. https://doi.org/10.1128/mcb.00325-13

Quadrato, G., Elnaggar, M. Y., Duman, C., Sabino, A., Forsberg, K., & Di Giovanni, S. (2014). Modulation

of GABAA receptor signaling increases neurogenesis and suppresses anxiety through NFATc4. *Journal of Neuroscience*, *34*(25), 8630–8645. https://doi.org/10.1523/JNEUROSCI.0047-14.2014

Quadrato, G., Nguyen, T., Macosko, E. Z., Sherwood, J. L., Yang, S. M., Berger, D. R., Maria, N., Scholvin, J., Goldman, M., Kinney, J. P., Boyden, E. S., Lichtman, J. W., Williams, Z. M., McCarroll, S. A., & Arlotta, P. (2017). Cell diversity and network dynamics in photosensitive human brain organoids. *Nature*, *545*(7652), 48–53. https://doi.org/10.1038/nature22047

Quattrocolo, G., Fishell, G., & Petros, T. J. (2017). Heterotopic Transplantations Reveal Environmental Influences on Interneuron Diversity and Maturation. *Cell Reports*, *21*(3), 721–731. https://doi.org/10.1016/j.celrep.2017.09.075

Racaud-Sultan, C., & Vergnolle, N. (2021). GSK3β, a Master Kinase in the Regulation of Adult Stem Cell Behavior. In *Cells* (Vol. 10, Issue 2). https://doi.org/10.3390/cells10020225

Raja, W. K., Mungenast, A. E., Lin, Y.-T., Ko, T., Abdurrob, F., Seo, J., & Tsai, L.-H. (2016). Self-Organizing 3D Human Neural Tissue Derived from Induced Pluripotent Stem Cells Recapitulate Alzheimer's Disease Phenotypes. *Plos One*, *11*(9), e0161969. https://doi.org/10.1371/journal.pone.0161969

Rakic, P. (2009). Evolution of the neocortex: A perspective from developmental biology. *Nature Reviews Neuroscience*, *10*(10), 724–735. https://doi.org/10.1038/nrn2719

Ramos-Fernández, E., Tapia-Rojas, C., Ramírez, V. T., & Inestrosa, N. C. (2019). Wnt-7a Stimulates Dendritic Spine Morphogenesis and PSD-95 Expression Through Canonical Signaling. *Molecular Neurobiology*, *56*(3), 1870–1882. https://doi.org/10.1007/s12035-018-1162-1

Ramsden, H. L., Sürmeli, G., McDonagh, S. G., & Nolan, M. F. (2015). Laminar and Dorsoventral Molecular Organization of the Medial Entorhinal Cortex Revealed by Large-scale Anatomical Analysis of Gene Expression. *PLoS Computational Biology*, *11*(1), 1–38. https://doi.org/10.1371/journal.pcbi.1004032

Rankin, J., Strachan, T., Lako, M., & Lindsay, S. (1999). Partial cloning and assignment of WNT6 to human

chromosome band 2q35 by in situ hybridization. *Cytogenetics and Cell Genetics*, *84*(1–2), 50–52. https://doi.org/10.1159/000015212

Regalado-Reyes, M., Furcila, D., Hernández, F., Ávila, J., Defelipe, J., & León-Espinosa, G. (2019). Phospho-tau changes in the human CA1 during Alzheimer's disease progression. *Journal of Alzheimer's Disease*, *69*(1), 277–288. https://doi.org/10.3233/JAD-181263

Reilly, P., Winston, C. N., Baron, K. R., Trejo, M., Rockenstein, E. M., Akers, J. C., Kfoury, N., Diamond, M., Masliah, E., Rissman, R. A., & Yuan, S. H. (2017). Novel human neuronal tau model exhibiting neurofibrillary tangles and transcellular propagation. *Neurobiology of Disease*, *106*, 222–234. https://doi.org/10.1016/j.nbd.2017.06.005

Ren, A., Zhang, H., Xie, Z., Ma, X., Ji, W., He, D. Z. Z., Yuan, W., Ding, Y. Q., Zhang, X. H., & Zhang, W. J. (2012). Regulation of hippocampus-dependent memory by the zinc finger protein Zbtb20 in mature CA1 neurons. *Journal of Physiology*, *590*(19), 4917–4932. https://doi.org/10.1113/jphysiol.2012.234187

Repina, N. A., Mcclave, T., Johnson, H. J., Bao, X., Kane, R. S., Schaffer, D. V, Repina, N. A., Mcclave, T., Johnson, H. J., Bao, X., & Kane, R. S. (2020). Resource Engineered Illumination Devices for Optogenetic Control of Cellular Signaling Dynamics ll ll Engineered Illumination Devices for Optogenetic Control of Cellular Signaling Dynamics. *CellReports*, *31*(10), 107737. https://doi.org/10.1016/j.celrep.2020.107737

Reshef, R., Kreisel, T., Beroukhim Kay, D., & Yirmiya, R. (2014). Microglia and their CX3CR1 signaling are involved in hippocampal- but not olfactory bulb-related memory and neurogenesis. *Brain, Behavior, and Immunity*, *41*(1), 239–250. https://doi.org/10.1016/j.bbi.2014.04.009

Richardson, M., Redmond, D., Watson, C. J., & Mason, J. O. (1999). Mouse Wnt8B is expressed in the developing forebrain and maps to Chromosome 19. *Mammalian Genome*, *10*(9), 923–925. https://doi.org/10.1007/s003359901115

Rickmann, M., Amaral, D. G., & Cowan, W. M. (1987). Organization of radial glial cells during the development of the rat dentate gyrus. *Journal of Comparative Neurology*, *264*(4), 449–479. https://doi.org/10.1002/cne.902640403

Riederer, B. M. (1992). Differential phosphorylation of some proteins of the neuronal cytoskeleton during brain development. *Histochemical Journal*, *24*(11), 783–790. https://doi.org/10.1007/BF01046350

Ripamonti, S., Shomroni, O., Rhee, J. S., Chowdhury, K., Jahn, O., Hellmann, K. P., Bonn, S., Brose, N., & Tirard, M. (2020). SUMOylation controls the neurodevelopmental function of the transcription factor Zbtb20. *Journal of Neurochemistry*, *March*, 1–15. https://doi.org/10.1111/jnc.15008

Rodriguez, A. (2004). Identification of Mammalian microRNA Host Genes and Transcription Units. *Genome Research*, *14*(10a), 1902–1910. https://doi.org/10.1101/gr.2722704

Roelink, H., & Nusse, R. (1990). Expression of two members of the Wnt family during mouse development-restricted temporal and spatial patterns in the developing neural tube. *Genes and Development*, *5*(3), 381–388. https://doi.org/10.1101/gad.5.3.381

Roelink, H., Wagenaar, E., Lopes Da Silva, S., & Nusse, R. (1990). Wnt-3, a gene activated by proviral insertion in mouse mammary tumors, is homologous to int-1/Wnt-1 and is normally expressed in mouse embryos and adult brain. *Proceedings of the National Academy of Sciences of the United States of America*, *87*(12), 4519–4523. https://doi.org/10.1073/pnas.87.12.4519

Roelink, Henk, Wang, J., Black, D. M., Solomon, E., & Nusse, R. (1993). Molecular cloning and chromosomal localization to 17q21 of the human wnt3 gene. In *Genomics* (Vol. 17, Issue 3, pp. 790–792). https://doi.org/10.1006/geno.1993.1412

Romito, A., & Cobellis, G. (2016). Pluripotent stem cells: Current understanding and future directions. *Stem Cells International*, *2016*(Icm). https://doi.org/10.1155/2016/9451492

Rose, G. M., & Dunwiddie, T. V. (1986). Induction of hippocampal long-term potentiation using

physiologically patterned stimulation. *Neuroscience Letters*, *69*(3), 244–248. https://doi.org/10.1016/0304-3940(86)90487-8

Rosenthal, E. H., Tonchev, A. B., Stoykova, A., & Chowdhury, K. (2012). Regulation of archicortical arealization by the transcription factor Zbtb20. *Hippocampus*, *22*(11), 2144–2156. https://doi.org/10.1002/hipo.22035

Rosso, S. B., & Inestrosa, N. C. (2013). WNT signalling in neuronal maturation and synaptogenesis. *Frontiers in Cellular Neuroscience*, *7*(JUNE), 1–11. https://doi.org/10.3389/fncel.2013.00103

Rueckeman, J. W., Di Mauro, A. J., Rangel, L. M., Han, X., Boyden, E. S., & Eichenbaum, H. (2016). Transient optogenetic inactivation of the medial entorhinal cortex biases the active population of hippocampal neurons. *Hippocampus*, *26*(2), 246–260. https://doi.org/10.1002/hipo.22519

Rutecki, P. A., Grossmann, R. G., Armstrong, D., & Irish-Loewen, S. (1989). Electrophysiological connections between the hippocampus and entorhinal cortex in patients with complex partial seizures. *Journal of Neurosurgery*, *70*(5), 667–675. https://doi.org/10.3171/jns.1989.70.5.0667

Ryu, J. R., Hong, C. J., Kim, J. Y., Kim, E. K., Sun, W., & Yu, S. W. (2016). Control of adult neurogenesis by programmed cell death in the mammalian brain. *Molecular Brain*, *9*(1), 1–20. https://doi.org/10.1186/s13041-016-0224-4

Sahel, J., Boulanger-Scemama, E., Pagot, C., Arleo, A., Galluppi, F., Martel, J. N., Esposti, S. D., Delaux, A., de Saint Aubert, J.-B., de Montleau, C., Gutman, E., Audo, I., Duebel, J., Picaud, S., Dalkara, D., Blouin, L., Taiel, M., & Roska, B. (2021). Partial recovery of visual function in a blind patient after optogenetic therapy. *Nature Medicine*. https://doi.org/10.1038/s41591-021-01351-4

Saitoh, T., Hirai, M., & Katoh, M. (2001). Molecular cloning and characterization of WNT3A and WNT14 clustered in human chromosome 1q42 region. *Biochemical and Biophysical Research Communications*, *284*(5), 1168–1175. https://doi.org/10.1006/bbrc.2001.5105

Saitoh, T., & Katoh, M. (2001a). Molecular cloning and characterization of human WNT8A. *International*

Journal of Oncology, *9*(2), 153–157. https://doi.org/10.3892/ijo.19.1.123

Saitoh, T., & Katoh, M. (2001b). Molecular cloning and characterization of human WNT5B on chromosome 12p13.3 region. *International Journal of Oncology*, *19*(5), 977–982. https://doi.org/10.3892/ijo.19.2.347

Sakaguchi, H., Kadoshima, T., Soen, M., Narii, N., Ishida, Y., Ohgushi, M., Takahashi, J., Eiraku, M., & Sasai, Y. (2015). Generation of functional hippocampal neurons from self-organizing human embryonic stem cell-derived dorsomedial telencephalic tissue. *Nature Communications*, *6*, 1–11. https://doi.org/10.1038/ncomms9896

Salas, C., Broglio, C., & Rodríguez, F. (2003). Evolution of forebrain and spatial cognition in vertebrates: Conservation across diversity. *Brain, Behavior and Evolution*, *62*(2), 72–82. https://doi.org/10.1159/000072438

Sarkar, A., Mei, A., Paquola, A. C. M., Stern, S., Bardy, C., Klug, J. R., Kim, S., Neshat, N., Kim, H. J., Ku, M., Shokhirev, M. N., Adamowicz, D. H., Marchetto, M. C., Jappelli, R., Erwin, J. A., Padmanabhan, K., Shtrahman, M., Jin, X., & Gage, F. H. (2018). Efficient Generation of CA3 Neurons from Human Pluripotent Stem Cells Enables Modeling of Hippocampal Connectivity In Vitro. *Cell Stem Cell*, *22*(5), 684-697.e9. https://doi.org/10.1016/j.stem.2018.04.009

Sasaki, T., Takagi, J., Giudici, C., Yamada, Y., Arikawa-hirasawa, E., Deutzmann, R., Timpl, R., Sonnenberg, A., Peter, H., & Tonge, D. (2010). Laminin-121 — Recombinant expression and interactions with integrins. *Matrix Biology*, *29*(6), 484–493. https://doi.org/10.1016/j.matbio.2010.05.004

Scalise, M., Galluccio, M., Console, L., Pochini, L., & Indiveri, C. (2018). The human SLC7A5 (LAT1): The intriguing histidine/large neutral amino acid transporter and its relevance to human health. *Frontiers in Chemistry*, *6*(JUN), 1–12. https://doi.org/10.3389/fchem.2018.00243

Scharfman, H. E., & MacLusky, N. J. (2006). Estrogen and brain-derived neurotrophic factor (BDNF) in hippocampus: Complexity of steroid hormone-growth factor interactions in the adult CNS.

Frontiers in Neuroendocrinology, *27*(4), 415–435. https://doi.org/10.1016/j.yfrne.2006.09.004

Schie, I. W., Weeks, T., McNerney, G. P., Fore, S., Sampson, J. K., Wachsmann-Hogiu, S., Rutledge, J. C., & Huser, T. (2008). Simultaneous forward and epi-CARS microscopy with a single detector by time-correlated single photon counting. *Optics Express*, *16*(3), 2168–2175. https://doi.org/10.1364/OE.16.002168

Schild, L. C., & Glauser, D. A. (2015). Dual Color Neural Activation and Behavior Control with Chrimson and CoChR in Caenorhabditis elegans. *Genetics*, *200*(4), 1029–1034. https://doi.org/10.1534/genetics.115.177956

Schmidt-Hieber, C., Jones, P., & Bischofberger, J. (2004). Enhanced synaptic plasticity in newly generated granule cells of the adult hippocampus. *Nature*, *429*(6988), 184–187. https://doi.org/10.1038/nature02553

Schobert, B., & Lanyi, J. K. (1982). Halorhodopsin is a light-driven chloride pump. *Journal of Biological Chemistry*, *257*(17), 10306–10313.

Schwarz, B. A., Bar-Nur, O., Silva, J. C. R., & Hochedlinger, K. (2014). Nanog is dispensable for the generation of induced pluripotent stem cells. *Current Biology*, *24*(3), 347–350. https://doi.org/10.1016/j.cub.2013.12.050

Schwarz, T. J., Ebert, B., & Lie, D. C. (2012). Stem cell maintenance in the adult mammalian hippocampus: A matter of signal integration? *Developmental Neurobiology*, *72*(7), 1006–1015. https://doi.org/10.1002/dneu.22026

Schwerdtfeger, W. K. (1979). Direct efferent and afferent connections of the hippocampus with the neocortex in the marmoset monkey. *American Journal of Anatomy*, *156*(1), 77–82. https://doi.org/10.1002/aja.1001560107

Seki, T., Sato, T., Toda, K., Osumi, N., Imura, T., & Shioda, S. (2014). Distinctive population of Gfap-expressing neural progenitors arising around the dentate notch migrate and form the granule cell

layer in the developing hippocampus. In *Journal of Comparative Neurology* (Vol. 522, Issue 2, pp. 261–283). https://doi.org/10.1002/cne.23460

Sengupta, A., Chaffiol, A., Macé, E., Caplette, R., Desrosiers, M., Lampič, M., Forster, V., Marre, O., Lin, J. Y., Sahel, J., Picaud, S., Dalkara, D., & Duebel, J. (2016). Red-shifted channelrhodopsin stimulation restores light responses in blind mice, macaque retina, and human retina. *EMBO Molecular Medicine*, *8*(11), 1248–1264. https://doi.org/10.15252/emmm.201505699

Shi, G., & Jin, Y. (2010). Role of Oct4 in maintaining and regaining stem cell pluripotency. *Stem Cell Research & Therapy*, *1*(5), 39. https://doi.org/10.1186/scrt39

Shi, Y., Kirwan, P., & Livesey, F. J. (2012). Directed differentiation of human pluripotent stem cells to cerebral cortex neurons and neural networks. *Nature Protocols*, *7*(10), 1836–1846. https://doi.org/10.1038/nprot.2012.116

Shi, Y., Kirwan, P., Smith, J., Robinson, H. P. C., & Livesey, F. J. (2012). Human cerebral cortex development from pluripotent stem cells to functional excitatory synapses. *Nature Neuroscience*, *15*(3), 477–486. https://doi.org/10.1038/nn.3041

Siano, G., Caiazza, M. C., Ollà, I., Varisco, M., Madaro, G., Quercioli, V., Calvello, M., Cattaneo, A., & Di Primio, C. (2019). Identification of an ERK Inhibitor as a Therapeutic Drug Against Tau Aggregation in a New Cell-Based Assay. *Frontiers in Cellular Neuroscience*, *13*(August), 1–10. https://doi.org/10.3389/fncel.2019.00386

Sierra, A., Encinas, J. M., Deudero, J. J. P., Chancey, J. H., Enikolopov, G., Overstreet-Wadiche, L. S., Tsirka, S. E., & Maletic-Savatic, M. (2010). Microglia Shape Adult Hippocampal Neurogenesis through Apoptosis-Coupled Phagocytosis. *Cell Stem Cell*, *7*(4), 483–495. https://doi.org/10.1016/j.stem.2010.08.014

Sievers, J., Hartmann, D., Pehlemann, F. W., & Berry, M. (1992). Development of astroglial cells in the proliferative matrices, the granule cell layer, and the hippocampal fissure of the hamster dentate

gyrus. *Journal of Comparative Neurology*, *320*(1), 1–32. https://doi.org/10.1002/cne.903200102

Simon, R., Baumann, L., Fischer, J., Seigfried, F. A., De Bruyckere, E., Liu, P., Jenkins, N. A., Copeland, N. G., Schwegler, H., & Britsch, S. (2016). Structure-function integrity of the adult hippocampus depends on the transcription factor Bcl11b/Ctip2. *Genes, Brain and Behavior*, *15*(4), 405–419. https://doi.org/10.1111/gbb.12287

Simon, Ruth, Brylka, H., Schwegler, H., Venkataramanappa, S., Andratschke, J., Wiegreffe, C., Liu, P., Fuchs, E., Jenkins, N. A., Copeland, N. G., Birchmeier, C., & Britsch, S. (2012). A dual function of Bcl11b/Ctip2 in hippocampal neurogenesis. *EMBO Journal*, *31*(13), 2922–2936. https://doi.org/10.1038/emboj.2012.142

Snyder, J. S., Kee, N., & Wojtowicz, J. M. (2001). Effects of adult neurogenesis on synaptic plasticity in the rat dentate gyrus. *Journal of Neurophysiology*, *85*(6), 2423–2431. https://doi.org/10.1152/jn.2001.85.6.2423

Soldner, F., Hockemeyer, D., Beard, C., Gao, Q., Bell, G. W., Cook, E. G., Hargus, G., Blak, A., Cooper, O., Mitalipova, M., Isacson, O., & Jaenisch, R. (2009). Parkinson's Disease Patient-Derived Induced Pluripotent Stem Cells Free of Viral Reprogramming Factors. *Cell*, *136*(5), 964–977. https://doi.org/10.1016/j.cell.2009.02.013

Song, J., Sun, J., Moss, J., Wen, Z., Sun, G. J., Hsu, D., Zhong, C., Davoudi, H., Christian, K. M., Toni, N., Ming, G. L., & Song, H. (2013). Parvalbumin interneurons mediate neuronal circuitry-neurogenesis coupling in the adult hippocampus. *Nature Neuroscience*, *16*(12), 1728–1730. https://doi.org/10.1038/nn.3572

Song, J., Zhong, C., Bonaguidi, M. A., Sun, G. J., Hsu, D., Gu, Y., Meletis, K., Huang, Z. J., Ge, S., Enikolopov, G., Deisseroth, K., Luscher, B., Christian, K., Ming, G., & Song, H. (2012). Neuronal circuitry mechanism regulating adult quiescent neural stem cell fate decision. *Nature*, *489*(7414), 150–154. https://doi.org/10.1038/nature11306

Sposito, T., Preza, E., Mahoney, C. J., Set??-Salvia, N., Ryan, N. S., Morris, H. R., Arber, C., Devine, M. J., Houlden, H., Warner, T. T., Bushell, T. J., Zagnoni, M., Kunath, T., Livesey, F. J., Fox, N. C., Rossor, M. N., Hardy, J., & Wray, S. (2015). Developmental regulation of tau splicing is disrupted in stem cell-derived neurons from frontotemporal dementia patients with the 10 + 16 splice-site mutation in MAPT. *Human Molecular Genetics*, *24*(18), 5260–5269. https://doi.org/10.1093/hmg/ddv246

Stanfield, B. B., & Cowan, W. M. (1979). The development of the hippocampus and dentate gyrus in normal and reeler mice. *Journal of Comparative Neurology*, *185*(3), 423–459. https://doi.org/10.1002/cne.901850303

Staubli, U., & Lynch, G. (1990). Stable depression of potentiated synaptic responses in the hippocampus with 1-5 Hz stimulation. *Brain Research*, *513*(1), 113–118. https://doi.org/10.1016/0006-8993(90)91096-Y

Stellacci, E., Steindl, K., Joset, P., Mercurio, L., Anselmi, M., Cecchetti, S., Gogoll, L., Zweier, M., Hackenberg, A., Bocchinfuso, G., Stella, L., Tartaglia, M., & Rauch, A. (2018). Clinical and functional characterization of two novel ZBTB20 mutations causing Primrose syndrome. *Human Mutation*, *39*(7), 959–964. https://doi.org/10.1002/humu.23546

Stepan, J., Dine, J., & Eder, M. (2015). Functional optical probing of the hippocampal trisynaptic circuit in vitro: Network dynamics, filter properties, and polysynaptic induction of CA1 LTP. *Frontiers in Neuroscience*, *9*(APR), 1–9. https://doi.org/10.3389/fnins.2015.00160

Streckfuss-Bömeke, K., Vlasov, A., Hülsmann, S., Yin, D., Nayernia, K., Engel, W., Hasenfuss, G., & Guan, K. (2009). Generation of functional neurons and glia from multipotent adult mouse germ-line stem cells. *Stem Cell Research*, *2*(2), 139–154. https://doi.org/10.1016/j.scr.2008.09.001

Sugar, J., Witter, M. P., van Strien, N. M., & Cappaert, N. L. M. (2011). The retrosplenial cortex: Intrinsic connectivity and connections with the (para)hippocampal region in the rat. An interactive connectome. *Frontiers in Neuroinformatics*, *5*(July), 1–13.

https://doi.org/10.3389/fninf.2011.00007

Sugiyama, Y., Yamada, N., & Mukohata, Y. (1994). The light-driven proton pump, cruxrhodopsin-2 in Haloarcula sp. arg-2 (bR+, hR-), and its coupled ATP formation. In *BBA - Bioenergetics* (Vol. 1188, Issue 3, pp. 287–292). https://doi.org/10.1016/0005-2728(94)90047-7

Sun, X.-Y., Tuo, Q.-Z., Liuyang, Z.-Y., Xie, A.-J., Feng, X.-L., Yan, X., Qiu, M., Li, S., Wang, X.-L., Cao, F.-Y., Wang, X.-C., Wang, J.-Z., & Liu, R. (2016). Extrasynaptic NMDA receptor-induced tau overexpression mediates neuronal death through suppressing survival signaling ERK phosphorylation. *Cell Death and Disease*, *7*(11), e2449. https://doi.org/10.1038/cddis.2016.329

Takahashi, K., & Yamanaka, S. (2006). Induction of Pluripotent Stem Cells from Mouse Embryonic and Adult Fibroblast Cultures by Defined Factors. *Cell*, *126*(4), 663–676. https://doi.org/10.1016/j.cell.2006.07.024

Tanapat, P., Hastings, N. B., Reeves, A. J., & Gould, E. (1999). Estrogen stimulates a transient increase in the number of new neurons in the dentate gyrus of the adult female rat. *Journal of Neuroscience*, *19*(14), 5792–5801. https://doi.org/10.1523/jneurosci.19-14-05792.1999

Tang, X., Kim, J., Zhou, L., Wengert, E., Zhang, L., Wu, Z., Carromeu, C., Muotri, A. R., Marchetto, M. C. N., Gage, F. H., & Chen, G. (2016). KCC2 rescues functional deficits in human neurons derived from patients with Rett syndrome. *Proceedings of the National Academy of Sciences of the United States of America*, *113*(3), 751–756. https://doi.org/10.1073/pnas.1524013113

Tashiro, A., Makino, H., & Gage, F. H. (2007). Experience-specific functional modification of the dentate gyrus through adult neurogenesis: A critical period during an immature stage. *Journal of Neuroscience*, *27*(12), 3252–3259. https://doi.org/10.1523/JNEUROSCI.4941-06.2007

Taylor, A. M., Blurton-Jones, M., Rhee, S. W., Cribbs, D. H., Cotman, C. W., & Jeon, N. L. (2005). A microfluidic culture platform for CNS axonal injury, regeneration and transport. *Nature Methods*, *2*(8), 599–605. https://doi.org/10.1038/nmeth777

Telias, M., Segal, M., & Ben-Yosef, D. (2013). Neural differentiation of fragile X human embryonic stem cells reveals abnormal patterns of development despite successful neurogenesis. *Developmental Biology*, *374*(1), 32–45. https://doi.org/10.1016/j.ydbio.2012.11.031

Terrigno, M., Busti, I., Alia, C., Pietrasanta, M., Arisi, I., D'Onofrio, M., Caleo, M., & Cremisi, F. (2018). Neurons Generated by Mouse ESCs with Hippocampal or Cortical Identity Display Distinct Projection Patterns When Co-transplanted in the Adult Brain. *Stem Cell Reports*, *10*(3), 1016–1029. https://doi.org/10.1016/j.stemcr.2018.01.010

Theil, T., Aydin, S., Koch, S., Grotewold, L., & Rüther, U. (2002). Wnt and Bmp signalling cooperatively regulate graded Emx2 expression in the dorsal telencephalon. *Development*, *129*(13), 3045–3054. https://doi.org/10.1242/dev.129.13.3045

Thompson, L. T., & Best, P. J. (1990). Long-term stability of the place-field activity of single units recorded from the dorsal hippocampus of freely behaving rats. *Brain Research*, *509*(2), 299–308. https://doi.org/10.1016/0006-8993(90)90555-P

Till, J. E., & McCulloch, E. A. (1961). A Direct Measurement of the Radiation Sensitivity of Normal Mouse Bone Marrow Cells Author (s): J . E . Till and E . A . McCulloch Published by : Radiation Research Society Stable URL : http://www.jstor.org/stable/3570892 A Direct Measurement of the Rad. *Radiation Research Society*, *14*(2), 213–222.

Tole, S., Christian, C., & Grove, E. A. (1997). Early specification and autonomous development of cortical fields in the mouse hippocampus. *Development*, *124*(24), 4959–4970.

Tole, S., & Grove, E. A. (2001). Detailed field pattern is intrinsic to the embryonic mouse hippocampus early in neurogenesis. *Journal of Neuroscience*, *21*(5), 1580–1589. https://doi.org/10.1523/jneurosci.21-05-01580.2001

Tonchev, A. B., Tuoc, T. C., Rosenthal, E. H., Studer, M., & Stoykova, A. (2016). Zbtb20 modulates the sequential generation of neuronal layers in developing cortex. *Molecular Brain*, *9*(1), 1–15.

https://doi.org/10.1186/s13041-016-0242-2

Tong, M., Hernandez, J. L., Purcell, E. K., Altschuler, R. A., & Duncan, R. K. (2010). The intrinsic electrophysiological properties of neurons derived from mouse embryonic stem cells overexpressing neurogenin-1. *American Journal of Physiology - Cell Physiology*, *299*(6), 1335–1344. https://doi.org/10.1152/ajpcell.00207.2010

Tozzini, E. T., Baumgart, M., Battistoni, G., & Cellerino, A. (2012). Adult neurogenesis in the short-lived teleost Nothobranchius furzeri: Localization of neurogenic niches, molecular characterization and effects of aging. *Aging Cell*, *11*(2), 241–251. https://doi.org/10.1111/j.1474-9726.2011.00781.x

Tukker, A. M., Wijnolts, F. M. J., de Groot, A., & Westerink, R. H. S. (2018). Human iPSC-derived neuronal models for in vitro neurotoxicity assessment. *NeuroToxicology*, *67*(June), 215–225. https://doi.org/10.1016/j.neuro.2018.06.007

Udo, H., Yoshida, Y., Kino, T., Ohnuki, K., Mizunoya, W., & Mukuda, T. (2008). *Enhanced Adult Neurogenesis and Angiogenesis and Altered Affective Behaviors in Mice Overexpressing Vascular Endothelial Growth Factor 120*. *28*(53), 14522–14536. https://doi.org/10.1523/JNEUROSCI.3673-08.2008

Uegaki, K., Sugiyama, Y., & Mukohata, Y. (1991). Archaerhodopsin-2, from Halobacterium sp. aus-2 further reveals essential amino acid residues for light-driven proton pumps. *Archives of Biochemistry and Biophysics*, *286*(1), 107—110. https://doi.org/10.1016/0003-9861(91)90014-a

Van den Heuvel, M., Harryman-Samos, C., Klingensmith, J., Perimon, N., & Nusse, R. (1993). Mutations in the segment polarity genes wingless and porcupine impair secretion of the wingless protein. *EMBO Journal*, *12*(13), 5293–5302. https://doi.org/10.1002/j.1460-2075.1993.tb06225.x

van Praag, H., Schinder, A. F., Christie, B. R., Toni, N., Palmer, T. D., Gage, F. H., Sito, E. ´, H, • Neuronal Development In The Adult Hippocampus Van Praag, Af, S., Br, C., N, T., Td, P., & Fh, G. (2002). Functional neurogenesis in the adult hippocampus. *Nature*, *415*(6875), 1030–1034.

https://doi.org/10.1038/4151030a

Van Praag, H., Shubert, T., Zhao, C., & Gage, F. H. (2005). Exercise enhances learning and hippocampal neurogenesis in aged mice. *Journal of Neuroscience*, *25*(38), 8680–8685. https://doi.org/10.1523/JNEUROSCI.1731-05.2005

Velasco, S., Kedaigle, A. J., Simmons, S. K., Nash, A., Rocha, M., Quadrato, G., Paulsen, B., Nguyen, L., Adiconis, X., Regev, A., Levin, J. Z., & Arlotta, P. (2019). Individual brain organoids reproducibly form cell diversity of the human cerebral cortex. *Nature*, *570*(7762), 523–527. https://doi.org/10.1038/s41586-019-1289-x

Vermersch, P., Frigard, B., David, J. P., Fallet-Bianco, C., & Delacourte, A. (1992). Presence of abnormally phosphorylated Tau proteins in the entorhinal cortex of aged non-demented subjects. *Neuroscience Letters*, *144*(1–2), 143–146. https://doi.org/10.1016/0304-3940(92)90736-Q

Villeda, S. A., Plambeck, K. E., Middeldorp, J., Castellano, J. M., Mosher, K. I., Luo, J., Smith, L. K., Bieri, G., Lin, K., Berdnik, D., Wabl, R., Udeochu, J., Wheatley, E. G., Zou, B., Simmons, D. A., Xie, X. S., Longo, F. M., & Wyss-Coray, T. (2014). Young blood reverses age-related impairments in cognitive function and synaptic plasticity in mice. *Nature Medicine*, *20*(6), 659–663. https://doi.org/10.1038/nm.3569

Vitali, I., Fièvre, S., Telley, L., Oberst, P., Bariselli, S., Frangeul, L., Baumann, N., McMahon, J. J., Klingler, E., Bocchi, R., Kiss, J. Z., Bellone, C., Silver, D. L., & Jabaudon, D. (2018). Progenitor Hyperpolarization Regulates the Sequential Generation of Neuronal Subtypes in the Developing Neocortex. *Cell*, *174*(5), 1264-1276.e15. https://doi.org/10.1016/j.cell.2018.06.036

Vivar, C., Potter, M. C., Choi, J., Lee, J. Y., Stringer, T. P., Callaway, E. M., Gage, F. H., Suh, H., & Van Praag, H. (2012). Monosynaptic inputs to new neurons in the dentate gyrus. *Nature Communications*, *3*(May). https://doi.org/10.1038/ncomms2101

Vlasits, A. (2016). He may have invented one of neuroscience's biggest advances. But you've never heard of him. *Stat*, 1–22.

Wainwright, B. J., Scambler, P. J., Stanier, P., Watson, E. K., Bell, G., Wicking, C., Estivill, X., Courtney, M., Boue, A., & Pedersen, P. S. (1988). Isolation of a human gene with protein sequence similarity to human and murine int-1 and the Drosophila segment polarity mutant wingless. *The EMBO Journal*, *7*(6), 1743–1748. https://doi.org/10.1002/j.1460-2075.1988.tb03003.x

Wamsley, B., Jaglin, X. H., Favuzzi, E., Quattrocolo, G., Nigro, M. J., Yusuf, N., Khodadadi-Jamayran, A., Rudy, B., & Fishell, G. (2018). Rbfox1 Mediates Cell-type-Specific Splicing in Cortical Interneurons. *Neuron*, *100*(4), 846-859.e7. https://doi.org/10.1016/j.neuron.2018.09.026

Wang, H. Y., Hsieh, P. F., Huang, D. F., Chin, P. S., Chou, C. H., Tung, C. C., Chen, S. Y., Lee, L. J., Gau, S. S. F., & Huang, H. S. (2015). RBFOX3/NeuN is Required for Hippocampal Circuit Balance and Function. *Scientific Reports*, *5*, 1–16. https://doi.org/10.1038/srep17383

Wang, J, & Shackleford, G. M. (1996). Murine Wnt10a and Wnt10b: cloning and expression in developing limbs, face and skin of embryos and in adults. *Oncogene*, *13*(7), 1537—1544. http://europepmc.org/abstract/MED/8875992

Wang, Jianlong, Levasseur, D. N., & Orkin, S. H. (2008). Requirement of Nanog dimerization for stem cell self-renewal and pluripotency. *Proceedings of the National Academy of Sciences*, *105*(17), 6326–6331. https://doi.org/10.1073/pnas.0802288105

Wang, L. P., Kempermann, G., & Kettenmann, H. (2005). A subpopulation of precursor cells in the mouse dentate gyrus receives synaptic GABAergic input. *Molecular and Cellular Neuroscience*, *29*(2), 181–189. https://doi.org/10.1016/j.mcn.2005.02.002

Wang, Sabrina, Scott, B. W., & Wojtowicz, J. M. (2000). Heterogenous properties of dentate granule neurons in the adult rat. *Journal of Neurobiology*, *42*(2), 248–257. https://doi.org/10.1002/(SICI)1097-4695(20000205)42:2<248::AID-NEU8>3.0.CO;2-J

Wang, Shuyan, Wang, B., Pan, N., Fu, L., Wang, C., Song, G., An, J., Liu, Z., Zhu, W., Guan, Y., Xu, Z. Q. D., Chan, P., Chen, Z., & Zhang, Y. A. (2015). Differentiation of human induced pluripotent stem cells to

mature functional Purkinje neurons. *Scientific Reports*, *5*, 1–9. https://doi.org/10.1038/srep09232

Wataya, T., Ando, S., Muguruma, K., Ikeda, H., Watanabe, K., Eiraku, M., Kawada, M., Takahashi, J., Hashimoto, N., & Sasai, Y. (2008). Minimization of exogenous signals in ES cell culture induces rostral hypothalamic differentiation. *Proceedings of the National Academy of Sciences of the United States of America*, *105*(33), 11796–11801. https://doi.org/10.1073/pnas.0803078105

Watson, L. M., Wong, M. M. K., Vowles, J., Cowley, S. A., & Becker, E. B. E. (2018). A Simplified Method for Generating Purkinje Cells from Human-Induced Pluripotent Stem Cells. *Cerebellum*, *17*(4), 419–427. https://doi.org/10.1007/s12311-017-0913-2

Werk, C. M., Klein, H. S., Nesbitt, C. E., & Chapman, C. A. (2006). Long-term depression in the sensorimotor cortex induced by repeated delivery of 10 Hz trains in vivo. *Neuroscience*, *140*(1), 13–20. https://doi.org/10.1016/j.neuroscience.2006.02.004

Wernig, M., Benninger, F., Schmandt, T., Rade, M., Tucker, K. L., Büssow, H., Beck, H., & Brüstle, O. (2004). Functional integration of embryonic stem cell-derived neurons in vivo. *Journal of Neuroscience*, *24*(22), 5258–5268. https://doi.org/10.1523/JNEUROSCI.0428-04.200

Wexler, E. M., Paucer, A., Kornblum, H. I., Plamer, T. D., & Geschwind, D. H. (2009). Endogenous Wnt signaling maintains neural progenitor cell potency. *Stem Cells*, *27*(5), 1130–1141. https://doi.org/10.1002/stem.36

Wichterle, H., Wichterle, H., Lieberam, I., Lieberam, I., Porter, J. a, Porter, J. a, Jessell, T. M., & Jessell, T. M. (2002). Directed differentiation of embryonic stem cells into motor neurons. *Cell*, *110*(3), 385–397. https://doi.org/10.1016/S0092-8674(02)00835-8

Wiebe, S. P., & Stäubli, U. V. (1999). Dynamic filtering of recognition memory codes in the hippocampus. *Journal of Neuroscience*, *19*(23), 10562–10574. https://doi.org/10.1523/jneurosci.19-23-10562.1999

Wietek, J., & Prigge, M. (2016). Enhancing Channelrhodopsins: An Overview. In *Methods in*

MolecularBiology 1408 (Vol. 1408, Issue March, pp. 141–165). https://doi.org/10.1007/978-1-4939-3512-3_10

Wietek, J., Wiegert, J. S., Adeishvili, N., Schneider, F., Watanabe, H., Tsunoda, S. P., Vogt, A., Elstner, M., Oertner, T. G., & Hegemann, P. (2014). Conversion of channelrhodopsin into a light-gated chloride channel. *Science*, *344*(6182), 409–412. https://doi.org/10.1126/science.1249375

Wilson, I. A., Ikonen, S., Gureviciene, I., McMahan, R. W., Gallagher, M., Eichenbaum, H., & Tanila, H. (2004). Cognitive Aging and the Hippocampus: How Old Rats Represent New Environments. *Journal of Neuroscience*, *24*(15), 3870–3878. https://doi.org/10.1523/JNEUROSCI.5205-03.2004

Wiseman, J. W., Goddard, C. A., McLelland, D., & Colledge, W. H. (2003). A comparison of linear and branched polyethylenimine (PEI) with DCChol/DOPE liposomes for gene delivery to epithelial cells in vitro and in vivo. *Gene Therapy*, *10*(19), 1654–1662. https://doi.org/10.1038/sj.gt.3302050

Witter, M. P. (2010). *Connectivity of the Hippocampus BT - Hippocampal Microcircuits: A Computational Modeler's Resource Book* (V. Cutsuridis, B. Graham, S. Cobb, & I. Vida (eds.); pp. 5–26). Springer New York. https://doi.org/10.1007/978-1-4419-0996-1_1

Wray, S. (2017). Modeling tau pathology in human stem cell derived neurons. *Brain Pathology*, *27*(4), 525–529. https://doi.org/10.1111/bpa.12521

Wullimann, M. F., & Mueller, T. (2004). Teleostean and mammalian forebrains contrasted: Evidence from genes to behavior. *Journal of Comparative Neurology*, *475*(2), 143–162. https://doi.org/10.1002/cne.20183

Xie, Y., Schutte, R. J., Ng, N. N., Ess, K. C., Schwartz, P. H., & O'Dowd, D. K. (2018). Reproducible and efficient generation of functionally active neurons from human hiPSCs for preclinical disease modeling. *Stem Cell Research*, *26*, 84–94. https://doi.org/10.1016/j.scr.2017.12.003

Xu, H. T., Han, Z., Gao, P., He, S., Li, Z., Shi, W., Kodish, O., Shao, W., Brown, K. N., Huang, K., & Shi, S. H. (2014). Distinct lineage-dependent structural and functional organization of the hippocampus. *Cell*,

157(7), 1552–1564. https://doi.org/10.1016/j.cell.2014.03.067

Yamagishi, S., Bando, Y., & Sato, K. (2021). Involvement of Netrins and Their Receptors in Neuronal Migration in the Cerebral Cortex. *Frontiers in Cell and Developmental Biology*, *8*(January), 1–12. https://doi.org/10.3389/fcell.2020.590009

Yang, Y., & Wang, J. Z. (2017). From structure to behavior in basolateral amygdala-hippocampus circuits. *Frontiers in Neural Circuits*, *11*(October), 1–8. https://doi.org/10.3389/fncir.2017.00086

Ying, Q.-L., Nichols, J., Chambers, I., & Smith, A. (2003). BMP Induction of Id Proteins Suppresses Differentiation and Sustains Embryonic Stem Cell Self-Renewal in Collaboration with STAT3. *Cell*, *115*(3), 281–292. https://doi.org/10.1016/S0092-8674(03)00847-X

Yizhar, O., Fenno, L. E., Davidson, T. J., Mogri, M., & Deisseroth, K. (2011). Optogenetics in neural systems. *Neuron*, *71*(1), 9–34. https://doi.org/10.1016/j.neuron.2011.06.004

Yizhar, O., Fenno, L. E., Prigge, M., Schneider, F., Davidson, T. J., O'Shea, D. J., Sohal, V. S., Goshen, I., Finkelstein, J., Paz, J. T., Stehfest, K., Fudim, R., Ramakrishnan, C., Huguenard, J. R., Hegemann, P., & Deisseroth, K. (2011). Neocortical excitation/inhibition balance in information processing and social dysfunction. *Nature*, *477*(7363), 171–178. https://doi.org/10.1038/nature10360

Yoon, K. J., Nguyen, H. N., Ursini, G., Zhang, F., Kim, N. S., Wen, Z., Makri, G., Nauen, D., Shin, J. H., Park, Y., Chung, R., Pekle, E., Zhang, C., Towe, M., Hussaini, S. M. Q., Lee, Y., Rujescu, D., St. Clair, D., Kleinman, J. E., … Ming, G. L. (2014). Modeling a genetic risk for schizophrenia in iPSCs and Mice reveals neural stem cell deficits associated with adherens junctions and polarity. *Cell Stem Cell*, *15*(1), 79–91. https://doi.org/10.1016/j.stem.2014.05.003

Yoon, S. J., Elahi, L. S., Pașca, A. M., Marton, R. M., Gordon, A., Revah, O., Miura, Y., Walczak, E. M., Holdgate, G. M., Fan, H. C., Huguenard, J. R., Geschwind, D. H., & Pașca, S. P. (2019). Reliability of human cortical organoid generation. *Nature Methods*, *16*(1), 75–78. https://doi.org/10.1038/s41592-018-0255-0

Yoshinaga, Y., Kagawa, T., Shimizu, T., Inoue, T., Takada, S., Kuratsu, J. I., & Taga, T. (2010). Wnt3a promotes hippocampal neurogenesis by shortening cell cycle duration of neural progenitor cells. *Cellular and Molecular Neurobiology*, *30*(7), 1049–1058. https://doi.org/10.1007/s10571-010-9536-6

Yu, Diana X., Marchetto, M. C., & Gage, F. H. (2014). How to make a hippocampal dentate gyrus granule neuron. *Development (Cambridge)*, *141*(12), 2366–2375. https://doi.org/10.1242/dev.096776

Yu, Diana Xuan, Di Giorgio, F. P., Yao, J., Marchetto, M. C., Brennand, K., Wright, R., Mei, A., McHenry, L., Lisuk, D., Grasmick, J. M., Silberman, P., Silberman, G., Jappelli, R., & Gage, F. H. (2014). Modeling hippocampal neurogenesis using human pluripotent stem cells. *Stem Cell Reports*, *2*(3), 295–310. https://doi.org/10.1016/j.stemcr.2014.01.009

Yu, Z., Pestell, T. G., Lisanti, M. P., & Pestell, R. G. (2012). Cancer stem cells. *International Journal of Biochemistry and Cell Biology*, *44*(12), 2144–2151. https://doi.org/10.1016/j.biocel.2012.08.022

Yuste, R., Hawrylycz, M., Aalling, N., Aguilar-Valles, A., Arendt, D., Arnedillo, R. A., Ascoli, G. A., Bielza, C., Bokharaie, V., Bergmann, T. B., Bystron, I., Capogna, M., Chang, Y., Clemens, A., de Kock, C. P. J., DeFelipe, J., Dos Santos, S. E., Dunville, K., Feldmeyer, D., … Lein, E. (2020). A community-based transcriptomics classification and nomenclature of neocortical cell types. *Nature Neuroscience*, *23*(12), 1456–1468. https://doi.org/10.1038/s41593-020-0685-8

Zakin, L. D. J., Mazan, S., Maury, M., Martin, N., Guénet, J. L., & Brûlet, P. (1998). Structure and expression of Wnt13, a novel mouse Wnt2 related gene. *Mechanisms of Development*, *73*(1), 107–116. https://doi.org/10.1016/S0925-4773(98)00040-9

Zemelman, B. V., Lee, G. A., Ng, M., & Miesenböck, G. (2002). Selective photostimulation of genetically chARGed neurons. *Neuron*, *33*(1), 15–22. https://doi.org/10.1016/S0896-6273(01)00574-8

Zhang, F., Prigge, M., Beyrière, F., Tsunoda, S. P., Mattis, J., Yizhar, O., Hegemann, P., & Deisseroth, K. (2008). Red-shifted optogenetic excitation: A tool for fast neural control derived from Volvox

carteri. *Nature Neuroscience*, *11*(6), 631–633. https://doi.org/10.1038/nn.2120

Zhang, F., Wang, L. P., Brauner, M., Liewald, J. F., Kay, K., Watzke, N., Wood, P. G., Bamberg, E., Nagel, G., Gottschalk, A., & Deisseroth, K. (2007). Multimodal fast optical interrogation of neural circuitry. *Nature*, *446*(7136), 633–639. https://doi.org/10.1038/nature05744

Zhang, Q. G., Wang, R. M., Scott, E., Han, D., Dong, Y., Tu, J. Y., Yang, F., Reddy Sareddy, G., Vadlamudi, R. K., & Brann, D. W. (2013). Hypersensitivity of the hippocampal CA3 region to stress-induced neurodegeneration and amyloidogenesis in a rat model of surgical menopause. *Brain*, *136*(5), 1432–1445. https://doi.org/10.1093/brain/awt046

Zhang, W., Mi, J., Li, N., Sui, L., Wan, T., Zhang, J., Chen, T., & Cao, X. (2001). Identification and characterization of DPZF, a novel human BTB/POZ zinc finger protein sharing homology to BCL-6. *Biochemical and Biophysical Research Communications*, *282*(4), 1067–1073. https://doi.org/10.1006/bbrc.2001.4689

Zhang, X., Schlögl, A., & Jonas, P. (2020). Selective Routing of Spatial Information Flow from Input to Output in Hippocampal Granule Cells. *Neuron*, *107*(6), 1212-1225.e7. https://doi.org/10.1016/j.neuron.2020.07.006

Zhang, Yalin, Kim, M. S., Jia, B., Yan, J., Zuniga-Hertz, J. P., Han, C., & Cai, D. (2017). Hypothalamic stem cells control ageing speed partly through exosomal miRNAs. *Nature*, *548*(7665), 52–57. https://doi.org/10.1038/nature23282

Zhang, Ye, Xie, Z., Zhou, L., Li, L., Zhang, H., Zhou, G., Ma, X., Herrera, P. L., Liu, Z., Grusby, M. J., & Zhang, W. J. (2012). The Zinc Finger Protein ZBTB20 Regulates Transcription of Fructose-1,6-Bisphosphatase 1 and β Cell Function in Mice. *Gastroenterology*, *142*(7), 1571-1580.e6. https://doi.org/10.1053/j.gastro.2012.02.043

Zhang, Ying, Schulz, V. P., Reed, B. D., Wang, Z., Pan, X., Mariani, J., Euskirchen, G., Snyder, M. P., Vaccarino, F. M., Ivanova, N., Weissman, S. M., & Szekely, A. M. (2013). Functional genomic screen

of human stem cell differentiation reveals pathways involved in neurodevelopment and neurodegeneration. *Proceedings of the National Academy of Sciences of the United States of America*, *110*(30), 12361–12366. https://doi.org/10.1073/pnas.1309725110

Zhang, Z., Marro, S. G., Zhang, Y., Arendt, K. L., Patzke, C., Zhou, B., Fair, T., Yang, N., Südhof, T. C., Wernig, M., & Chen, L. (2018). The fragile X mutation impairs homeostatic plasticity in human neurons by blocking synaptic retinoic acid signaling. *Science Translational Medicine*, *10*(452), 1–16. https://doi.org/10.1126/scitranslmed.aar4338

Zhao, C., Teng, E. M., Summers, R. G., Ming, G. L., & Gage, F. H. (2006). Distinct morphological stages of dentate granule neuron maturation in the adult mouse hippocampus. *Journal of Neuroscience*, *26*(1), 3–11. https://doi.org/10.1523/JNEUROSCI.3648-05.2006

Zhao, X., Ueba, T., Christie, B. R., Barkho, B., McConnell, M. J., Nakashima, K., Lein, E. S., Eadie, B. D., Willhoite, A. R., Muotri, A. R., Summers, R. G., Chun, J., Lee, K. F., & Gage, F. H. (2003). Mice lacking methyl-CpG binding protein 1 have deficits in adult neurogenesis and hippocampal function. *Proceedings of the National Academy of Sciences of the United States of America*, *100*(11), 6777–6782. https://doi.org/10.1073/pnas.1131928100

Zhou, G., Jiang, X., Zhang, H., Lu, Y., Liu, A., Ma, X., Yang, G., Yang, R., Shen, H., Zheng, J., Hu, Y., Yang, X., Zhang, W. J., & Xie, Z. (2015). Zbtb20 regulates the terminal differentiation of hypertrophic chondrocytes via repression of Sox9. *Development (Cambridge, England)*, *142*(2), 385–393. https://doi.org/10.1242/dev.108530

Zhu, Z., & Huangfu, D. (2013). Human pluripotent stem cells: An emerging model in developmental biology. *Development (Cambridge)*, *140*(4), 705–717. https://doi.org/10.1242/dev.086165

Acknowledgements

I have come to the conclusion that despite my best efforts over the past decade and a half, I will never fully release an album with acknowledgments like “Thanks to T-Bone for zipping and ripping, much luv bruv.” So instead, I convey my gratitude to my little international community I have established in the last 5-6 years here and everyone else who has been integral to my journey.

On the Pisan side: to all my friends and colleagues who have provided unconditional support (and ~milliliters in antibodies), both in the lab and out, I could not have done this you, my sincerest gratitude to Leo, Raffa, Manu, Ajesh, Fabri, Ele, Edo, Enrico, Fra, Silvia, Nadia, Giac, Claudia, Vere, Gianluca, Akash, Neeraj, Omar, Mehdi, Ayush, Giovanna, Irene, Alessio, Marco T., Marco S., Lenny, Didi, Giampi, Alice, Gael, Vinoshene, Andrea I.

To my collaborators and laboratory heads: Prof. Antonino Cattaneo, Prof. Alessandro Cellerino., Prof. Tommaso Pizzorusso, Prof. Matteo Caleo, Prof. Vanessa Hall, Dr. Cristina DiPrimio, Dr. Elena Novelli, Dr. Marco Mainardi, and Prof. Roberto Vignali (my fellow Hoosier).

To the greatest and most enduring lab technicians of all time: Dr. Vania Liverani and Dr. Mariantoniella Calvello.

To Ricerca for all your help with realizing OPAL’s potential: Marco, Sabrina, Claudia, Edoardo, Alla

To my young prodigy, Anna Maria Frontino, it has been a genuine pleasure to watch you grow as a scientist, I am so proud of you and your accomplishments, and I am honored beyond measure to have played a part in your training. I know you have a very bright future in front of you and I hope that we remain close collaborators and friends.

And finally, to the rarest bird I have ever met, a man who wholeheartedly believes in the integrity of science and all the wonder it could ever hold. I want to thank you for taking a chance on me and inviting me into your laboratory. I wish I could fully express what this opportunity has meant to me, and I have thrived under your guidance these past four years. I am privileged and honored to say that I studied under you, Dr. Federico Cremisi. Mi mancherai tantissimo. Bah. Marcello.

On the Emerald Isle: to my friends who sincerely encouraged me to stay abroad and supported me during my time with Kumlesh and continued well past my goodbyes: Adam, Christine, Charlotte, Teresa, Rob & Rhona & Anya & Olya & Mikey, Emanuele & Kiaran & Oisín.

To my conference cohorts: Istvan, Giordano, Mae, Nour, Ed, Erik, Jeremy, Sara, Ingie, Wen-Hsien, Elisabetta, Giulia, Max, Dennis. Your experimental/job/life advice was always welcome.

Thanks to my Norwegian community, Giulia, Max, Bianca, Maike, and Ingvild for welcoming me to the lab, I’m really looking forward to the next adventure.

Back stateside: to my friends and most crucial support group, who gave me everything I needed to keep pushing forward: Trev & Kayla, Ferg, Ian, Arielle & Tyler & Asher, Pep, Charles Oliver, Joe (rest well), Emily R., Jeremy &

Gwen, Alex, Jake, Good Kyle, Amber & Jimmy, Rachel P., Zavi, Fagrell. To my wonderful nookfinderinos: Nat, Sei, Al, Mel, Leah, & Crystal.

To my family: Mom & Dad, Bren, Cam, Ava, Fin, & Chuck, Gram, Gump, Nana, Papa, Linda, Greg, Andy & Heather & Addie, Brad & Natalie & Chloe & Katelyn & Logan & Kingston, Wes, and Doris and all my extended family in IN/MA/KS.

And finally, to my best friend, my one and forever, thank you so much for undertaking this adventure with me. I wouldn't trade these past five years for anything, and I will be eternally grateful that you crossed oceans for me to pursue my dream. There is no way I can ever pay you back for all you have done and all you have sacrificed. Thank you for supporting me unconditionally and thank you for believing in me with your all. You are truly a wonder and the most genuine and caring individual I know. Thank you, Shelley, I love you.

"Nobody ever accomplishes anything alone." -Leslie Knope

"On a mission, your worst enemy is idle time."- Nipsey Hussle

Anyway. That's it. Thanks for reading.